Quantitative Basis for Component Factors of Gas Flow Proportional Counting Efficiencies

A Dissertation
Presented to
the Academic Faculty

By

Michael C. Nichols

In Partial Fulfillment
of the Requirements for the Degree
Doctor of Philosophy in Radiological Engineering

Georgia Institute of Technology

December 2009

Quantitative Basis for Component Factors of Gas Flow Proportional Counting Efficiencies

Approved by:

Dr. Bernd Kahn, Advisor
Georgia Tech Research Institute
Georgia Institute of Technology

Dr. Nolan Hertel, Co-Chair
School of Mechanical Engineering
Georgia Institute of Technology

Dr. Chris Wang
School of Mechanical Engineering
Georgia Institute of Technology

Dr. W. David Kulp, III
School of Physics
Georgia Institute of Technology

Dr. Eva Lee
School of Industrial Systems Engineering
Georgia Institute of Technology

Date Approved: May 1, 2009

ACKNOWLEDGEMENTS

I would like to acknowledge the support of Georgia Power by providing the opportunity to develop and manage the environmental radiochemistry program of the Environmental Laboratory. This work developed from an interest in improving the quality of specific measurements, and the contributions from Patrick Bell, Health Physicist in this program, are appreciated.

I particularly appreciate the patience, scrupulous attention to detail, and encouragement provided by my advisor, Dr. Bernd Kahn. This work could not have been completed without the support of my co-advisor, Dr. Nolan Hertel, and my reading committee, Dr. Chris Wang, Dr. David Kulp, III, and Dr. Eva Lee.

William Cross, Canberra, provided detailed information regarding the design of the gas flow proportional counter and available information regarding the composition and specification of the detector window. Avneet Snood, Los Alamos National Laboratory Monte Carlo Development Team, provided confirmation and detailed explanation of the MCNP normalization routines.

I wish to particularly acknowledge the support and understanding from my family, Lee, Maggie, Nancy, and Pete Nichols.

TABLE OF CONTENTS

LIST OF TABLES

LIST OF FIGURES

LIST OF SYMBOLS

R_m = observed count rate

A_R = source disintegration rate for radionuclide "R"

G = geometry factor of counting system

f_w = attenuation correction factor due to absorption between the source and the detector

f_b = source-mount backscatter correction factor

ε_β = intrinsic detector counting efficiency for beta particles

f_m = multiple count factor

f_s = source self absorption factor

f_τ = dead-time correction

f_{sc} = fraction scattered into detector volume

Ω = solid angle

D = distance from the point source to the center of the detector window

θ = angle between the line from the center of the point source to the center of the detector and the line from the center of the point source to the edge of the detector window

I/I_o = fraction of initial interactions measured after beta particles are attenuated

μ/ρ = empirical mass absorption coefficient, area / unit mass

$x\rho$ = areal thickness, mass per area

T_{el} = kinetic energy of electrons, MeV

Z = atomic number of the scattering material

p = probability of forming ion pair (Equation 2-9)

b = number of ion pairs (Equation 2-9)

N = number of segments (Equation 2-9)

I_n = true interaction rate, per second

τ = system dead time, seconds

R_m = measured count rate, min^{-1}

E_n = energy of beta particles, MeV, for interval "n"

s_n = path length, cm

$E_R(xp)$ = counting efficiency (count rate per disintegration rate) as a function of areal denisty for radionuclide "R"

R_{net} = net count rate for the source (min^{-1})

C_R = concentration of the source solution (min^{-1} mL^{-1}) at a specified date and time for radionuclide "R"

V_R = volume of the source solution (mL) for radionuclide "R"

λ_R = decay constant (s^{-1}) for radionuclide "R"

T = elapsed time from the source date to the mid-point of the count time for radionuclide "R"

W_{f+p} = weight of filter plus precipitate (g)

W_f = weight of filter (g)

W_{net} = net weight of precipitate

V_c = Volume of carrier added (mL)

C_c = Concentration of carrier (mg mL^{-1})

R_g = gross count rate for the source (min^{-1})

R_b = background count rate for a blank filter on a ring and disk mount (min^{-1})

W_{Net} = Net weight of precipitate (g)

X_s = areal density of precipitate (mg cm^{-2})

$A_{R,T}$ = Activity for radionuclide "R" at time "T", (min^{-1})

Y = fractional yield, the fraction of carrier recovered from the mass added.

$I_{Y\text{-}90,T}$ = fraction of yttrium-90 ingrowth occurring between the time of yttrium hydroxide precipitation and the midpoint of the counting period

$R_{Yttirum\text{-}90}$ = count rate attributed to ingrowth of yttrium-90

S_m = standard deviation of a new measurement of mass “m”

$\widehat{\sigma}$ = estimated variance by Mean Square Error (MSE) from linear regression

n = number of observations

M_I = indicated mass measured by the balance

M_{cal} = mass of calibration weight

$\overline{X}$ = average value

X_i = individual values

S_{xx} = variance of independent values “x”

$u(M_I)$ = uncertainty of balance measurements of mass “M_I”

S_r = standard uncertainty due to repeatability

S_{aL} = standard uncertainty due to balance linearity

I^2 = balance indication

φ_{env} = relative standard uncertainty due to environmental factors estimated as S_m/m

$u(V_I)$ = uncertainty of volume measurements “V_I”

V_I = measured volume

δ_{cap} = manufacturer’s specification for accuracy of volume measurements

S_p = manufacturer’s specification for precision of volume measurements

Z = volume indication

S(i) = standard deviation of the volume indication estimated from replicate weighing

E_i = predicted efficiency for the coefficients E_0 and μ’

ρ_m = density for material “m”

df = degrees of freedom

SS = Sums of Squared deviations

MS = Mean Square

F = F-ratio

P_n^i = normalized probability for beta particle in energy bin i

P_i = specified probability for beta particle in energy bin i, with i an integer

P_c^i = corrected probability for beta particle in energy bin i, with i an integer

$E_{R(x\rho)}$ = efficiency estimated by equation 3-1 or 3-8 for radionuclide R and areal thickness xρ

$E_{MCNP,\ R(x\rho)}$ = fractional energy deposition estimated with the MCNP model for radionuclide R and areal thickness xρ

$u(E_{R(x\rho)})$ = total propagated uncertainty for the measured efficiency for radionuclide R and areal thickness xρ

$u(E_{MCNP,\ R,\ x\rho})$ = uncertainty for the MCNP model, for radionuclide R and areal thickness xρ.

SUMMARY

This dissertation investigates the counting efficiency calibration of a gas flow proportional counter with beta-particle emitters in order to 1) determine by measurements and simulation the values of the component factors of beta-particle counting efficiency for a proportional counter, 2) compare the simulation results and measured counting efficiencies, and 3) determine the uncertainty of the simulation and measurements.

Monte Carlo simulation results by the MCNP5 code were compared with measured counting efficiencies as a function of sample thickness for ^{14}C, ^{89}Sr, ^{90}Sr, and ^{90}Y. The Monte Carlo model simulated strontium carbonate with areal thicknesses from 0.1 to 35 mg cm^{-2}.The samples were precipitated as strontium carbonate with areal thicknesses from 3 to 33 mg cm^{-2} , mounted on membrane filters, and counted on a low background gas flow proportional counter. The estimated fractional standard deviation was 2–4% (except 6% for ^{14}C) for efficiency measurements of the radionuclides. The Monte Carlo simulations have uncertainties estimated to be 5 to 6 percent for carbon-14 and 2.4 percent for strontium-89, strontium-90, and yttrium-90. The curves of simulated counting efficiency *vs*. sample areal thickness agreed within 3% of the curves of best fit drawn through the 25 - 49 measured points for each of the four radionuclides.

Contributions from this research include development of uncertainty budgets for the analytical processes; evaluation of alternative methods for determining chemical yield critical to the measurement process; correcting a bias found in the MCNP normalization

of beta spectra histogram; clarifying the interpretation of the commonly used ICRU beta-particle spectra for use by MCNP; and evaluation of instrument parameters as applied to the simulation model to obtain estimates of the counting efficiency from simulated pulse height tallies.

Chapter 1. Introduction

This dissertation investigates the counting efficiency calibration of a gas flow proportional counter with beta-particle emitters in order to 1) determine by measurements and simulation the values of the component factors of beta-particle counting efficiency for a proportional counter, 2) compare the simulation results and measured counting efficiencies, and 3) determine the uncertainty of the simulation and measurements.

The study of absolute counting efficiencies for gas ionization detectors began in the 1940s at a time when known radionuclide standards for beta-emitting radionuclides were not readily available and there was a need for determining counting efficiencies for gas filled detectors. Early measurements, particularly those described by Zumwalt (1950), consisted of carefully varying counting conditions for end-window Geiger-Mueller counters so correction factors were as close to unity as feasible. These studies provide conceptual models to describe empirical data based on specific counting geometries. Additional studies of parameters determined from empirical data are presented in a series of papers in Coryell and Sugarman (1951) and summarized in Steinberg (1962) and Price (1964).

The detector system studied is a low-background gas flow proportional counter configured to count samples emitting beta-particle radiation. The counting efficiencies of interest are for the following radionuclides: strontium-90; yttrium-90; and strontium-89. Calibration curves of counting efficiency as a function of areal thickness are constructed

for a range of strontium carbonate masses for typical analytical processes. Carbon-14 efficiencies are also evaluated in order to extend the range of measurements to lower beta-particle energies.

Strontium-90, yttrium-90, and strontium-89 efficiencies are used for measurements of radioactivity in water, vegetation, soil, and other matrices. Reference methods requiring these counting efficiencies include EPA 905 (Krieger et. al, 1980) for measurements in water, HASL 300 method Sr-01 for water and soil (EML, 1997), and Standard Methods 7500-Sr for water (APHA, 1992).

A detailed evaluation of the preparation of calibration standards also addresses requirements for establishing uncertainties meeting requirements of USNRC Regulatory Guide 4.15 Revision 2 (USNRC, 2007). Constructing an uncertainty budget provides insight regarding important parameters affecting the overall measurement uncertainty.

The development of Monte Carlo codes for modeling electron interactions permits further study of the parameters identified by earlier empirical studies. Constructing a model of beta-particle interactions within gas-filled detectors requires evaluation of detector dimensions, material composition, and evaluation of assumptions in the Monte Carlo simulation. Verification of the suitability of the model for estimating the fraction of interactions within the detector depends on demonstrating the measured counting efficiencies are a reasonable fit to the model output and that the model output is consistent with the operational characteristics of gas ionization detectors. The model results can then provide insight into components of the detector geometry and responses that are not directly measurable.

Chapter 2. Literature

Counting efficiency parameters for gas ionization detectors were developed from empirical measurements for calibrating end-window Geiger Mueller counters and proportional counters. One approach to determining the magnitude of parameter values is to vary conditions for a single parameter while controlling all other parameter values. The rigorous evaluation first presented by Zumwalt (1950) requires extensive measurement and evaluation. This approach is limited by parameters that may be correlated except under specific conditions.

2.1 Parameters determining beta-particle counting efficiency

The parameters that affect absolute beta-particle counting are summarized by Burtt (1949), Zumwalt (1950) and Gleason et al. (1951). The overall efficiency for counting of beta particles may be expressed as

$$R_m / A_R = G \bullet f_w \bullet f_b \bullet \varepsilon_\beta \bullet f_m \bullet f_s \bullet f_\tau \qquad \text{Equation 2-1}$$

where

R_m = observed count rate

A_R = source disintegration rate

G = geometry factor of counting system

f_w = attenuation correction factor due to absorption between the source and the detector

f_b = source-mount and backing backscatter correction factor

ε_β = intrinsic detector counting efficiency for beta particles

f_m = multiple count factor

f_s = source self absorption factor

f_τ = dead-time correction

following the notation used by Price (1964).

Zumwalt (1950) also considered scattering of beta particles into the detector, a cylindrical Geiger-Mueller counter, from the source housing, from air outside the solid angle subtended by the detector, and by preferential scattering toward the detector from within the source. Bailey and Steigerwalt (1975) point out additional factors affecting beta-particle counting efficiency, including 1) loss of scattered secondary electrons by total or partial escape from the detector volume; 2) scattered secondary electrons entering the detector volume but originating outside the detector; and 3) energy lost in the form of characteristic x-rays.

The following discussion considers the parameters that affect absolute beta-particle counting, and then the Monte Carlo simulation of electron transport.

2.1.1 Geometry of counting system (G)

Beta particle radiation from the source is initially emitted isotropically. If factors such as scattering and attenuation are negligible, the amount of radiation incident on the detector is proportional to the solid angle Ω, in steradians, which the detector subtends at some fixed distance with respect to the source. The geometry factor, G, is equal to $\Omega/4\pi$. Early

work on empirical corrections for beta-particle counting used small geometry factors to avoid scattering when counting sources were in close proximity to the detector, but resulted in lower counting efficiencies. Gleason et al. (1951) simplified the evaluation of equation 2-1 by standardizing the counting geometry with a collimating orifice placed between the source and the end window of the detector. The collimating orifice effectively eliminates corrections for scattering from air, counter supports, and the sample holder. In addition, it restricts interactions to the sensitive volume of the detector.

Several methods of estimating the solid angle are available. The solid angle subtended by a point source can be calculated:

$$\Omega = 2 \bullet \pi \bullet D^2 \bullet \left(1 - Cos\ \theta\right) \qquad \text{Equation 2-2}$$

where D = distance from the point source to the center of the detector window,

θ = is the angle between the line from the center of the point source to the center of the detector and the line from the center of the point source to the edge of the detector window.

Solid angles subtended by circular apertures from circular sources have been estimated from infinite series expansions tabulated for point and spread sources by Jaffey (1953) and solid angle contour integrals (Masket 1957). Solid angle values are also tabulated for various circular source-detector configurations by Bland (1984) and approximated as described by Burtt (1949, Appendix C).

2.1.2 Attenuation correction due to absorption between the source and the sample detector (f_w)

The number of beta particles leaving a radioactive source and depositing energy in a gas filled detector is reduced by attenuation in the intervening materials, including any source covering, air between the source and the detector window, and the detector window. The fraction of beta particles reaching the detector volume after penetrating a specified distance expressed as areal density, xρ, is approximated by an exponential attenuation equation:

$$I / I_0 = e^{\frac{-\mu}{\rho} \bullet x\rho} \qquad \text{Equation 2-3}$$

where I/I_o = fraction of initial ionization measured after beta particles are attenuated,

μ/ρ = empirical mass absorption coefficient, area / unit mass, and

$x\rho$ = areal density in mass per area.

The exponential attenuation of beta particles is largely independent of the atomic weight, Z, of the material, with u/ρ rising only slightly with increasing Z. The attenuation of β-ray spectra is a function of E_{max}, the maximum or endpoint energy (Evans, 1955) and is independent of distance within the range of the beta particles. Absorption curves for thin absorbers, absorbers close to the source, and measurements near the range of beta particles, however, are poorly fit by exponential absorption curves. Scattering by an absorber close to the detector has been noted by Zumwalt (1950) and Elliott et al. (1951). Zumwalt (1950) also noted that an absorber placed on the source may increase

the fraction of radiation observed in a detector by causing scattering into the solid angle subtended by the detector.

The exponential attenuation of beta particles results from electron interactions satisfying approximately the postulates of a Poisson process. The exponential distribution has a memory-less property such that regardless of the previous history, the probability of interaction over the next unit distance is the same as the probability over any other equivalent distance (Evans, 1955; Hogg and Craig, 1978). The exponential attenuation of beta particles is an approximation limited by the finite range of electrons from a specific radionuclide.

The mass attenuation coefficients from Baltakmens (1970, 1977) (see Table 2-1) are based on attenuation by aluminum absorbers counted in a Beckman "Widebeta" proportional counter with 0.5 mg cm^{-2} end window and sample-to-window distances of 1 mm and 5 mm. Attenuation coefficients in Baltakmens' studies were related to the maximum energy of the beta-particle spectra and the beta-particle energy distribution. These data are sometimes used to identify beta-particle emitters by their maximum energy.

Table 2-1. Empirical attenuation coefficients from Baltakmens (1970) for select materials and radionuclides.

Radionuclide	***Emax MeV***	***Aluminum Z=13 cm^2 g^{-1}***	***Copper Z=29 cm^2 g^{-1}***
Cobalt-60	0.32	104	99
Strontium-90	0.54	35	35.4
Strontium-89	1.46	7.2	11.0
Yttrium-90	2.26	4.9	6.0

Gleason et al (1951) report estimates of absorption factors for beta particles by extrapolating from measurements of an aluminum absorption curve back to the areal thickness equivalent to the thickness of the intervening air and mica window. They note that this estimate is an approximation that may be biased if significant scattering from the backing or surrounding material occurs. They provide an equation estimating the mass absorption coefficient for beta particles from allowed transitions dependent on the maximum beta particle energy for range from 0.15 to 3.5 MeV as

$$\mu_0 = 0.017 E_{\max}^{-1.43} \qquad \text{Equation 2-4}$$

where

$\mu_{0\ is}$ the mass absorption coefficient near zero thickness

E_{max} is the maximum energy of the beta particle spectrum.

2.1.3 Source-mount backscatter correction (f_b)

Two sources of information regarding backscatter corrections are available: empirical measurements with radionuclides emitting beta particles; and measurements of monoenergetic electrons in electron beams. Backscatter of beta particles has been determined empirically as the ratio f_b = (count rate with backing)/ (count rate without backing), or

.

$$f_b = R_m \,/\, A_R \bullet G \bullet f_w \bullet \varepsilon_\beta \bullet f_m \bullet f_s \bullet f_\tau \qquad \text{Equation 2-5}$$

where the parameters are as defined for equation 2-1.

In empirical determination of backscatter, the source count rate is obtained with a thin backing, less than 1 mg cm^{-2}, and compared with the source count rate when backed with the material in question (Burtt, 1949; Seliger, 1952; and Zumwalt, 1950).

The solid angle subtended by the detector typically is held constant in empirical studies and has ranged from small angles to 2 π geometry. The beta-particle source has a spectrum of energies initially emitted isotropically and interacting with the backing in non-uniform geometry (Baker and Katz, 1953; Zumwalt, 1950). Estimates of backscatter for beta particles indicate that the saturation thickness is reached at two-tenths the range of the beta particles (Burtt, 1949; Price, 1964; Zumwalt, 1950).

Measurements by Seliger (1952) of the backscattering of positrons and electrons from point sources shows electrons are backscattered to a greater extent than positrons and backscattering is approximately independent of energy. Seliger demonstrated that backscatter is a function of atomic number. He described the backscattering coefficients qualitatively as a function of angle and atomic number in terms of a “diffused” component and a “side scattered” component. This qualitative view describes the initial increase in counting efficiency with thickness until a maximum is reached. Zumwalt (1950) provided backscatter measurements for nearly weightless phosphorous-32 sources (Emax 1.70 MeV) of high specific activity with a cylindrical Geiger Mueller counter for small solid angles (ranging from 0.016 to 0.069 sr). The sources were mounted on films of 50 μg cm^{-2} and the increase in count rate measured when backed by materials of different atomic numbers. He also observed increased backscatter with increasing atomic number. In addition, he found that backscatter increased with increased maximum beta-particle energy using cobalt-60, iodine-131, and phosphorous-32 sources.

Balfour (1954) provides additional information regarding back-scattering of electrons with energies in the range from 28 to 105 keV as a function of atomic number. He notes the importance of change in counting geometries toward detectors subtending greater solid angles relative to source emissions. He also notes that the effect of atomic number on backscattering from thin sources is relative minor for low-Z materials but may be considerable for high Z-values.

Many backscatter estimates were developed from measurements of monoenergetic electrons impinging targets in a vacuum. The following studies include electron microprobe data with energies from approximately 4 keV to 100 keV and electron beam data for energies from 1.0 MeV to 22 MeV. The primary geometry is a normally incident beam on a semi-infinite target.

Darlington (1975), Hünger and Kuchler (1979), and Neubert and Rogachewski (1980) provide backscatter coefficients for electron beams in the range from 4 to 100 keV for semi-infinite targets with atomic numbers ranging from 5 to 92. Darlington (1975), and Neubert and Rogachewski (1980) also provide backscattering coefficients as a function of angle.

Rester and Derrickson (1970) provide the energy distribution of backscattered electrons for perpendicular and non-perpendicular measurements of 1.0-MeV electron beams measured with a Si(Li) detector. In addition, Monte Carlo results are presented which approximate the energy distribution measured for backscattered electrons.

Tabata (1967) provides backscattering coefficients for electrons from 3.2 MeV to 14 MeV impinging normal on semi-infinite targets made of beryllium, carbon, aluminum, copper,

silver, gold, and uranium. Variation of backscattering coefficients with the target thickness and the angular distribution of backscattered electrons as a function of atomic number and electron energy are provided.

Schimizu and Ichimura (1983) compared Monte Carlo calculations with Auger microprobe measurements for 1.5 and 3.0 keV electrons at normal and 45 degree incidence on thick aluminum targets. The measured results were also simulated with a Monte Carlo model.

Backscatter of monoenergetic electrons measured by electron beams normal to targets of differing atomic number are summarized by Tabata et al. (1971). In the case of monoenergetic electron measurements, backscatter is a function of atomic number of the scattering material, kinetic energy of the incident electron, and angle of incidence (Rester and Derricksen, 1970; Tabata et al. 1971). These measurements indicate that a saturation thickness where there is no further increase in the fraction backscattered is reached at one half the range of the electron (cf. Tabata et al. 1971, Figure 7).

Tabata et al. (1971) fitted empirical equations to the data:

$$f_b = a_1 \Big/ \left(1 + a_2 \bullet \left(\frac{T_{el}}{mc^2}\right)^{a^3}\right) \qquad \text{Equation 2-6}$$

where f_b = fraction backscattered,

$$a_1 = b_1 \bullet e^{-b_2 \cdot Z^{-b_3}}$$

$$a_2 = b_4 + b_5 \bullet Z^{-b_6}$$

$$a_3 = b_7 - b_8 / Z$$

with

T_{el} = kinetic energy of electrons

m = particle mass

c = velocity of light

Z = atomic number of the scattering material

and the eight fitted constants in Table 2-2.

Table 2-2. Backscatter coefficients for normally incident monoenergetic electrons, Tabata et al. 1971).

Constant	*Value*
b_1	1.15 ± 0.06
b_2	8.35 ± 0.25
b_3	0.525 ± 0.020
b_4	0.0185 ± 0.0019
b_5	15.7 ± 3.1
b_6	1.59 ± 0.07
b_7	1.56 ± 0.02
b_8	4.42 ± 0.18

The empirical equation is applicable for energies from 50 keV to 22 MeV for $Z \geq 6$, but is of limited use in counting applications as they are based on monoenergetic electrons incident on semi-infinite targets in a vacuum.

2.1.4 Source self-absorption factor (f_s)

The source self-absorption factor, f_s, estimates the fraction of beta particles reaching the surface of the source as a function of the areal thickness of the source. The self-absorption factor assumes exponential absorption and the absence of scattering from the source into the detector. These conditions apply for small solid angles and

detectors counting radiation normal to the surface (Baker and Katz, 1953). The self-absorption factor is estimated by:

$$f_s = \frac{\left[1 - e^{\frac{-\mu}{\rho} \bullet x\rho}\right]}{\frac{\mu}{\rho} \bullet x\rho}$$ Equation 2-7

where μ/ρ = mass attenuation coefficient, area per mass

$x\rho$ = areal thickness, mass per area

with the product equal to μx.

The self-absorption factor described by equation 2-7 is derived by integrating equation 2-3 over the distance penetrated, with the distance measured in units of areal density.

Sources counted close to the detector or covered by thin absorbers exhibit scattering which complicates correction for self absorbance. The generally observed pattern is an increase in count rate with additional absorber until a maximum is reached, followed by an approximately exponential decrease in count rate with continued increase in absorber thickness (Novey and Elliot, 1951). The maximum count rate appears to be a function of atomic number and absorber thickness. Work with beta particles emitted from thick plane sources suggests the distribution is I_o* Cos θ and not isotropic (Elliot et al. 1951), where I_o is the initial intensity of the radiation.

Zumwalt (1950) describes scattering with increasing source thickness as “forescattering” with beta particles initially emitted isotropically preferentially scattered in the direction normal to the absorber. As reported in Zumwalt, thick uranium foils produce angular distribution of radiation following the distribution

$$A = A_0 \frac{Cos\theta}{\mu x}\left(1 - e^{\frac{-\mu x}{Cos\theta}}\right) \qquad \text{Equation 2-8}$$

where

A_o = the count rate at zero thickness

Θ = angle between the axis normal to the source and detector and the direction of the beta radiation, and

μx = attenuation coefficient times the thickness, see Equation 2-7.

Baker and Katz(1953) note the difficulty of separating self-scattering and self-absorption for sources of finite mass. They studied self-absorption in a 4π counting geometry with sources mounted on thin Mylar film to effectively minimize backscatter that complicates evaluation of these two components. They suggest that beta particles from thin sources and the initial material for thicker sources (Figure 2-1, layer “a”) are emitted isotropically. As the source thickness increases, beta particles originating at greater depths (Figure 2-1, layer “b”) are preferentially scattered in a direction normal to the surface, emerging as a cosine distribution with respect to an axis normal to the plane of the surface. Scattering from this intermediate layer consists of elastic scattering, favoring a forward direction, and more infrequently, inelastic scattering resulting in large changes in energy (Lorence

and Beutler, 1997). Beta particles originating at greater depths (Figure 2-1, layer “c”) have a great probability of undergoing multiple scattering and if they emerge from the source surface will travel in random directions.

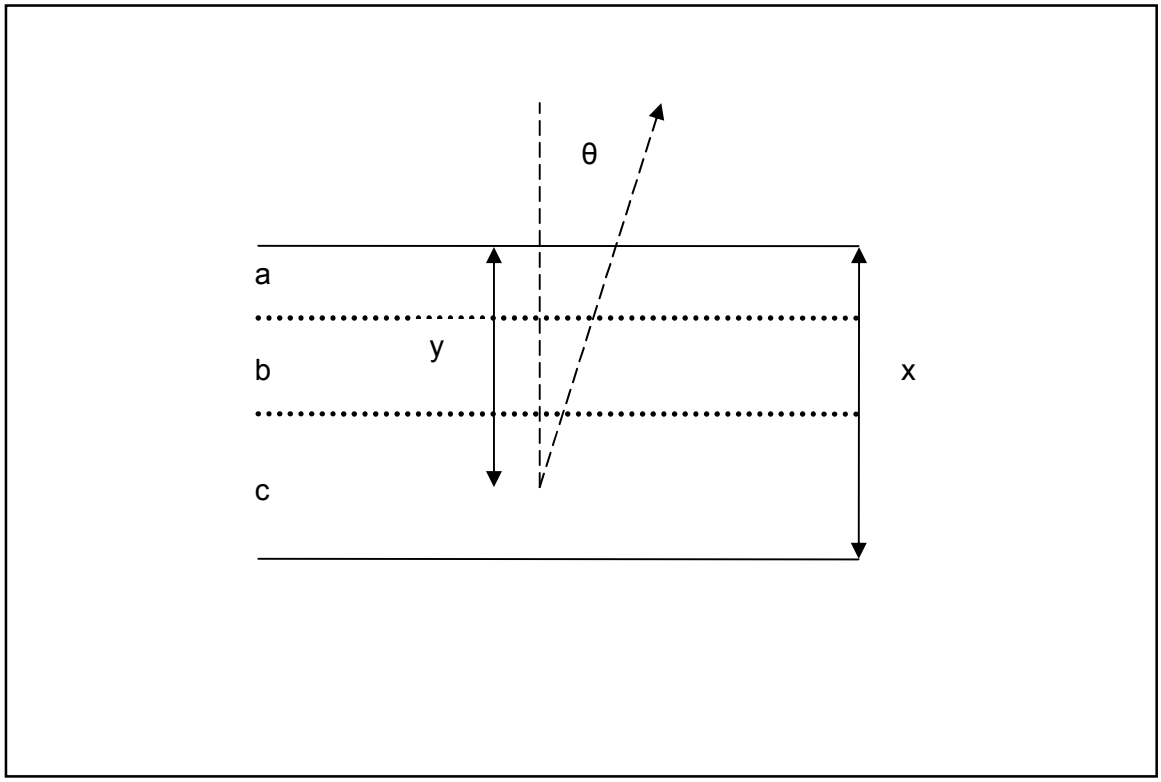

Figure 2-1. Conceptual representation of the origin of beta-particles and the resulting qualitative distribution as a function of material depth, from Baker and Katz (1953). Beta-particle distributions are expected to be (a) isotropic, (b) cosine, and (c) random depending on the distance and angle traversed to the surface.

This distribution is presented in Figure 2-2 for A_0=100 and μx =1 is the expected angular distribution of beta-particle tracks crossing a plane for thin sources counted in close proximity to the detector window.

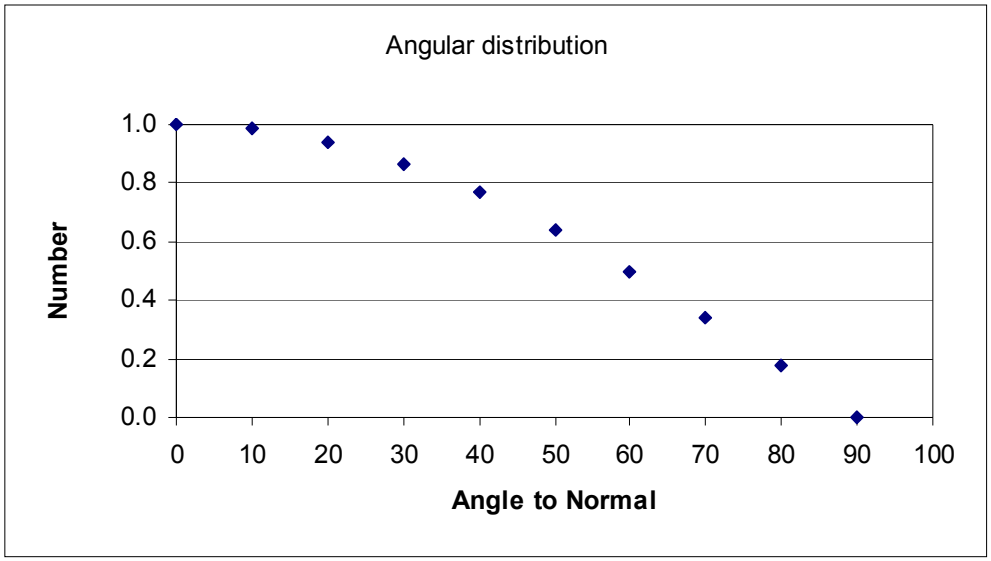

Figure 2-2. Angular distribution of beta-particle radiation for equation 2-8, from the distribution by Engelkemeir, Rubinson, and Elliot (Zumwalt, 1950).

2.1.5 Intrinsic efficiency for beta particles (ε_β)

The intrinsic efficiency for beta particles is defined as the fraction of the particles which produces a discharge upon entering the sensitive volume of the detector. This factor is dependent on the specific ionization constant of the gas mixture, the pressure of the gas, the path length, the energy of the particle, and the multiplication that takes place in the detector following interaction. Large detectors are usually designed with an intrinsic efficiency approaching 1. The intrinsic efficiency of the detector is an estimate of the probability of interactions within the detector volume that result in a signal sufficient to be measured above electronic noise.

The intrinsic efficiency for beta particles has two components: the probability of interaction with the counter gas; and the amplification of the resulting signal to a level sufficient for measurement above the electronic noise threshold. Counting losses may

result from pulse height discrimination, including events which do not exceed the lower level discriminator and also events that exceed the upper level discriminator. The lower level discriminator is set to exclude electronic noise from the detector and amplifier system and places a lower limit on the peak height which is counted. The counting system can be evaluated to estimate the incident energy which will be excluded by the lower level discriminator. In gas flow proportional counters, an upper level discriminator may exclude pulses above a specified voltage which may occur when counting alpha particles in addition to beta particles. The frequency with which beta-particle sources produce counts above the upper level discriminator is typically 1% or less in conventionally configured systems (Tennelec, undated).

The probability of beta-particle tracks producing ionization sufficient to produce a discharge can be estimated from the binomial-distribution law. The probability of producing a single ion pair can be estimated by considering a distance divided into N segments, with “b” ion pairs produced along the path, so that

$$p = \frac{b}{N}$$ Equation 2-9

where

p = probability of forming and ion pair, and

N is sufficiently large that only one ion pair is formed per segment.

Then the probability that no ionizations will be produced is estimated by the Poisson approximation to the binomial distribution, with

$$P(x=0)=\frac{N!}{N!x!}\left(p^{x}\right)(1-p)^{N}=\left(1-\frac{b}{N}\right)^{N}\simeq e^{-b}$$ Equation 2-10

for large N (Price, 1964), where "x" is the number of events. The probability of no ionizations as N increases and b/N is small is typically less than $1x10^{-6}$. Given a set of one or more ionizations, however, the multiplication within the detector must be sufficient to exceed the level of the electronic discriminator. The probability of any integer number of events n, given p, is

$$f(x \mid n, p)=\frac{e^{-np}\bullet np^{x}}{x!}$$ Equation 2-11

(DeGroot, 1986).

2.1.6 Multiple count factor (f_m)

The multiple count factor is the fraction of the number of counts relative to the number of primary discharges which occur in the sensitive volume of the detector. Multiple count interactions may result from secondary processes which arise from effects within the primary avalanche. Spurious after-pulses are often very small and are eliminated from consideration by simple amplitude discrimination. At moderate values of the electric field, their rate of occurrence may not exceed a few hundredths of a percent of the primary count rate. The need for corrections for multiple counts if f_m is larger than 1.0 can result from operating the counter near the end of the counting plateau where the applied voltage may be sufficiently high to permit counting after-pulses (Knoll, 2000).

2.1.7 Dead-time correction (f_τ)

Dead time losses may result for events occurring within a specified time interval for the counting system. Two types of dead time behavior are commonly used, paralysable and nonparalysable models (Albert and Nelson, 1953). The paralysable case can be modeled as an exponential probability density function for the distribution of intervals between random events

$$R_m = I_n \bullet e^{-I_n \bullet \tau} \qquad \text{Equation 2-12}$$

The non-paralysable model is based on the absence of a response for a fixed length of time following an initiating event. In the non-paralysable case,

$$I_n - R_m = I_n \bullet R_m \bullet \tau \qquad \text{Equation 2-13}$$

can be solved for I_n, the true interaction rate,

where

I_n = true interaction rate,

R_m = observed count rate, and

τ = system dead time

The non-paralysable model is appropriate for the gas-flow proportional counters used in this research since the counting system is designed to have a fixed dead time following an event (Tennelec, undated). The ratio of the interaction rate to the observed count rate is given by rearranging equation 2-12 to

$$\frac{I_n}{R_m} = \frac{1}{1 - R_m \bullet \tau} \qquad \text{Equation 2-14}$$

2.1.8 Other factors

Other factors may affect beta-particle counting efficiencies, including additional dead time corrections from the anti-coincidence signal from guard detector, and creation of secondary electrons that may scatter into the detector volume. These factors are evaluated to estimate the effect on beta-particle counting efficiency.

In low background anticoincidence detectors, an additional correction for the dead time introduced by the guard detector must be considered. Signals from the guard detector are fed to an amplifier/discriminator. The amplifier/discriminator is set to discriminate against electronic noise and produce a 45-50 microsecond logic pulse for pulses exceeding the discriminator level. The logic pulses inhibit the scaler from counting pulses received from the sample detector. As a result, counting of cosmic rays by the sample detector is greatly reduced, but an additional dead time correction is required.

In considering the creation of secondary electrons through inelastic collisions, by convention, the lower energy electron from a scattering event is assumed to be the scattered electron and the higher energy electron the beta particle. Secondary electrons of less than 40 keV created within or near the source would be unlikely to reach the detector volume. This is the lower energy for beta particle emitted normal to the source surface and capable of penetrating the detector window based on the tabulated range for electrons (Turner, 1986) and the thickness of the intervening material. However, secondary electrons created by interactions in the intervening layers or by interactions with the detector walls may interact within the detector volume.

2.2 Monte Carlo simulation of electron transport

Monte Carlo methods provide a useful means of exploring the mechanism of radiation interaction. The code MCNP simulates electron transport with regard to transmission, absorption, and scattering (LANL, 2005). Electrons are transported in Monte Carlo methods in a schematized random walk in which each step approximates a large number of interactions. This approach is used instead of sampling each interaction as implemented for photon and neutron transport. Each step represents a condensed history with an average energy loss estimated by the continuous-slowing-down-approximation (Berger, 1963).

MCNP implements the "condensed history" Monte Carlo method developed by Berger (1963). This method considers the interaction occurring in major energy steps, defined such that the kinetic energy T is reduced by $2^{-1/k}$ per step, or

$$T_{n+1} / T_n = 2^{-1/k} \qquad \text{Equation 2-15}$$

where k is commonly set to 8, resulting in an average energy loss per major energy step of 8.3%.

Electron steps with path length, s_n, are determined from the total stopping power for a given material and electron energy, with the relationship between the total stopping power and the major energy step given by

$$T_n - T_{n+1} = -\int_{s_n}^{s_{n+1}} \frac{dT}{ds} ds$$ Equation 2-16

The path length "s" differs from the material thickness because scattered electrons travel complex paths. The electron stopping power and electron range from the MCNP electron cross section library are tabulated in MCNP so that values correspond to the energy differences of equations 2-15 and 2-16. Energy loss is computed once per energy step based on the Landau-Blunck-Leisegang theory of energy loss fluctuations. Each major energy step is further divided into "m" sub-steps, with path length s/m, in order to meet assumptions for modeling the angular deflection of electrons. The number of sub-steps, m, is a function of the average atomic number, Z, of the material and ranges by default from m= 2 for Z < 6 to m = 15 for Z > 15. The actual number of substeps completed by electrons in crossing a given volume is also a function of the dimensions of the material. The sub-steps may be increased for specific materials, at the expense of increased computational time, in order to adequately sample electron interactions for a major energy step within the dimensions of the material. Within the sub-steps, the angular deflections of electrons are estimated following the multiple scattering theory of Goudsmit-Saunderson. The production of secondary radiation including fluorescent x-rays, "knock-on" electrons, Auger electrons, and bremsstrahlung photons is also sampled in the sub-steps (LANL 2005, 2006).

Codes for examining the transport of electrons include CYLTRAN, TIGER, GEANT4, Penelope, and MCNP. The electron transport approach in CYLTRAN uses the techniques described in Berger (1963). This is one of the Integrated Tiger Series codes which implements three- dimensional particle trajectories for axially symmetric geometries (Halbleib, 1988). This code is available as CYLTRAN, CYLTRANP, and CYLTRANM. CYLTRAN is designed to transport at energies which are large compared

to the binding energies of the atomic electrons. CYLTRANM consists of the collisional transport of CYLTRAN with transport in macroscopic electric and magnetic fields of arbitrary spatial dependence. CYLTRANP includes a more elaborate ionization and relaxation model in order to have a more detailed model of low energy transport.

Horowitz et al. (1994) used CYLTRANP to estimate monoenergetic electron depth dose distributions for construction of beta-particle correction factors for LiF dosimeters. Monte Carlo estimates were compared with measurements of beta particle fields based on plastic scintillators. Difficulties encountered included uncertainties in shape of the beta-particle spectra below 500 keV, variations in beta spectra with the source-dosimeter geometry, and the unknown angular distribution of radiation incident to the detector. Horowitz et al. considered both normal and isotropic incidence, but simulated an isotropic geometry.

Pregenzer (1985) used Monte Carlo calculations to estimate low-energy electron back-scatter coefficients and compared results with empirically determined coefficients for normally incident electrons in the 3 - 100 keV range. Both TIGER and TIGERP (based on ETRAN) were evaluated for gold and aluminum. This study found back scatter was underestimated at all atomic weights, with increasing divergence at lower energies, particularly less than 10 keV. Calculations by single scattering Monte Carlo may be necessary to adequately model electron interactions (Shimizu and Ichimura, 1983).

Lockwood et al. (1981) performed calorimetric measurements of electron energy deposition and compared results with Monte Carlo simulations with the TIGER code. This study examined predictions for homogeneous and multilayer materials including beryllium, carbon, aluminum, copper, tantalum, and molybdenum exposed to electrons

from 0.05 to 1.0 MeV at angles of 0, 30, and 60 degrees. The TIGER code produced results in good agreement with measurements, except at low energies and high Z material where model results underestimated electron energy deposition.

Jun (2003) evaluated MCNP4C and TIGER for energy deposition by electrons with energies of 0.5, 1 and 2 MeV in elemental slabs. The energy deposition profiles were modeled for semi-infinite elemental slabs for carbon, aluminum, copper, and tantalum and compared to experimental measurements. The experimental results and energy deposition profiles agreed within the combined uncertainties of the measurements and calculations. Observed differences resulted from different energy-indexing algorithms employed in the two codes, the effects of sub-zone thickness, and facilities for modeling complex geometries provided by the two different codes.

Martin et al. (2003) reported detailed measurements of electron backscattering from low beryllium and silicon targets for electron energies of 42.5 and 124 keV. These measured results for energy distribution and angular distribution were compared with simulations based on GEANT4 and Penelope Monte Carlo codes. Normalized results from Monte Carlo simulations were found to provide reasonable representations of the distribution of backscattered electrons in angle and energy. Martin et al. (2006) extended this work, reporting detailed measurements of electron backscattering from plastic scintillators targets. The simulations by the Penelope Monte Carlo code was found to give a better fit to the measurement data.

Results from Monte Carlo model results have been compared to measurements of backscatter coefficients for monoenergetic electrons normally incident to an aluminum surface (Berger, 1963). Berger compared electron backscatter as a function of source

energy for perpendicular incidence on aluminum to experimental measurements by Kanter (1957) for energies between 10 and 70 keV, Agu et al. (1958) for energies between 0.4 and 0.8 MeV, Trump and Van de Graaf (1949) for energy of 0.2 MeV, and Frank (1959) for energies up to 1.7 MeV. He used a simple Monte Carlo model with a relative small number of histories per case, 1000, to tabulate backscatter for normal incidence, as a function of beta-particle angle incident with the surface, and for isotropic incidence. Berger reported agreement between values for isotropic incidence and measurements by Kanter with a rubidium-87 beta-particle source (maximum beta energy of 0.275 MeV), and with measurements by Suzor and Charpak (1952) for beta-particle sources with maximum energies ranging from 0.17 to 1.7 MeV. He noted that the results for the isotropic incidence were approximately 10 percent lower than the measurements reported by Seliger (1952) for phosphorous-32, with maximum beta energy of 1.7 MeV.

Dapor(1975) describes a Monte Carlo simulation to calculate the electron backscattering and average backscatter energy for bulk targets at various angles of incidence over the energy range from 5 keV to 30 keV. His simulation results for backscattering coefficients are in close agreement with experimental data in this energy range.

Chapter 3. Methods

This chapter outlines the methods for preparing efficiency standards, estimating the uncertainty of measurements, and constructing the Monte Carlo model. Carbon-14, strontium-89, strontium-90, and yttrium-90 sources of varying areal thicknesses were prepared and counted with a gas flow proportional counter under conditions of large solid angle counting geometry. Preparation of sources includes carrier standardization, determining chemical yield, checking results through mass balance measurements, counting samples, and calculating counting efficiencies. In addition, the preparation of other radionuclide sources for specific measurements is described.

The basis for measurement uncertainties used to construct total measurement uncertainties is provided. Measurement uncertainties include the uncertainty of the radioactive material activity, gravimetric measurements, volumetric measurements, and counting measurements.

This chapter also describes the dimensions and densities needed to construct a Monte Carlo model, methods for estimating the energy of events occurring within the detector and excluded by the amplifier discriminator, and the amplification resulting from multiplication within the detector volume. The section describing the Monte Carlo model lists assumptions and modifications necessary to model the source-detector system.

3.1 Radiochemical and analytical methods

Radiochemical and analytical methods include description of the radionuclide standard solutions, stable carriers for determining chemical yield, preparation of sources, and mass balance measurements.

3.1.1 Radionuclide standard solutions

Sources were prepared from carbon-14, strontium-89, and strontium-90/yttrium-90 standards obtained from Eckert and Zeigler (formerly Analytics, Incorporated), a commercial supplier of calibration standards with measurements traceable to National Institute of Standards and Technology (NIST). Source solutions were prepared by transferring a weighed amount of the standard to a class A volumetric flask and diluting to the specified volume, typically 100 mL, with 0.024 N HNO_3.

3.1.2 Carrier standardization

Strontium carrier was prepared as strontium nitrate, $Sr(NO_3)_2$, in deionized water for a nominal carrier concentration of 20 mg strontium mL^{-1}. Yttrium carrier was prepared as yttrium nitrate, $Y(NO_3)_3 \cdot 6H_2O$, with a nominal concentration of 10 mg yttrium mL^{-1}.

The strontium carrier was standardized gravimetrically by precipitation as strontium carbonate with excess sodium carbonate, filtration onto a fine-pore Gooch filter crucible, and drying and weighing the precipitate. Five mL of the carrier was pipetted into each of

three separate centrifuge tubes and 20 mL of deionized water was added. The solution was made basic by adding 5 mL of 15 N ammonium hydroxide. Five mL of 1.5 N sodium carbonate was added to precipitate strontium carbonate. The strontium carbonate precipitate was collected by filtering with previously dried and weighed Gooch crucibles. The crucibles with precipitate were dried at 104 º C overnight, placed in a desiccator until they have reached room temperature, and then weighed on an analytical balance.

Independent measurements of strontium and yttrium carrier concentrations were made with a Themo Jarell-Ash Polyscan 61E inductively coupled plasma spectrometer. A wavelength calibration was performed prior to measurements to calibrate the sequential monochromator. The instrument emission intensity was calibrated from known concentrations of strontium and yttrium standards, prepared from commercial standards from High Purity and ERA. The commercial solutions contained 1000 $\pm$ 3 μg strontium and yttrium and were diluted volumetrically to obtain concentrations of 10, 20, 40, and 50 μg per mL Sources were made by pipetting the required volume of standard with Rainen Model EDP2 1000 pipette and diluted in Type A volumetric flasks with an acid solution of 0.024 N HCl and 0.024 N HNO_3 in deionized water. The calibration relationship was checked for linearity before measuring unknown concentrations. Analyzed samples were preceded and followed by measurement of spiked samples prepared from strontium and yttrium standards from different standard solutions. Blank solutions consisted of 0.024 N HCl-HNO_3 in deionized water. In the event the spiked sample recoveries exceeded ± 5% of the known value, the sample set was reanalyzed. Carrier concentrations were measured following volumetric dilution of the carrier solution to a concentration within the linear range of the calibration.

A sodium carbonate carrier (Na_2CO_3) was used for carbon-14 efficiency measurements. The sodium carbonate carrier was standardized by titrating with 0.1 F HCl with methyl-orange as an endpoint indicator (Standard Method 2310, APHA, 1992). The sodium carbonate carrier was also standardized gravimetrically following addition of excess strontium nitrate, filtration onto a fine-pore Gooch filter crucible, and drying and weighing the precipitate. Five mL of the 0.25 M sodium carbonate carrier were pipetted into four separate centrifuge tubes and 20 mL of deionized water was added to each centrifuge tube. Two mL of 1.5 M strontium nitrate was added to each centrifuge tube, precipitating strontium carbonate. The strontium carbonate precipitate was collected by filtering with previously dried and weighed Gooch crucibles. The crucibles with precipitate were dried at 104 º C overnight, placed in a desiccator until they reached room temperature, and then weighed on an analytical balance.

3.1.3 Source preparation

Strontium carbonate sources of various areal thickness containing strontium-89, or strontium-90 and yttrium-90, were prepared by varying the amount of strontium nitrate carrier. Radionuclide sources were prepared by transferring a volume measured with a Rainen Model EDP2 micro-liter pipette and weighing the amount placed in a tared 25 mL disposable plastic centrifuge tube with an analytical balance. Carrier amounts were also measured with a Rainen Model EDP2 pipette and a specific volume of carrier was transferred from a standardized solution. For strontium-90 plus yttrium-90, the radionuclides with carrier solution were diluted to 25 mL with deionized water. The solution was acidified with two to three drops 16 N nitric acid and 1 mL of 10 mg yttrium per mL carrier was added. Yttrium hydroxide was precipitated following the addition of 5

mL 15 N ammonium hydroxide and the precipitate separated by centrifugation for 10 minutes at 3,000 rpm with an IEC Model HN-SII centrifuge. The date and time of yttrium hydroxide precipitation is the beginning of yttrium-90 ingrowth from the decay of strontium-90. The supernatant containing strontium nitrate was transferred to another centrifuge tube and precipitated as strontium carbonate following the addition of 5 mL 1.5 N sodium carbonate.

The prepared $SrCO_3$ precipitates with the strontium-90 or strontium-89 were filtered on a tared Supor 0.45 micron membrane filter 25 millimeter in diameter with a Millipore glass frit vacuum filtering support. The precipitate was then washed with 10 mL each of water, ethanol, and ether. The filters were placed in aluminum weighing pans and dried at 104˚ C for at least 15 minutes, and then placed in a desiccator containing dry silica to cool to room temperature. The filter and filtrate were weighed and then mounted on nylon ring and disc mounts with a Mylar cover. These ring and disc mounted filters were typically counted for 60 minutes. Efficiencies were calculated for the mid-point of the counting period as described in sections 3.2.1 and 3.2.2 below. Strontium carbonate sources are identified by the date prepared and the number in the set, with a maximum of eight sources prepared on a given date.

Carbon-14 sources were made from a calibration solution that contains carbon-14 as sodium carbonate. The NaOH solution used to maintain an alkaline pH (greater than 10) was heated prior to preparation to drive off dissolved carbon dioxide. One mL 1 N sodium hydroxide was added to 20 mL of deionized water to raise the pH and prevent loss of carbon-14 from conversion of carbonate to carbon dioxide. Carbon-14 was added from the calibration solution and varying amounts of sodium carbonate carrier were pipetted with a Rainen pipette. One mL of 1.5 N strontium nitrate was added to

precipitate strontium carbonate and the solution was heated in a water bath for 10 minutes. Supor 0.45 micron membrane filters were dried at 104 º C for 15 minutes, cooled to room temperature in a desiccator, and weighed prior to use. The precipitated strontium carbonate was collected on a previously weighed membrane filter The precipitate was washed with deionized water, ethanol, and ethyl ether to remove moisture and then dried at 104 º C for 15 minutes. The filter with precipitate was weighed and mounted on nylon ring and disk mounts with a Mylar cover. The ring and disk mounted filters were counted for 60 minutes.

3.1.4 Yield

The chemical yield of sources was determined gravimetrically following drying to assure attaining constant weight. The effect of drying time and temperature were examined by repeated mass measurements of a set of three strontium carbonate carriers over time with increasing drying temperatures. In addition, the mass of precipitated strontium carbonate and possible co-precipitated yttrium was evaluated by measuring strontium and yttrium concentrations following dissolution of selected blank sources. The strontium carbonate precipitate for blank sources were dissolved in 3N nitric acid, transferred to a volumetric flask, and diluted to 100 mL for analysis by ICP as described in section 3.1.5 Mass balance, below.

3.1.5 Mass balance

Byproducts of the preparation process were collected for mass balance measurements to check the gravimetric yield of precipitates. Fractions collected include 1 mL of the

strontium nitrate supernatant collected after separating yttrium hydroxide; the supernatant poured off the precipitated strontium carbonate prior to filtering; and the filtrate collected during filtration of strontium carbonate. The filtrate was reduced in volume on a hotplate in a laboratory hood to evaporate ethyl ether and ethanol present from washing the precipitate. These organic solvents were removed because they interfere with subsequent measurements of strontium and yttrium concentrations by inductively coupled plasma emission. All glassware was rinsed with 0.1N nitric acid and the rinsate was collected to capture any residual strontium carbonate. The volume of each fraction was recorded along with the date and the source identification number.

The filtrate and yttrium hydroxide precipitate collected during source preparation were analyzed for strontium and yttrium following removal of ethanol and ether by heating and volume reduction. The samples were acidified to pH less than 2 with 1 mL 16 N nitric acid. The samples were analyzed by inductively coupled plasma spectrometry (ICP) calibrated with standard solutions. Each batch included an independent measurement of a calibration standard at 50 μg strontium and yttrium per mL, a blank solution, a sample of the strontium carrier, and a sample of the yttrium carrier. The blank and independent calibration standards were measured at the beginning and end of each batch.
The net strontium mass was estimated from the difference between the strontium added as carrier minus the mass of strontium measured in the filtrate and the mass of strontium measured in the hydroxide precipitate. This value was converted to mass of strontium carbonate and compared with the gravimetrically measured mass of strontium carbonate.

3.2 Efficiency calculations

Efficiency estimates were made for radionuclides undergoing a simple one step disintegration, carbon-14 and strontium-89, and for the pair of radionuclides decaying sequentially, strontium-90 and yttrium-90. The efficiencies for strontium-89 and carbon-14 were determined from a single count. The strontium-90 and yttrium-90 efficiencies were determined by a double count method (Bowman et al., 1976) with the strontium-90 efficiency determined by the first count, and the Y-90 efficiency determined following ingrowth from decay of strontium-90. The counting efficiencies for measured calibration sources were calculated by two different methods. Initially, all efficiency estimates were made in an Excel™ spreadsheet through calculations of the components of the efficiency equation. Efficiency estimates were also independently determined using the complete efficiency equation in the general uncertainty model with GumCalc (McCroan, 2005). The efficiency estimates from GumCalc were compared with the values in the spreadsheet estimates and any discrepancies resolved. The total uncertainties of the measured efficiencies were determined by GumCalc through propagation of error following the General Uncertainty Model (Ellison et al., 2000).

The data and results for each source are provided in Appendix A. The tables in Appendix A provide data for sample preparation and sample counting. The steps in the efficiency calculation found in Appendix A reference the equations below. The complete efficiency equation used in the GUM efficiency calculation is presented first, followed by the steps used to calculate efficiencies in the spreadsheet.

3.2.1 Strontium-89 and carbon-14 efficiency estimates

Counting efficiencies for strontium-89 and carbon-14 are calculated for a single count with the following equation:

$$\mathrm{E}_R(x\rho) = \frac{R_{net}}{\left(C_R \bullet V_R \bullet e^{-(\lambda_R \bullet T_{El})} \bullet \frac{\left(W_{f+p} - W_f\right) \bullet 1000}{\left(V_c \bullet C_c\right)} \right)} \qquad \text{Equation 3-1}$$

Where

$E_R(xp)$ = expected count rate per disintegration rate as a function of areal thickness for carbon-14 or strontium-89

R_{net} = net count rate for the source (min^{-1}) (see equation 3-2)

C_R = concentration of the source solution (min^{-1} mL^{-1}) at a specified date and time

V_R = volume of the source solution (mL)

λ_R = decay constant for strontium-89 or carbon-14 (s^{-1})

T_{El}= elapsed time (s) from the source date to the mid-point of the count time.

W_{f+p} = mass of filter plus precipitate (g)

W_f = mass of filter (g)

1000 = conversion factor, mg g^{-1}

V_c = Volume of carrier added (mL)

C_c = Concentration of carrier (mg mL^{-1})

In addition, the sample count time (T_g = 60 minutes) and background count time (T_b = 100 minutes) are required to estimate the uncertainty of the counting data.

This equation is the function modeled with GumCalc to estimate the total uncertainty of the efficiency estimate described in section 3.3.

The net count rate for the source was determined by subtracting the background count rate for a blank ring and disk. The blank ring and disk consists of a filter mounted on a nylon ring and disk under Mylar. The average background count rate for one year of measurements was used as the expected background count rate.

$$R_{Net} = R_g - R_b \qquad \text{Equation 3-2}$$

where

R_{Net} = net count rate (min^{-1})

R_g = gross count rate for the source (min^{-1})

R_b = background count rate for a blank filter on a ring and disk mount (min^{-1})

The following intermediate results are components of Equation 3-1 and included in tables found in Appendix A. The estimated counting efficiency given by equations 3-1 and 3-7 are equivalent.

The net mass of the precipitate is given by

$$W_{net} = \left(W_{f+p} - W_f\right) \bullet 1000 \qquad \text{Equation 3-3}$$

where

W_{Net} = Net mass of precipitate (mg)

W_{f+p} = mass of filter plus precipitate (g)

W_f = mass of filter (g)

1000 = conversion factor from gram to milligram

The thickness of the standard in mass per unit area is given by

$$x_s \rho = W_{net} / 2.138 \qquad \text{Equation 3-4}$$

where

$x_s\rho$ = areal thickness of precipitate (mg cm^{-2})

W_{Net} = Net mass of precipitate (milligram) from Equation 3-3

2.138 = area of the precipitate (cm^2)

The yield is given by

$$Y = W_{Net} / (V_C * C_C) \qquad \text{Equation 3-5}$$

Where

Y = Yield

W_{Net} = Net mass of precipitate (mg)

V_C = Volume of carrier (mL)

C_C = Concentration of carrier in mg $SrCO_3$ mL^{-1}

The activity at the date and time of counting is given by

$$A_{R,T} = C_R \bullet V_R \bullet Y \bullet \mathrm{e}^{\left(\frac{-0.693*(\mathrm{Date}_{\mathrm{Count}} - \mathrm{Date}_{\mathrm{Activity}})}{HalfLife}\right)} \qquad \text{Equation 3-6}$$

where

$A_{R,T}$ = Activity for radionuclide R at time T, (min^{-1})

V_R = volume of radionuclide solution added (mL)

C_R = Concentration of radionuclide solution (min^{-1} mL^{-1})

Y = fractional yield from Equation 3-5

$Date_{Count}$ = Date and Time of first count as mid-point of the counting period (year)

$Date_{Activity}$ = Date and Time for activity (year)

HalfLife = half life of radionuclide (years)

The counting efficiency is given by

$$\mathrm{E}_R(x\rho) = \frac{R_{net}}{A_{R,T}} \qquad \text{Equation 3-7}$$

where

$E_R(xp)$ = measured counting efficiency for carbon-14 or strontium-89,

R_{net} = net count rate (min^{-1}), and

$A_{R,T}$ = activity at the time of counting, corrected for yield (min^{-1})

3.2.2 Strontium-90 and yttrium-90 efficiency estimates

The strontium-90 and yttrium-90 efficiencies were determined by a double count method (Bowman et al., 1976). The first count following precipitation of yttrium hydroxide is dominated by beta-particle radiation from strontium-90 with a small contribution from yttrium-90. The source standard is counted a second time following ingrowth of yttrium-90 from the decay of strontium-90. The increase in count rate resulting from ingrowth following decay of strontium-90 provides an estimate of the yttrium counting efficiency. The yttrium-90 counting efficiency is estimated from the change in net count rate and fraction of yttrium-90 present as

$$E_{Y-90}(x\rho) = \frac{(R_{net2}) - (R_{net1})}{C_R \bullet V_R \bullet e^{-(\lambda_R \bullet T_{EI})} \bullet \frac{(W_{f+p} - W_f) \bullet 1000}{V_C \bullet C_C} \bullet (I_{Y-90,second} - I_{Y-90,first})} \qquad \text{Equation 3-8}$$

where

$E_{Y\text{-}90}(x\rho)$ = yttrium-90 counting efficiency

R_{net1} = net count rate of the first count (see Equation 3-2)

R_{net2} = net count rate of the second count (see Equation 3-2)

C_R = activity of the source standard (min^{-1} mL^{-1})

V_R = volume of the source standard used (mL)

λ_R = decay constant for strontium-90 (days)

T_{El} = time elapsed from the standardization of the source standard to the mid-point of the count date and time (days)

W_{f+p} = mass of the filter and precipitate (g)

W_f = mass of the filter (g)

1000 = conversion factor from gram to milligram (mg g^{-1})

V_c = volume of carrier added (mL)

C_c = carrier concentration as mg $SrCO_3$ mL^{-1}

$I_{Y\text{-}90,\ second}$ = fraction of yttrium-90 ingrowth occurring between the time of yttrium hydroxide precipitation and the midpoint of the second count, $I_{Y\text{-}90,T}$

$I_{Y\text{-}90,first}$ = fraction of yttrium-90 ingrowth occurring between the time of yttrium hydroxide precipitation and the midpoint of the first count, $I_{Y\text{-}90,T}$

The ingrowth fraction $I_{Y\text{-}90,T}$ is given by

$$I_{Y-90,T} = (1 - e^{-\lambda_{Y-90}(Date_{CountDate} - Date_{Yppt})}) \qquad \text{Equation 3-9}$$

where

$\lambda_{Y\text{-}90}$ = decay constant for yttrium-90 (hr^{-1})

$Date_{CountDate}$ = date and time the standard is counted

$Date_{Yppt}$ = date and time yttrium hydroxide is precipitated and ingrowth begins and the difference (T) is in hours.

The strontium-90 counting efficiency is estimated by correcting the first net count rate for the contribution to the count rate from yttrium-90 as

$$E_{Sr-90}(x\rho) = \frac{(R_{net1}) - (E_{Y-90} * A_{Sr-90,first} * I_{Yttrium-90,first})}{C_R \bullet V_R \bullet e^{-(\lambda_R \cdot T_{E1})} \bullet \frac{(W_{f+p} - W_f) \bullet 1000}{V_C \bullet C_C}} \qquad \text{Equation 3-10}$$

Where the parameters are defined for Equation 3-8 above and

$E_{Sr-90}(x\rho)$ = strontium-90 counting efficiency as a function of areal thickness

$E_{Y-90}(x\rho)$ = counting efficiency for yttrium-90 as a function of areal thickness

$A_{Sr-90,\ First}$ = strontium-90 activity at first count (min^{-1})

$I_{Yttrium-90,first}$ = Ingrowth of yttrium-90 by mid-point of first count (Equation 3-9)

Note that the product of $E_{Y-90} \cdot A_{Sr-90,First} \cdot I_{Yttrium-90,first}$ is the estimated count rate from yttrium-90.

The parameters measured for the efficiency determination and components of the efficiency equations are provided in Appendix A for strontium-90 and yttrium-90. The components are described by sections of each table as follows, with the section headings corresponding to the sections in Tables A-15 through A-24.

3.2.2.1 Preparation

The net mass of the precipitate is given by equation 3-3 above. The yield for the stable carrier is given by equation 3-5 above.

3.2.2.2 First count

The strontium-90 activity at the mid-point of the first counting period is determined from

$$A_{Sr-90,first} = V_R \bullet C_R \bullet \mathrm{Y} \bullet \mathrm{e}^{\left(\frac{-0.693*(\mathrm{Date}_{\mathrm{First\ Count}} - \mathrm{Date}_{\mathrm{Activity}})}{365.25 \bullet 28.79}\right)} \qquad \text{Equation 3-11}$$

$A_{Sr\text{-}90,first}$ = Activity of Sr-90 at first count (min^{-1})

V_R = volume of radionuclide solution added (mL)

C_R = Concentration of radionuclide solution (min^{-1} mL^{-1})

Y = fractional yield from Equation 3-5

$Date_{First\ Count}$ = Date and Time of first count as mid-point of the counting period (day)

$Date_{Activity}$ = Date and Time for activity (day)

365.25 = days per year

28.79 = half life of Sr-90 (years)

and the elapsed time is in days.

The fraction of the activity resulting from the ingrowth of yttrium-90 by decay of strontium-90 is given by Equation 3-9.

The count rate in the first count is primarily from the decay of strontium-90 plus a small contribution from the yttrium-90 that is present from ingrowth following decay of strontium-90. This count rate is given by

$$R_{Yttrium-90,T} = E_{Y-90} \bullet A_{Sr-90,first} \bullet I_{Yttrium-90,first} \qquad \text{Equation 3-12}$$

where

$R_{Yttirum\text{-}90,T}$ = count rate attributed to ingrowth of yttrium-90 at time "T"

$E_{Y\text{-}90}(x\rho)$ = counting efficiency for Yttrium-90

$A_{Sr\text{-}90,\ first}$ = strontium-90 activity at first count (min^{-1})

$I_{Yttrium\text{-}90,first}$ = Ingrowth of yttrium-90 by mid-point of first count (Equation 3-9)

3.2.2.3 Second count

The strontium-90 efficiency is determined once the efficiency of yttrium-90 is known following the second count. The strontium-90 activity at the mid-point of the second count is estimated from

$$A_{Sr-90,Second} = Y \bullet V_R \bullet C_R \bullet e^{\left(\frac{-0.693 * Date_{Second\ Count} - Date_{Precipitation}}{365.25 \bullet 28.79} \right)} \quad \text{Equation 3-13}$$

Y = fractional yield from Equation 3-5

V_R = volume of radionuclide added (mL)

C_R = Concentration of strontium-90 (min^{-1} mL^{-1})

$Date_{Second\ Count}$ = Date and Time of count as mid-point of the counting period (day)

$Date_{Precipitation}$ = Date and Time for yttrium precipitation (day)

$A_{Sr\text{-}90,Second\ Count}$ = strontium-90 activity at the mid point of the second count

28.79 = half life of strontium-90 (years)

365.25 = days per year

and the elapsed time is in days.

The ingrowth of yttrium-90 by the midpoint of the second count is estimated by Equation 3-9.

3.2.2.4 Efficiency

The yttrium-90 efficiency was determined from the change in the count rate between the first count and the second count that results from the ingrowth of yttrium-90 activity due to the decay of strontium-90.

$$E_{Y-90}(x\rho) = \left(\frac{R_{\text{net2}} - R_{\text{net1}}}{A_{Sr-90,1} \bullet (I_{\text{Y90,2}} - I_{Y90,1})} \right) \qquad \text{Equation 3-14}$$

where

R_{net2} = net count rate from the second time the source was counted from equation 3-2

R_{net1} = net count rate from the first time the source was counted

$A_{Sr\text{-}90,1}$ = strontium-90 activity determined for the first count from Equation 3-10

$I_{Y\text{-}90,\,2}$ = fraction of yttrium-90 activity from ingrowth of yttrium-90 by the second count following precipitation of yttrium hydroxide and ingrowth due to decay of strontium-90 from Equation 3-9.

$I_{Y\text{-}90,1}$ = fraction of yttrium-90 activity from ingrowth of yttrium-90 by the first count following precipitation of yttrium hydroxide and ingrowth due to decay of strontium-90 from Equation 3-9.

The strontium-90 efficiency is determined from the first count by correcting the net count rate for the small contribution from yttrium-90 (Equation 3-12) as

$$E_{Sr-90}(x\rho) = \left(\frac{R_{first} - R_{Y-90,T}}{A_{Sr-90,first}} \right)$$ Equation 3-15

where

R_{first} = net count rate for first count (min^{-1})

$R_{Y-90,T}$ = count rate due to ingrowth of yttrium=90 (min^{-1}) from Equation 3-12

$A_{Sr-90,first}$ = strontium-90 activity at first count (min^{-1}) from Equation 3-11

3.2.3 Other radionuclide sources

Additional radionuclide sources were used as controls and to provide specific measurements. These include check sources in one-inch diameter plastic mounts, sources prepared by evaporation on stainless steel planchets, and carrier-free sources prepared using sealed filters. Radionuclides of interest include strontium-89, strontium-90/yttrium-90 in equilibrium, cadmium-109, and iron-55.

Manufactured check sources in the form of a one inch diameter plastic disk with activity deposited in the center and sealed with plastic were used for an instrument control source and to provide x-ray photons. A 0.037 MBq (1 microCurie) strontium-90/yttrium-90 check source is used for daily instrument control measurements and determining the beta counting plateau. A cadmium-109 check source provided x-ray photons for estimating the energy calibration for the Nuclear Data MCA.

An iron-55 source provided x-ray photons for estimating the energy calibration for the Nuclear Data MCA as well as the energy cutoff of the amplifier discriminator. An iron-55 source was prepared by depositing 1 mL of a standard iron-55 calibration solution on a stainless steel planchet. The planchet was heated under an infra-red lamp until the solution evaporated.

Strontium-90/yttrium-90 and strontium-89 sources were prepared without carrier to provide estimates of counting efficiencies for carrier free sources. These sources were prepared by randomly distributing the calibration standard drop wise within a 0.825 cm radius from the center of sealed membrane filters. The membrane filters were sealed by

spraying the filters with a thin coat of acrylic. The liquid was allowed to evaporate and the filters further dried at 104˚ C in a drying oven. Carbon-14 sources were prepared in a similar manner, but the carbon-14 as carbonate did not appear to be stable.

3.3 Estimating components of measurement uncertainty

Measurement uncertainties are estimated as the combined standard uncertainty following propagation of error rules. The following section presents the methods used to derive the uncertainties of individual components for the efficiency measurement, and the results are provided in section 4.1, Measurement uncertainty estimates. The uncertainties of the individual components, or standard uncertainties, are provided as one standard deviation (1S) to simplify incorporating these values in the uncertainty model. The total measurement uncertainties are provided as 95% confidence limits (CL), equivalent to two standard deviations, from combined standard uncertainties. These estimates follow the nomenclature found in NIST Technical Note 1297 (Taylor and Kuyatt, 1994) and MARLAP (2004) and are calculated with GUMCalc (McCroan, 2005). The uncertainty models were based on the calculations provided in section 3.2.

The standard uncertainties are estimated by statistical, or type A evaluation of standard uncertainty expressed as one sigma values, and non-statistical or type B evaluation of standard uncertainty. Statistical estimates are based on the mean and variance of repeated independent measurements, and least square fit to measurement data. Non-statistical estimates include manufacturer's specifications for volumetric glassware and pipettes, uncertainties provided with calibration radionuclide certificates and Poisson

estimates for the uncertainty of counting data (see Taylor and Kuyatt, 1994). Uncertainty budgets for measurement efficiencies were constructed for representative sources covering the range of areal thicknesses.

3.3.1 Balance measurements

The uncertainty of mass measurements was assessed from the manufacturer's specification for linearity of the balance, the uncertainties in the mass of a set of class 1 calibration weights, the precision of replicate measurements of a check weight measured each day the balance was in use, and the variability in the balance measurements assessed from a series of linearity measurements collected every four months.

The uncertainty of balance measurements due to variations in environmental factors was estimated from regression results from "as found" and "as left" responses to Class 1 weights evaluated with the model $M_I = B_1 \bullet M_{cal} + B_0$, where M_I is the balance indication for calibration mass $M_{cal,}$ and B_1 and B_0 are the slope and intercept of a linear regression, respectively.

The regression analysis is reported in a standard Analysis of Variance (ANOVA) Table specifying the sources of variation, the degrees of freedom for each source of variation (df), the Sums of Squared deviations for each source of variation (SS), Mean Square for the Regression (MSR), the Mean Square Error (MSE), and results for the Fisher F test. The Mean Square Error (MSE) is an estimate of the variance of the measurements about the fitted regression coefficients necessary to estimate the uncertainty of future measurements (Neter et al. 1990).

The uncertainty for future measurements is estimated by

$$S_m = \sqrt{\hat{\sigma}^2 \bullet \left(1 + \frac{1}{\mathrm{n}} + \frac{\left(M_I - \overline{M_{cal}}\right)^2}{\sum_{i=1}^{n} (M_i - \overline{M_{cal}})^2}\right)} \qquad \text{Equation 3-16}$$

where:

S_m = standard deviation of a new measurement of mass *m*;

$\hat{\sigma}$ = estimated by the Mean Square Error (MSE) for the regression;

n = number of observations;

M_I = indicated mass by the balance;

$\overline{M_{cal}}$ = average value of the calibration masses;

M_i = indicated mass for calibration mass "i"; and

$\sum_{i=1}^{n} (M_i - \overline{M_{cal}})^2 = \sum_{i=1}^{n} (X_i - \bar{X})^2$ = variance of the known masses, also denoted as S_{xx}

The uncertainty of balance measurements are estimated as described in MARLAP (2004) Attachment 19E with

$$u(m) = \sqrt{\left(s_r^2 + s_{a_L}^2 + M_I^2 \cdot \phi_{env}^2\right)} \qquad \text{Equation 3-17}$$

where:

S_r = standard uncertainty due to repeatability;

S_{a_L} = standard uncertainty due to balance linearity;

M_I^2 = balance indication (variable); and

φ_{env} = relative standard uncertainty due to environmental factors, estimated from S_m/I_m from Equation 3-16.

The standard uncertainty due to repeatability is evaluated from replicate measurements of a calibrated mass over an extended period of time. The standard uncertainty due to balance linearity is based upon the linearity tolerance limit for the balance specified by the manufacturer. The relative standard uncertainty due to environmental factors is evaluated from routine linearity measurements providing multiple measurements over time of the balance reading versus the known calibration masses.

3.3.2 Variable volume pipettes

An initial estimate of the standard uncertainty for variable volume pipets was made following MARLAP (2004, equation 19.31). This uncertainty based on the manufacturer's specification and estimated as

$$u(V) = \sqrt{S_P{}^2 + \frac{\delta_{cap}^2}{6}} \qquad \text{Equation 3-18}$$

where:

δ_{cap} = manufacturer's specification for accuracy; and

S_P = manufacturer's specification for precision.

The variability of future volume measurements was estimated following MARLAP equation 19.75

Based on experience, the estimates from equation 3-18 were believed to underestimate the uncertainty of volume measurements by variable volume pipettes.

A more realistic estimate of the uncertainty of variable volume pipette measurements could be made from ongoing control data.

$$u(V) = Z \bullet S(i) \bullet \sqrt{1 + \frac{1}{n}}$$ Equation 3-19

where

Z = volume indication;

n = number of observations; and

S(i) = standard deviation of the volume indication estimated from replicate weighing estimated by equation 3-16, with volume replace mass.

.

3.3.3 Counting statistics

The uncertainties in counting statistics were estimated by the Poisson approximation of a normal distribution. Most sources were counted for sixty minutes and have sufficient activity to result in at least 10,000 accumulated counts, for a relative standard uncertainty of less than 1%. Results where fewer counts were collected are noted in the Appendix A for specific measurements.

3.4 Counting system

The counting system is a Tennelec LB 5100 Series 3 gas flow proportional counter. The system includes detectors, shielding, and electronics. The relationship of the source to the detector is presented in Figure 3-1. The configuration of the detectors and electronics are summarized in Figure 3-2. The sample and guard detectors are located within a 4 inch thick lead shield. The detectors are operated with a mixture of 90%

argon and 10% methane (ultra P-10) at a flow rate of 4.25 liter per hour. The detectors are operated anticoincident to a guard detector to reduce the count rate from cosmic background radiation.

Physical dimensions of the source mount, source holder, and detector are necessary for specifying the dimensions of the Monte Carlo model. Larger dimensions were determined with a Mitutoyo dial caliper, Model 505-636, with a range to 10 cm and precision of ± 0.05 millimeter. If dimensions exceeded the range of the dial caliper, measurements were made by ruler. Smaller dimensions, including the thickness of sources, were measured with a Mitutoyo micrometer (range from 0.1 to 25 mm, with precision of ± 0.01 mm).

The sample detector entrance window is 57 mm in diameter and consists of a proprietary hydrocarbon film on which a gold conducting layer is deposited[1]. The total areal thickness of the detector window is 80 μg cm^{-2}.

[1] William Cross, Canberra 2005. Email describing thickness of detector window and method of production.

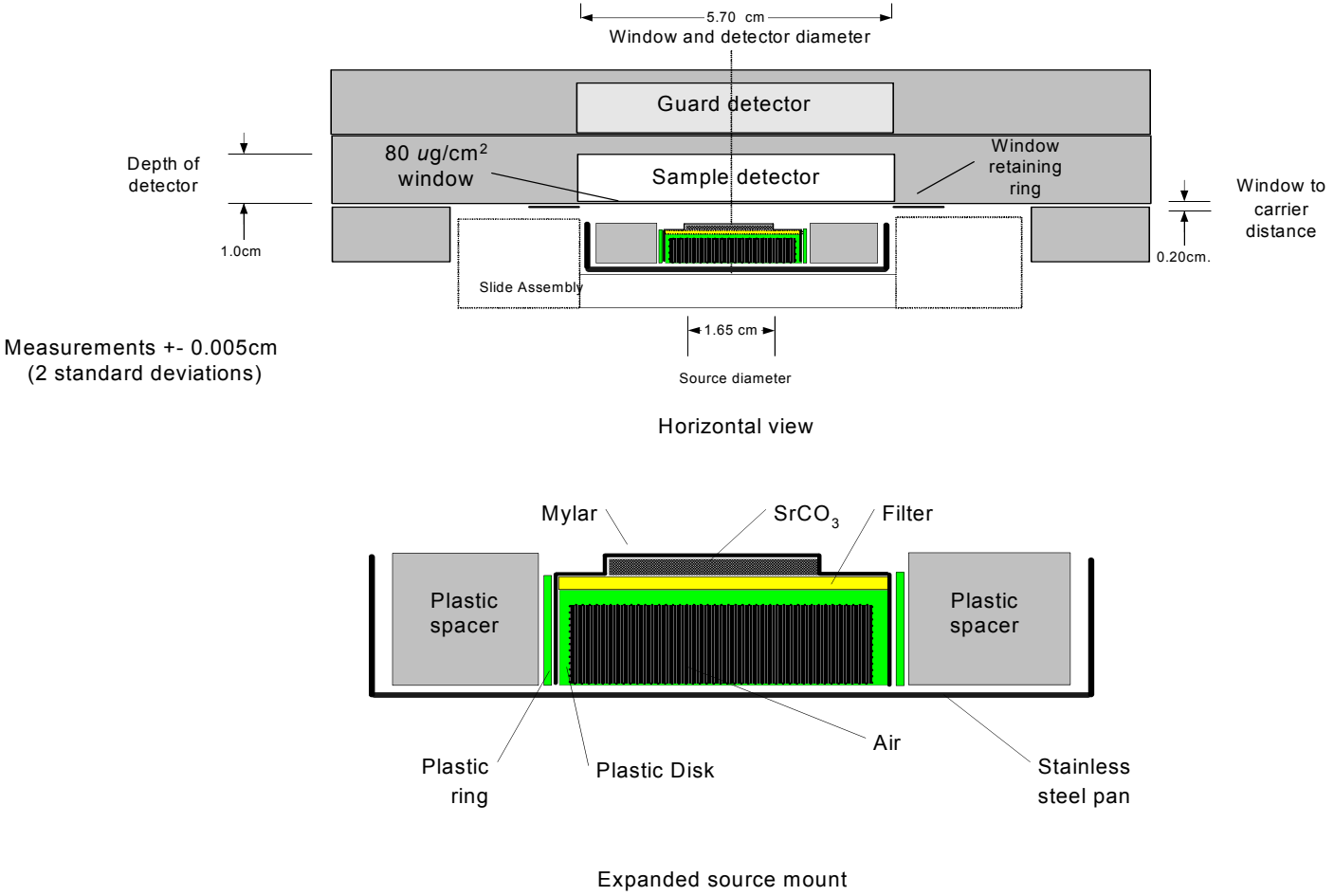

Figure 3-1. Detector block and ring and source mount cross section

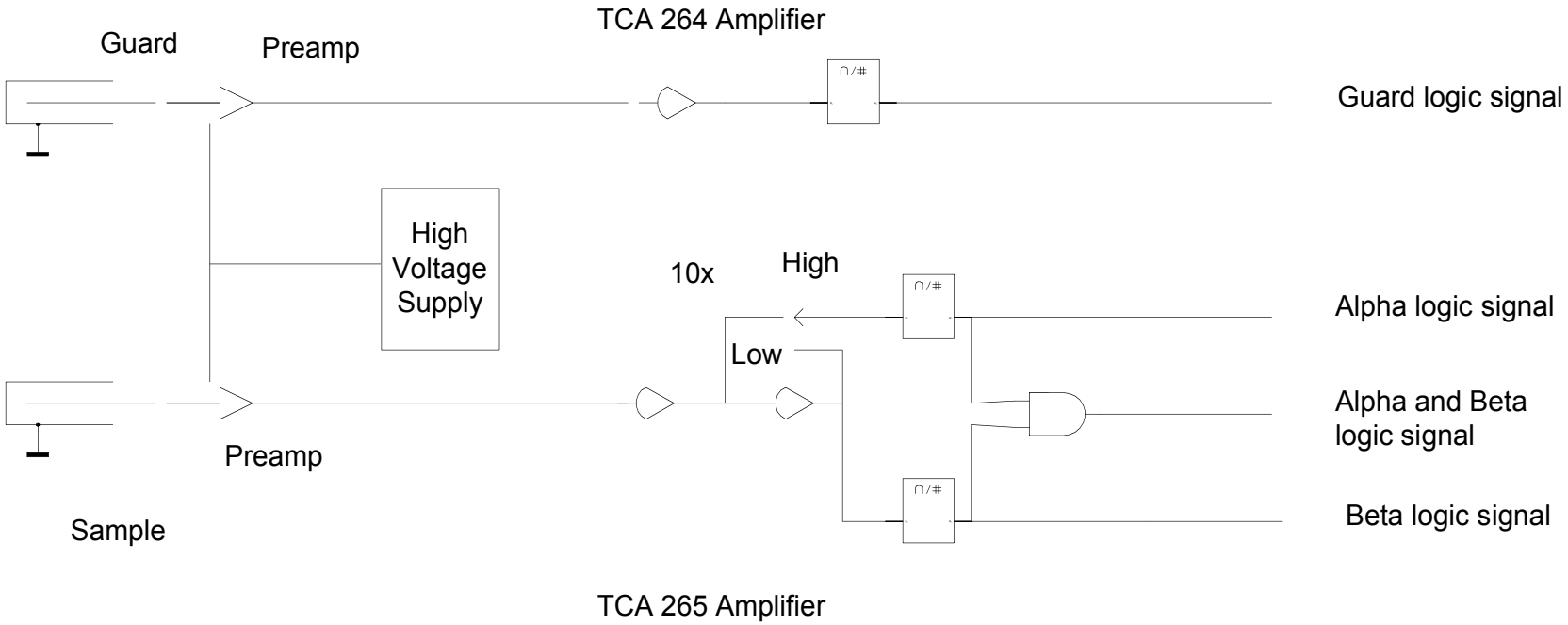

Figure 3-2. Electronic components for Tennelec LB5100 gas flow proportional counter.

Signals from ionizing the gas in the sample detector are fed through a Tennelec TC 175 preamplifier to a Tennelec Model TC 265 amplifier and single channel analyzer. The TC 265 amplifier/single channel analyzer uses discriminators to separate electronic noise from pulses with peak heights below a "beta" particle threshold and pulses above an "alpha" particle threshold. Logic signals generated when these thresholds are exceeded are delayed approximately 10 microseconds and are counted when no signal is coincident from the guard detector (Figure 3-2).

3.4.1 Source

Gas flow proportional counters used for measurement of beta-particle emitters require calibration sources in specified geometries. Calibration sources for this application were 1.65 cm diameter strontium carbonate precipitates ranging in areal thickness from 3 to 33 mg cm^{-2} containing strontium-89, strontium-90. Yttrium-90 is produced from the decay of strontium-90 and reaches equilibrium after approximately 18 days. Strontium carbonate precipitates containing carbon-14 were prepared with areal thickness ranging from 3.5 to 29 mg cm^{-2}. The precipitates were deposited on 25 millimeter diameter membrane filters, which were mounted on nylon disks and held in place under Mylar film, 1.67 mg cm^{-2} thick, by an outer nylon ring. Beta-particle sources included carbon-14, Emax 0.156 MeV; strontium-90, Emax 0.546 MeV; strontium-89, Emax 1.492 MeV; and yttrium-90, Emax 2.28 MeV.

3.4.2 Source holder

The ring and disk assembly is centered under the detector window with a plastic spacer on a stainless steel support. The stainless steel support sits within a numerically coded sample holder read by the counting system. The sample holder is mechanically moved into position by sliding horizontally within an opening 1.5 cm in height and 10.4 cm in width. The sides of the opening consist of copper plate 7 millimeter in thickness. The manufacturer's specification for the clearance between the window retaining ring and the slide assembly is 0.2 cm (see Figure 3-1).

3.4.3 Geometrical efficiency

The geometrical efficiency was estimated for a point located on the plane of the supporting filter and as a circular source with the average diameter measured for strontium carbonate source located on the plane of the supporting filter and centered on the axis of the detector. The geometrical efficiency for a circular source on the plane of the source filter was estimated to be 0.425 based on Table 2 from Bland (1984). The geometrical efficiency for a point source calculated by equation 2-2 was found to be 0.427.

3.4.4 Self-absorption curves

The self-absorption equation provided in Equation 2-7 is typically used to estimate counting efficiencies for sources where efficiency varies with areal thickness from E_0, the efficiency with no self-absorption. Note E_0 differs from the geometrical counting efficiency G because of scattering into the detector.

Self-absorption coefficients were fit to the measured efficiency data by iteratively selection of E_0 and μ/ρ to minimize the bias and variance from the empirical measurements.

The bias is estimated from

$$Bias = \frac{\sum_i \left(\left| E_R(x\rho) - E_0 \bullet f_s \right| \right)}{n} \qquad \text{Equation 3-20}$$

where:

$E_R(x\rho)$ = measured efficiency for areal thickness $x\rho$ for measurements i to n;

$E_0 \cdot f_s$ = predicted efficiency for the coefficients E_0 and μ with equation 2-7; and

n = total number of measurements.

The variance is estimated from

$$Var = \frac{\sum_i \left(E_R(x\rho) - E_0 \bullet f_i \right)^2}{(n-2)} \qquad \text{Equation 3-21}$$

for 2 degrees of freedom, given the two parameters E_0 and μ.

The fitted self-absorption coefficients μ' were compared to values provided in the literature by Baltakmens (1970) in Table 1, "Absorption coefficients in cm^2g^{-1} for beta particles", determined for a Beckman Widebeta gas flow proportional counter with a 0.5 mg cm^{-2} end window, and source to window distances of 1 mm and 5 mm (see Table 2-1).

3.4.5 Detector window density

The detector window is composed of a proprietary hydrocarbon film which is anodized with a thin gold layer to provide a conducting surface[2]. The total areal thickness is specified as 80 μg cm^{-2} by the manufacturer. The actual deposited gold layer was measured on a single detector window with a Rigaku CSX 101E X-ray fluorescence spectroscopy system. The x-ray fluorescence system is designed to measure bulk elemental concentrations and is calibrated at eight points over a range of elements from fluorine to uranium. The accuracy specification, based on the manufacturer's specification for bulk concentration measurements by the x-ray fluorescence system, is 10% (one standard deviation). The detector window was mounted on a nylon ring and disk with a Mylar backing and measured for the gold thickness by the Au – L_α X-ray fluorescence line. Repeated measurements resulted in an estimated gold areal

[2] William Cross, Canberra 2005. Email describing the thickness of detector window, the approximate window composition, and the specification for the sample holder to window clearance.

thickness of 22 μg cm^{-2}. An adjacent peak was identified as a Zn $K_{\beta}1$ X-ray fluorescence line and found to be present in the Mylar backing of a blank mount.

The window composition was estimated from the measured areal thickness for gold and the specified areal thickness for the window. The difference between the total areal thickness and the gold areal thickness was assigned to a hydrocarbon base. The composition of Mylar was used to approximate the unknown base material with mass fractions for carbon (45.3%), hydrogen (3.0%), and oxygen (24.1%) from ICRU 56 Appendix A Table 1 (ICRU, 1997). The composite density of the detector window is estimated to be 6.3 g cm^{-3}.

3.4.6 Electronic measurements

The response of the detector system to known inputs was measured to establish the relationship between energy deposited, the corresponding peak voltages produced, and the spectral distribution of recorded events. Peak height and voltage measurements of the signal were made with a Techtronix model 2246 oscilloscope. This instrument is calibrated annually by a vendor to provide traceability to the National Institute of Science and Technology. Reference pulses were supplied by a model 1407 Canberra Reference pulse generator set to produce pulses corresponding to detector pulses. The pulse output at the preamplifier test output was measured with the oscilloscope when counting a strontium-90/yttrium-90 check source. The pulse generator was set to produce a similar pulse shape when input to the test input of the preamplifier, with rise time set to 250 microseconds and fall time to 200 microseconds. Negative pulses were provided by

the pulse generator at the preamplifier test input. The pulse generator provides 3600 pulses per minute; this frequency was verified by oscilloscope measurement. Pulse-height spectra were collected with a Nuclear Data multichannel analyzer. The energy distributions of the spectra were scaled to volts by the relationship between the measured voltage at the amplifier output and the channel the pulse is counted. Alternatively, the energy distributions were scaled to energy of photoelectric interactions from cadmium-109 and iron-55 within the detector by relating the peak centroid channel to photoelectron energy. Cadmium-109 emits the following major radiations: 88 keV gamma rays (3.6%); 63 keV conversion electrons (41.8%); 85 keV conversion electrons (total 41%); and 22 keV x-rays (total 83.7%). Iron-55 emits in 5.9 keV x-rays (total of 25%), 6.5 keV x-rays (total of 3.4%), and electrons at 5.1 keV (49.5%) and 5.8 keV (11.2%). The conversion electrons and Auger electrons are attenuated and do not penetrate the detector window, with the predominant interactions in the detector fill gas resulting from photoelectric interactions by the gamma rays and x-rays.

3.4.7 Minimum energy cutoff

The energy excluded by the LB5100 lower level discriminator was estimated from count data from the 5.9-keV X-ray of Fe-55. At low detector voltages, the detector does not provide sufficient multiplication for photoelectron events in the detector volume to produce a signal that exceeds the level of the amplifier discriminator. As the detector voltage is increased, the gain resulting from multiplication within the detector increase, and a point is reached were photoelectric interactions are recorded. The detector voltage where the multiplication is sufficient for some of the interactions to exceed the threshold

is marked by an increase in count rate with increasing voltage. Further increases in detector gain produce the characteristic counting plateau for proportional counters, where increases in high voltage no longer produce significant changes in count rate until the voltage is great enough to produce non-proportional electron cascades. The difference between the voltage where multiplication within the detector is just sufficient for the 5.9-keV photoelectron interactions to be counted above the amplifier discriminator, and the plateau voltage where the further increases in count rate are limited, is proportional to the increase in multiplication occurring from the change in detector voltage (Zumwalt, 1950).

The energy that must be deposited to just exceed the discriminator was estimated from the ratio of the total energy deposited (5.9 keV) to the change in multiplication occurring as a result of the change in the detector voltage. The multiplication that occurs with increasing detector bias was estimated from plateau counting data at amplifier gains of 2, 4, 8, 16, 32, and 64 to estimate the change in voltage required to reach a constant count rate for each doubling of amplification.

The level of the amplifier voltage discriminator was also measured with a known test signal provided by a Canberra Model 1407 reference pulse generator configured to approximate the pulse shape when counting strontium-90 and yttrium-90, with rise time of 250 usec, fall time of 200 usec, and negative pulse amplitude. The attenuated output of the pulse generator was connected to the test input of the Tennelec model 145 preamplifier. The count rate was recorded for 10 minutes for each pulse height with a count rate of 3600 counts per minute. As the test signal pulse height is decreased, a point is reached where further reductions result in a decrease in count rate from 3600

counts per minute to the counter background count rate. The voltage level of the amplifier discriminator is determined from the pulse height setting that result in a reduction in recorded count rate to 1800 counts per minute. A separate output from the preamplifier was routed to a separate Tennelec 247 amplifier with gain of 50 and pulse height was recorded on a Canberra Genie 2000 multi-channel analyzer. The MCA was calibrated against the voltage signal measured with an oscilloscope. In addition, the energy deposited in the detector was estimated form the spectra recorded for photoelectric interactions from a Fe-59 5.9keV x-ray and Cd-109 22 keV and 84 keV x-rays counted under the same conditions.

3.4.8 Intrinsic efficiency

The intrinsic efficiency was estimated as a range, first based on approximation of the average primary ionization in air, and then based on the stopping power for P-10 gas. The average primary ionization in air passes through a minimmum of 21 ion pairs percentimeter at approximately 1 MeV, with a corresponding total ionization rate of 42 ion pairs percentimeter (Price, 1964). The average primary ionization in P-10 is directly proportional to the atomic number of the gas, adjusting for the fact that air is diatomic and argon monatomic, resulting in an estimated primary ionization rate of 21.2 ion pairs percentimeter at 1 MeV.

The total ionization in P-10 for beta particles of a specific energy can be estimated from corresponding total stopping power (MeV g^{-1} cm^2) by multiplying by the P-10 density,

assumed to be 1.68E-03 g cm^{-3}, and dividing by the energy dissipation per ion pair, 26.4 eV per ip for argon.

The intrinsic efficiency is estimated with equation 2-10, assuming beta particles cross the 1 cm depth of the detector for both the approximation based on the primary ionization rate and the total ionization rate from stopping power cross sections.

3.5 Monte Carlo model

The Monte Carlo model was developed and run with MCNP4C. The Monte Carlo software was installed on a Shuttle PC with a 2.4 MHertz Pentium IV processor running the Redhat Linux 7 operating system. The model also was run with the subsequent release of MCNP5 version 1.4. Geometry plots were obtained from Vised, a visual editor included in the release of MCNP5 (LANL, 2006). The following description includes information on the definition of the cells, the surfaces defining the cells, and the probability distribution for the source spectra.

Components of the MCNP model results provide information regarding the contribution of geometry, scattering, attenuation, and backscattering to the fraction of interactions within the detector. The geometrical efficiency of the model was evaluated by setting all cell importances to zero, eliminating scattering and absorption, and noting the fraction of particles entering the detector cell. Attenuation and scattering interactions in specific cells were evaluated by setting the cell importances to zero and examining the resulting

change in pulse height tallies. Specific cells of interest include the window, air space between the window and the Mylar surface, and the Mylar cover.

In addition to models emitting electrons 4 π from the source (designated as total), each beta-particle distribution was also biased to initiate electrons into a 2 π geometry initially directed away from the plane of the detector window (designated as indirect) or toward the detector plane (designated as direct) in order to estimate the contribution from backscatter and scatter.

3.5.1 Orientation of the model

The model is specified in a rectangular coordinate system with the z-axes oriented vertically through the center of the circular source and detector.

3.5.2 Assumptions

The following assumptions were made in constructing the model and are discussed further in the description of the model. The actual measured material densities were used when available; otherwise the physical density found in CRC Handbook of Chemistry and Physics (CRC, 1984) or ICRU 56 (ICRU, 1997) was used in material specifications. The measured densities apply to the Mylar covering, strontium carbonate, and detector window. The beta-particle spectra are from ICRU Report 56 Appendix D (ICRU, 1997). The input probabilities for the first energy interval were adjusted to eliminate a bias introduced when MCNP normalizes the probabilities for the beta-particle spectra. The energy binning follows the Integrated Tiger Series (ITS) model of using the

nearest group boundary of the energy bin instead of the MCNP default bin-centered treatment (Schaart, 2002; see also LANL, 2006, page 2-74).

3.5.3 Materials

Materials are specified for all cells described in the model. These specifications, found in Table 3-1, consist of a material name, material designation used to reference the material for each cell, and the mass fraction of elements forming the compound. Mass fractions are indicated as negative fractions. The mass fractions include the element specified by atomic number, followed by the fractional mass of each component. The composition and mass fractions are required for MCNP to establish the electron stopping powers for materials using data in the EL03 electron stopping power library. Calculations by default assume the materials are in the condensed (solid) phase. A density-effect correction to the electron stopping power is indicated for P-10 gas and air by setting the keyword GAS=1. Materials where the conduction state is evaluated in determining the electron stopping power include iron and copper, where the keyword is COND=1.

Where thin materials are modeled, the number of steps is increased above the default that MCNP determines from the average atomic number (see Table 3-2). The number of energy sub-steps was evaluated as described in the MCNP documentation (LANL 2005, page 2-69). Sub-steps were increased from the MCNP default value to values in Table 3-2 to ensure that at least 10 sub-steps were sampled in crossing each cell. Materials where the number of sub-steps was increased include the P-10 in the detector volume, air between the Mylar surface and the detector window, the Mylar cover, and the

detector window. The number of sub-steps for strontium carbonate varies with the areal thickness of the source as well as the maximum energy of the beta particle. In the case of strontium carbonate, the step values are provided as the range corresponding to the thinnest source at 0.1 mg cm^{-2} to the step values for the thickest source at 35 mg cm^{-2}.

Table 3-1. Material designations, mass fractions, and physical state specified for the MCNP model.

Name	*Material Designation*	*Mass fractions*	*Gas state*	*Cond*
P-10	M1	18000 -0.643 6000 -0.071 1000 -0.286	1	
Air	M2	8000 -0.232 7000 -0.755 18000 -0.013	1	
Strontium Carbonate	M3	3800 -0.0961 6000 -0.0132 8000 -0.2471 7000 -0.6328 18000 -0.0109		
Polyethersulfone filter	M4	1000 -0.0072 6000 -0.1301 8000 -0.2267 7000 -0.5967 18000 -0.0103 16000 -0.029		
Nylon	M5	1000 -0.098 8000 -0.141 6000 -0.637 7000 -0.124		
Plastic	M6	1000 -0.098 8000 -0.141 6000 -0.637 7000 -0.124		
Copper	M7	29000 1		1
Mylar	M8	1000 -0.042 8000 -0.333 6000 -0.625		
Iron	M9	26000 1		1
Window	M10	1000 -0.0304 8000 -0.2414 6000 -0.4531 79000 -0.275		

Table 3-2. Number of steps by material designation and radionuclide for the MCNP model. Note that the numbers of steps for strontium carbonate vary with the areal thickness of the source from 0.1 mg cm^{-2} to 35 mg cm^{-2}.

Description	*Material Designation*	*C-14*	*Sr-90*	*Sr-89*	*Y-90*
P-10	M1	10	30	140	150
Air	M2	20	140	600	700
Strontium Carbonate	M3	80 -10	600 -10	3000 -10	3500 -10
Polyethersulfone filter	M4	10	15	70	75
Nylon	M5	10	10	10	10
Plastic support	M6	10	10	10	10
Copper	M7	10	10	10	10
Mylar	M8	10	40	170	180
Steel	M9	10	10	10	10
Window	M10	100	800	4000	4250

3.5.4 Mass fractions for composite materials.

The window composition is specified from the areal thickness measured for gold, 22 μg cm^{-2}, and the manufacturer's specification for the total areal thickness, 80 μg cm^{-2} as described in section 3.4.5. The mass fraction for carbon (45.3%), hydrogen (3.0%), and oxygen (24.1%) are specified from the composition of Mylar (ICRU, 1997). The composite window composition is proportional to the areal thickness of gold, 22 μg cm^{-2}, to the total areal thickness, 80 μg cm^{-2}. The sensitivity of the model to bias in this estimate was evaluated assuming the measured gold areal thickness was within the range from 17.6 μg cm^{-2} to 26.4 μg cm^{-2}, a range representing twice the analytical uncertainty for the gold areal thickness measurement.

The composition of the strontium carbonate source and the polyethersulfone filter were constructed by adjusting the volume fraction of air and strontium carbonate or air and polyethersulfone so the product of the compound densities times the volume fraction of each compound when summed achieves the measured density for the strontium carbonate precipitate. For example, the fraction of strontium carbonate resulting in a measured density of 0.6 gram cm^{-3} is estimated by:

$$Fraction_{SrCO_3} = \frac{\rho_{precipitate} - \rho_{Air}}{\rho_{SrCO_3} - \rho_{Air}} \qquad \text{Equation 3-22}$$

.

The remaining fraction is assumed to be air and hence the air fraction is

$$Fraction_{Air} = (1 - Fraction_{SrCO_3}) \quad \text{Equation 3-23}$$

The respective mass fractions composing the material are estimated by multiplying the respective elemental mass fractions for each compound by the required component fraction and then summing the elemental fractions for the two components for each element. The mass fraction specifying strontium carbonate at 0.6 gm cm^{-3} is provided in Table 3-3.

The composition of the filter is estimated similarly by weighting the fraction of polyethersulfone with density 3.45 g cm^{-3} and air with density 1.205E-03 g cm^{-3} to produce a material with measured density 0.295 g cm^{-3}. The normalized mass fraction specifying the membrane filter at 0.295 gm cm^{-3} is provided in Table 3-4.

Table 3-3. Example of strontium carbonate composition determined from the proportional addition of mass fractions of strontium carbonate and air resulting in a density of 0.6 g cm^{-3}. Mass fractions determined as volumetric fraction times compound volume fraction and summed.

$SrCO_3$ composition	Fraction	Strontium	Carbon	Oxygen	Nitrogen	Argon
Atomic Number		38	6	8	7	18
Mass		87.62	12.01	15.99	14.0067	39.948
$SrCO_3$ Mass Fraction		0.5936	0.0814	0.3250		
Fractional volume x mass fraction	0.16	0.0950	0.0130	0.0520		
Air Mass Fraction				0.2320	0.7550	0.0130
Fractional volume x mass fraction	0.84			0.1949	0.6342	0.0109
Mass fraction		0.0950	0.0130	0.2469	0.6342	0.0109

Table 3-4. Filter composition from the proportional addition of mass fractions equivalent to polyethersulfone and air resulting in a density 0.295g cm^{-3}. Mass fractions determined as volume fraction times compound mass fraction and summed.

Polyethersulfone composition	Fraction	Hydrogen	Carbon	Oxygen	Nitrogen	Argon	Sulfur
Molecular composition (number)		8	12	3			1
Atomic number		1	6	8	7	18	16
Mass		1	12.01	15.99	14.0067	39.95	32.065
Polyethersulfone mass fraction		0.0345	0.6208	0.2066			0.1381
Fractional volume x mass fraction	0.21	0.00722	0.1301	0.0433			0.029
Air Mass Fraction				0.232	0.755	0.013	
Fractional volume x mass fraction	0.79			0.1834	0.5967	0.0103	
Mass fraction		0.0072	0.1301	0.2267	0.5967	0.0103	0.029

3.5.5 Cells

The following cells are defined for this model (see Table 3-5 and Figure 3-3). The model includes twenty cells that are described in three groups: cells in order from the detector to the source; components of the source holder; and components of the surrounding detector.

The detector volume is a right circular cylinder 5.7 cm in diameter and 1.0 cm in depth filled with P-10 at a density of 1.68 x 10^{-3} g cm^{-3}, designated as cell 1. The detector volume is bordered by the detector window, cell 2, and the detector wall, cell 12. The detector window is composed of a proprietary hydrocarbon film and anodized with a gold conducting layer with an estimated combined density of 1.8 g cm^{-3}. The detector wall and back are constructed of oxygen-free copper and are specified with a physical density of 8.96 g cm^{-3}. The detector window is mounted with an oxygen free copper disk contiguous with a copper plate 7 millimeter in thickness, specified as cell 13. Outside of the detector walls, the detector blocks that contain passages for gas flow and holding the sample and guard detectors, are designated as cells 14 and 15, respectively, with a physical density for plastic of 1.1045 g cm^{-3}. The guard detector and upper detector assembly noted in Figure 3-1 are not modeled because beta particles do not penetrate the walls of the sample detector, based on monitoring the guard detector count rate when counting strontium-90 and yttrium-90 in equilibrium.

Below the detector window is an air gap, cell 3, which includes the volume from the plane of the window ring and copper sheet to the sample slide, as well as the space from the detector window to the Mylar surface. Cell 3 is specified with a density of 1.205E-3 g

cm^{-3} and the composition of air in ICRU Report 56 Table A-1 (ICRU, 1997). Note for areal thickness 35 mg cm^{-2} the plane of the Mylar (41) is above the plane specifying the slide surface (52), at which point the air space is specified as noted in Table 3-5.

The strontium carbonate source assembly (see Figures 3-1 and 3-3) consists of the precipitate (Cell 5) mounted on a filter (Cell 8), covered by Mylar film (cells 4, 6, and 7), and held on a nylon ring and disk (Cells 9 and 10). The density of the strontium carbonate was measured and ranged from 0.6 g cm^{-3} to 0.8 g cm^{-3}.
The measured density of the filter of porous polyethersulfone is 0.295 g cm^{-3}. The supporting nylon ring and disk consists of a flat disc shaped supporting surface (cell 10) and supported by a plastic ring (cell 9). The air space within this ring and disk is specified as cell 11. The nylon ring and disk uses the composition for nylon specified in ICRU Report 56, Appendix A-1 (ICRU, 1997). The density of the ring and disk was measured as 1.1 g cm^{-3} and is consistent with the value of 1.14 g cm^{-3} in ICRU Report 56, Table A-1, for nylon.

The source assembly is placed in a plastic spacer to center the assembly within the sample holder. The spacer is represented by Cell 18 and the sample holder by Cell 17, with physical density of 1.104 gm cm^{-3} and the material specification for nylon 6.

Underlying the source assembly and counter spacer is a stainless steel pan 0.1 cm thick and 5.7 cm diameter designated Cell 19, specified with a density of 7.874 g cm^{-3}.

Cell 20 designates everything outside of the model geometry. Beta particles and electrons that may leave the model and enter cell 20 have no further interactions relative to the detector.

Table 3-5. MCNP cell specifications for model including description, cell number, material number, density, and defining surfaces.

Description	*Cell*	*Material*	*Density (g cm^{-3})*	*Surfaces (Table 3-6)*
Detector volume with P10	1	M1	-0.00168	-30 -37 +38
Entrance Window	2	M10	-1.8	-30 -38 39
Air between source and sample surface, inside surface 30	3	M2	-0.001205	(-30 -39 52):(-32 -52 41):(35 -32 -41 43) (34 -30 -39 41):(32 -30 -41 52)[3]
Mylar	4	M8	-1.35	(-34 -41 42)
$SrCO_3$ precipitate	5	M3	-0.60 to -1.0	(-34 -42 44)
Mylar in contact with filter	6	M8	-1.35	(34 -32 44 -43)
Mylar to side of source	7	M8	-1.35	(34 -35 -41 43)
Filter	8	M4	-0.295	(-44 45 -32)
Nylon support sides	9	M5	-1.1045	(-46 47 33 -32)
Nylon support	10	M5	-1.1045	(-45 46 -32)
Air gap under disk	11	M2	-0.001205	(-46 47 -33)
Detector wall (Cu)	12	M7	-8.96	(-31 37 -54):(-31 39 -37)
Metal plate/detector ring (Cu)	13	M7	-8.96	(40-39 30)(-51 48 -49 50 40 -39)
Detector Block (plastic)	14	M5	-1.1045	(31 39 -36)(39 -36 -51 48 -49 50)
Detector Block (plastic)	15	M5	-1.1045	(-31 -36 54)
Air between slide and metal plate, outside surface 30	16	M2	-0.001205	(30 -40 52)(-40 52 -51 48 -49 50)
Slide (Fe)	17	M9	-7.874	30 (-52 53 -51 48 -49 50)
Sample assembly spacer	18	M6	-1.1045	(-52 47 32 -30)
Stainless steel support (Fe)	19	M9	-7.874	(-47 53 -30)
Everything else	20	Void	NA	-53:-50:49:-48:51:36

[3] Except at 35 mg cm^{-2},(-34 -39 41):(-32 -52 41):(35 -32 -41 43):(34 -30 -39 41):(32 -30 -41 52)

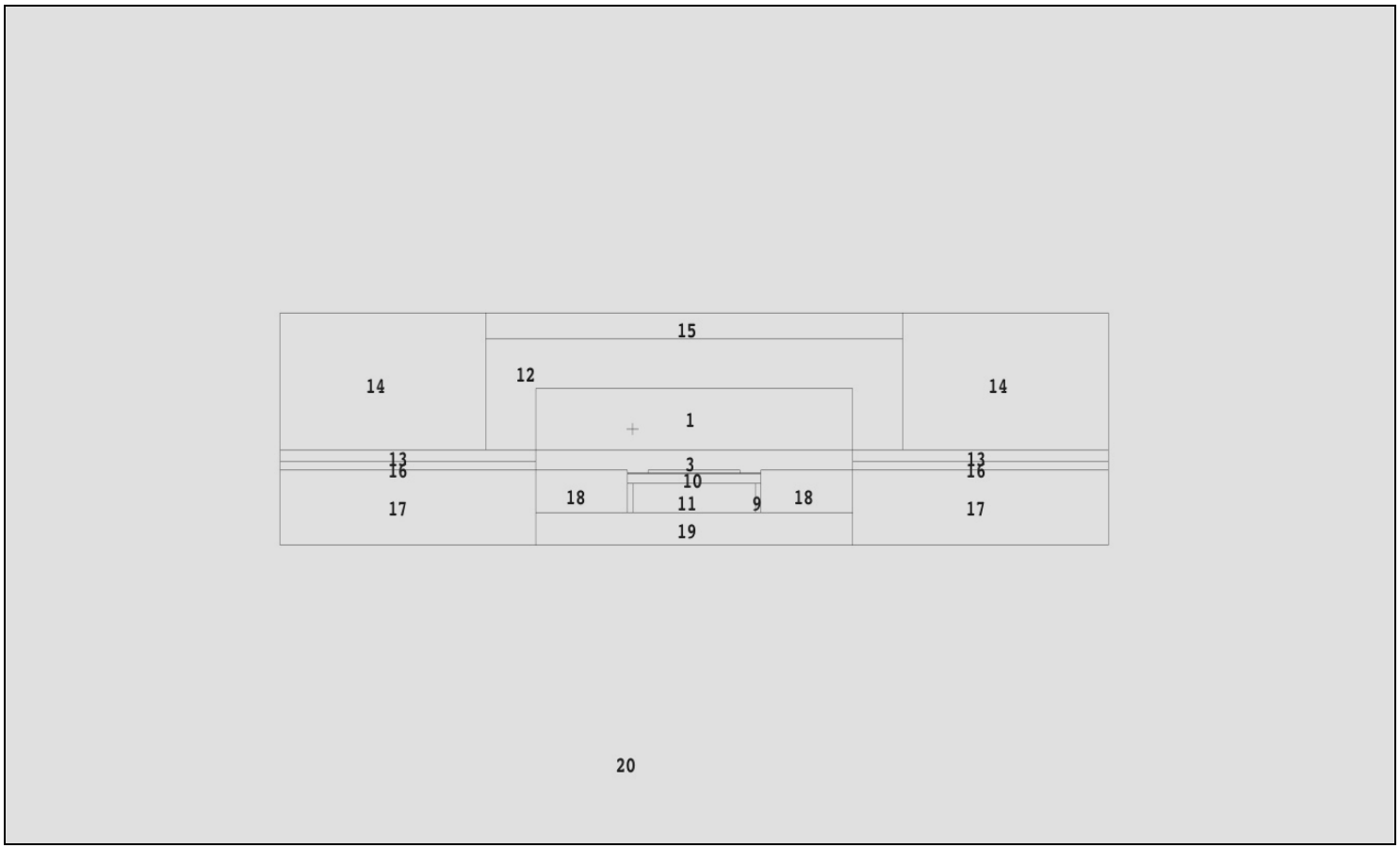

Figure 3-3. Major cells of the MCNP model corresponding to cell descriptions in Table 3-5. Window (Cell 2) and source (Cells 4 through 8) are not visible.

3.5.6 Surfaces

The detector volume, detector window, filter, source, and Mylar are radially symmetrical about the z-axis and defined by the radius of the respective geometry. The detector volume and detector window have a radius of 2.85 cm. The detector window is retained by a mounting ring 3.75 cm in outside diameter. These cylindrical surfaces defined with respect to the Z-axis are designated by “CZ” in Table 3-6.

The filter is mounted on a disk support with radius of 1.20 cm, and the sample precipitate is 0.825 cm in radius. The base of the ring and disk is hollow, with inside radius of 1.10 cm and a wall thickness of 0.1 cm.. Outside the source precipitate, the Mylar is in contact with the filter surface. The transition of the Mylar from the surface of the source precipitate and to the filter is approximated as a step over the equivalent thickness of Mylar (0.012 cm).

The detector and sample assembly are defined in part by a series of horizontal planes perpendicular to the z-axis specified as the distance from the x-y plane. These surface planes are defined with respect to the X-Y plane as the intersection on the Z-axis and are designated by “PZ” in Table 3-6. The guard detector and associated upper detector block are not included in the model because count rate measurements demonstrated beta particles from the sources do not register in the guard detector. The uppermost plane, surface 36, represents the upper surface of the detector wall. The next plane, surface 37, defines the transition between the detector volume and the detector wall. Surface 38 specifies the transition between the detector window and the detector

volume. Surface 39 specifies the transition between the detector window and the air space below the detector.

The next series of planes defined for the z-axis are a function of the source thickness. These include the upper plane specifying the transition between the Mylar covering and the air space (Surface 41), and the transition between the Mylar and the source (Surface 42). These planes are a function of the areal thickness of the source as indicated in Table 3-6 and listed in Table 3-7.

The remaining planes defined for the z-axis are at a fixed distance from the detector window. They are, in order, the upper boundary of the counter slide (surface 52), the upper boundary of the Mylar in contact with the filter (surface 43), the transition between the filter and the ring and disk support (surface 45), the lower plane of the ring and disk support and transition to the supporting pan (surface 47), and finally the lower extent of the supporting stainless steel pan (surface 53).

The distance from the upper boundary of the counter slide to the bottom of the detector assembly is estimated to be 0.2 cm. This is based on the difference between the measured vertical opening to the detector assembling and the height of the slide assembly, and was confirmed by design parameters provided by Canberra[4]. This distance determines the plane of the top of the sample holder and also the base of the sample assembly. The plane of the transition between the Mylar and the source (surface

[4] William Cross, Canberra 2005. Email describing thickness of detector window and method of production.

42) changes as precipitates of increasing mass per unit area are modeled. Note that for the 35 mg cm^{-2} source model, the plane of the Mylar surface is above the plane of the sample slide and requires modification of the cell specification to correctly represent the air space between the source assembly and the detector window.

The four remaining planes define the extent of the detector block holding the detector cell. These planes are parallel to the z-axis and form the sides of a rectangular box. These surface planes are defined with respect to the X-Z plane or Y-Z plane, intersect the Y or X-axis, respectively, and are designated by “PY” or “PX” in Table 3-6. When facing the detector from the side the sample will enter, the planes include: surface 48, forming the left side; surface 49, forming the front side; surface 50, forming the back side; and surface 51, forming the right side.

Table 3-6. MCNP surfaces for a detector to carrier distance of 0.2 cm, with $SrCO_3$ density of 0.6 g cm^{-3}. Vertical distances are relative to the X-Y plane of the detector entrance. The detector to carrier distance is the difference between surface planes 40 and 52.

Surface	*Reference*	*Specification (cm)*	*Description*
30	CZ	2.85	Detector window, 28.5 mm cylinder
31	CZ	3.75	Detector window ring, outer radius
32	CZ	1.20	Filter diameter, 2.4 cm diameter
33	CZ	1.10	Inside diameter disk
34	CZ	0.825	Source, 1.65 cm diameter
35	CZ	0.8262	Mylar transition from source to filter
36	PZ	3.61	Upper plane of detector block
37	PZ	2.150	Upper boundary for detector volume
38	PZ	1.150	Entrance window boundary
39	PZ	1.150	Plane of detector entrance
40	PZ	0.948	Plane of window ring
41	PZ	See Table 3-7	Upper Mylar
42	PZ	See Table 3-7	Upper source surface
43	PZ	0.6914	Upper boundary, Mylar to side of source
44	PZ	0.6902	Upper filter boundary
45	PZ	0.676	Lower filter boundary
46	PZ	0.506	Lower horizontal support boundary of disk
47	PZ	-0.024	Lower boundary for ring and disk/upper pan boundary
48	PX	-7.45	Left side detector block
49	PY	7.45	Front side detector block
50	PY	-7.45	Back side detector block
51	PX	7.45	Right side detector block
52	PZ	0.748	Upper boundary of slide/disk
53	PZ	-0.611	Lower pan boundary
54	PZ	3.15	Upper boundary of detector wall (back)

3.5.7 Source specification

The MCNP program was used to sample source particles from a right circular cylinder, representing the strontium carbonate precipitate, centered on the z-axis. The location of the starting particle is determined by sampling uniformly from the z-axes to the radial extent defined by the edge of the source, or from 0 to a radial distance of 0.824 cm. The vertical extent is sampled uniformly above and below the center plane of the source to determine the starting coordinates in x, y, and z. The vertical extent of the source is calculated for a specific areal thickness from the area mass of the source and the precipitate density. The series of areal thicknesses and dimensions are provided in Table 3-7. The center plane of the source is the midpoint of the distance from the filter and source plane to the vertical extent of the source at the transition to Mylar and is also provided in Table 3-7.

Table 3-7. Model designation and specifications for variable planes in Table 3-6 as a function of density and areal density. Dimensions are based on a $SrCO_3$ density of 0.6 g cm^{-3} and clearance between window ring and sample slide of 0.2 cm. Specifications for the source definition include the plane of the midpoint of the source and the vertical extent sampled above and below the midpoint.

Model designation and specifications			***A***	***B***	***E***	***F***	***G***
Surface	Areal thickness	mg cm^{-2}	0	0.1	2.339	4.677	9.354
41	Upper Mylar	cm	0.6914	0.6916	0.6953	0.6992	0.7070
42	Upper source surface	cm	0.6902	0.6904	0.6941	0.6980	0.7058
Source Definition	Vertical extent (D2)	cm	0.0000	0.0001	0.0019	0.0039	0.0078
	Midpoint	cm	0.6902	0.6903	0.6921	0.6941	0.6980
	Height	cm	0.0000	0.0002	0.0039	0.0078	0.0156
Calculated	Geometrical Efficiency		0.425	0.425	0.425	0.426	0.427

Model designation and specifications (Continued)			***H***	***I***	***J***	***K***	***L***	***M***[5]
Surface	Areal thickness	mg cm^{-2}	14.03	18.71	23.39	28.06	32.74	35
41	Upper Mylar	cm	0.7148	0.7226	0.7304	0.7382	0.7460	0.7897
42	Upper source surface	cm	0.7136	0.7214	0.7292	0.7370	0.7448	0.7885
Source Definition	Vertical extent (D2)	cm	0.0117	0.0156	0.0195	0.0234	0.0273	0.0292
	Midpoint	cm	0.7019	0.7058	0.7097	0.7136	0.7175	0.7594
	Height	cm	0.0234	0.0312	0.0390	0.0468	0.0546	0.0583
Calculated	Geometrical Efficiency		0.429	0.430	0.432	0.433	0.434	0.435

[5] Areal thickness of 35 mg cm^{-2} requires redefinition of the cells for the air-space (see Table 3-5).

3.5.8 Source energy distribution

The energy of the beta particles is sampled from the distributions in Appendix D "Table of Calculated Beta-Ray Spectra" of ICRU Report 56 (ICRU, 1997). The ICRU beta-particle spectra provide the number of betas per disintegration per unit interval of energy divided by the maximum beta-particle energy (E / Emax) and energies as the fraction of E / Emax. The energy fraction bins are specified beginning with the energy fraction 0.0 to 0.025 and continues to 1.0, resulting in 40 bins, each bin 0.025 times Emax in width. The 41st value for E/Emax of 1.0 has probability of 0.00. The probabilities for each energy bin are specified per disintegration for the interval from the fraction E /Emax to the fraction E/Emax + 0.025. These probabilities are in the form of a histogram distribution. The energy intervals are converted from fraction of Emax to energy in MeV by multiplying each fraction by Emax. The probabilities per fractional energy interval can be converted to the probability for the corresponding energy interval by dividing each respective probability by Emax. MCNP normalizes the probabilities per energy interval when processing the beta-particle spectra input, so the table values can be used without conversion.

MCNP requires the first energy and probability entries to be zero. The MCNP code for normalizing histogram distributions assumes the probabilities are for the maximum energy of the interval, in contrast to the ICRU formulation. The probabilities for the ICRU bins are assigned to the upper energy of the energy bin in order to meet this assumption, with the first energy assignment set to zero with probability zero for the MCNP energy distribution.

The input is modified so the beta-particle probability distribution following normalization by MCNP matches the probability distribution provided by ICRU. Further discussion of this modification occurs in section 4.2.4 Beta-particle spectra. This modification consists of increasing the probability for the first non-zero energy bin by the fraction of energy in the interval below the MCNP default energy cut off for electrons of 1 keV or

$$P_c^2 = P_2 * E_2 / (E_2 - 0.001) \qquad \text{Equation 3-24}$$

where:

E_2 = energy for bin boundary 2 (in MeV);

P_2 = probability for the second interval;

0.001 = minimum energy cutoff for electrons in MeV ; and

P_c^2 = adjusted probability in the MCNP source distribution.

Note that MCNP requires the probability P_1 to be zero for E_1 equal to zero.

The beta-particle spectra for carbon-14, strontium-90, strontium-89, and yYttrium-90 are provided in the last two columns of Tables 3-8 through 3-11, respectively.

Table 3-8. Carbon-14 beta-particle spectrum and corresponding input to MCNP for beta-particle energy and histogram probability distribution.

E/Emax	*Number per disintegration per interval, ICRU 56*	*Energy (MeV)*	*Number per disintegration per interval for MCNP source specification*
0.000	1.549	0.0000	0.000
0.025	1.594	0.0039	2.083*
0.050	1.690	0.0078	1.594
0.075	1.756	0.0117	1.690
0.100	1.798	0.0156	1.756
0.125	1.820	0.0195	1.798
0.150	1.825	0.0234	1.820
0.175	1.817	0.0273	1.825
0.200	1.798	0.0312	1.817
0.225	1.768	0.0351	1.798
0.250	1.730	0.0390	1.768
0.275	1.685	0.0429	1.730
0.300	1.633	0.0468	1.685
0.325	1.576	0.0507	1.633
0.350	1.514	0.0546	1.576
0.375	1.447	0.0585	1.514
0.400	1.378	0.0624	1.447
0.425	1.305	0.0663	1.378
0.450	1.231	0.0702	1.305
0.475	1.154	0.0741	1.231
0.500	1.077	0.0780	1.154
0.525	0.999	0.0819	1.077
0.550	0.920	0.0858	0.999
0.575	0.842	0.0897	0.920
0.600	0.765	0.0936	0.842
0.625	0.689	0.0975	0.765
0.650	0.615	0.1014	0.689
0.675	0.543	0.1053	0.615
0.700	0.473	0.1092	0.543
0.725	0.406	0.1131	0.473
0.750	0.343	0.1170	0.406
0.775	0.284	0.1209	0.343
0.800	0.229	0.1248	0.284
0.825	0.179	0.1287	0.229
0.850	0.134	0.1326	0.179
0.875	0.095	0.1365	0.134
0.900	0.062	0.1404	0.095
0.925	0.036	0.1443	0.062
0.950	0.016	0.1482	0.036
0.975	0.004	0.1521	0.016
1	0	0.1560	0.004

*The second entry for MCNP number per disintegration per interval is by equation 3-24.

Table 3-9. Strontium-90 beta-particle spectrum and corresponding input to MCNP for beta-particle energy and histogram probability distribution.

E/Emax	*Number per disintegration per interval, ICRU 56*	*Energy (MeV)*	*Number per disintegration per interval for MCNP source specification*
0	1.597	0.0000	0.000
0.025	1.538	0.0137	1.723*
0.050	1.532	0.0273	1.538
0.075	1.526	0.0410	1.532
0.100	1.518	0.0546	1.526
0.125	1.509	0.0683	1.518
0.150	1.500	0.0819	1.509
0.175	1.490	0.0956	1.500
0.200	1.479	0.1092	1.490
0.225	1.466	0.1229	1.479
0.250	1.453	0.1365	1.466
0.275	1.439	0.1502	1.453
0.300	1.422	0.1638	1.439
0.325	1.404	0.1775	1.422
0.350	1.384	0.1911	1.404
0.375	1.361	0.2048	1.384
0.400	1.335	0.2184	1.361
0.425	1.306	0.2321	1.335
0.450	1.274	0.2457	1.306
0.475	1.238	0.2594	1.274
0.500	1.198	0.2730	1.238
0.525	1.154	0.2867	1.198
0.550	1.106	0.3003	1.154
0.575	1.053	0.3140	1.106
0.600	0.997	0.3276	1.053
0.625	0.935	0.3413	0.997
0.650	0.870	0.3549	0.935
0.675	0.801	0.3686	0.870
0.700	0.729	0.3822	0.801
0.725	0.654	0.3959	0.729
0.750	0.577	0.4095	0.654
0.775	0.498	0.4232	0.577
0.800	0.420	0.4368	0.498
0.825	0.343	0.4505	0.420
0.850	0.268	0.4641	0.343
0.875	0.198	0.4778	0.268
0.900	0.135	0.4914	0.198
0.925	0.081	0.5051	0.135
0.950	0.038	0.5187	0.081
0.975	0.010	0.5324	0.038
1	0	0.5460	0.010

*The second entry for MCNP number per disintegration per interval is by equation 3-24.

Table 3-10. Strontium-89 beta-particle spectrum and corresponding input to MCNP for beta-particle energy and histogram probability distribution.

E/Emax	*Number per disintegration per interval, ICRU 56*	*Energy (MeV)*	*Number per disintegration per interval for MCNP source specification*
0	1.064	0.0000	0.000
0.025	1.107	0.0373	1.093*
0.050	1.167	0.0746	1.107
0.075	1.218	0.1119	1.167
0.100	1.263	0.1492	1.218
0.125	1.300	0.1865	1.263
0.150	1.331	0.2238	1.300
0.175	1.356	0.2611	1.331
0.200	1.376	0.2984	1.356
0.225	1.390	0.3357	1.376
0.250	1.401	0.3730	1.390
0.275	1.407	0.4103	1.401
0.300	1.410	0.4476	1.407
0.325	1.409	0.4849	1.410
0.350	1.404	0.5222	1.409
0.375	1.397	0.5595	1.404
0.400	1.386	0.5968	1.397
0.425	1.381	0.6341	1.386
0.450	1.357	0.6714	1.381
0.475	1.330	0.7087	1.357
0.500	1.299	0.7460	1.330
0.525	1.263	0.7833	1.299
0.550	1.223	0.8206	1.263
0.575	1.178	0.8579	1.223
0.600	1.128	0.8952	1.178
0.625	1.073	0.9325	1.128
0.650	1.011	0.9698	1.073
0.675	0.944	1.0071	1.011
0.700	0.872	1.0444	0.944
0.725	0.794	1.0817	0.872
0.750	0.711	1.1190	0.794
0.775	0.624	1.1563	0.711
0.800	0.534	1.1936	0.624
0.825	0.443	1.2309	0.534
0.850	0.353	1.2682	0.443
0.875	0.265	1.3055	0.353
0.900	0.184	1.3428	0.265
0.925	0.112	1.3801	0.184
0.950	0.054	1.4174	0.112
0.975	0.014	1.4547	0.054
1	0	1.4920	0.014

*The second entry for MCNP number per disintegration per interval is by equation 3-24.

Table 3-11. Yttrium-90 beta-particle spectrum and corresponding input to MCNP for beta-particle energy and histogram probability distribution.

E/Emax	*Number per disintegration per interval, ICRU 56*	*Energy (MeV)*	*Number per disintegration per interval for MCNP source specification*
0	0.761	0.0000	0.000
0.025	0.849	0.0570	0.775*
0.050	0.945	0.1141	0.849
0.075	1.031	0.1711	0.945
0.100	1.110	0.2281	1.031
0.125	1.179	0.2851	1.110
0.150	1.239	0.3422	1.179
0.175	1.291	0.3992	1.239
0.200	1.335	0.4562	1.291
0.225	1.372	0.5132	1.335
0.250	1.401	0.5703	1.372
0.275	1.435	0.6273	1.401
0.300	1.443	0.6843	1.435
0.325	1.446	0.7413	1.443
0.350	1.444	0.7984	1.446
0.375	1.438	0.8554	1.444
0.400	1.428	0.9124	1.438
0.425	1.414	0.9694	1.428
0.450	1.395	1.0265	1.414
0.475	1.373	1.0835	1.395
0.500	1.347	1.1405	1.373
0.525	1.315	1.1975	1.347
0.550	1.279	1.2546	1.315
0.575	1.238	1.3116	1.279
0.600	1.191	1.3686	1.238
0.625	1.138	1.4256	1.191
0.650	1.078	1.4827	1.138
0.675	1.012	1.5397	1.078
0.700	0.939	1.5967	1.012
0.725	0.86	1.6537	0.939
0.750	0.775	1.7108	0.860
0.775	0.684	1.7678	0.775
0.800	0.589	1.8248	0.684
0.825	0.492	1.8818	0.589
0.850	0.394	1.9389	0.492
0.875	0.298	1.9959	0.394
0.900	0.207	2.0529	0.298
0.925	0.127	2.1099	0.207
0.950	0.061	2.1670	0.127
0.975	0.017	2.2240	0.061
1	0	2.2810	0.017

*The second entry for MCNP number per disintegration per interval is by equation 3-24.

3.5.9 Particle flux

The particle flux is measured by surface current tally (F1 tally in MCNP) flagged by the number of the plane the particles are crossing. These planes include the upper boundary for the detector volume (37), plane between the detector volume and the window surface (38), plane of the detector window surface facing the source (39), upper Mylar surface (41), and upper source surface (42). The direction of particles is determined by flagging the direction measured normal to the surface for particle trajectories as particles may be scattered back across these surfaces. These directions are specified as the cosine of the angle normal to the surface plane, consisting of 1 to 0 for particles traveling away from the source and 0 to -1 for particles scattered back across the surface.

The direction of the particle tracks as they cross into the detector volume are tabulated as a function of the cosine of the angle between the current trajectory and a vector normal to the window surface.

3.5.10 Pulse height tally

The pulse-height tally (F8 tally in MCNP) is used to estimate the energy distribution of pulses deposited within the detector volume by beta particles and associated scattered electrons. This tally includes separate bins to account for knock-on electrons, beta particles that enter the detector volume but may not have an interaction before leaving the volume, and interactions that deposit energy less than required to register above the counter discriminator (0.3 keV, discussed in section 4.2.1). Energy deposition is tallied in

one keV increments through 50 keV and the remainder is tallied in the interval between 50 keV and the maximum energy that may be emitted.

3.5.11 Energy binning of electrons

The cross-section tables are assessed for a given particle energy using the nearest group boundary of the energy bin instead of the MCNP default bin-centered treatment (Schaart, 2002, See also LANL, 2006, page 2-74). This is achieved through setting the 18th parameter of the DBCN card to 1, implementing cross section look-up as implemented in ITS codes. The EI03 electron interaction data library is used (LANL, 2006).

3.6 Comparison of measured efficiencies with MCNP model results

The measured efficiencies include estimates of the total propagated uncertainty as described in section 3.3. A sensitivity analysis of varying the model parameters described in section 3.5 provides an estimated of the uncertainty of the MCNP model energy deposition estimates. The individual measurements are compared with estimates based on the MCNP model assuming the measurements and model estimates are normally distributed with the standard normal statistic

$$Z = \frac{(\mathrm{E}_R(x\rho) - \mathrm{E}_{MCNP,R}(x\rho))}{\sqrt{u(\mathrm{E}_R(x\rho))^2 + u(\mathrm{E}_{MCNP,R}(x\rho))^2}} \qquad \text{Equation 3-25}$$

(DeGroot, 1986), where:

$E_R(x\rho)$ is the efficiency estimated by equation 3-1 or 3-8 for radionuclide R and areal thickness xρ;

$E_{MCNP,\,R}\,(x\rho)$ is the fractional energy deposition estimated with the MCNP model for radionuclide R and areal thickness xρ ;

$u(E_R(x\rho))$ is the total propagated uncertainty for the measured efficiency for radionuclide R and areal thickness xρ; and

$u(E_{MCNP,\,R}\,(x\rho))$ is the uncertainty for the MCNP model, for radionuclide R and areal thickness xρ.

Chapter 4. Measurement uncertainties, parameter estimates, and total uncertainty budgets.

This chapter presents results of uncertainty estimates and parameters for efficiency measurements and Monte Carlo modeling. Uncertainty estimates that are described include gravimetric and volumetric measurements with their associated uncertainties, activity of radionuclide standards, and parameters characteristic of the counting system. Specific parameters for the Monte Carlo model include specification of the beta spectra, composition of materials, and the estimated energy cutoff.

4.1 Measurement uncertainty estimates

The uncertainty estimates describe the components affecting measurement uncertainty, the data used to develop uncertainty estimates, and either the uncertainty estimate for constant values or the equation for estimating the uncertainty component as a function of the measured value. An example of the estimated uncertainty value for a constant value is the uncertainty associated with volumetric measurements of a constant volume. Examples of estimating uncertainty for measured values include gravimetric and variable volume pipette measurements. The results for uncertainty estimates are provided below, including the estimates for gravimetric measurements, volumetric measurements, and the activity of calibration standards. The specific values are provided in Appendix A and the uncertainty budgets are presented in sections 4.3 and 4.4.

4.1.1 Gravimetric measurements

The uncertainty components in gravimetric measurements include the repeatability of measurements, uncertainty in the linearity of the balance, uncertainty of calibration masses, and uncertainty due to variation in environmental factors. The sources of uncertainty data include measurements of a known traceable mass prior to each set of measurements, the balance manufacturer's specifications, and measurements over time from routine linearity checks. Uncertainty estimates were made following MARLAP Attachment 19E "Uncertainties of Mass and Volume Measurements" (MARLAP, 2004) and are described in section 3.3 Estimating components of measurement uncertainty.

Mass measurements were obtained from an AND FR-300 analytical balance. Repeatability was estimated from repeated measurements of a calibrated 0.5000 gram mass. The test mass is weighed and the results recorded each time the balance is used. The mass of the test mass is verified annually by a calibration service maintaining traceability to National Institute of Standards and Technology (NIST). The acceptance criteria for this balance check is plus or minus 0.0001 gram (ASTM, 1987). Results for one year of measurements from April 2001 through April 2002 averaged 0.5000 ± 0.00008 gram (1 standard deviation) for 102 measurements with a range in measurements from 0.4999 to 0.5001 gram. The standard uncertainty due to repeatability is 8.0×10^{-05} gram.

The linearity tolerance limit for the balance specified by the manufacturer is ±0.0002 gram. This linearity tolerance limit is treated as the half-width of a rectangular distribution and the standard uncertainty due to linearity is estimated by dividing the tolerance limit by $\sqrt{3}$. The standard uncertainty associated with linearity is 1.4×10^{-04} gram.

The AND FR-300 analytical balance is evaluated for linearity every four months by Rite-Weight, Inc., using a set of Troemmer Analytical ASTM Class 1 weights with calibrations traceable to NIST. These data were used to evaluate uncertainties created by environmental variations including vibration, use of the balance, and temperature fluctuations as described in section 3.3.1. The two components of this uncertainty estimate are the tolerances of the calibration masses and the measured variability in response over time. The mass in air calibration data for a representative set calibrated December 22, 2004 was examined during a routine audit of Rite Weight, Inc. The uncertainties in calibration masses are expressed as tolerance limits. Tolerances for calibration masses used in routine linearity checks include 200 ± 0.0005; 100 ± 0.00025; 50 ± 0.00012; 10 ± 0.00005; and 1 ± 0.00034 gram.

The uncertainty in the calibration and measurement with an analytical balance is largely the result of variation from environmental factors including temperature, humidity, operation of the instrument, and vibration. The uncertainty in the calibration and environmental factors were evaluated by measurements from routine linearity checks for calibration mass sets of 1, 10, 50, 100, and 200 grams. The uncertainty due to environmental factors was estimated from multiple calibrations over the period from 2000 through 2006 and by including the “as found” measurements” as well as the “as left” measurements. Results were evaluated by linear regression with the calibration masses as the independent variable and the balance indication as the dependent variable as described in section 3.3.1. The Mean Square Error (MSE) provided in the Analysis of Variance is an estimate of the variance from environmental factors. The uncertainty in future measurements is estimated by Equation 3-16 and expressed as the relative uncertainty, S_m/M_l. The average value of the calibration mass data was 77.75

gram, and the estimated relative uncertainty is 2.17x 10^{-05} gram for the average of the calibration masses (see Table 4-1). Similar results were found for a subset of the results for either 100 gram or 200 gram calibration masses.

The combined uncertainty for individual gravimetric measurements, U(m), in grams, is estimated from

$$u(M) = \sqrt{(8.0x10^{-5})^2 + (1.4x10^{-4})^2 + (M_I \bullet 2.17x10^{-5})^2} \qquad \text{Equation 4-1}$$

where:

8.0x10^{-5} = uncertainty due to repeatability;

1.4x10^{-4} = uncertainty due to linearity;

M_I = balance indication; and

2.17x10^{-5} = relative uncertainty due to environmental variations

Table 4-1. FR 300 balance estimate of uncertainty due to environmental variations based on linearity checks. Masses include 0, 1, 10, 50, 100, and 200 gram. MSE is an estimate of the random error about the linear regression. Results for the uncertainty estimate are given as the uncertainty, S_m, and the relative uncertainty, $S_m/M_{I,}$ below the ANOVA results.

Model FR-300 Balance
ANOVA

Source of variation	*df*	*SS*	*MS*	*F*	*Significance F*
Regression	1	207366.5	207366.5	75330461262	1.45E-142
Residual	30	8.26E-05	2.75E-06	MSE Equation 3-16	
Total	31	207366.5			

	Coefficients	*Standard Error*	*t Stat*	*P-value*	*Lower 95%*	*Upper 95%*
Intercept	-4.01E-05	0.00041	-0.0984	0.92	-0.0009	0.0008
X Variable 1	1.0000	3.64E-06	274464	1.4522E-142	1.0000	1.0000

Xbar	77.75	$\overline{M}$
Sxx	6689.24	Variance of the calibration masses
Balance Indication	77.75	M_I
Uncertainty	0.0017	S_m from Equation 3-16
Relative Uncertainty	2.167E-05	S_m/M_I

4.1.2 Volumetric measurements

The concentration of radionuclide standards and the amount of carrier added in preparing standards were determined from volumetric measurements. The primary sources of uncertainty were volumetric measurements with a variable volume pipette and volumetric flasks in preparing radionuclide source solutions.

4.1.2.1 Variable volume pipette

The radionuclide standards were pipetted with a Rainen EDP-2 variable volume pipette with a working range from 100 µL to 1000 µL (0.100 mL to 1.000 mL). The uncertainty components in pipette measurements include the repeatability of measurements, the uncertainty from the linearity of pipette, and the uncertainty due to variation in environmental factors, evaluated as described in section 3.3.2.

The manufacturer's specification for accuracy and precision at specific volumes are provided in Table 4-2. The relative uncertainty based on the manufacturer's specification range from 0.35% at 1000 µL to 1.36% at 100 µL.

Table 4-2. Accuracy and precision specifications for the Rainen EDP-2 variable volume pipette. µ (V) is the propagated uncertainty based on the manufacturer's specification for accuracy and precision.

Volume	Accuracy Specification		Precision Specification		MARLAP	Relative
µL	Relative%	Absolute µL	Relative %	Absolute µL	µ(V)	Uncertainty
100	3	3	0.6	0.6	1.36	1.36%
500	0.8	4	0.13	0.65	1.76	0.35%
1000	0.8	8	0.13	1.3	3.52	0.35%

Additional quality control data including information from quarterly checks of repeatability and specific evaluations of linearity were available and included in the estimate of the combined standard uncertainty of pipette measurements.

The repeatability of pipette measurements was estimated from replicate measurements of deionized water. The volumetric pipettes were evaluated monthly by weighing 1.000 mL of deionized water in three replicate measurements on a calibrated analytical balance. The average precision of 1.000 mL measurements from 2002 through 2006 (n = 51) was ± 0.0012 mL, in agreement with the precision specification provided by the manufacturer of ± 0.0013 mL.

The uncertainty from pipetting variable volumes was estimated by linear regression of the indicated volume against the mass recorded for deionized water for 100 µL to 1000 µL for five replicate measurements at each volume. These measurements were made at various times and include variability due to operation of the pipette and variations in the environmental conditions. The results of the regression analysis are provided in Table 4-3. The uncertainty of pipette measurements is estimated by combining the accuracy specification from the manufacture with the uncertainty from the linear regression. Relative uncertainties of pipette measurements are provided in Table 4-4 for representative volumes.

Table 4-3. Estimate of relative uncertainty in volumetric pipette measurements due to environmental variations based on linearity checks. Data are replicate measurements of delivered mass. MSE is an estimate of the random error about the linear regression. Results for the uncertainty estimate are given as the uncertainty, S_m and the relative uncertainty, S_m/V_l, below the ANOVA results

Mass = 0.001005*Volume-0.00662
SUMMARY OUTPUT
ANOVA

Source of variation	*df*	*SS*	*MS*	*F*	*Significance F*
Regression	1	4.15078	4.1508	470239	1.76E-88
Residual	43	0.00038	8.83E-06	**MSE Equation 3-16**	
Total	44	4.15115			

	Coefficients	*Standard Error*	*t Stat*	*P-value*	*Lower 95%*	*Upper 95%*
Intercept	-0.0066	0.0009	-7.3	5.46E-09	-0.0085	-0.0048
Volume	0.001004812	1.4653E-06	685.7	1.76E-88	0.0010	0.0010

Xbar	544.4	$\overline{V}$
Sxx	17146843.4	Variance of the calibration masses
Volume	500	V_l
Uncertainty	3.0	S_m from Equation 4-16
Relative Uncertainty	0.6%	S_m/V_l

Table 4-4. Relative uncertainty of variable pipette measurements.

Volume (mL)	Uncertainty (1S)	Relative
1	0.015	1.5%
0.9	0.012	1.3%
0.8	0.009	1.2%
0.7	0.008	1.1%
0.6	0.007	1.2%
0.5	0.008	1.7%
0.4	0.011	2.7%
0.3	0.013	4.4%
0.2	0.016	8.0%

4.1.2.2 Volumetric glassware

100 mL volumetric flasks were used in the preparation of radionuclide standards. The manufacturer tolerances for Type A glassware are specified in Table 4-5. The total uncertainty was estimated to be ± 0.04 mL. Variations due to temperature were evaluated and found to be small relative to the uncertainties for the tolerance specification and repeatability.

Table 4-5. Uncertainty specifications for volumetric 100-mL volumetric flask.

Quantity	Unit	Uncertainty	Definition
Tolerance	mL	0.04	Type B rectangular distribution as half width
Repeatability	mL	0.03	Type A statistical evaluation, N=10

4.1.3 Calibration Standards

The calibration standards are NIST traceable and purchased from Eckert and Zeigler (formerly Analytics, Incorporated). The radionuclide, serial number, concentration, and total uncertainties are provided in Table 4-6. The total uncertainty components include

the total propagated uncertainty for the initial activity, the uncertainty for the mass of material transferred (estimated in section 4.1.1), and the uncertainty for the volumetric container (estimated in section 4.1.2.2).

Table 4-6. Calibration standard activities and expanded uncertainties (1S).

Radionuclide	Source Standard Serial Number	Source Activity (Uncertainty, 1S) s^{-1} g^{-1}	Concentration (Uncertainty, 1S) s^{-1} mL^{-1}
Strontium-89	54195-163	7.81E+04(0.13)	391.4(3.8)
Strontium-89	56950-163	4.00E+04(0.04)	200.5(1.3)
Strontium-90a	54194-163-a	4.00E+04(0.08)	15.79(0.23)
Strontium-90b	54194-163-b	4.00E+04(0.08)	58.79(0.85)
Carbon-14	66404-163	768(12)	771.3(7.3)

4.1.4 Counting system

The uncertainties in the counting system include counting statistics (section 3.3.3), variations in counting efficiency of the instrument, and variations in background count rate. The controls and magnitude of these variations are discussed below.

The counting plateau is evaluated following change in the P-10 counting gas cylinder or any change made in the counting system. The evaluation includes the slope of the beta-particle counting plateau, the statistical independence of 20 repetitive counts, and the fraction of beta particles counted above the alpha discriminator. Long and short term variations in counting efficiency were monitored with a beta-particle point source that was counted each day the system was used and the count rate was evaluated against established control limits. The control limits for a nominal count rate of 50,000 min^{-1} is ± 269 min^{-1} (95% confidence limits), equivalent to ±0.5%.

An instrument background was measured each day the instrument was used by counting an empty planchet for 100 minutes at the beta-particle plateau operating voltage and the results were evaluated against control limits. Control limits based on one year of data collected in 2005 were 1.19 ± 0.23 min^{-1} (95% confidence limits). A background measurement with a blank filter was made each time a set of sources or samples were counted. Control limits for filter background measurements based on one year of data, collected in 2005 were 1.90 ± 0.34 min^{-1} (95% confidence limits). The difference in blank filter measurements and empty planchet measurements represents the contribution from the filter material.

Calibration sources were not counted if control limits were exceeded for counting efficiency, instrument background measurements, or background measurements. No data were collected when instrument controls indicated out-of-specification conditions.

The intrinsic efficiency of the detector is estimated by an approximation based on the specific ionization in air and separately by the stopping power of electrons in P-10 to provide a range in estimates. The energy of beta particle tracks from an MCNP model of yttrium-90 was examined to assess the range of energies for tracks crossing the window boundary into the detector volume (Figure 4-1). Ytttium-90 beta-particle tracks may have energies up to approximately E_{max}, or 2.28 MeV. Intrinsic efficiency estimates are made for a particle energy of 1 MeV since the corresponding specific ionization by beta particles of this energy is at a minimum and the estimated intrinsic efficiency will be at a corresponding minimum. The probability of zero interactions estimated with equation 2-10 is 6×10^{-10}. However, in order to deposit sufficient energy to exceed the estimated 0.3 keV energy cut-off, at least 12 ion pairs must be created along the beta particle track. The cumulative probability for 12 and fewer interactions by equation 2-11 is 0.02,

resulting in an intrinsic efficiency of 0.98 for a beta particle history. This is the minimum intrinsic efficiency based on the extrapolation for specific ionization in air.

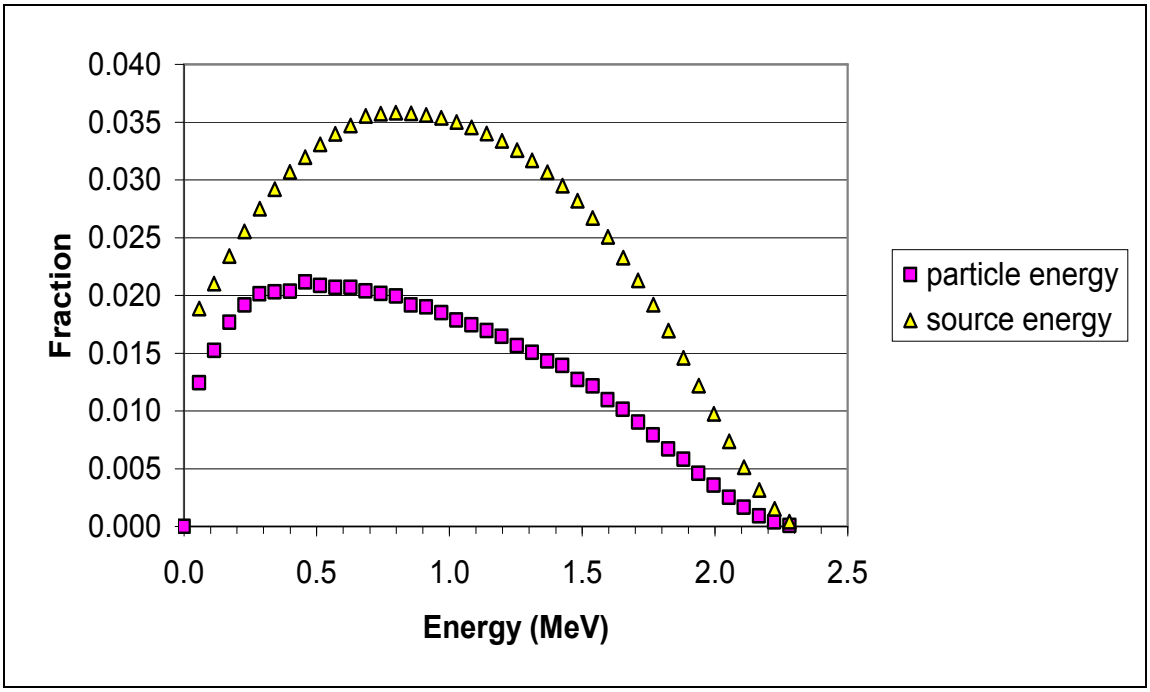

Figure 4-1. Energy of beta particle tracks crossing into the detector volume from 14 mg cm^{-2} yttrium-90 source. Yttrium-90 source energy distribution is provided for comparison.

The total stopping power for electrons in P-10 gas shows a minimum at 1.0 MeV of 2.10 MeV cm^2 g^{-1} (MCNP Table 170, for P-10 gas). This corresponds to a total specific ionization rate of 134 ion pairs percentimeter. The probability of having 12 and fewer interactions decreases rapidly as the specific ionization rate increases, with intrinsic efficiency of 0.991 for 23 ion pairs per cm and 0.995 for 24 ion pairs per cm, well below that expected for 1.0 MeV beta particles. The MCNP model results for yttrium-90 are consistent with this estimate for intrinisic efficiency, with the maximum fraction of beta-particle histories escaping without interaction plus the fraction below the energy cut-off

(0.3 keV) equal to 7.86E-03, corresponding to an intrinsic efficiency of 0.992 (see Table 5-11). The intrinsic efficiency is believed to be greater than 0.99 for this detector based on the MCNP model results and the total stopping power for electrons in P-10.

4.2 Parameters affecting Monte Carlo results

Specific parameters are required to estimate counting system efficiencies by Monte Carlo methods. For example, the model estimates all interactions within the detector volume. The counting system, on the other hand, is designed to eliminate signals from the detector below an amplifier voltage threshold to reduce the effects of electrical noise. The effect of voltage discrimination on the pulse height excluded within the counting system was evaluated and the results applied to the Monte Carlo efficiency estimates. In addition, specific parameters were selected that affect energy binning, and an adjustment was made in the specification of the beta-particle particle spectra to properly match the MCNP normalization scheme to the specified beta-particle particle energy distribution.

4.2.1 Energy cutoff

The energy excluded by the LB 5100 lower level discriminator was estimated as described in section 3.4.7. The distribution of pulse heights produced by a strontium-90/yttrium-90 source is provided in Figure 4-2. The pulse height spectrum was obtained as described in section 3.4.6. The threshold for counting beta-particle particle tracks above a specific energy is determined by the discriminator setting of the TC 247

amplifier. The distribution of pulses recorded with a multi-channel analyzer is skewed to the lower voltages, with the mode of the distribution between 0.125 and 0.130 Volts, and the pulse distribution tailing to higher voltages. The counting efficiency is maximized by setting the discriminator below voltages where the distribution shows a rapid decrease, approximately 0.03 Volts, and above the level where electronic noise would increase the counting background. This threshold voltage can be measured directly using a pulse generator and oscilloscope, and the corresponding energy estimated by relating the voltage to the pulse height from photoelectric interactions in the detector or by changing the gain of the detector by changing the detector bias and estimating the change in gain for a specific photoelectric interaction.

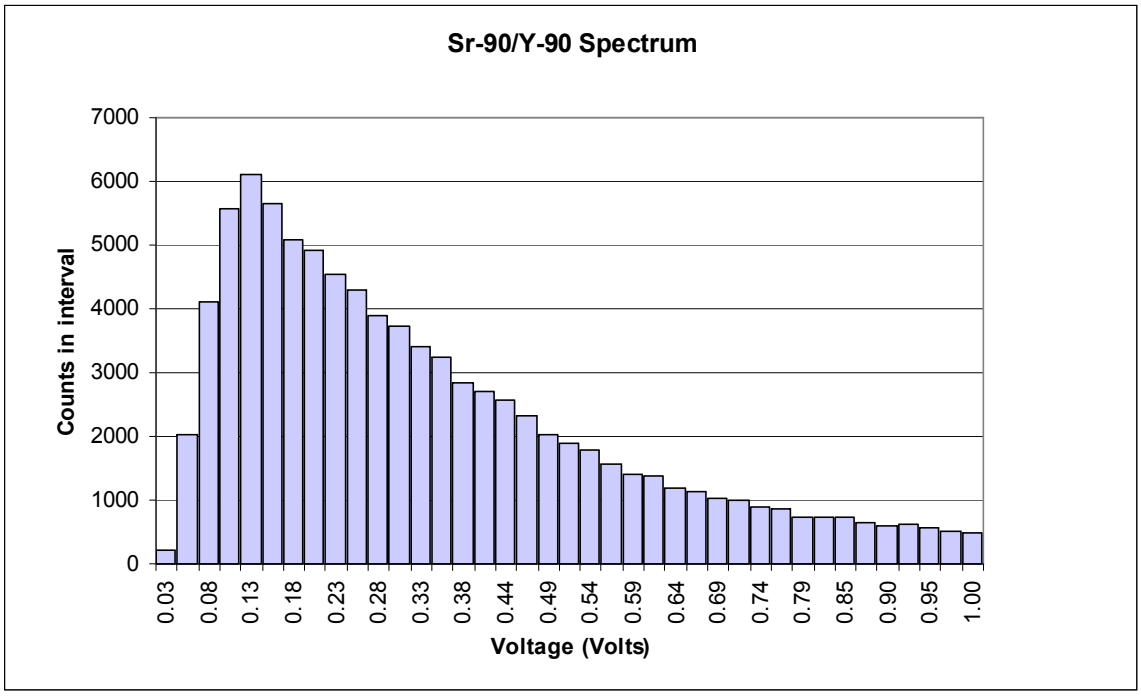

Figure 4-2. Strontium and yttrium-90 signal spectrum measured from the LB-5100 detector.

A Canberra Model 1407 reference pulse generator was configured to provide a pulse approximating the signal observed when counting strontium-90 and yttrium-90 as described in section 3.4.6. The pulse height was gradually reduced until the count rate decreased from 3600 min^{-1} to 1800 min^{-1}. The pulse generator signal was found to record counts in channel 6 of the MCA and based on the energy calibration the corresponding energy for photo-electric interactions is estimated to be 0.4 keV.

The energy deposited within the detector volume was also estimated by scaling the multiplication that occurs with increasing detector bias from the point where interactions were measured just exceeding the discriminator level to the full detector bias used at the counting plateau. The energy deposited within the detector and amplified proportionately by gas multiplication was estimated from the photoelectric interaction by the 5.9 keV x-ray from Fe-55 and the increase in multiplication that occurs as the detector high voltage increases. The recorded pulse height spectrum for iron-55 is provided in Figure 4-3.

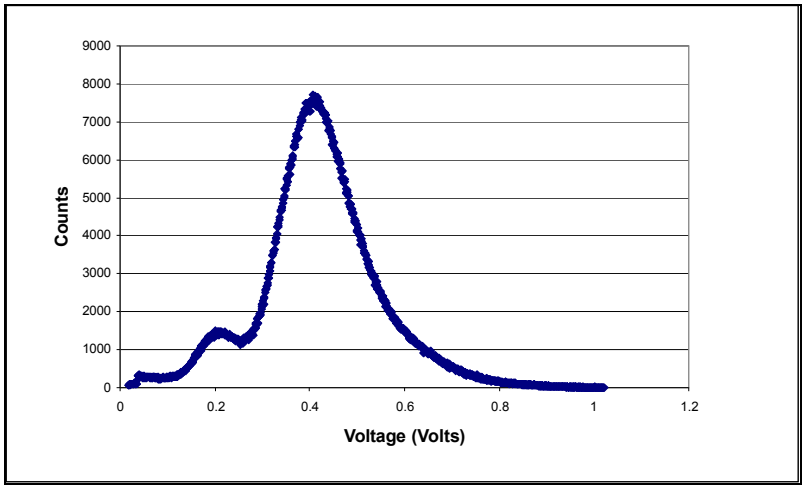

Figure 4-3. Spectrum for Fe-55 photoelectric interactions measured from the LB-5100 detector.

The multiplication that occurs with increasing detector voltage was estimated by varying the amplifier gain and recording the voltage that produces the same count rate. The difference in detector voltage as the gain was increased by a factor of two provides an estimate of the voltage change needed to double the multiplication, or "doubling voltage". Beta-particle plateaus for strontium-89 were collected with amplifier gain settings including 2, 4, 8, 16, 32, and 64 (Figure 4-4). The voltage resulting in a constant count rate of 5000 min^{-1}, approximately half the plateau count rate, was estimated from the linear portion of the counting plateau by solving the linear equation Count Rate = B_1*Voltage + B_0, for the voltage providing 5000 min^{-1} at a given gain. The difference in voltages at a constant count rate is an estimate of the doubling voltage. The average doubling voltage as the amplifier gain was varied from 2 to 64 is estimated to be 62.3 ± 1.2 Volts (standard error of the mean) (Table 4-7).

Table 4-7. Doubling voltage measurements with strontium-89.

Gain	Slope (min^{-1}/ volt)	Intercept (min^{-1})	Estimated voltage for 5000 min^{-1} (Volts)	Difference (Volts)
2	46.6	-62819	1454.2	-
4	43.4	-55607	1394.9	59.3
8	46.8	-57745	1340.4	54.5
16	43.8	-51021	1279.5	60.9
32	43.3	-47432	1210.3	69.1
64	44.8	-46142	1142.7	67.7
Average	44.79		Average	62.3
			Standard Deviation (1S)	6.1
			Standard Error (1S)	1.2

The estimated doubling voltage for the counting system allows scaling of a known energy event in the detector from the plateau operating voltage to a voltage just sufficient to trigger the counting system above the amplifier discriminator. The 5.9 keV photoelectric interactions from x-rays produced following the decay of Fe-55 were used to provide an estimate of the energy excluded by the amplifier discriminator.
The Auger electrons produced following decay of Fe-55 by electron capture were absorbed by an aluminum foil. The counting plateau provided in Figure 4-4 shows the Fe-55 source registering when the detector voltage was 1200 volts. The maximum count rate of 2491 min^{-1} was reached at the operating plateau voltage of 1500 volts. The point where multiplication results in the 5.9 keV interaction producing voltage pulses exceeding the discriminator threshold in half of the events corresponds to the voltage where the count rate was one half the count rate at 1500 volts and was estimated by interpolation to occur at 1240 volts.

The proportional counter multiplication increases by $2^{260/62.3}$ or 18.3 times between 1240 volts and 1500 volts based on 62.3 volts per doubling in multiplication,. Dividing the energy deposited from the photoelectric interaction by the change in multiplication provides an estimate of 0.33 ± 0.09 keV (1S expanded uncertainty) for the energy that was excluded by the lower level discriminator. MCNP model pulse height tallies (section 3.5.10) record results for beta-particle histories depositing less than 0.3 keV in the detector volume and this contribution is subtracted from the fraction of interactions estimated for the detector.

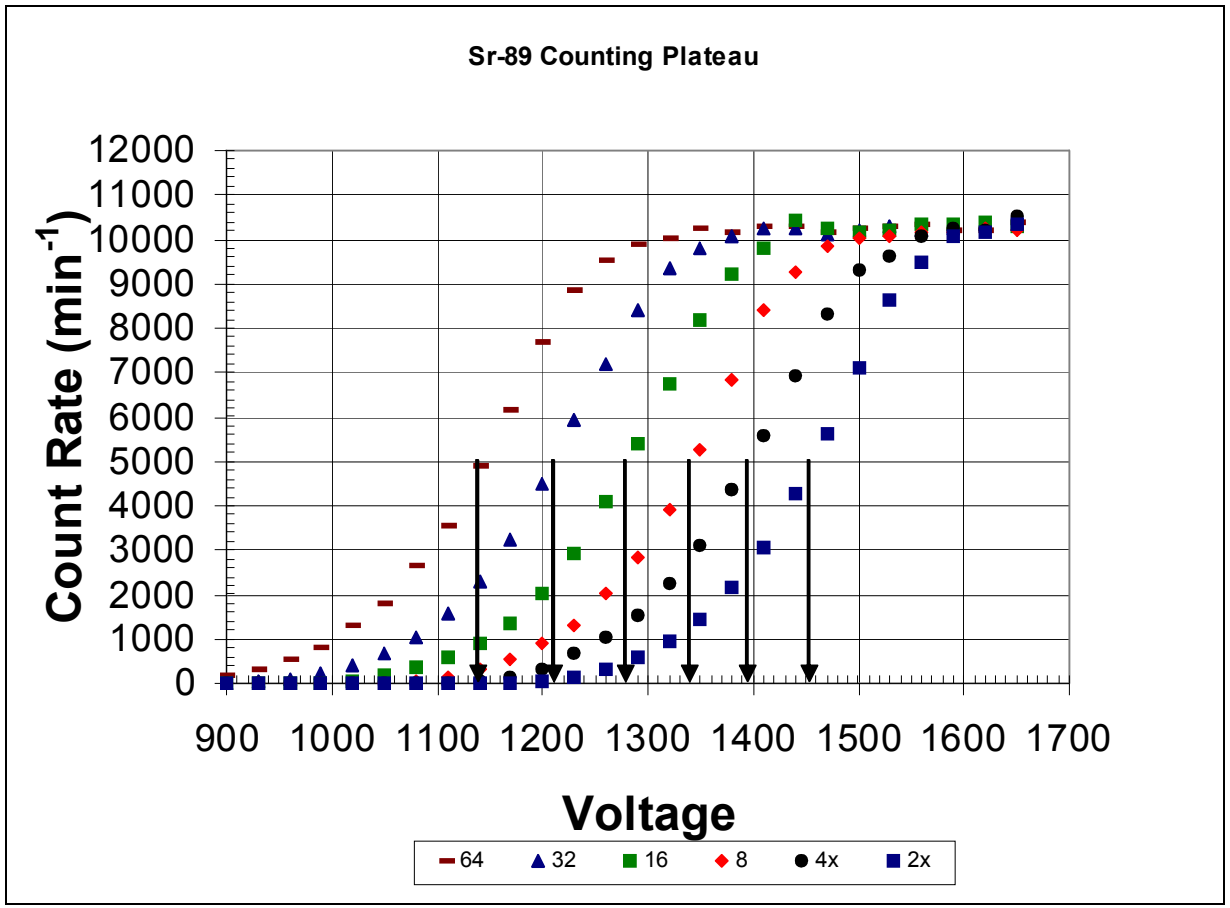

Figure 4-4. Doubling voltage estimated from strontium-89 beta-particle plateau with amplifier gain varied from 2 to 64. Voltage corresponding to a count rate of 5000 min^{-1} is estimated from Table 4-7.

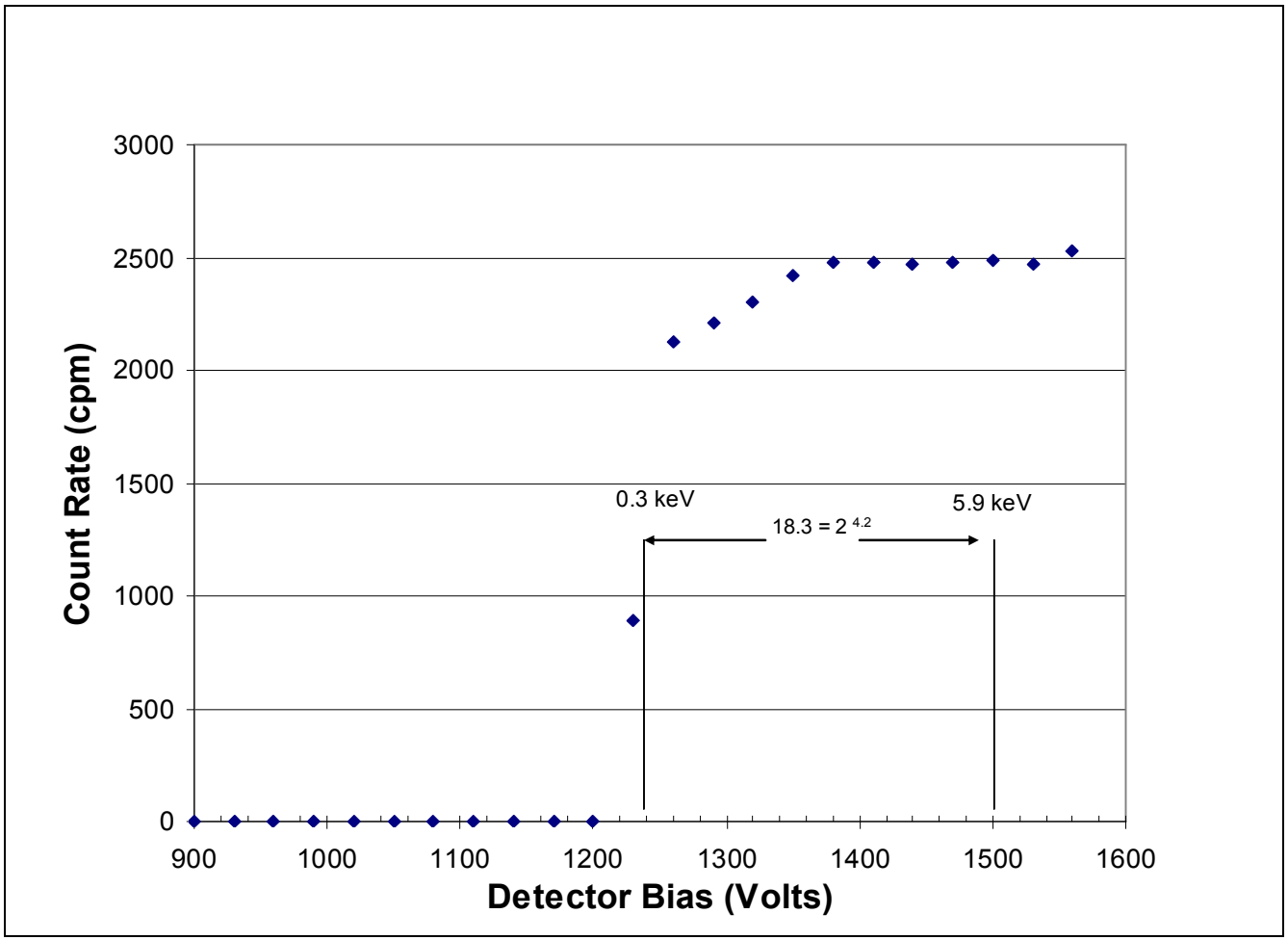

Figure 4-5. Iron-55 counting plateau and estimated gas multiplication. Source covered by aluminum foil and amplifier gain of 16.

4.2.2 Material densities

Densities were measured (see Table 4-8) when practical and compared to tabulated values found in ICRU 56, Table A.1 (ICRU, 1997). The densities of the nylon ring and disk mount, Mylar film, and filter were determined from physical dimensions and mass measurements of representative samples.

The density of the nylon ring and disk mount was estimated from a set of 10 randomly selected sets with average weight of 0.8342 g and volume of 0.755 cm^{-3}, resulting in a measured density of 1.1049 ± 0.0096 g cm^{-3}. This measurement is slightly less than the value of 1.14 g cm^{-3} found in ICRU 56 Table A-1.

The density of the Mylar covering was estimated from the mass of a strip 207.6 cm in length and 3.79 cm in width, weighing 1.2940 gram. Replicate measurements (n=5) of the thickness of 100 sheet stack provided an average thickness of 0.0122 ± 0.00005 (1S) mm. The resulting density of 1.35 g cm^{-3} is in agreement with the ICRU value of 1.35 g cm^{-3} (ICRU, 1997)

The density of filters was obtained from replicate measurement the mass and thickness of a stack of five filters. The filters are constructed from polyethersulfone with a physical density of 3.45 g cm^{-3}. The filters are 24.65 mm in diameter, with an average mass of 0.0200 ± 0.0004 (95% CL). The average thickness measured with a micrometer is 0.142 mm based on measurement of replicate measurement of a stack of five filters. The estimated density of Gelman Supor filters is 0.295 ± 0.003 g cm^{-3} (N= 5 replicate measurements).

The density of the strontium carbonate precipitate was obtained from nineteen calibration sources ranging from 8 to 31 mg cm^{-2}. The density ranged from 0.79 ± 0.04 g cm^{-3} (N=14) to 0.58 ± 0.07 (N = 5) with the greater density occurring with sources less than 20 mg cm^{-2}. The densities modeled included the range from 0.6 to 1.0 g cm^{-3}.

Table 4-8. Material descriptions and measured densities.

Description	Material	Density g cm^{-3}	Uncertainty (1S) g cm^{-3}	Basis
Ring and disk mount	Nylon	1.1049	0.0096	Measured mass and dimensions, n=10
Mylar film	Polyethylene terepthalate	1.35	0.02	Measured 208 cm length 3.79 cm wide and weighed
Filter	Polyethersulfone	0.295	0.003	Replicate measurement of thickness for set of five filters and weighed.
Window	Gold on hydrocarbon substrate	1.8	0.4	Manufacturer's specification for total mass per unit area and measured mass per unit area of gold.
Sample precipitate	$SrCO_3$	Range 0.6 to 0.8	0.07 to 0.04, respectively	Measured mass and thickness

4.2.3 Energy binning

MCNP by default uses a "bin-centered" treatment for assigning electrons to energy bins. This approach was used to assign electron energies to the interval $E_n > E > E_{n+1}$ in a way that corresponds to the midpoints of energy groups for straggling losses estimated by MCNP at the beginning of each model run. The result is a small but systematic bias as discussed by Schaart et al. (2002) occurring when electrons do not actually lose sufficient energy before reaching a cell boundary. MCNP provides an option to assign electron energies based on the "nearest-group-boundary" (LANL, 2005, page 2-75) so that an electron is assigned to a group n with $(E_{n-2} + E_n)/2 > E > (E_n + E_{n+1})/2$. The nearest-group-boundary was specified for all MCNP model results.

4.2.4 Beta-particle spectra

The probability distributions for beta-particle spectra are from ICRU Report 56, Appendix D, Table D.1 "Calculated Beta Spectra". Other earlier sources of beta-particle spectra include Murthy (1971) and Dickens (1982). The energy distribution is specified in the MCNP model by a "Source Information" (SI) card indicating the energy and a corresponding "Source Probability" (SP) card indicating the probability for a source defined in a "Source Definition" (SDEF) card.

MCNP provides the source distribution frequency table (MCNP Table 170) as part of the normal output file. This table lists the bin energies, fraction sampled, fraction expected, and ratio of sampled to expected particles based both on number and particle weight.

The expected frequency distribution for particle numbers produced by the “normh” subroutine for histogram distributions given a specified a beta-particle energy spectrum exhibit lower than expected frequencies in the first energy bin for carbon-14, strontium-90, strontium-89, and yttrium-90. Slightly greater frequencies are observed for higher energy bins. For example, the source energy distributions provided in Figures 4-6 for carbon-14 compare the expected frequency from the ICRU 56 spectrum to the expected number after normalization by MCNP.

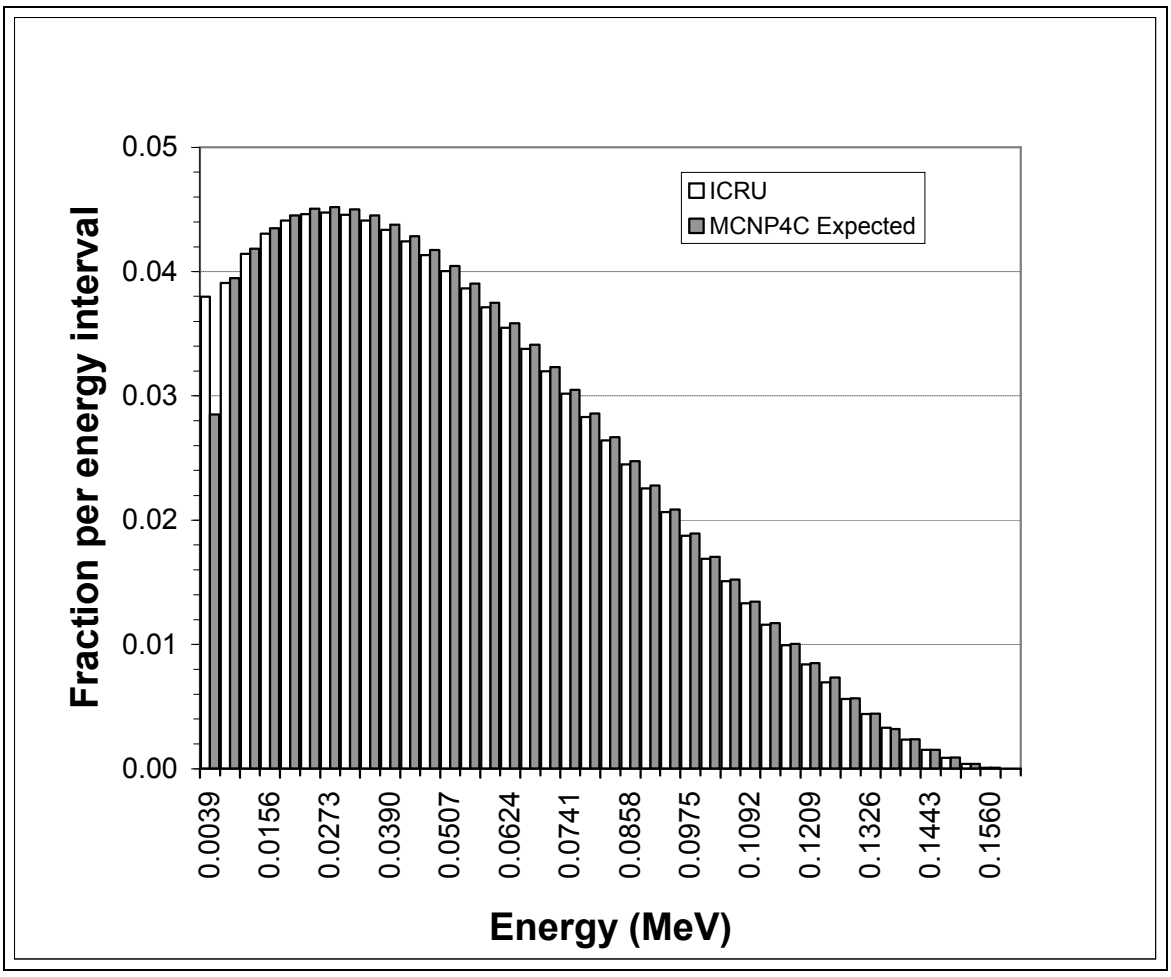

Figure 4-6. Carbon-14 beta-spectrum probabilities specified as a histogram distribution from ICRU 56 and expected values after normalization by MCNP. Bin energies are labeled for every third entry and correspond to entries in Table 3-8 except the second entry is not modified (1.549).

The hypothesis that the probabilities produced by the histogram normalization sub-routine within MCNP compared to the expected frequencies based on the ICRU 56 distribution is rejected for all comparisons made with carbon-14 and yttrium-90 (Table 4-9). Goodness of fit was evaluated by comparing the MCNP sampled frequencies as the observed results of the normalization process for 100,000 initial particles with the ICRU 56 frequencies as the expected values. The observed and expected frequencies were compared for the forty bins comprising the beta-particle spectra. This hypothesis was not rejected when using the histogram distribution with strontium-90 and strontium-89. As the number of particle histories run increases beyond 320,000, however, the goodness of fit statistic for strontium-90 spectra specified as a histogram will exceed the acceptance criteria. The fit remains acceptable for strontium-89 until the number of beta particles sampled exceeds 3.5 million. The hypothesis that the normalized probabilities produced by the histogram normalization sub-routine is rejected when using either maximum bin energies or bin mid-point energies for strontium-90 and strontium-89, as well as for carbon-14 and yttrium-90.

Table 4-9. Chi-square statistics for comparison of MCNP expected values with ICRU 56 specified frequencies for 40 energy bins, N= 100,000.The energy distribution is specified as a histogram. The critical value of $\boldsymbol{X}^2(0.05, 40) = 55.8$.

Radionuclide	Chi-Square Statistic
C-14	247.3
Sr-90	20.3
Sr-89	1.8
Y-90	949.6

MCNP uses one of two normalization algorithms depending on the input distribution specified, “normh” for histogram distributions, and “norma” for probability density functions. The normalization provided for probability density functions was evaluated as

an alternative to the histogram normalization routine and found to be not applicable to beta-particle energy distributions.

The purpose of normalizing the probability distribution is to predetermine a table for sampling the beta-particle particle energy using a uniformly distributed random number between zero and one. The beta-particle particle energy table maps the cumulative probability of a beta particle (between zero and one) to energy by first selecting the appropriate cumulative probability interval and then estimating the beta-particle particle energy by interpolation.

In the following discussion, input energies (E_i) and probabilities (P_i) are denoted with subscripts. The normalized probability calculated by MCNP in the subroutine "normh" is represented with superscripts(P_n^i).The subroutine "normh" evaluates and normalizes distributions specified as a histogram, where probabilities are defined for the energy interval. Specifying a histogram distribution requires that the first probability entered is zero ($P_1 = 0$) with a corresponding E_1 of zero MeV. The second energy bin is adjusted by the subroutine "normh" to remove the probability between $E_1 = 0$ and the minimum beta particle energy that will be tracked, which is 1 keV (see Figure 4-7). Assuming a uniform probability from E_1 (zero) to E_2, this probability is given by

$$P_n^2 = P_2 \bullet (E_2 - 0.001) \qquad \text{Equation 4-2}$$

where:

P_n^2 = normalized probability for the second energy bin;

P_2 = probability for the second interval specified in the source definition;

E_2 = energy for the second energy bin; and

0.001 = MCNP minimum energy cutoff for electrons in keV .

Note that MCNP requires the probability P_1 to be zero for E_1 equal to zero (see Figure 4-7).

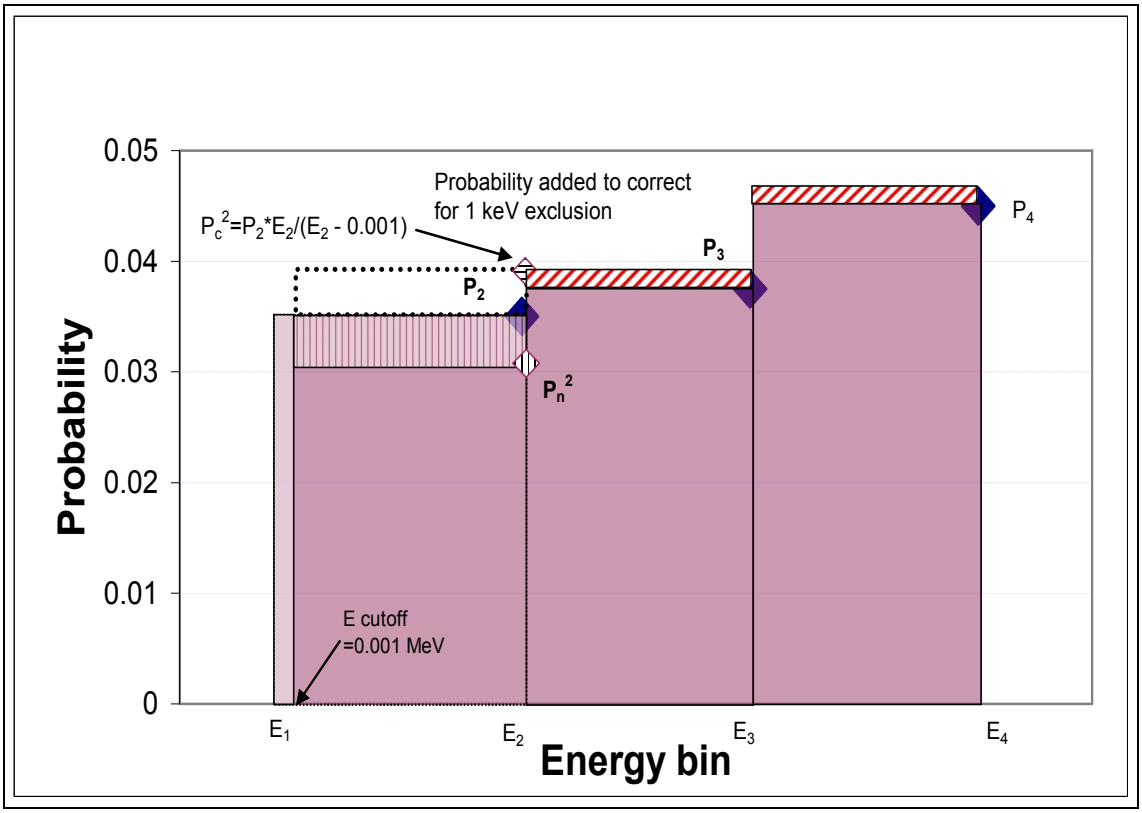

Figure 4-7. Graphical representation of normalization by MCNP subroutine "normh". P_n^2 is the normalized probability, with the subtracted area normalized across the remaining 39 energy bins (diagonal cross hatched area added to E_2 and E_3). P_2 is the probability corresponding to E_2. P_c^2 is the adjusted probability required in the source definition to remove the bias introduced by the MCNP normalization routine.

The correction described in section 3.5.8 by equation 3-24 adds the probability subtracted in the “normh” routine, preserving the probability distribution. Referring to Figure 4-7, increasing the first non-zero probability by the area removed between E_1 (zero) and the energy cutoff at 1 keV results in the correct probability in the normalized beta energy spectrum.

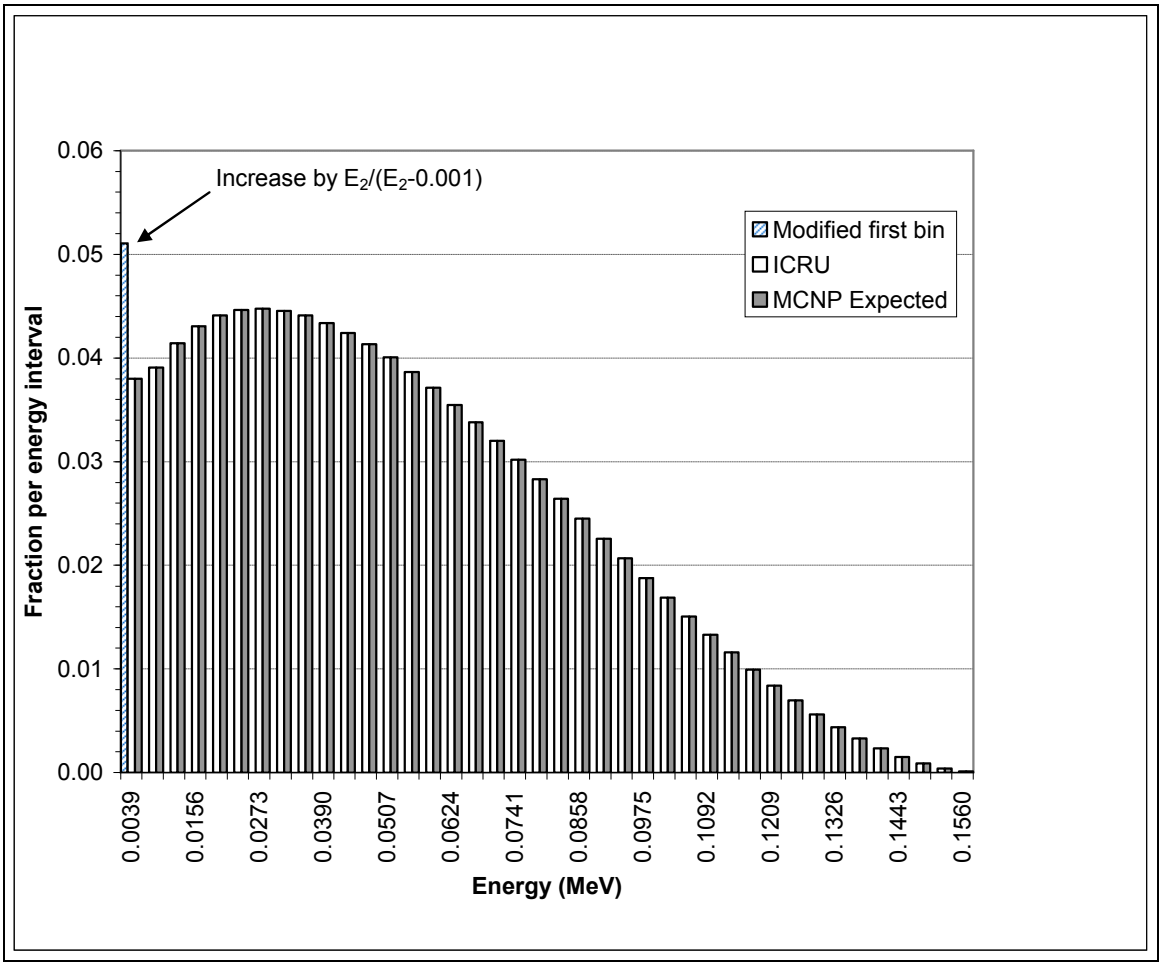

Figure 4-8. Probabilities for carbon-14 based on modifying the probability of the second energy bin for a histogram distribution. Bin energies correspond to entries in Table 3-8 and are labeled for every third entry.

The goodness of fit statistics are provided in Table 4-10. Correcting for the renormalization performed in subroutine “normh” results in no significant differences between the original ICRU 56 distribution and the distribution produced by normalization within MCNP.

Table 4-10. Chi-square goodness of fit for normalized beta-particle histogram distributions with modified beta probability distributions from tables 3-8 through 3-11.

The goodness of fit statistic is estimated for 1 million histories. The critical value of $X^2(0.05, 40) = 55.8$.

Radionuclide	Chi-Square Statistic
Carbon-14	1.97E-04
Strontium-90	9.47E-04
Strontium-89	2.14E-03
Yttrium-90	1.01E-04

The probabilities in the ICRU beta-particle spectra are normalized by multiplying the number of betas per disintegration per unit interval by the bin width in MeV, and dividing by Emax. The sum of the products of the bin energies and the probabilities result in average energies within 2.2% of the values found in ICRU 36 for carbon-14, strontium-90, strontium-89, and yttrium-90, which is within the uncertainties for the calculated beta-ray spectra in ICRU 56 of "…a few percent" (ICRU,1997).

Table 4-11. Average energy estimated by MCNP for 1 million particles and compared to the average energy from ENDF/B-VI.

Radionuclide	Average Energy MCNP5, MeV	Average Energy ENDF/B-VI [6], MeV
Carbon-14	0.0503	0.04945
Strontium-90	0.199	0.1959 (0.0007)
Strontium-89	0.596	0.5833 (0.0012)
Yttrium-90	0.954	0.934 (0.001)

[6] *Average energy from ENDF/B-VI with one sigma uncertainty, from* http://t2.lanl.gov/data/data.html

4.3 Measured results uncertainty – single efficiency estimates

The total propagated uncertainties for efficiency measurements are evaluated following the methods described in section 3.3. The uncertainty components change in importance with the areal thickness so uncertainty budgets are provided for representative examples for sources less than 7 mg cm^{-2}, approximately 14 mg cm^{-2}, and about 32 mg cm^{-2}. The uncertainty budgets for carbon-14 and strontium-89 are based on single efficiency measurements and calculations described in section 3.2.1. The uncertainty budgets for strontium-90 and yttrium-90 are based on sequential efficiency measurements and calculations described in section 3.2.2.

4.3.1 Carbon-14 uncertainty budgets

Carbon-14 efficiency measurements were made for areal thicknesses from 3.5 mg cm^{-2} to 25 mg cm^{-2}. Efficiencies for carbon-14 ranged from 0.107± 0.014 at 3.5 mg cm^{-2} to 0.025 ± 0.002at 24.9 mg cm^{-2}. Total uncertainties are reported with 95% confidence limits for single efficiency measurements. Uncertainty budgets for representative carbon-14 efficiency measurements are provided in Tables 4-12 through 4-14. The parameters defined for estimating the counting efficiency by Equation 3-1 are listed with the contribution to the uncertainty estimate u(i) $E_R(x\rho)$ and the percent of the total variance estimate for the efficiency measurement.

Important parameters, indicated in bold, contributing to the total uncertainty of the efficiency measurements for thin sources, less than 7 mg cm^{-2}, include the carrier concentration (55%) and filter and filter plus precipitate masses (12% each) (see Table 4-12). At 6.9 mg cm^{-2}, the contributions from the uncertainty of the carrier concentration increased to 72% of the total variance and from the concentration of carbon-14 to 9% (cf. Table 4-13). The uncertainty components for the thickest carbon-14 sources, 24.9 mg cm^{-2}, include the carrier concentration (84%), and the concentration of carbon-14 (11%), (Table 4-14).

Table 4-12. Carbon-14 uncertainty budget for source 07/05/04 7- 8, 3.5 mg cm^{-2}, with efficiency 0.106 and total uncertainty of 0.014 (95% CL).

x[i]	$U(E_R(x\rho))$	Units	% of variance
Concentration of radionuclide (C_R)	0.00176	min^{-1} mL^{-1}	7.2 %
Volume of source solution (V_A)	0.0016	mL	5.9 %
Mass of filter plus precipitate (W_{f+p})	0.0023	g	**12.4 %**
Mass of filter (W_f)	0.0023	g	**12.4 %**
Volume of carrier (V_c)	0.0016	mL	5.94 %
Gross count rate (R_g)	0.000463	min^{-1}	0.50%
Background count rate (R_b)	1.68e-05	min^{-1}	0.001 %
Concentration of carrier (C_c)	0.00488	mg mL^{-1}	**55.7 %**
Decay constant (λ_R)	1.58e-07	s^{-1}	0.00 %

Table 4-13. Carbon-14 uncertainty budget for source 07/05/04 4-8, 6.9 mg cm^{-2}, with efficiency 0.072 and total uncertainty 0.008 (95% CL).

x[i]	$u(E_R(x\rho))$	Units	% of variance
Concentration of radionuclide (C_R)	0.00119	min^{-1} mL^{-1}	9.3 %
Volume of source solution (V_A)	0.00108	mL	7.7 %
Mass of filter plus precipitate (W_{f+p})	0.000776	g	4.0 %
Mass of filter (W_f)	0.000776	g	4.0 %
Volume of carrier (V_c)	0.000539	mL	1.9 %
Gross count rate (R_g)	0.000381	min^{-1}	0.96 %
Background count rate (R_b)	1.68e-05	min^{-1}	0.002 %
Concentration of carrier (C_c)	0.0033	mg mL^{-1}	**72.1 %**
Decay constant (λ_R)	1.07e-07	s^{-1}	0.001%

Table 4-14. Carbon-14 uncertainty budget for source 08/13/04 4- 8, 24.9 mg cm^{-2}, with efficiency 0.025 and total uncertainty 0.002 (95% CL).

x[i]	$u(E_R(x\rho))$	Units	% of variance
Concentration of radionuclide (C_R)	0.000405	min^{-1} mL^{-1}	**10.9 %**
Volume of source solution (V_A)	0.000184	mL	2.2 %
Mass of filter plus precipitate (W_{f+p})	7.37e-05	g	0.36 %
Mass of filter (W_f)	7.37e-05	g	0.36 %
Volume of carrier (V_c)	7.36e-05	mL	0.36 %
Gross count rate (R_g)	0.000155	min^{-1}	1.6%
Background count rate (R_b)	8.17e-06	min^{-1}	0.004 %
Concentration of carrier (C_c)	0.00113	mg mL^{-1}	**84.2 %**
Decay constant (λ_R)	3.64e-08	s^{-1}	0.000 %

4.3.2 Strontium-89 uncertainty budgets

Strontium-89 efficiency measurements were made for areal thicknesses from 5.7 mg cm^{-2} to 31.4 mg cm^{-2}. Efficiencies for strontium-89 ranged from 0.495 ± 0.022 at 5.7 mg cm^{-2} to 0.438 ± 0.029 at 31.4 mg cm^{-2}. Total uncertainties are reported with 95% confidence limits for single efficiency measurements. Uncertainty budgets for strontium-89 efficiency measurements are provided in Tables 4-15 through 4-17.

The parameters defined for estimating the counting efficiency by Equation 3-1 are listed with the contribution to the uncertainty estimate u(i) $E_R(x\rho)$ and the percent of the total variance estimate for the efficiency measurement. Important parameters, indicated in bold, contributing to the total uncertainty of the efficiency measurements for thin sources, less than 10 mg cm^{-2}, include the filter and filter plus precipitate masses (31.9% each), volume of carrier (10.8%), and the concentration of the carrier (10.1%). These four parameters account for approximately 85% of the uncertainty of the efficiency estimate. Table A-6 shows relative uncertainties for efficiency estimates ranging from 2 to 4 percent in calibration standards with low areal thicknesses. One limitation in the strontium-89 efficiency measurements is the increasing uncertainty of the radionuclide concentration as the strontium-89 decays with a 50.53 day half-life. The data sets with greater uncertainties were made from radionuclide solutions with lower activity and a subsequent set produced on April 15, 1999 were made with greater activity from a new standard (Table 4-17).

Table 4-15. Strontium-89 uncertainty budget for source 04/15/99 1-8, 6.0 mg cm^{-2}, with efficiency 0.480 and total uncertainty 0.022 (95% CL).

x[i]	$u(E_R(x\rho))$	Units	% of variance
Concentration of radionuclide (C_R)	0.003	min^{-1} mL^{-1}	8.065%
Volume of source solution (V_A)	1.86e-04	mL	0.031 %
Mass of filter plus precipitate (W_{f+p})	0.00596	g	**31.91 %**
Mass of filter (W_f)	0.00596	g	**31.91%**
Volume of carrier (V_c)	0.00347	mL	**10.84 %**
Gross count rate (R_g)	0.00266	min^{-1}	6.36 %
Background count rate (R_b)	0.000131	min^{-1}	0.015 %
Concentration of carrier (C_c)	0.00336	mg mL^{-1}	**10.12** %
Decay constant (λ_R)	0.000917	s^{-1}	0.756 %

Approximately 86% of the uncertainty for sources of uncertainty for intermediate areal thickness, between 10 and 20 mg cm^{-2} are contributed by the uncertainty of the carrier concentration, radionuclide concentration, volume of source solution, and the gross count rate. Efficiency measurements made with lower activity standards due to decay of strontium-89 have increased uncertainty from the uncertainty of the activity.

Table 4-16. Strontium-89 uncertainty budget for source 03/28/99 5-8, 18.5 mg cm^{-2}, with efficiency 0.453 and total uncertainty 0.012 (95% CL).

x[i]	$u(E_R(x\rho))$	Units	% of variance
Concentration of radionuclide (C_R)	0.00283	min^{-1} mL^{-1}	**20.6 %**
Volume of source solution (V_A)	0.00269	mL	**18.7 %**
Mass of filter plus precipitate (W_{f+p})	0.00184	g	8.72 %
Mass of filter (W_f)	0.00184	g	8.72 %
Volume of carrier (V_c)	0.00148	mL	5.64 %
Gross count rate (R_g)	0.00202	min^{-1}	**10.5 %**
Background count rate (R_b)	8.12E-05	min^{-1}	0.017%
Concentration of carrier (C_c)	0.00317	mg mL^{-1}	**25.9 %**
Decay constant (λ_R)	0.000652	s^{-1}	1.10 %

Approximately 86% of the uncertainties for sources of areal thickness greater than 20 mg cm^{-2} results from use of a solution with radionuclide concentration with relatively low activity of 825 min^{-1} mL^{-1}.

Table 4-17. Strontium-89 uncertainty budget for source 03/19/99 5-8, 31.4 mg cm^{-2}, with efficiency 0.438 and total uncertainty 0.029 (95% CL).

x[i]	u($E_R(x\rho)$)	Units	% of variance
Concentration of radionuclide (C_R)	0.0138	min^{-1} mL^{-1}	**85.8 %**
Volume of source solution (V_A)	7.0e-05	mL	0.002 %
Mass of filter plus precipitate (W_{f+p})	0.00104	g	0.49 %
Mass of filter (W_f)	0.00104	g	0.49 %
Volume of carrier (V_c)	0.000919	mL	0.38 %
Gross count rate (R_g)	0.00434	min^{-1}	8.50 %
Background count rate (R_b)	0.00038	min^{-1}	0.065 %
Concentration of carrier (C_c)	0.00306	mg mL^{-1}	4.22 %
Decay constant (λ_R)	0.000439	s^{-1}	0.087 %

4.4 Measured results uncertainty – equilibrium efficiency estimates

Source counting efficiencies for strontium-90 and yttrium-90 are estimated from the change in counting rate as the yttrium-90 daughter count rate increases due to the decay of strontium-90. The parameters for estimating the counting efficiency by Equation 3-8 are listed in the uncertainty budgets with the contribution to the uncertainty estimate u(i) E_r and the percent of the total variance estimate for the efficiency measurement.

4.4.1 Strontium-90 uncertainty budgets

Strontium-90 efficiency measurements were made for areal thicknesses from 2.9 mg cm^{-2} to 33.3 mg cm^{-2}. Efficiencies for strontium-90 ranged from 0.403 ± 0.018 at 2.9 mg cm^{-2} to 0.237 ± 0.006 at 33.3 mg cm^{-2}. Total uncertainties are reported with 95% confidence limits for single efficiency measurements. Parameters affecting the total uncertainty of the efficiency measurements varied with areal thickness and are provided in Tables 4-18 through 4-20.

The largest contribution to the variance of sources from 2.9 to 7.7 results from measuring the small difference between the mass of the filter and filter plus precipitate, with each measurement contributing 31% to the total variance. The two mass measurements, combined with the concentration of strontium-90 (19%), the carrier volume (11%) account for 91.7% of the combined variance (see Table 4-18).

Table 4-18. Strontium-90 uncertainty budget for source 11/11/01 6 - 8, 3.0 mg cm^{-2}, with efficiency 0.407 and total uncertainty 0.018 (95%CL).

x[i]	$u(E_R(x\rho)$	Units	% of variance
Gross count rate, first count(R_{g1})	0.00248	min^{-1}	1.802 %
Background count rate, first count (R_{b1})	0.000113	min^{-1}	0.004 %
Gross Count rate, second count (R_{g2})	0.000274	min^{-1}	0.022 %
Background count rate second count (R_{b2})	8.55e-06	min^{-1}	0.000 %
Concentration of radionuclide (C_R)	0.00805	min^{-1} mL^{-1}	**19.012 %**
Volume of source solution (V_R)	0.00246	mL	1.776 %
Mass of filter plus precipitate (W_{f+p})	0.0102	g	**30.839 %**
Mass of filter (W_f)	0.0102	g	**30.839 %**
Volume of carrier (V_c)	0.00615	mL	**11.102 %**
Concentration of carrier (C_c)	0.00396	mg $SrCO_3$ mL^{-1}	4.596 %
Decay constant Y-90 ($\lambda_{Y\text{-}90}$)	0.000138	min^{-1}	0.006 %
Decay constant Sr-90($\lambda_{Sr\text{-}90}$)	9.01e-05	min^{-1}	0.002 %

At intermediate areal thicknesses for sources from 10 to 20 mg cm^{-2} the concentration of strontium-90 (60%), and the carrier concentration (15%) contributed to 75% of the total efficiency variance (Table 4-19).

Table 4-19. Strontium-90 uncertainty budget for source 09/03/01 8- 8, 14.2 mg cm^{-2}, with efficiency 0.318 and total uncertainty 0.008 (95%CL).

x[i]	$u(E_R(x\rho))$	Units	% of variance
Gross count rate, first count(R_{g1})	0.00233	min^{-1}	8.50 %
Background count rate, first count (R_{b1})	10.00	min^{-1}	0.023 %
Gross Count rate, second count (R_{g2})	0.000327	min^{-1}	0.167 %
Background count rate second count (R_{b2})	1.13e-05	min^{-1}	0.000 %
Concentration of radionuclide (C_R)	0.00623	min^{-1} mL^{-1}	**60.7 %**
Volume of source solution (V_R)	0.00191	mL	5.67 %
Mass of filter plus precipitate (W_{f+p})	0.00168	g	4.39%
Mass of filter (W_f)	0.00168	g	4.39 %
Volume of carrier (V_c)	0.000953	mL	1.42 %
Concentration of carrier (C_c)	0.00306	mg $SrCO_3$ mL^{-1}	**14.68 %**
Decay constant Y-90 ($\lambda_{Y\text{-}90}$)	0.000154	min^{-1}	0.037 %
Decay constant Sr-90($\lambda_{Sr\text{-}90}$)	6.68e-05	min^{-1}	0.007 %

In thick sources greater than 30 mg cm^{-2}, the concentration of strontium-90 (64%), the carrier concentration (15%), and the counting uncertainty for the first source count (12%) contributed to 91% of the variance (Table 4-20).

Table 4-20. Strontium-90 uncertainty budget for source 09/07/01 8-8, 33.3 mg cm^{-2}, with efficiency 0.237 and total uncertainty 0.006 (95%CL).

x[i]	$u(E_R(x\rho))$	Units	% of variance
Gross count rate, first count(R_{g1})	0.00206	min^{-1}	**12.46 %**
Background count rate, first count (R_{b1})	0.000117	min^{-1}	0.040 %
Gross Count rate, second count (R_{g2})	0.000345	min^{-1}	0.35 %
Background count rate second count (R_{b2})	1.23e-05	min^{-1}	0.000 %
Concentration of radionuclide (C_R)	0.00466	min^{-1} mL^{-1}	**63.7%**
Volume of source solution (V_R)	0.00142	mL	5.96%
Mass of filter plus precipitate (W_{f+p})	0.000532	g	0.83 %
Mass of filter (W_f)	0.000532	g	0.83 %
Volume of carrier (V_c)	0.000316	mL	0.29%
Concentration of carrier (C_c)	0.00229	mg $SrCO_3$ mL^{-1}	**15.4 %**
Decay constant Y-90 ($\lambda_{Y\text{-}90}$)	0.000175	min^{-1}	0.090 %
Decay constant Sr-90($\lambda_{Sr\text{-}90}$)	5e-05	min^{-1}	0.007 %

4.4.2 Yttrium-90 uncertainty budgets

Yttrium-90 efficiency measurements were made for areal thicknesses from 2.9 mg cm^{-2} to 33.3 mg cm^{-2}. Efficiencies for Yttrium-90 ranged from 0.542 ± 0.024 at 2.9 mg cm^{-2} to 0.505 ± 0.012 at 33.3 mg cm^{-2}. Total uncertainties are reported with 95% confidence limits for single efficiency measurements. Parameters affecting the total uncertainty of the efficiency measurements varied with areal thickness and are provided in Tables 4-21 through 4-23.

At low areal thicknesses, sources from 2.9 to 7.7 mg cm^{-2}, the uncertainties due to measuring the mass of the filter and filter plus precipitate contribute 30% each, respectively. The remaining parameters contributed 3% to the total uncertainty (Table 4-21).

Table 4-21. Yttrium-90 uncertainty budget for source 11/11/01 6- 8, 3.0 mg cm^{-2}, with efficiency 0.533 and total uncertainty 0.024 (95%CL).

x[i]	$u(E_R(x\rho))$	Units	% of variance
Gross count rate, first count(R_{g1})	0.00249	min^{-1}	0.98 %
Background count rate, first count (R_{b1})	0.000113	min^{-1}	0.002 %
Gross Count rate, second count (R_{g2})	0.00364	min^{-1}	2.08 %
Background count rate second count (R_{b2})	0.000113	min^{-1}	0.002 %
Concentration of radionuclide (C_R)	0.0109	min^{-1} mL^{-1}	**18.8** %
Volume of source solution (V_R)	0.00333	mL	1.75%
Mass of filter plus precipitate (W_{f+p})	0.0139	g	**30.4%**
Mass of filter (W_f)	0.0139	g	**30.4%**
Volume of carrier (V_c)	0.00833	mL	**11.0%**
Concentration of carrier (C_c)	0.00536	mg $SrCO_3$ mL^{-1}	4.54 %
Decay constant Y-90 ($\lambda_{Y\text{-}90}$)	7.63e-05	min^{-1}	0.001 %
Decay constant Sr-90($\lambda_{Sr\text{-}90}$)	0.000122	min^{-1}	0.002 %

At intermediate areal thicknesses for sources from 10 to 20 mg cm^{-2} the concentration of strontium-90 (60%), and the carrier concentration (14%), contributed to 74% of the total efficiency variance (Table 4-22).

Table 4-22. Yttrium-90 uncertainty budget for source 09/03/01 8- 8, 14.2 mg cm^{-2}, with efficiency 0.519 and total uncertainty 0.013 (95%CL).

x[i]	$u(E_R(x\rho))$	Units	% of variance
Gross count rate, first count(R_{g1})	0.00237	min^{-1}	3.22 %
Background count rate, first count (R_{b1})	0.000122	min^{-1}	0.009 %
Gross Count rate, second count (R_{g2})	0.00356	min^{-1}	7.28 %
Background count rate second count (R_{b2})	0.000122	min^{-1}	0.009 %
Concentration of radionuclide ($_{CR}$)	0.0102	min^{-1} mL^{-1}	**59.5 %**
Volume of source solution (V_R)	0.00311	mL	5.60 %
Mass of filter plus precipitate (W_{f+p})	0.00274	g	4.31%
Mass of filter (W_f)	0.00274	g	4.31 %
Volume of carrier (V_c)	0.00155	mL	1.39 %
Concentration of carrier (C_c)	0.005	mg $SrCO_3$ mL^{-1}	**14.4 %**
Decay constant Y-90 ($\lambda_{Y\text{-}90}$)	5.08e-05	min^{-1}	0.001 %
Decay constant Sr-90($\lambda_{Sr\text{-}90}$)	0.000109	min^{-1}	0.007 %

Significant contributors to uncertainty for thick sources greater than 30 mg cm^{-2} include the concentration of strontium-90 (66%), and the carrier concentration (16%), accounting for 82% of the total variance (Table 4-23).

Table 4-23. Yttrium-90 uncertainty budget for source 09/07/01 8- 8, 33.3 mg cm^{-2}, with efficiency 0.505 and total uncertainty 0.012 (95%CL).

x[i]	$u(E_R(x\rho))$	Units	% of variance
Gross count rate, first count(R_{g1})	0.00208	min^{-1}	2.888 %
Background count rate, first count (R_{b1})	0.000118	min^{-1}	0.009 %
Gross Count rate, second count (R_{g2})	0.0033	min^{-1}	7.309 %
Background count rate second count (R_{b2})	0.000118	min^{-1}	0.009 %
Concentration of radionuclide ($_{CR}$)	0.0099	min^{-1} mL^{-1}	**65.721 %**
Volume of source solution (V_R)	0.00303	mL	6.140 %
Mass of filter plus precipitate (W_{f+p})	0.00113	g	0.859 %
Mass of filter (W_f)	0.00113	g	0.859 %
Volume of carrier (V_c)	0.000673	mL	0.303 %
Concentration of carrier (C_c)	0.00487	mg $SrCO_3$ mL^{-1}	**15.887 %**
Decay constant Y-90 ($\lambda_{Y\text{-}90}$)	0.000109	min^{-1}	0.008 %
Decay constant Sr-90($\lambda_{Sr\text{-}90}$)	.000106	min^{-1}	0.008 %

4.5 Major contributions to uncertainty budgets

Uncertainty budgets for precipitates vary among the radionuclides and with increasing areal thickness. The largest contribution to the uncertainties for carbon-14 is the concentration of the carrier, with increasing contribution to the uncertainty budget as the areal thickness increases. At low mass area for carbon-14 standards, the small difference in masses of the filter and filter plus precipitate contributes to 25% of the estimated variation, but this contribution becomes minimal above approximately 7 mg cm^{-2}. The contribution from the uncertainty of the radionuclide concentration ranges from 7% to 11%.

The sources of uncertainty for strontium-89 efficiency measurements are greatly affected by the concentration of the radionuclide standard. The contribution from the uncertainty of the radionuclide concentration is minimized when using concentrations above approximately 10,000 min^{-1} mL^{-1}. The primary contributors to the uncertainty budget in these cases are the small differences in masses of the filter and filter plus precipitate for low areal thickness, the uncertainty in the carrier concentration, and the volumetric measurements for the carrier and radionuclide solutions. Uncertainties from small mass differences become insignificant as areal mass increases above approximately 10 mg cm^{-2}.

Strontium-90 and yttrium-90 are dependent measurements and as would be expected the uncertainty budgets are related. For low mass area standard, 3 mg cm^{-2}, the uncertainty of strontium-90/yttrium-90 efficiencies is largely affected by the small difference in masses of the filter and filter plus precipitate with 60% of the estimated variation resulting from these two measurements. The contribution from the masses of the filter and filter plus precipitate becomes small for intermediate 14 mg cm^{-2} and thicker standards. The uncertainty associated with the concentration of the radionuclide increases from 19% for low mass area source of 3 mg cm^{-2} to 60% at 14 mg cm^{-2} and 64% to 66% at 33 mg cm^{-2}.

Chapter 5. Measured efficiencies and Monte Carlo results

This chapter provides the results for measured counting efficiencies and estimates from simulations by the Monte Carlo model for beta particles including carbon-14, strontium-90, strontium-89, and yttrium-90. The measured counting efficiencies are presented with the total expanded uncertainties of the efficiency measurements. Then the estimates from the MCNP model and estimated model uncertainty are provided. The MCNP model results for the energy distribution of electrons and the direction of beta-particle tracks crossing the detector window are presented and demonstrate that the energy and direction of beta particles are a function of the source areal thickness. As a result, parameters for estimating scattering and attenuation by equation 2-1 are correlated. The parameters for equation 2-1 are estimated from simulation results and empirical measurements, providing estimates for the components comprising the counting efficiency for the four radionuclides.

5.1 Measured counting efficiencies

Measured counting efficiencies for carbon-14, strontium-90, strontium-89, and yttrium-90 are presented in order of increasing maximum beta-particle particle energy. The components of the total expanded uncertainties vary with the areal thickness of the source and are summarized in sections 4.3 and 4.4. In addition, measured counting efficiencies are provided for carrier free strontium-89 and strontium-90/yttrium-90 sources.

Self-absorption equations of the form described in equation 2-7 were fit to the efficiency measurements for each radionuclide by minimizing the average bias and the variance of the measured values from the predicted values as described in section 3.4.4. The efficiencies for zero areal thickness, E_0, and self-absorption coefficients that minimize the bias and variance are presented in Table 5-1 for each radionuclide. The self-absorption coefficients in strontium carbonate are presented as the expected value where the bias is minimum, or zero, followed by the range in values where the bias does not differ significantly from zero. Note that the efficiency at zero areal thickness, E_0, differs from the estimate made in section 3.4.3 for the geometrical efficiency of 0.425 due to attenuation and scattering components discussed in section 5.5.1 and 5.5.2 below. The self-absorption equations are plotted in Figures 5-1 through 5-5 as a dashed line.

The standard deviations provided in Table 5-1 are estimates of the variation in the efficiency measurements about the self-absorption equation with the value of the self-absorption coefficient set at the expected value. The bias is less than the variation about the fitted self-absorption equation in all four cases.

Table 5-1. Efficiency and empirical self-absorption coefficients for carbon-14, strontium-89, strontium-90, and yttrium-90 fit to measured efficiencies. Coefficients are provided with estimated range in values. Bias (Equation 3-20) and standard deviation (Equation 3-21) are based on comparison of the fitted curve to the measured efficiencies.

Radionuclide	***Efficiency, E_0***	***Self-absorption coefficient, μ/p ($cm^2\ g^{-1}$)***	***N***	***Bias***	***Standard Deviation (1S)***
Carbon-14	0.174	304 (288 - 320)	25	0.001	0.002
Strontium-90	0.430	44 (38 - 50)	48	0.000	0.010
Strontium-89	0.520	12 (10 – 14)	34	-0.007	0.011
Yttrium-90	0.540	6.6 (5.2 – 7.9)	48	-0.003	0.015

The efficiency at zero areal thickness increases from 0.174 for carbon-14 to 0.540 for yttrium-90 (Table 5-1). The lower efficiency at zero areal thickness for carbon-14 results from attenuation of the lower energy beta particles from carbon-14 by Mylar, air, and the detector window. Scattering and back-scatter of beta particles into the detector volume results in greater counting efficiencies at zero areal thickness than expected from geometrical counting efficiencies for strontium-89 and yttrium-90. As expected, the self-absorption coefficient decreases as the maximum beta-particle energy increases from 0.156 MeV for carbon-14 through 2.28 MeV for yttrium-90.

Carbon-14 efficiency was measured for areal thickness from 3.5 mg cm^{-2} to 25 mg cm^{-2}. Efficiencies for carbon-14 ranged from 0.107 ± 0.014 at 3.5 mg cm^{-2} to 0.025 ± 0.002 at 24.9 mg cm^{-2}. Efficiency values are provided graphically in Figures 5-1 and 5-2 for 25 measurements summarized in Appendix A, Table A-1. The MCNP model estimates are also presented graphically and are not distinguishable from the results provided for the fitted self-absorption equation.

Strontium-90 efficiency was measured for areal thickness from 2.9 mg cm^{-2} to 33.3 mg cm^{-2}. Efficiencies for strontium-90 ranged from 0.403 ± 0.018 at 2.9 mg cm^{-2} to 0.237 ± 0.006 at 33.3 mg cm^{-2}. Efficiency values are provided graphically in Figures 5-3 for 49 measurements summarized in Appendix A, Table A-12. The fitted self-absorption equation is consistently greater than the results from the MCNP model estimates for areal thickness between 5 and 20 mg cm^{-2}, but differs in fractional efficiency by at most 0.007.

Strontium-89 efficiency was measured for areal thickness from 5.7 mg cm^{-2} to 31.4 mg cm^{-2}. Efficiencies for strontium-89 ranged from 0.495 ± 0.022 at 5.7 mg cm^{-2} to 0.438 ±

0.029 at 31.4 mg cm^{-2}. Total uncertainties are 95% confidence limits for single efficiency measurements. Efficiency values for sources prepared with strontium carrier are provided graphically in Figures 5-4 for 34 measurements summarized in Appendix A, Table A-6. The fitted self-absorption equation is consistent with the results from the specific Monte Carlo simulation results. The measured efficiencies in the range of areal thickness between 5.7 and 6.7 mg cm^{-2} are lower by 2 to 3 percent from the fitted self-absorption equation and Monte Carlo simulation results. This is believed to be a bias in the measurements for low areal thickness as both the fitted self-absorption curve and Monte Carlo simulation results are consistent with the measurements without carrier.

Yttrium-90 efficiency was measured for areal thickness from 2.9 mg cm^{-2} to 33.3 mg cm^{-2}. Efficiencies for Yttrium-90 ranged from 0.542 ± 0.024 at 2.9 mg cm^{-2} to 0.505 ± 0.012 at 33.3 mg cm^{-2}. Efficiency values are provided graphically in Figure 5-5 for 49 measurements summarized in Appendix A, Table A-12. The fitted self-absorption equation is consistent with the results from the specific Monte Carlo simulations.

Strontium-89 sources without carrier were counted to measure the efficiency with no self-absorption. Replicate measurements of strontium-89 efficiency from three evaporated sources on filters sealed with acrylic resulted in efficiency estimate of 0.530 ± 0.008 (standard error as 95% confidence limit). The measured efficiencies with no carrier are presented in figure 5-4 for strontium-89. The estimated value from the Monte Carlo simulation for strontium carbonate with areal thickness of 0.1 mg cm^{-2} of 0.531 is in good agreement with the measured value.

Similar measurements were made with strontium-90 sources in equilibrium with yttrium-90 and deposited without carrier. The measurement of counting efficiency for strontium-

90 and yttrium-90 without carrier is complicated by the secular equilibrium reached by these two radionuclides. Assuming the respective efficiencies for strontium-90 and yttrium-90 estimated from the Monte Carlo simulation for the source areal thickness of 0.10 mg cm^{-2} is a lower limit for the efficiency estimate with no self-absorption, the total efficiency is expected to be in the interval 0.986 < efficiency strontium-90+yttrium-90< 1.00, with 0.986 the sum of the efficiencies for strontium-90 (0.438) and yttrium 90 (0.546) at 0.1 mg cm^{-2}, respectively. Five strontium-90 and yttrium-90 sources were prepared without carrier and counted, with measured total efficiency (strontium-90 plus yttrium-90) of 0.999 ± 0.060 (95% confidence limits). Assuming the ratio of the respective efficiencies from the MCNP simulation for source areal thickness of 0.10 mg cm^{-2} for strontium-90 and yttrium-90 are approximately the ratio in the total efficiency measurement, the efficiency for strontium-90 for sources of zero areal thickness is estimated to be 0.445 and for yttrium-90 is estimated to be 0.554. These values are presented in figures 5-3 and 5-5 for strontium-90 and yttrium-90, respectively.

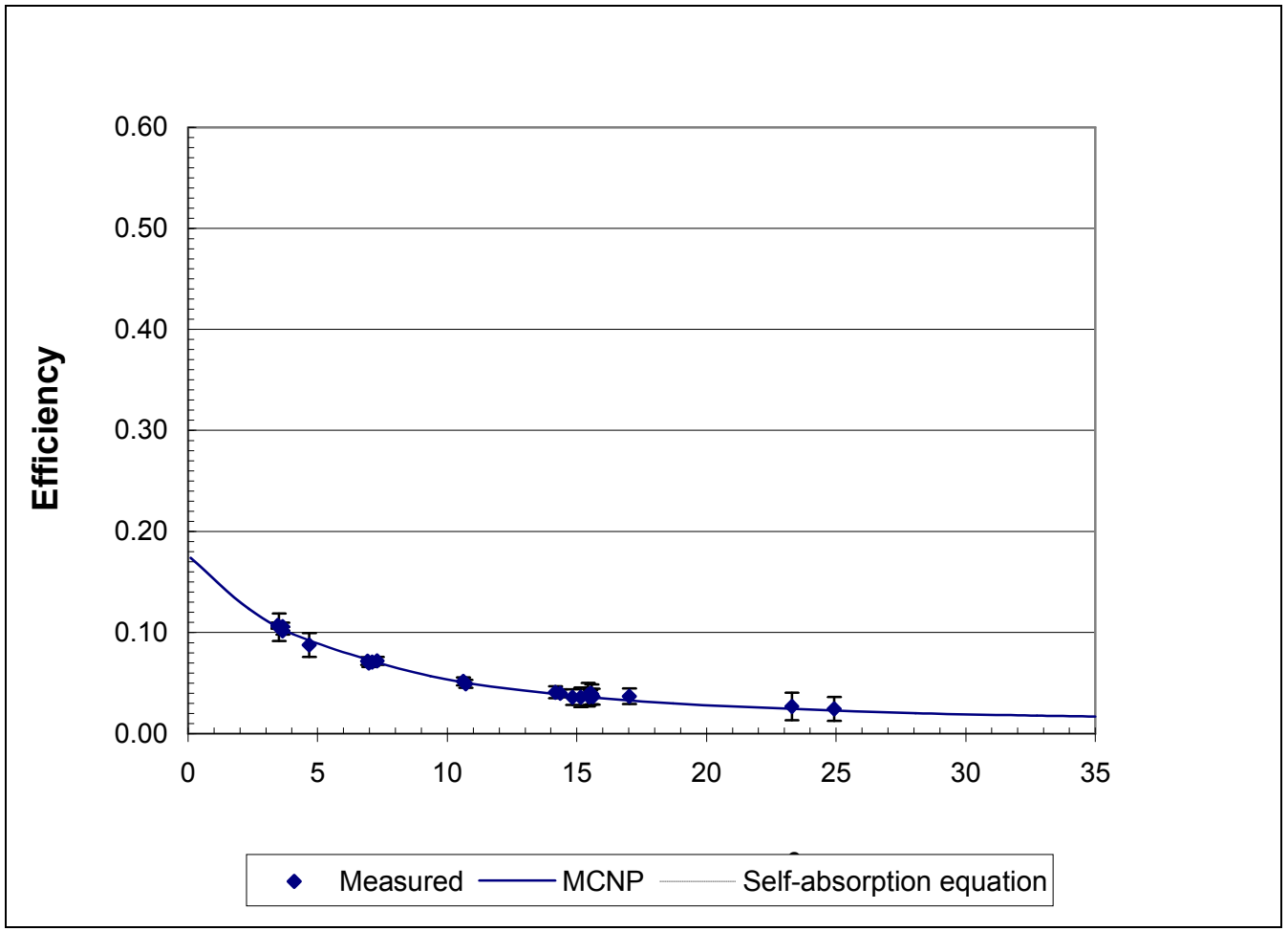

Figure 5-1. Measured counting efficiencies for carbon-14 and simulation estimates of the fraction of beta-particle particle histories interacting within a gas filled detector. Empirical self-absorption equation, the best fit to the measured values, is identical to simulation estimates. Measured efficiencies indicate total measurement uncertainty as 95% confidence intervals.

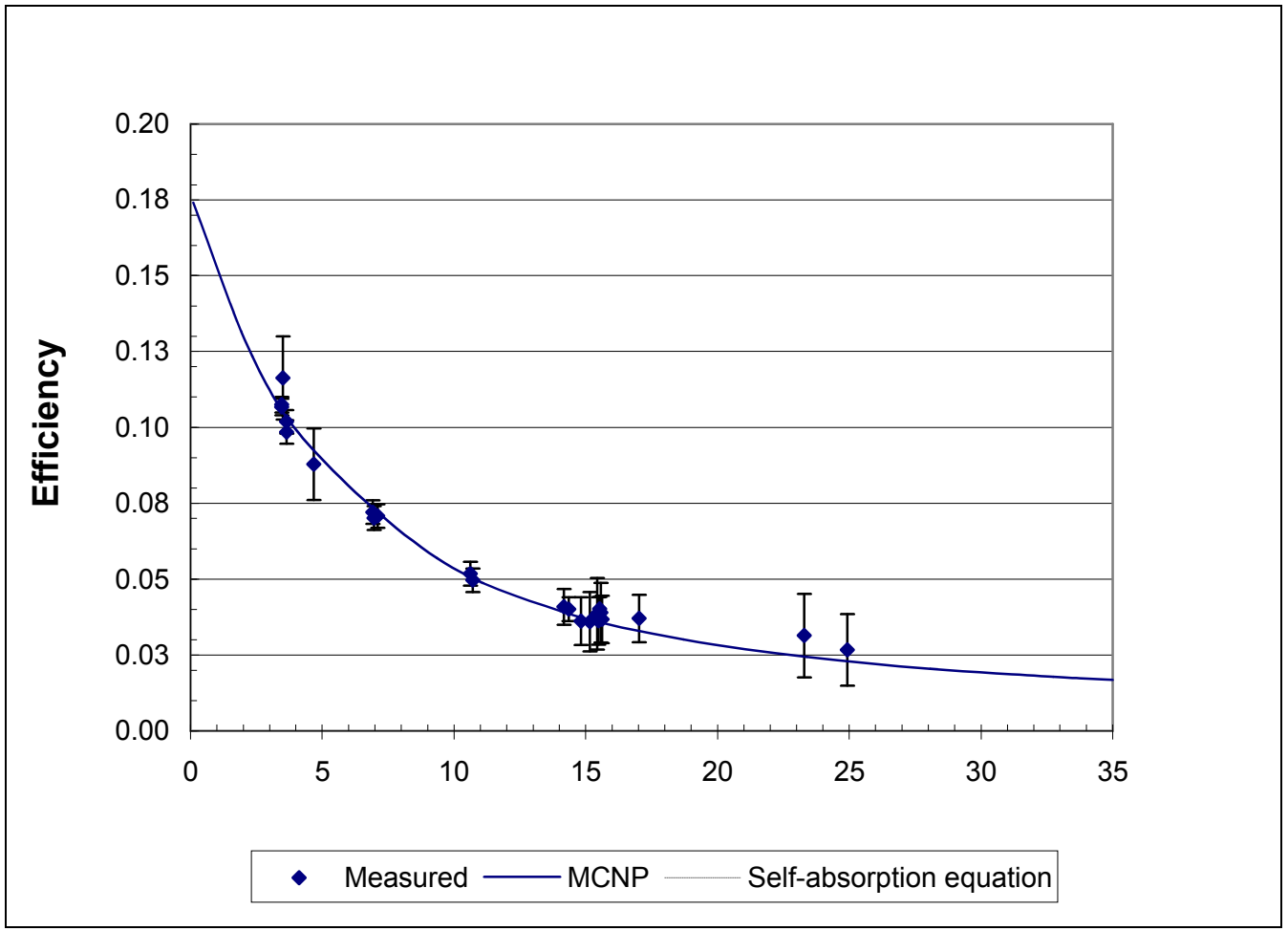

Figure 5-2. Measured counting efficiencies on expanded efficiency scale for carbon-14 and simulation estimates of the fraction of beta-particle particle histories interacting within a gas filled detector. Empirical self-absorption equation, the best fit to the measured values, is identical to simulation estimates. Measured efficiencies indicate total measurement uncertainty as 95% confidence intervals.

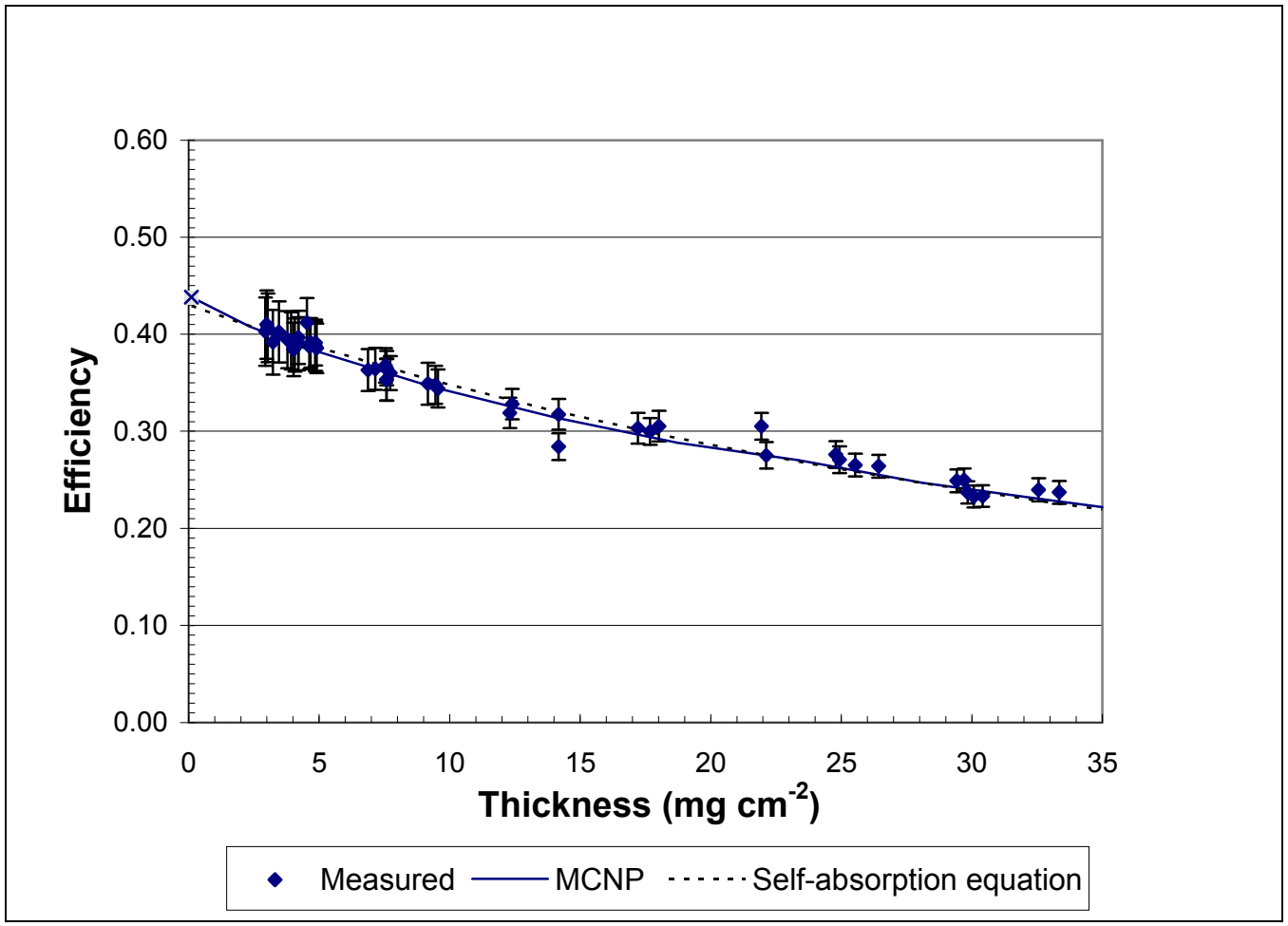

Figure 5-3. Measured counting efficiencies for strontium-90 and simulation estimates of the fraction of beta-particle particle histories interacting within a gas filled detector. Empirical self-absorption equation is the best fit to the measured values. X is the efficiency for a carrier free standard. Measured efficiencies indicate total measurement uncertainty as 95% confidence intervals.

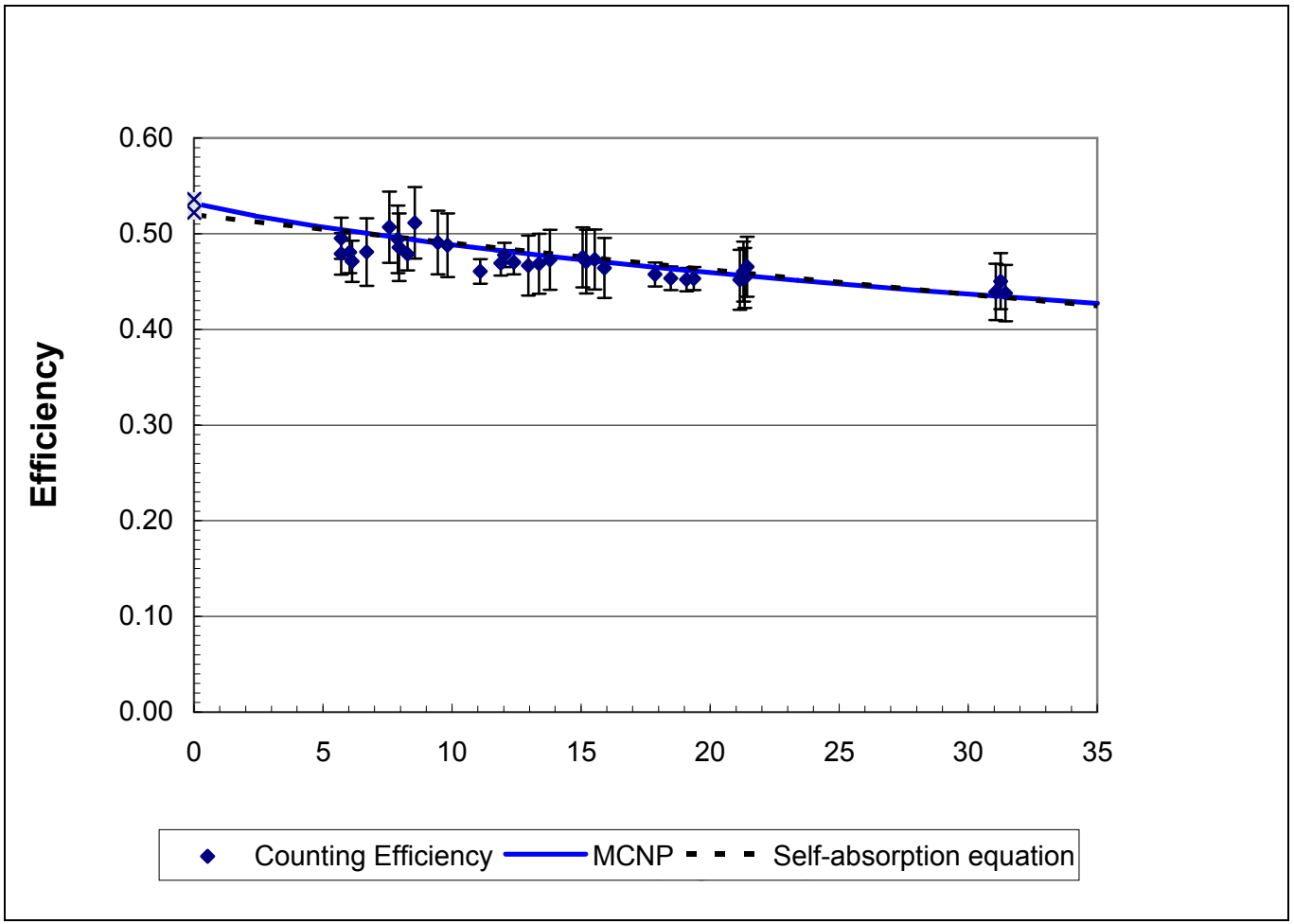

Figure 5-4. Measured counting efficiencies for strontium-89 and simulation estimates of the fraction of beta-particle particle histories interacting within a gas filled detector. Empirical self-absorption equation is the best fit to the measured values. X is the efficiency for a carrier free standard.

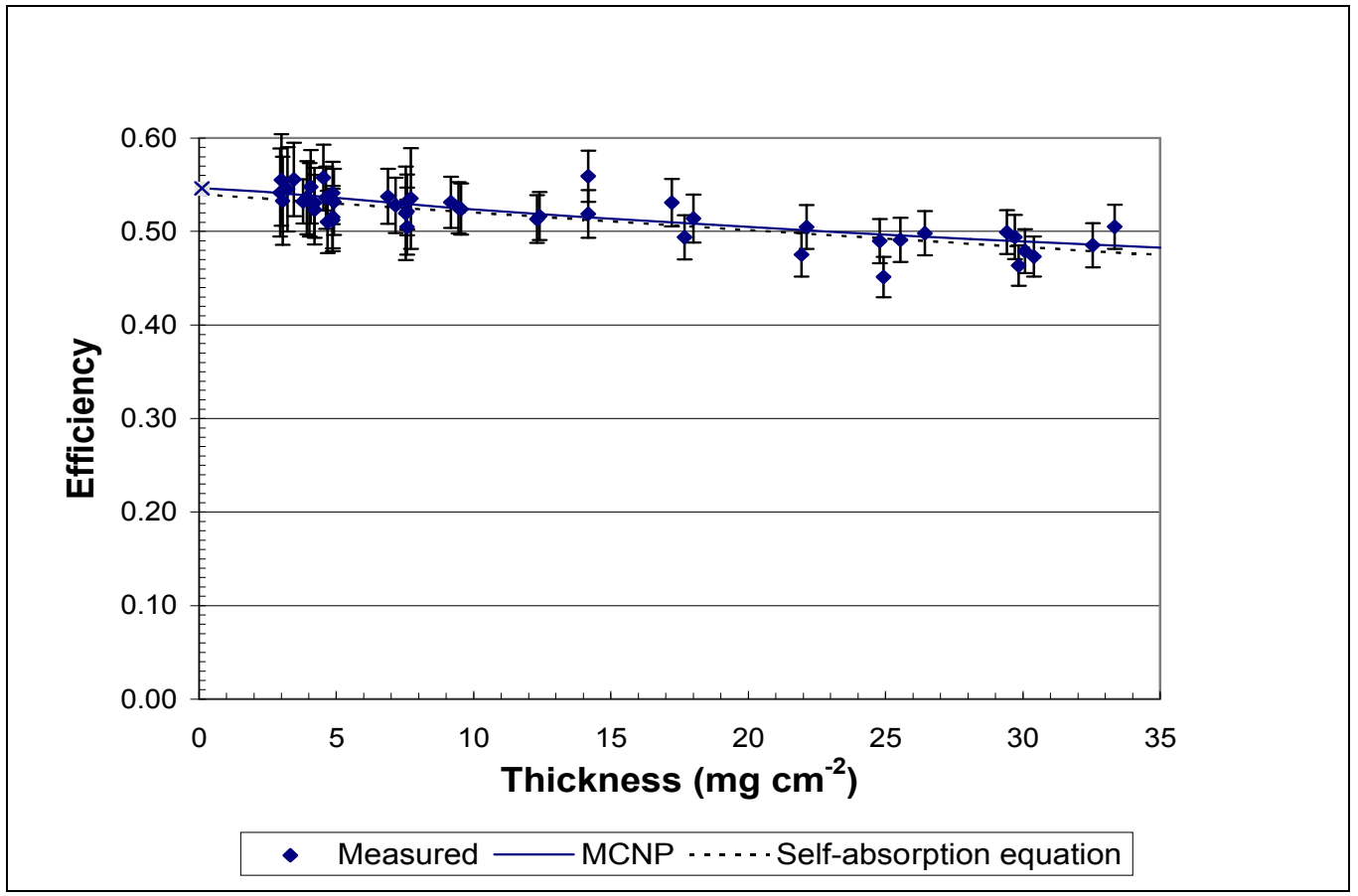

Figure 5-5. Measured counting efficiencies for yttrium-90 and simulation estimates of the fraction of beta particle histories interacting within a gas filled detector. Empirical self-absorption equation is the best fit to the measured values. X is the efficiency for a carrier free standard.

5.2 Efficiencies from the Monte Carlo simulation

The fraction of beta-particle histories interacting within the gas filled detector simulated by the MCNP model described in section 3.5 are presented here and summarized in Table 5-14 for sources ranging in areal thickness from 0.1 mg cm^{-2} to 35.0 mg cm^{-2}. The sensitivity of the model to biases in materials and dimensions are discussed in section 5.3 below.

The Monte Carlo simulation results are provided for model runs as a function of areal thickness with beta particles initially started isotropically in a 4 π geometry, biased 2 π toward the detector volume (direct), or biased 2 π away from the detector volume (indirect or backscattered). Selected simulation results presented graphically for visualizing attenuation by the intervening Mylar, air, and window cells are achieved by setting the importance of these cells to zero so electron interactions are ignored. The geometrical efficiency is only presented graphically in Figure 5-6 for carbon-14. The values corresponding to the 4 π and direction biased estimates are provided in tables 5-2 through 5-13 below. Each table includes the fraction of the pulse height tally entering the detector volume, the fraction of histories that escape without interacting, the fraction below the 0.3 keV energy cutoff, the number of knock-on electrons, and the resulting net fraction of histories interacting in the detector volume.

The fraction interacting for the 4 π models of carbon-14 decreases from 0.17 at 0.1 mg cm^{-2} to less than 0.03 at areal thicknesses greater than 14 mg cm^{-2} (Figure 5-6 and Table 5-2). The electrons initially started 2 π away from the detector provide a small contribution to the fraction of interactions, with the fraction interacting ranging from 0.03

at 0.1 mg cm^{-2} to 0.004 at 35 mg cm^{-2} (Table 5-3). The electrons initially started 2 π toward the plane of the detector entrance provide the dominate contribution to the fraction of interactions, with 0.144 at 0.1 mg cm^{-2} to 0.013 at 35 mg cm^{-2} interacting within the detector volume (Table 5-4). As expected, significant attenuation occurs across the Mylar, air space, and detector window. The counting efficiency varies by a factor of three between 2.3 mg cm^{-2} and 14 mg cm^{-2} and is less than three percent for areal thickness greater than 14 mg cm^{-2}.

The fraction interacting for the 4 π models of strontium-90 decreases from 0.44 at 0.1 mg cm^{-2} to 0.22 at an areal thickness of 35 mg cm^{-2} (Figure 5-7 and Table 5-5). The electrons initially started 2 π away from the detector have sufficient energy for a fraction of beta particles to scatter back into the detector volume, with the fraction of beta particle histories starting away from the detector and interacting ranging from 0.090 at 0.1 mg cm^{-2} to 0.072 at 14 mg cm^{-2} (Table 5-6). As the strontium carbonate areal thickness increases to 35 mg cm^{-2}, the contribution from scattering decreases and the fraction of interaction reaches 0.052. The electrons initially started 2 π toward the plane of the detector entrance result in 0.348 interactions within the detector volume at 0.1 mg cm^{-2} to 0.169 at 35 mg cm^{-2} interacting within the detector volume (Table 5-7).

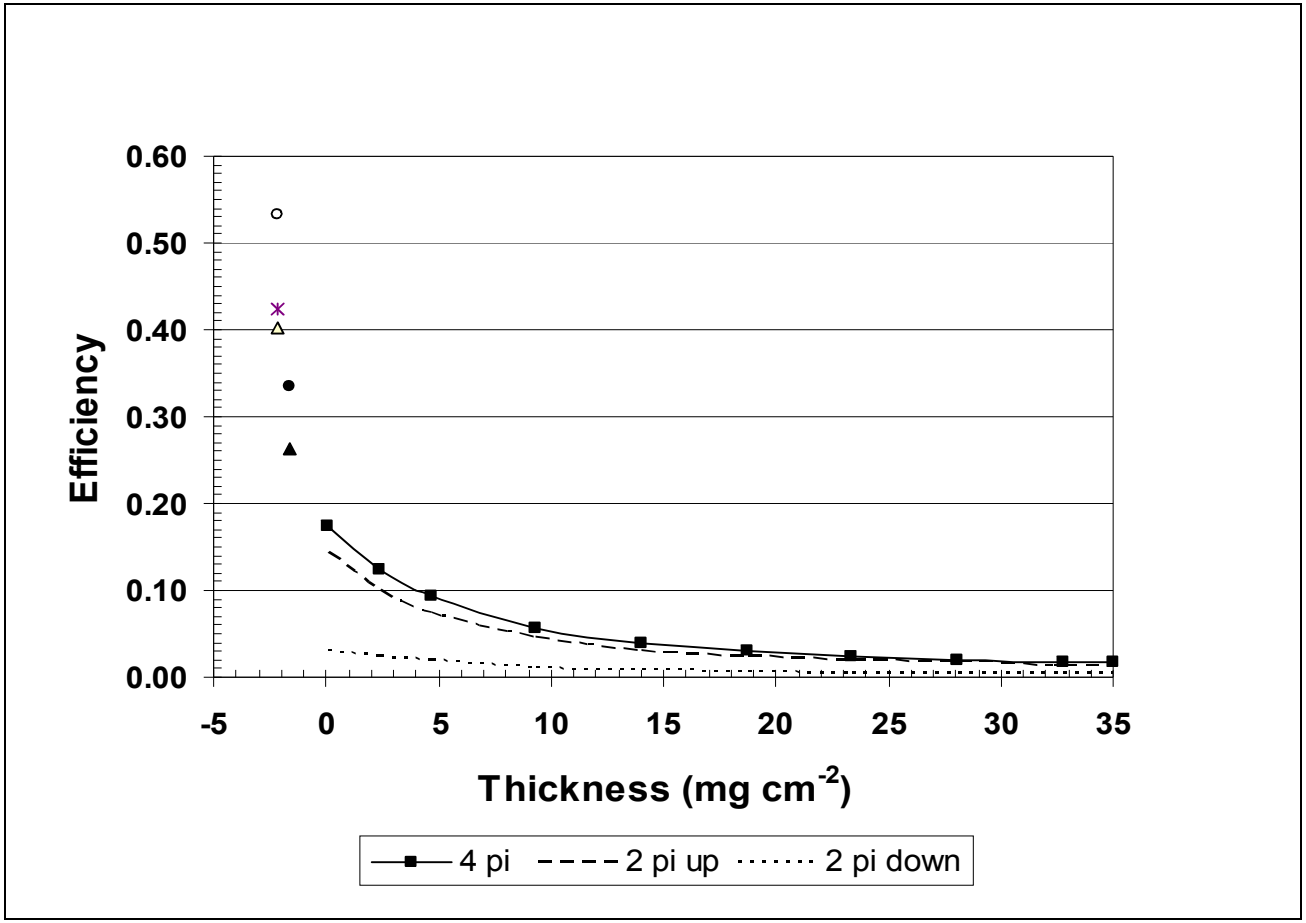

Figure 5-6. Carbon-14 efficiency estimates by MCNP for beta particles emitted in 4 π and 2 π geometries as a function of areal thickness from 0.1 to 35 mg cm^{-2}. Single point estimates of scattering and attenuation for 4 π source with self-absorption and no attenuation (○),and attenuation by window and air (●). Scattering and attenuation components for 2 π source emitting particles toward the detector with no attenuation (∆) and with attenuation by window and air (▲). The geometrical efficiency for the simulation at 0.1 mg cm^{-2} is presented (ж) and will be the same value (0.425) for subsequent radionuclides.

Table 5-2. Model estimates of the fraction of beta particles entering the detector volume from particles emitted isotropically by carbon-14. Fractions are for one million histories and are a function of areal thickness. Knock-on (scattered) electrons range from 0 to 1.97E-06 (0 to 2 per million histories).

Areal thickness $SrCO_3$ (mg cm^{-2})										
Category	0.1	2.3	4.7	9.4	14.0	18.7	23.4	28.1	32.7	35.0
Fraction entering detector	0.174	0.124	0.093	0.057	0.040	0.030	0.024	0.020	0.018	0.017
Escape without interaction	2.25E-04	1.91E-04	1.31E-04	6.91E-05	5.63E-05	3.85E-05	3.36E-05	2.17E-05	1.97E-05	2.07E-05
Below energy cutoff	9.87E-05	6.71E-05	5.23E-05	3.26E-05	2.27E-05	1.28E-05	1.97E-05	1.38E-05	1.28E-05	9.87E-06
Fraction of interactions	0.174	0.123	0.092	0.057	0.040	0.030	0.024	0.020	0.018	0.017

Table 5-3. Model estimates of the fraction of beta particles entering the detector volume by particles from carbon-14 initially emitted 2 pi downward. Fractions are for one million histories and are a function of areal thickness. Knock-on (scattered) electrons range from 6 to 62 per million histories.

Areal thickness $SrCO_3$ (mg cm^{-2})										
Category	0.1	2.3	4.7	9.4	14.0	18.7	23.4	28.1	32.7	35.0
Fraction entering detector	0.030	0.024	0.019	0.012	0.008	0.006	0.005	0.004	0.004	0.004
Escape without interaction	3.95E-06	9.87E-07	1.97E-06	0.00	9.87E-07	9.87E-07	0.00E+00	0.00E+00	9.87E-07	1.18E-05
Below energy cutoff	4.84E-05	3.55E-05	1.88E-05	1.97E-05	9.87E-06	5.92E-06	3.95E-06	4.94E-06	5.92E-06	3.95E-06
Fraction of interactions	0.030	0.024	0.019	0.012	0.008	0.006	0.005	0.004	0.004	0.004

Table 5-4. Model estimates of the fraction of beta particles entering the detector volume by particles from carbon-14 initially emitted 2 pi upward. Fractions are for one million histories and are a function of areal thickness. Knock-on (scattered) electrons range from 0 to 4 per million histories.

	Areal thickness $SrCO_3$ (mg cm^{-2})									
Category	0.1	2.3	4.7	9.4	14.0	18.7	23.4	28.1	32.7	35.0
Fraction entering detector	0.145	0.100	0.074	0.045	0.032	0.024	0.020	0.016	0.014	0.013
Escape without interaction	4.34E-04	2.79E-04	1.98E-04	1.15E-04	8.69E-05	5.43E-05	4.34E-05	3.85E-05	3.55E-05	3.65E-05
Below energy cutoff	1.67E-04	1.11E-04	6.71E-05	5.03E-05	3.06E-05	2.07E-05	1.88E-05	1.88E-05	1.88E-05	5.92E-06
Fraction of interactions	0.144	0.100	0.074	0.045	0.031	0.024	0.019	0.016	0.014	0.013

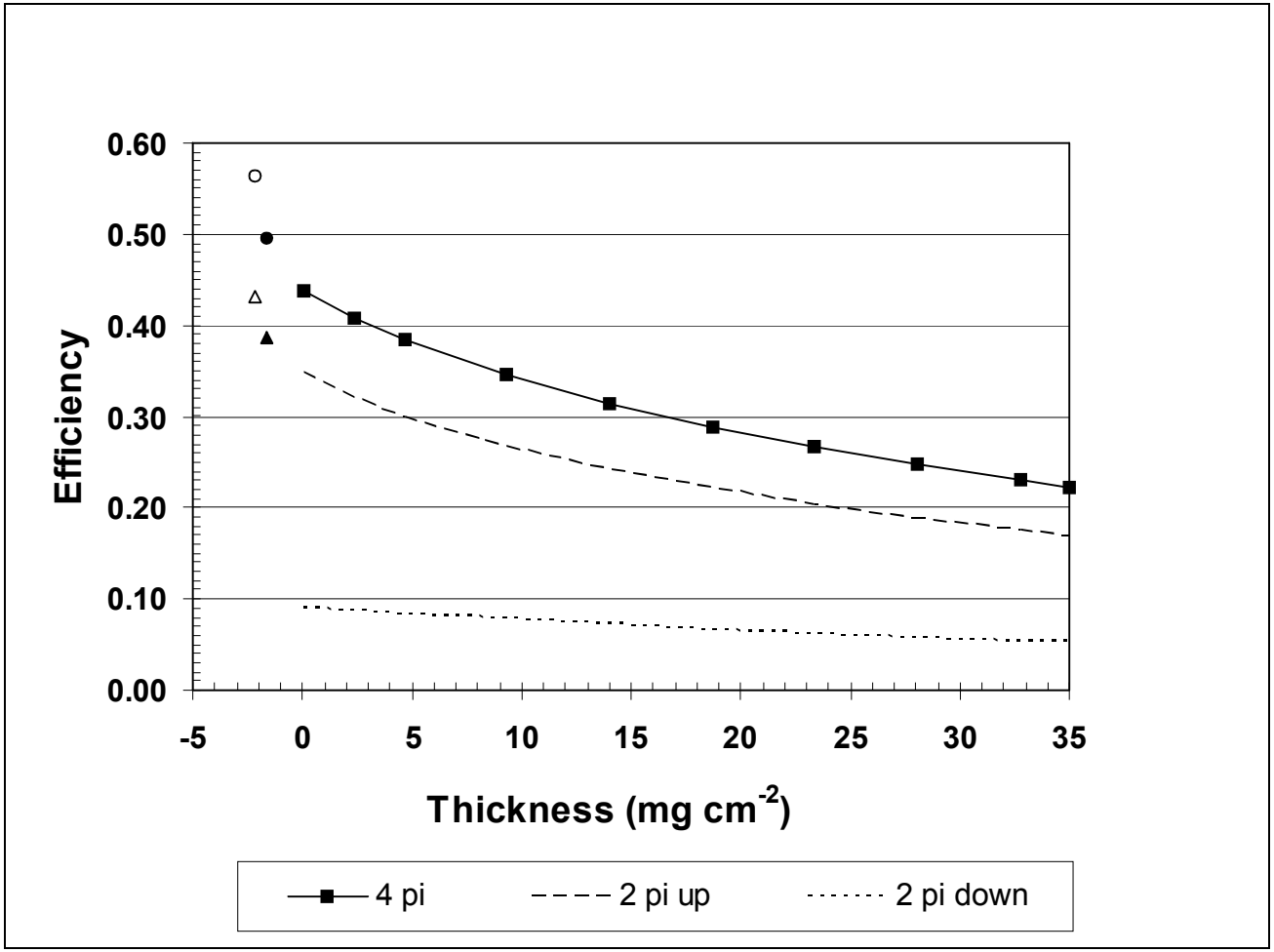

Figure 5-7. Strontium-90 efficiency estimates by MCNP for beta particles emitted in 4 π and 2 π geometries as a function of areal thickness from 0.1 to 35 mg cm-2. Scattering and attenuation components for 4 π source with no attenuation (○) and attenuation by window and air (●). Scattering and attenuation components for 2 π source emitting particles toward the detector with no attenuation (∆) and with attenuation by window and air (▲).

Table 5-5. Model estimates of fraction of beta particles entering the detector volume for particles emitted isotropically by strontium-90. Fractions are for one million histories and are a function of areal thickness. Knock-on (scattered) electrons range from 3 to 22 per million histories.

Areal thickness $SrCO_3$ (mg cm^{-2})										
Category	0.1	2.3	4.7	9.4	14.0	18.7	23.4	28.1	32.7	35.0
Fraction entering detector	0.442	0.411	0.387	0.348	0.317	0.291	0.269	0.249	0.232	0.224
Escape without interaction	3.24E-03	3.05E-03	2.81E-03	2.55E-03	2.40E-03	2.22E-03	2.05E-03	1.84E-03	1.71E-03	1.73E-03
Below energy cutoff	4.97E-04	3.61E-04	3.07E-04	1.90E-04	2.11E-04	2.03E-04	1.71E-04	1.48E-04	1.62E-04	1.42E-04
Fraction of interactions	0.438	0.408	0.384	0.346	0.314	0.288	0.267	0.247	0.230	0.220

Table 5-6. Model estimates of the fraction of beta particles entering the detector volume by particles from strontium-90 initially emitted 2 pi downward. Fractions are for one million histories and are a function of areal thickness. Knock-on (scattered) electrons range from 2 to 9 per million histories.

Areal thickness $SrCO_3$ (mg cm^{-2})										
Category	0.1	2.3	4.7	9.4	14.0	18.7	23.4	28.1	32.7	35.0
Fraction entering detector	0.090	0.088	0.085	0.079	0.072	0.0674	0.063	0.058	0.055	0.053
Escape without interaction	1.13E-03	1.11E-03	1.10E-03	1.02E-03	9.64E-04	8.70E-04	8.87E-04	8.04E-04	7.50E-04	7.89E-04
Below energy cutoff	2.38E-04	1.70E-04	1.71E-04	1.40E-04	9.77E-05	1.02E-04	1.24E-04	8.27E-05	9.17E-05	8.77E-05
Fraction of interactions	0.090	0.087	0.084	0.078	0.072	0.067	0.062	0.058	0.054	0.052

Table 5-7. Model estimates of the fraction of beta particles entering the detector volume by particles from strontium-90 initially emitted 2 pi upward. Fractions are for one million histories and are a function of areal thickness. Knock-on (scattered) electrons range from 5 to 21 per million histories.

Areal thickness $SrCO_3$ (mg cm^{-2})										
Category	0.1	2.3	4.7	9.4	14.0	18.7	23.4	28.1	32.7	35.0
Fraction entering detector	0.351	0.323	0.302	0.269	0.243	0.224	0.205	0.190	0.176	0.171
Escape without interaction	5.38E-03	4.98E-03	4.68E-03	4.07E-03	3.61E-03	3.48E-03	3.09E-03	2.90E-03	2.66E-03	2.55E-03
Below energy cutoff	8.08E-04	5.49E-04	4.80E-04	3.82E-04	3.12E-04	2.75E-04	2.76E-04	2.48E-04	2.07E-04	2.09E-04
Fraction of interactions	0.348	0.320	0.299	0.266	0.241	0.222	0.203	0.188	0.175	0.169

The fraction interacting for the 4 π models of strontium-89 decreases from 0.531 at 0.1 mg cm^{-2} to 0.427 for an areal thickness of 35 mg cm^{-2} (Figure 5-8 and Table 5-8). The electrons initially started 2 π away from the detector contribute fractions from 0.109 at 0.1 mg cm^{-2} to 0.096 at 35 mg cm^{-2} (Table 5-9), with the backscatter component largely unaffected by the areal thickness of the strontium carbonate. The backscatter and scatter increase the fraction of histories recorded within the detector volume relative to the geometrical efficiency. The electrons initially started 2 π toward the plane of the detector entrance result in 0.422 interactions within the detector volume at 0.1 mg cm^{-2} to 0.331 at 35 mg cm^{-2} interacting within the detector volume (Table 5-10).

The fraction interacting for the 4 π models of yttrium-90 decreases from 0.546 at 0.1 mg cm^{-2} to 0.483 at areal thickness of 35 mg cm^{-2} (Figure 5-9 and Table 5-11). The electrons initially started 2 π away from the detector contribute 0.111 at 0.1 mg cm^{-2} to 0.104 at 35 mg cm^{-2} (Table 5-12) with little attenuation of the scattered electrons with increasing areal thickness. The backscatter and scatter increase the fraction of histories recorded within the detector volume relative to the geometrical efficiency. The electrons initially started 2 π toward the plane of the detector entrance result in 0.436 interactions within the detector volume at 0.1 mg cm^{-2} to 0.379 at 35 mg cm^{-2} interacting within the detector volume (Table 5-13).

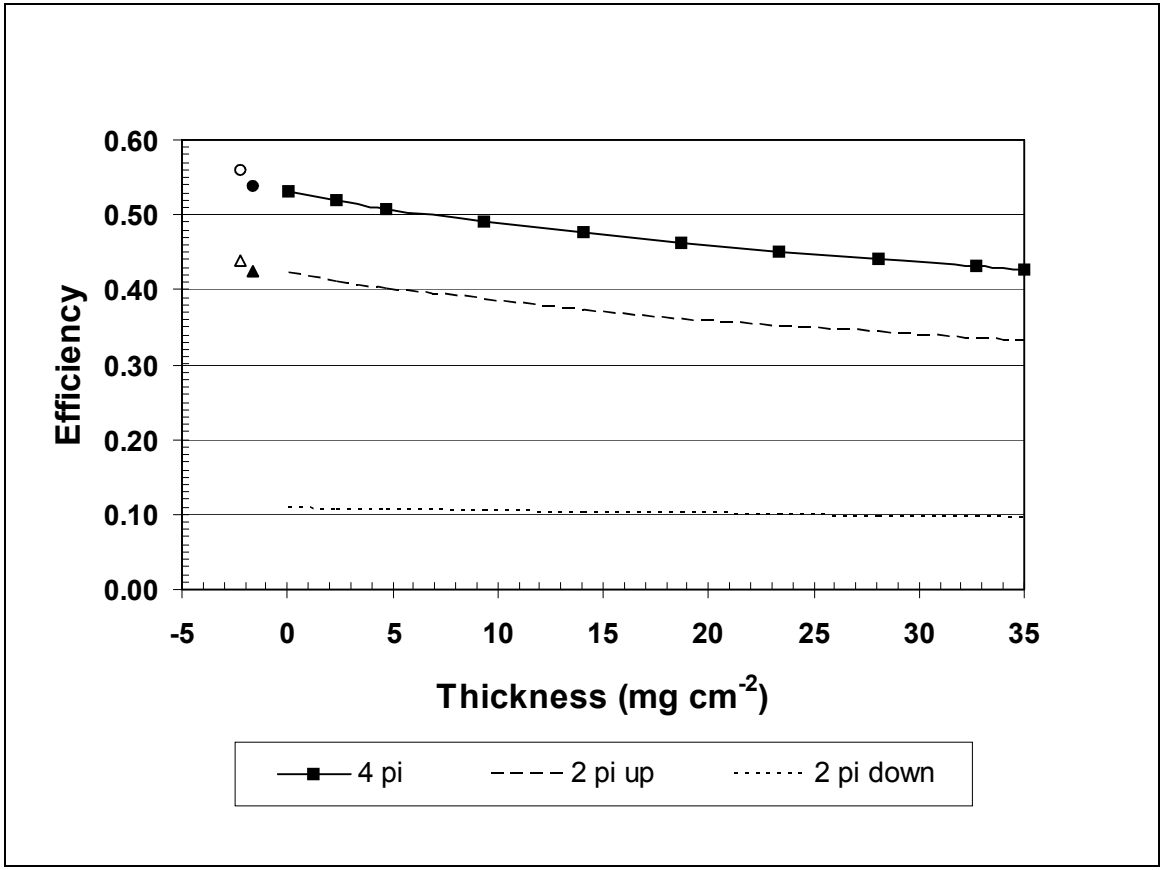

Figure 5-8. Strontium-89 efficiency estimates by MCNP for beta particles emitted in 4 π and 2 π geometries as a function of areal thickness from 0.1 to 35 mg cm^{-2}. Scattering and attenuation components for 4 π source with no attenuation (○) and attenuation by window and air (●). Scattering and attenuation components for 2 π source emitting particles toward the detector with no attenuation (∆) and with attenuation by window and air (▲).

Table 5-8. Model estimates of the fraction of beta particles entering the detector volume for particles emitted isotropically by strontium-89. Fractions are for one million histories and are a function of areal thickness. Knock-on (scattered) electrons range from 19 to 63 per million histories.

	Areal thickness $SrCO_3$ (mg cm^{-2})									
Category	0.1	2.3	4.7	9.4	14.0	18.7	23.4	28.1	32.7	35.0
Fraction entering detector	0.538	0.525	0.514	0.496	0.481	0.468	0.456	0.446	0.436	0.432
Escape without interaction	5.20E-03	5.28E-03	5.04E-03	5.00E-03	4.77E-03	4.63E-03	4.41E-03	4.41E-03	4.22E-03	4.12E-03
Below energy cutoff	1.65E-03	1.19E-03	1.13E-03	9.32E-04	7.47E-04	7.30E-04	6.24E-04	5.96E-04	5.60E-04	5.82E-04
Fraction of interactions	0.531	0.519	0.508	0.490	0.476	0.463	0.451	0.441	0.432	0.427

Table 5-9. Model estimates of the fraction of beta particles entering the detector volume by particles from strontium-89 initially emitted 2 pi downward. Fractions are for one million histories and are a function of areal thickness. Knock-on (scattered) electrons range from 14 to 34 per million histories.

	Areal thickness $SrCO_3$ (mg cm^{-2})									
Category	0.1	2.3	4.7	9.4	14.0	18.7	23.4	28.1	32.7	35.0
Fraction entering detector	0.110	0.109	0.108	0.106	0.104	0.102	0.100	0.099	0.097	0.097
Escape without interaction	2.05E-03	1.99E-03	2.05E-03	2.01E-03	1.99E-03	1.88E-03	1.90E-03	1.90E-03	1.79E-03	1.78E-03
Below energy cutoff	8.81E-04	6.85E-04	5.41E-04	5.15E-04	4.61E-04	4.02E-04	4.30E-04	4.37E-04	4.05E-04	3.61E-04
Fraction of interactions	0.109	0.108	0.107	0.104	0.103	0.101	0.099	0.098	0.096	0.096

Table 5-10. Model estimates of the fraction of beta particles entering the detector volume by particles from strontium-89 initially emitted 2 pi upward. Fractions are for one million histories and are a function of areal thickness. Knock-on (scattered) electrons range from 22 to 91 per million histories.

Areal thickness $SrCO_3$ (mg cm^{-2})										
Category	0.1	2.3	4.7	9.4	14.0	18.7	23.4	28.1	32.7	35.0
Fraction entering detector	0.427	0.416	0.407	0.390	0.377	0.366	0.356	0.347	0.338	0.335
Escape without interaction	8.56E-03	8.24E-03	8.01E-03	7.60E-03	7.47E-03	7.11E-03	6.97E-03	6.71E-03	6.62E-03	6.56E-03
Below energy cutoff	2.45E-03	1.74E-03	1.58E-03	1.24E-03	1.11E-03	9.46E-04	9.18E-04	8.58E-04	8.04E-04	7.73E-04
Fraction of interactions	0.422	0.411	0.402	0.386	0.373	0.362	0.352	0.343	0.335	0.331

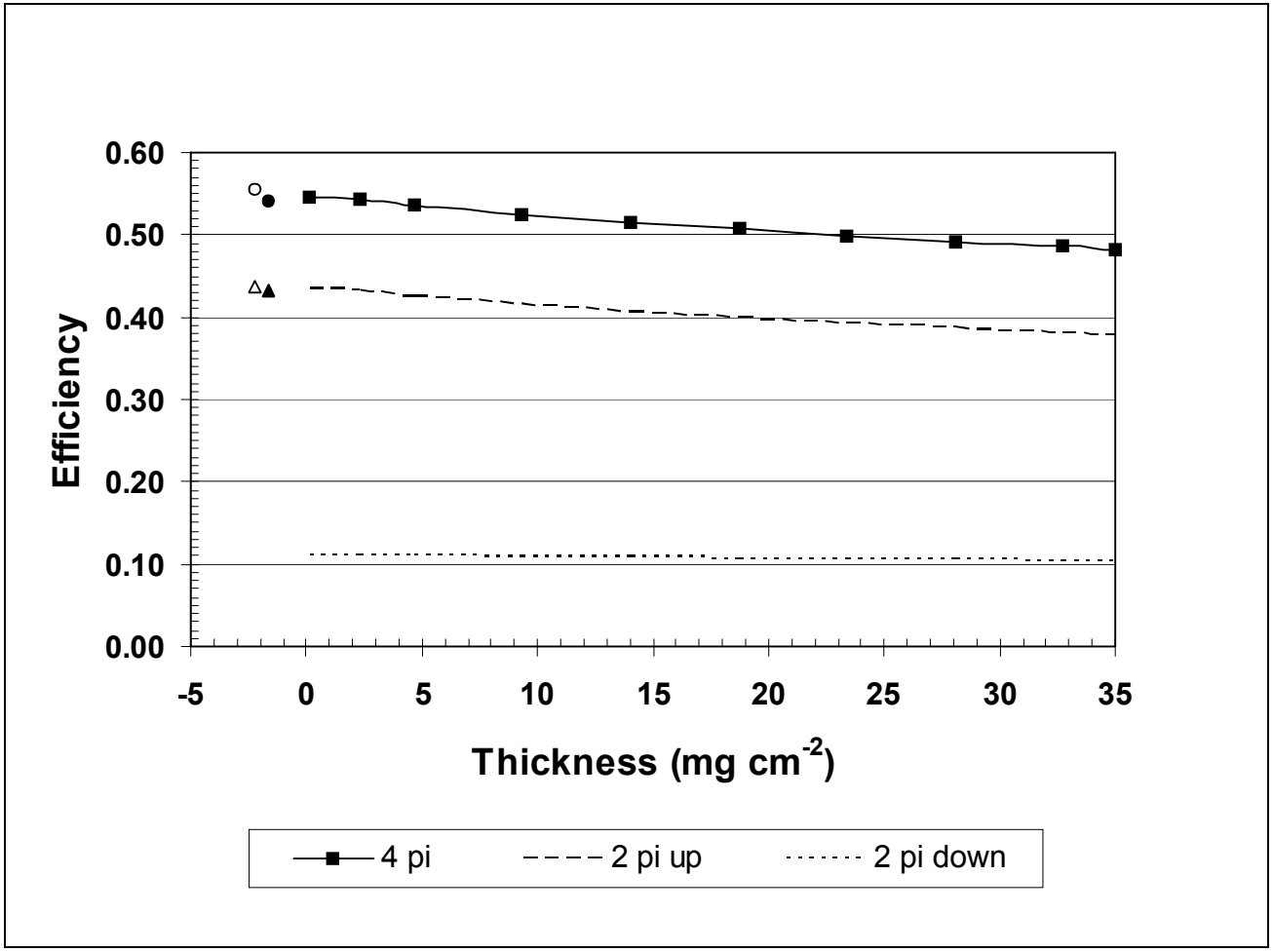

Figure 5-9. Yttrium-90 efficiency estimates by MCNP for beta particles emitted in 4 π and 2 π geometries as a function of areal thickness from 0.1 to 35 mg cm^{-2}. Scattering and attenuation components for 4 π source with no attenuation (○) and attenuation by

window and air (●). Scattering and attenuation components for 2 π source emitting particles toward the detector with no attenuation (∆) and with attenuation by window and air (▲).

Table 5-11. Model estimates of the fraction of beta particles entering the detector volume from particles emitted isotropically by yttrium-90. Fractions are for one million histories and are a function of areal thickness. Knock-on (scattered) electrons range from 33 to 81 per million histories.

	Areal thickness $SrCO_3$ (mg cm^{-2})									
Category	0.1	2.3	4.7	9.4	14.0	18.7	23.4	28.1	32.7	35.0
Fraction entering detector	0.540	0.550	0.544	0.531	0.522	0.514	0.505	0.498	0.492	0.489
Escape without interaction	5.56E-03	5.53E-03	5.48E-03	5.32E-03	5.28E-03	5.16E-03	5.09E-03	4.94E-03	4.87E-03	4.85E-03
Below energy cutoff	2.30E-03	1.88E-03	1.59E-03	1.27E-03	1.20E-03	1.08E-03	1.06E-03	9.63E-04	8.86E-04	9.31E-04
Fraction of interactions	0.546	0.542	0.537	0.525	0.516	0.507	0.499	0.492	0.486	0.483

Table 5-12. Model estimates of the fraction of beta particles entering the detector volume by particles from yttrium-90 initially emitted 2 pi downward. Fractions are for one million histories and are a function of areal thickness. Knock-on (scattered) electrons range from 17 to 46 per million histories.

	Areal thickness $SrCO_3$ (mg cm^{-2})									
Category	0.1	2.3	4.7	9.4	14.0	18.7	23.4	28.1	32.7	35.0
Fraction entering detector	0.113	0.112	0.112	0.111	0.110	0.108	0.107	0.10	0.106	0.105
Escape without interaction	2.17E-03	2.24E-03	2.24E-03	2.21E-03	2.10E-03	2.08E-03	2.18E-03	2.15E-03	2.14E-03	2.06E-03
Below energy cutoff	1.27E-03	9.93E-03	8.86E-03	7.70E-03	6.55E-03	7.01E-03	6.67E-03	5.75E-04	6.63E-04	5.91E-04
Fraction of interactions	0.111	0.110	0.110	0.109	0.108	0.107	0.106	0.105	0.105	0.104

Table 5-13. Model estimates of the fraction of beta particles entering the detector volume by particles from yttium-90 initially emitted 2 pi upward. Fractions are for one million histories and are a function of areal thickness. Knock-on (scattered) electrons range from 37 to 127 per million histories.

Areal thickness $SrCO_3$ (mg cm^{-2})										
Category	0.1	2.3	4.7	9.4	14.0	18.7	23.4	28.1	32.7	35.0
Fraction entering detector	0.442	0.437	0.432	0.421	0.412	0.404	0.398	0.391	0.386	0.383
Escape without interaction	8.93E-03	8.95E-03	8.84E-03	8.55E-03	8.27E-03	8.37E-03	7.93E-03	7.95E-03	7.62E-03	7.58E-03
Below energy cutoff	3.46E-03	2.58E-03	2.32E-03	1.86E-03	1.66E-03	1.53E-03	1.39E-03	1.30E-03	1.25E-03	1.19E-03
Fraction of interactions	0.436	0.431	0.426	0.416	0.407	0.399	0.393	0.387	0.381	0.379

The results of the Monte Carlo simulations are summarized in Table 5-14 for carbon-14, strontium-90, strontium-89, and yttrium-90 as a function of areal thickness.

Table 5-14. Monte Carlo simulation estimates of the fraction of electrons tracks depositing energy within the detector volume as a function of areal thickness of $SrCO_3$. Pulse height tallies excluding the fraction below the energy cutoff, knock-on electrons, and beta particles not interacting within the detector volume, for a strontium carbonate density of 0.6 g cm^{-3} and slide to window distance of 0.2 cm.

Areal thickness mg cm^{-2}	***Carbon-14***	***Strontium-90***	***Strontium-89***	***Yttrium-90***
0.10	0.174	0.438	0.531	0.546
2.34	0.123	0.408	0.519	0.542
4.68	0.092	0.384	0.508	0.537
9.35	0.057	0.346	0.490	0.525
14.03	0.040	0.314	0.476	0.516
18.71	0.030	0.288	0.463	0.507
23.39	0.021	0.270	0.451	0.499
28.10	0.020	0.247	0.441	0.492
32.70	0.018	0.230	0.432	0.486
35.0	0.017	0.222	0.427	0.483

Two comparisons are made between the results of the MCNP simulations and the measured efficiencies: the fit of the Monte Carlo simulation results to the measured efficiency data sets; and pair-wise comparison of measured efficiencies with interpolated values from simulation estimates. The fit of the Monte Carlo simulation results to the measured efficiency data sets are evaluated by the average bias with equation 3-20 and the variance of the measured values from the simulated values by equation 3-21. The difference between the simulation results and measured efficiency data are found in Appendix A, Tables A-1, A-6, and A-14 for carbon-14, strontium-89, strontium-90, and yttrium-90, respectively, and are summarized in Table 5-15.

The pair-wise comparison of measured efficiencies with the simulation results estimated from linear interpolation flagged measurement results that may be outliers. Each

measurement pair for carbon-14 (Table A-1), strontium-89 (Table A-6), strontium-90 (Table A-14), and yttrium-90 (Table A-14) was evaluated given the hypothesis

H_0: $E_R(x\rho) = E_{MCNP,\,R}(x\rho)$

H_A: $E_R(x\rho) \neq E_{MCNP,\,R}(x\rho)$

Where

$E_R(x\rho)$ is the measured efficiency by equation 3-1 or 3-8 for radionuclide R and areal thickness xρ;

$E_{MCNP,\,R}(x\rho)$ is the fractional energy deposition estimated by interpolation of the MCNP simulation results for radionuclide R and areal thickness xρ.

The null hypothesis was evaluated with the Z-statistic (equation 3-25), with the total uncertainties for the measurements estimated as described in section 4.3 and 4.4 and provided in Appendix A, and the estimated uncertainty for the MCNP simulation results from section 5.3. These uncertainties are 2.4% for strontium-89, strontium-90, and yttrium-90, and approximately 4.8 to 5.6% for carbon-14. The individual comparisons where the null hypothesis is rejected are noted in Appendix A Tables A-1, A-6, and A-14, and the number exceeding the Z-statistic, thus rejecting the null hypothesis, are summarized in Table 5-15. These specific measurements remain in the efficiency measurement data set as no other basis for rejecting the specific results was found.

The evaluation summarized in Table 5-15 found the average biases for estimates from the Monte Carlo simulations are less than the variation of measured efficiencies about the interpolated MCNP values. This comparison differs from the fit of the self-absorption curve to the measured efficiencies presented in Table 5-1.

Table 5-15. Bias and uncertainty (1S) of Monte Carlo simulation pulse height tally estimates in Table 5-1 compared with measured efficiency values in Appendix A. Number of measurement pairs exceeding the expected difference by equation 3-25, an estimate of the difference assuming the measurement uncertainties and MCNP model uncertainties are known.

Radionuclide	*N*	*Bias*	*Standard Deviation of model versus measured efficiencies*	*Number exceeding Z statistic*
Carbon-14	25	-0.0005	0.003	0
Strontium-90	48	-0.003	0.009	3
Strontium-89	34	-0.005	0.011	0
Yttrium-90	48	0.002	0.015	2

5.3 Sensitivity analysis of MCNP results

The uncertainty in Monte Carlo simulation estimates was evaluated from estimated uncertainties for beta spectra, examining the sensitivity to changes in model parameters, and variations in specific dimensions or material properties. Specific model parameters examined include comparing the effect of increasing the probability of the first energy bin in the beta-particle source spectrum described in section 3.5.8 and discussed in section 4.2.4, the effect of using the Integrated Tiger Series (ITS) energy binning algorithm versus the default MCNP energy binning, and the effect of increasing the number of sub-steps from the default for materials in cells with dimensions that are small in relation to the range of electrons. The sensitivity of the Monte Carlo simulation to modification of the probability of the first energy bin is not included in the uncertainty estimate for the models. Instead, the uncertainty of the calculated beta spectra is assigned a value of 3 percent based on the observation in ICRU 56 that the number of beta particles per MeV are calculated with "..uncertainties of a few percent" (ICRU, 1997). The effect of

variations in specific dimensions or material properties include evaluating the effect of changing the distance of the sample slide to the detector window retaining ring, variation in density of the strontium carbonate precipitate, and variation from the measured areal thickness of the gold layer deposited on the detector window.

The first non-zero energy bin in the sampled beta-particle spectrum based on ICRU 56 Appendix D were increased by the probability of beta particles excluded below 1keV as described in section 3.5.8. This modification of the source beta-particle spectrum results in probability distributions, following normalization by the MCNP algorithm "normh", that do not differ from the ICRU 56 distributions. The estimated fraction of electrons deposited in the detector were compared with and without this modification for a source mass area 14 mg cm^{-2}, density of 0.6 g cm^{-3}, and sample slide to window retention ring clearance of 0.2 cm. This modification changes the fraction of electrons deposited by 1.4% for carbon-14, and by -0.3% to +0.2% for strontium-89, strontium-90, and yttrium-90 (Table 5-16).

Table 5-16. Comparison of the effect of modifying the source beta spectrum on source counting efficiencies for 14 mg cm^{-2}, 0.6 g cm^{-3} source with window to slide distance of 0.2 cm.

Radionuclide	***Modified Beta spectra***	***ICRU***	***Percent Difference***
Carbon-14	0.037	0.037	1.4%
Strontium-90	0.311	0.312	-0.3%
Strontium-89	0.474	0.475	-0.2%
Yttrium-90	0.514	0.513	0.2%

The difference between the default MCNP energy binning and the optional ITS energy binning was evaluated for sources with areal thickness of 14 mg cm^{-2} and sample slide to window distance of 0.2 cm. Results provided in Table 5-17 indicate a 3.0% lower

estimated efficiency for carbon-14 when using the ITS energy binning, and increased efficiencies by 0.8% to 1.2% for strontium-89 and yttrium-90, respectively..

Table 5-17. Comparison of the effect of MCNP default energy binning and ITS energy binning for source counting efficiency for 14 mg cm^{-2} source at a source to window distance of 0.2 cm.

Radionuclide	MCNP	ITS	% difference
Carbon-14	3.86E-02	3.75E-02	-3.0%
Strontium-90	3.12E-01	3.13E-01	0.1%
Strontium-89	4.74E-01	4.78E-01	0.8%
Yttrium-90	5.12E-01	5.18E-01	1.2%

The effect of source density was evaluated by comparing the fractions of particles interacting within the detector volume for three source areal thicknesses of 0.1, 14, and 32.7 mg cm^{-2} for strontium carbonate densities of 0.6 g cm^{-3} and 0.8 g cm^{-3} and constant window to slide distance of 0.2 cm (Table 5-18). Strontium-90, strontium-89 and yttrium-90 results show minimal differences for densities in this range. The fraction of interactions for carbon-14 differs by 1.6% to 3.3% for 0.1 and 14 mg cm^{-2} sources, respectively. The fraction of interactions for strontium-90 differs by -0.4% to 0.8% for 14 and 32.7 mg cm^{-2} sources, respectively. The effect of source density is 0.1% to 0.2% for strontium-89 and yttrium-90 sources.

Table 5-18. Fraction of interactions within the detector volume as a function of strontium carbonate density and areal thickness for carbon-14, strontium-90, strontium-89 and yttrium-90 and constant slide to window distance of 0.2 cm.

Sample slide to window distance 0.2 cm, 0.6 g cm^{-3}				
mg cm^{-2}	C-14	Sr-90	Sr-89	Y-90
0.1	0.171	0.435	0.525	0.539
14	0.037	0.311	0.474	0.513
32.7	0.017	0.230	0.431	0.485
Sample slide to window distance 0.2 cm, 0.8 g cm^{-3}				
0.1	0.174	0.436	0.525	0.540
14	0.038	0.312	0.475	0.513
32.7	0.017	0.228	0.430	0.484
% difference comparing 0.8 g cm^{-3} to 0.6 g cm^{-3}				
mg cm^{-2}	C14	Sr-90	Sr-89	Y-90
0.1	-1.6%	-0.2%	-0.1%	-0.1%
14	-3.3%	-0.4%	-0.1%	0.0%
32.7	-0.6%	0.8%	0.2%	0.1%

The effect of the source distance on the fraction of interactions within the detector was evaluated for window to slide distances of 0.16 cm and 0.24 cm relative to the selected distance of 0.2 cm for constant density of 0.6 g cm^{-3} (Table 5-19). Strontium-89, strontium-90, and yttrium-90 results show small changes in the fraction interacting ranging from changes in efficiency from -1.5% to 1.3%, with the greatest changes occurring for 0.1 mg cm^{-2} sources. The results for carbon-14 are very sensitive with respect to the source – window distance, particularly for thin sources were self-absorption is minimal. The change in the fraction of interactions is 24.7% when comparing results for 0.16 cm and 0.20 cm at 0.1 mg cm^{-2} $SrCO_3$. As the carbon-14 source is moved further from the window, the fractional interaction decreases by 3.1%.

Table 5-19. Fraction of interactions within the detector volume as a function of distance and areal thickness for carbon-14, strontium-90, strontium-89 and yttrium-90 and constant source density of 0.6 g cm^{-3}.

0.16 cm, 0.6 g cm^{-3}				
mg cm^{-2}	C14	Sr-90	Sr-89	Y-90
0.1	0.214	0.438	0.531	0.546
14	0.038	0.314	0.476	0.516
32.7	0.017	0.232	0.432	0.486
0.2 cm, 0.6 g cm^{-3}				
0.1	0.171	0.435	0.525	0.539
14	0.037	0.311	0.474	0.513
32.7	0.017	0.230	0.431	0.485
0.24 cm, 0.6 g cm^{-3}				
0.1	0.166	0.430	0.518	0.531
14	0.036	0.309	0.471	0.509
32.7	0.016	0.227	0.428	0.481
% change from 0.16 cm to 0.20 cm				
0.1	24.7%	0.6%	1.2%	1.3%
14	4.4%	1.0%	0.4%	0.5%
32.7	2.5%	0.9%	0.3%	0.2%
% change from 0.24 cm to 0.20 cm				
0.1	-3.1%	-1.2%	-1.3%	-1.5%
14	-1.7%	-0.6%	-0.7%	-0.9%
32.7	-2.6%	-1.1%	-0.6%	-0.8%

The effect of variation in the gold areal thickness of the detector window was evaluated by comparing the fraction of interactions for areal thicknesses of 26.4 μg cm^{-2} and 17.6 μg cm^{-2} compared to the model value of 22 μg cm^{-2} (Table 5-20) for sources with constant strontium carbonate areal thickness of 14 mg cm^{-2}. No variation is found for models of strontium-90, strontium-89, or yttrium-90 interactions. Simulation results for carbon-14 fractions differed by 1.1% for windows specified with gold at 26.4 μg cm^{-2} and 17.6 μg cm^{-2}.

Table 5-20. Variation in source counting efficiency estimates resulting from differences in the window gold areal thickness. Results are for source areal thickness of 14.0 g cm^{-2} at slide to detector window distance of 0.16 cm.

Area thickness of gold for detector window			
Au µg cm^{-2}	26.4	22	17.6
Fraction of window thickness	0.33	0.275	0.22
Carbon-14	3.71E-02	3.75E-02	3.79E-02
% difference	-1.1%	0.0%	1.1%
Strontium-90	3.12E-01	3.12E-01	3.13E-01
% difference	0.0%	0.0%	0.3%
Strontium-89	4.77E-01	4.78E-01	4.83E-01
% difference	0.0%	0.0%	1.1%
Yttirum-90	5.18E-01	5.18E-01	5.18E-01
% difference	0.0%	0.0%	0.0%

The uncertainty for the Monte Carlo simulation estimates are summarized in Table 5-21. The uncertainties for the simulation results are based on the uncertainties in the beta spectra specification, density and composition of materials, distance from the plane of the detector window to the surface of the source, window composition, and the tally statistics. The estimated uncertainty for the Monte Carlo simulation results for strontium-90, strontium-89, and yttrium-90 is expected to be ±2.4 percent of the predicted efficiency (1 standard deviation). The estimated uncertainty for the Monte Carlo simulation results for carbon-14 is affected by areal thickness and ranges from 4.8 to 5.6 percent of the predicted efficiency.

Additional uncertainties exist for parameters and data such as elemental cross sections, bias in dimension measurements, uncertainty in the energy distribution of the beta spectra, variation in the actual material composition from the modeled composition, and correlations among parameters. These additional uncertainties are believed to be small components relative to the identified model uncertainties and uncertainties in the efficiency measurement process.

Table 5-21. Estimated uncertainty of Monte Carlo model for carbon-14, strontium-89, strontium-90, and yttrium-90.

Source of Uncertainty	***Type***	***Carbon-14***	***Strontium-90***	***Strontium-89***	***Yttrium-90***
Beta spectra	Rectangular distribution, from ICRU 56	1.7%	1.7%	1.7%	1.7%
Density and composition of material	Rectangular distribution, Table 5-18	1.6%	0.7%	0.2%	0.1%
Distance from detector window to source surface	Rectangular distribution, Table 5-19	4.0%	1.3%	1.4%	1.6%
Window composition	Rectangular distribution, Table 5-20	1.3%	0.8%	0.6%	0.2%
Tally uncertainty	Normal distribution, range in relative standard deviation from simulation	0.2 to 2.8%	0.1 to 0.2%	0.1%	0.1%
Total Uncertainty (1 standard deviation)	Propagated uncertainty	4.8% to 5.6%	2.4%	2.4%	2.4%

5.4 Monte Carlo simuation results and counting system characteristics.

There are two lines of evidence suggesting that the MCNP model provides a reasonable representation of the interactions occurring as result of the counting geometry and the resulting interactions within the detector volume. First, the fractions of interactions estimated from the MCNP model are an acceptable fit to the measured efficiencies for prepared sources. Second, the energy distribution of the interactions closely approximates the pulse height distribution measured at the test signal output of the linear amplifier and is consistent with the establishment of a counting plateau.

In a typical gas flow proportional counter, no counts are recorded until the detector bias is sufficient to cause multiplication of the ionization occurring from interactions of beta particles with the fill gas of the detector. Initially, only a few interactions deposit enough energy to result in pulses above the amplifier discriminator would be expected. Once sufficient multiplication occurs, the count rate gradually increases with increasing voltage until a point is reached where further increases result in small incremental changes in count rate. This region is the typical operating plateau for gas flow proportional counters used to measure beta-particle radiation.

When the cumulative fraction of interactions is plotted versus the natural logarithm of the energy deposited from highest energy to lowest in Figure 5-10, the resulting curve closely approximates the observed counting plateau from a gas flow proportional counter. The minimal increase with energy at the plateau, an increase of 1.6 percent per

100 V when lowering the acceptable pulse height from 300 eV to 1 eV, suggests that the low energy discriminator at 0.3 keV prevents few pulses from being counted.

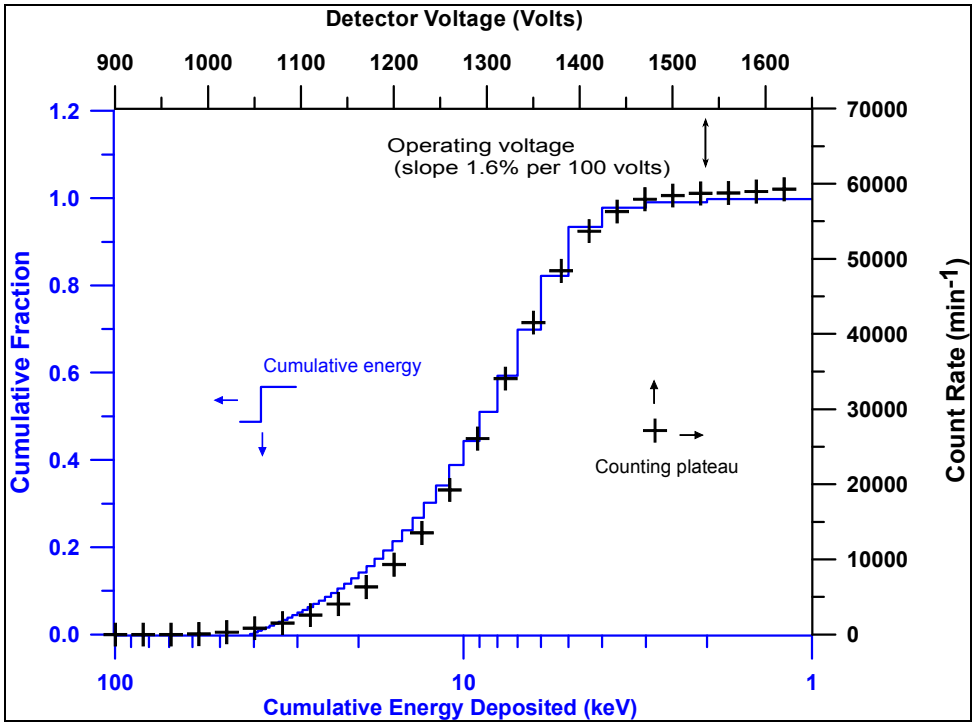

Figure 5-10. Counting plateau for strontium-90 and yttrium-90 in equilibrium and cumulative energy deposited in the detector volume estimated by MCNP.

5.4.1 Energy distribution of electrons deposited in the detector.

The distribution of energy deposited by beta particles is obtained from pulse height tallies from the MCNP simulations. The energy deposition of electron tracks within the detector volume is provided in Figures 5-11 through 5-14 for carbon-14, strontium-90, strontium-89, and yttrium-90 beta-particle spectra, respectively. The distributions are provided for source areal thicknesses of 0.1 mg cm^{-2} and 14mg cm^{-2} for carbon-14, and 0.1 mg cm^{-2} and 32.7 mg cm^{-2} for strontium-90, strontium-89, and yttrium-90.

The carbon-14 energy spectra display a broad range of energies with the largest fraction distributed around 10 keV, but broadly distributed and tailing off towards 80 keV (Figure 5-11). The fraction deposited and the energy distribution differs greatly between the strontium carbonate source at 0.1 mg cm^{-2} and the source at 14 mg cm^{-2}. The fraction of beta-particles reaching the detector for sources with areal thickness greater than 14 mg cm^{-2} is small and as a result the pulse height tally and energy distribution have large uncertainties.

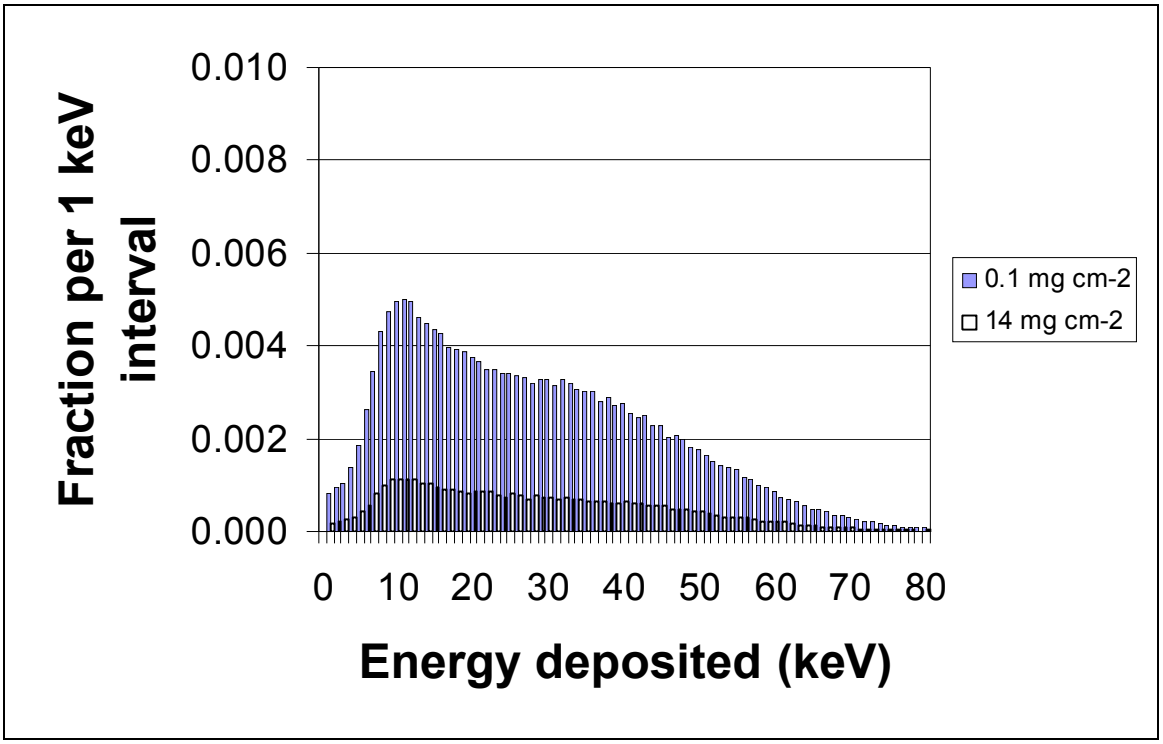

Figure 5-11. Energy distribution for carbon-14 model with areal thickness of 0.1 and 14 mg cm^{-2}. The fraction deposited totals 0.17 and 0.040 of beta particles emitted for areal thicknesses of 0.1 and 14.0 mg cm^{-2}, respectively.

The strontium-90 energy spectra have a broad peak in the range of 5-7 keV and decreasing fractions for histories depositing energies out to 50 keV. There is a noticeable difference in the energy distribution of histories for strontium carbonate sources of 0.1 mg cm^{-2} and 32.7 mg cm^{-2} (Figure 5-12) due to increased scatter and attenuation through self-absorption.

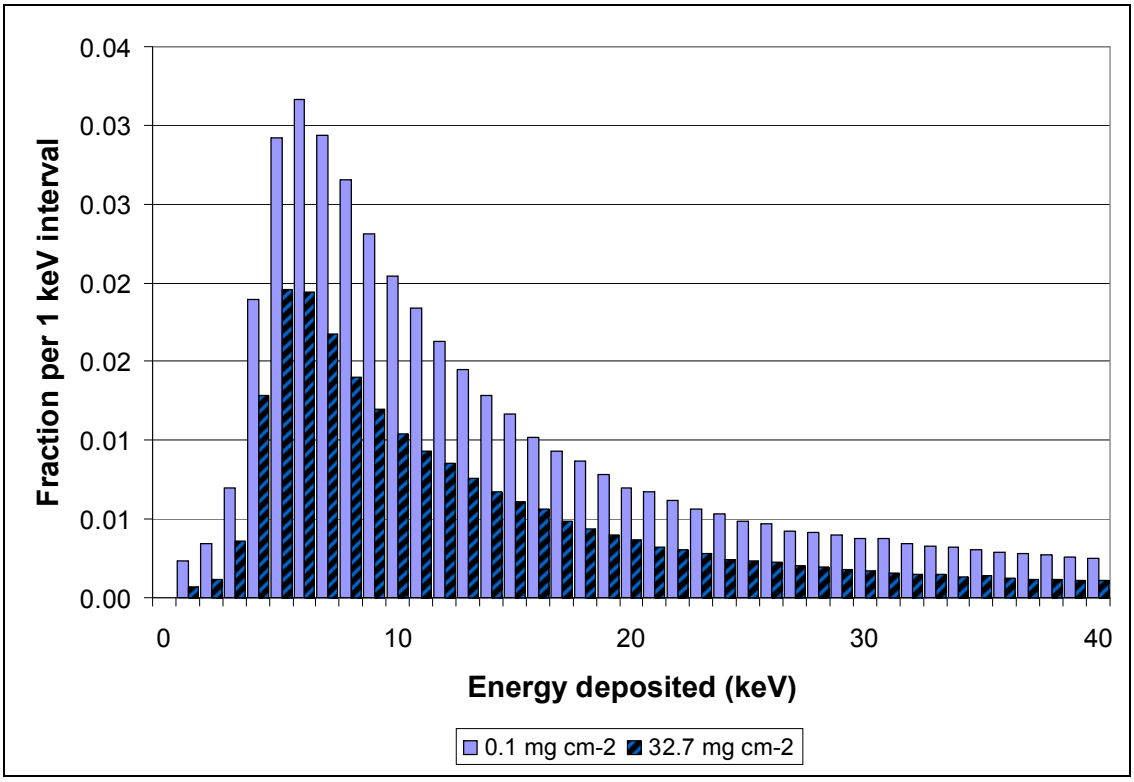

Figure 5-12 Energy distribution for strontium-90 model with areal thickness of 0.1 and 32.7 mg cm^{-2}. The fraction deposited totals 0.438 and 0.230 of beta particles emitted for areal thicknesses of 0.1 and 32.7 mg cm^{-2}, respectively.

The strontium-89 and yttrium-90 energy spectra continue this pattern, with a broad energy peak in the range of 4 to 6 keV and a sharply decreasing fraction for histories with greater energies. There is less difference between strontium carbonate sources of 0.1 mg cm^{-2} and 32.7 mg cm^{-2} for strontium-89 and yttrium-90 (Figures 5-13 and 5-14, respectively). The difference in energy distribution as the areal thickness increases is

greater for beta particle radiation from spectra with low maximum energies (carbon-14 and strontium-90) than from spectra with greater maximum energies (strontium-89 and yttrium-90).

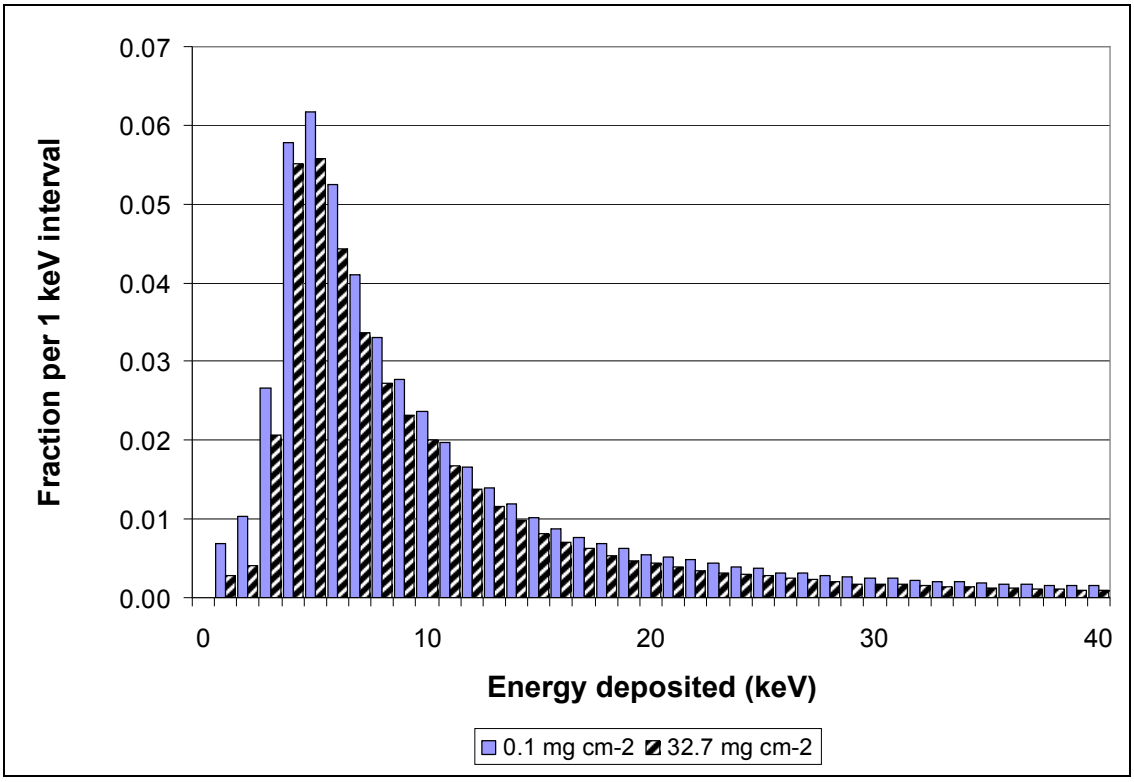

Figure 5-13. Energy distribution for strontium-89 model with areal thickness of 0.1 and 32.7 mg cm^{-2}. The fraction deposited totals 0.53 and 0.43 of beta particles emitted for areal thicknesses of 0.1 and 32.7 mg cm^{-2}, respectively.

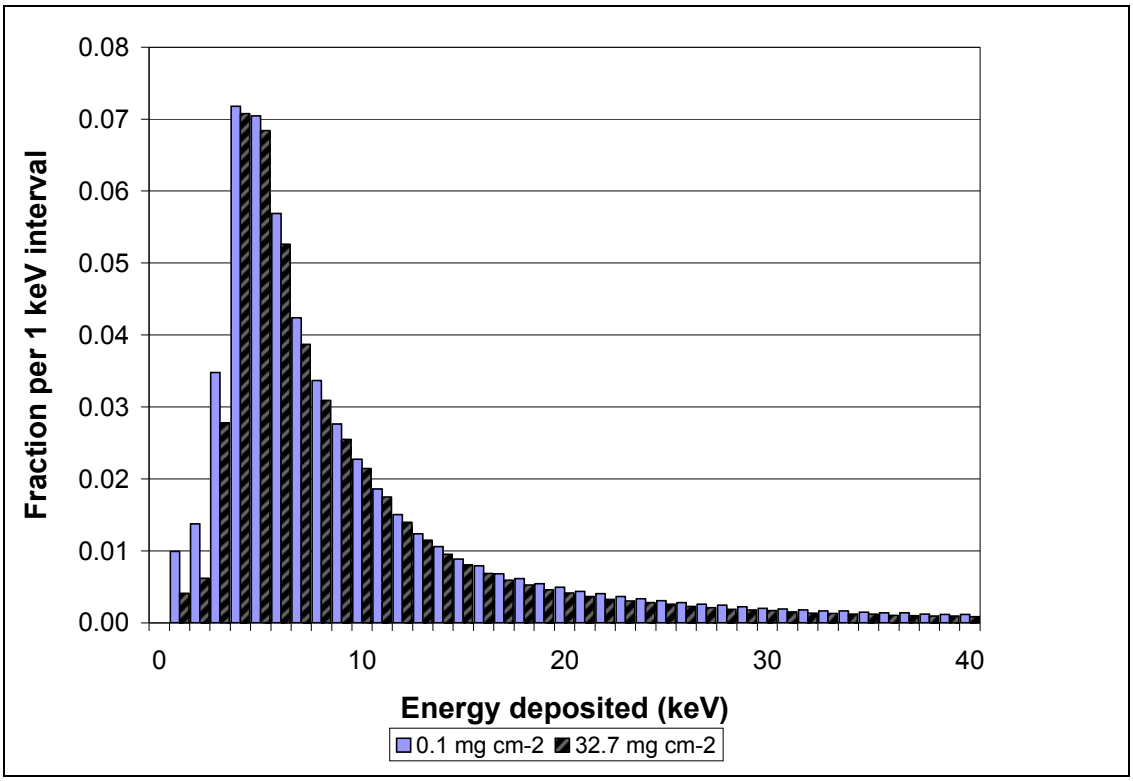

Figure 5-14. Energy distribution for yttrium-90 model with areal thickness of 0.1 and 32.7 mg cm^{-2}. The fraction deposited totals 0.546 and 0.486 of beta particles emitted for areal thicknesses of 0.1 and 32.7 mg cm^{-2}, respectively.

5.4.2 Direction of beta-particle tracks crossing the plane of the detector window.

The Monte Carlo simulations include information regarding the direction of electron tracks crossing the plane of the detector window. The distribution of trajectories for the surface current tally (F1) of electron tracks crossing the plane of the detector window were collected in 10 degree increments from the surface normal (parallel to the z-axis) and are presented in Figure 5-15 for strontium-90 sources with areal thickness of 0.1, 14, and 32.7 mg cm^{-2}. The beta-particles are biased 2 π toward the detector surface to minimize the contribution from backscattered beta particles and electrons. A source emitting beta particles isotropically would exhibit equal fractions in each increment when normalized to the bin width. The expected cosine distribution of a thicker source predicted by equation 2-8 is provided for comparison. The simulation for 0.1 mg cm^{-2} areal thickness source exhibits tracks that are strongly anisotropic with most crossing at angles within zero to 50 degrees to the normal and decreasing in number for angles in the range from 60 to 90 degrees. The 14 mg cm^{-2} areal thickness source exhibits trajectories closely approximating a cosine distribution and decreasing in number for angles in the range from 80 to 90 degrees. The 32.7 mg cm^{-2} areal thickness source exhibits trajectories closely approximating a cosine distribution for all angles, but exhibiting attenuation. These model results are consistent with the qualitative results presented by Baker and Katz (1973) and discussed in section 2.1.4.

Data collected for strontium-89 and yttrium-90 exhibit angular distributions that are strongly anisotropic with little evidence of attenuation at 32.7 mg cm^{-2} areal thickness. This is consistent with the energy distribution for beta-particle histories discussed in section 5.4.1.

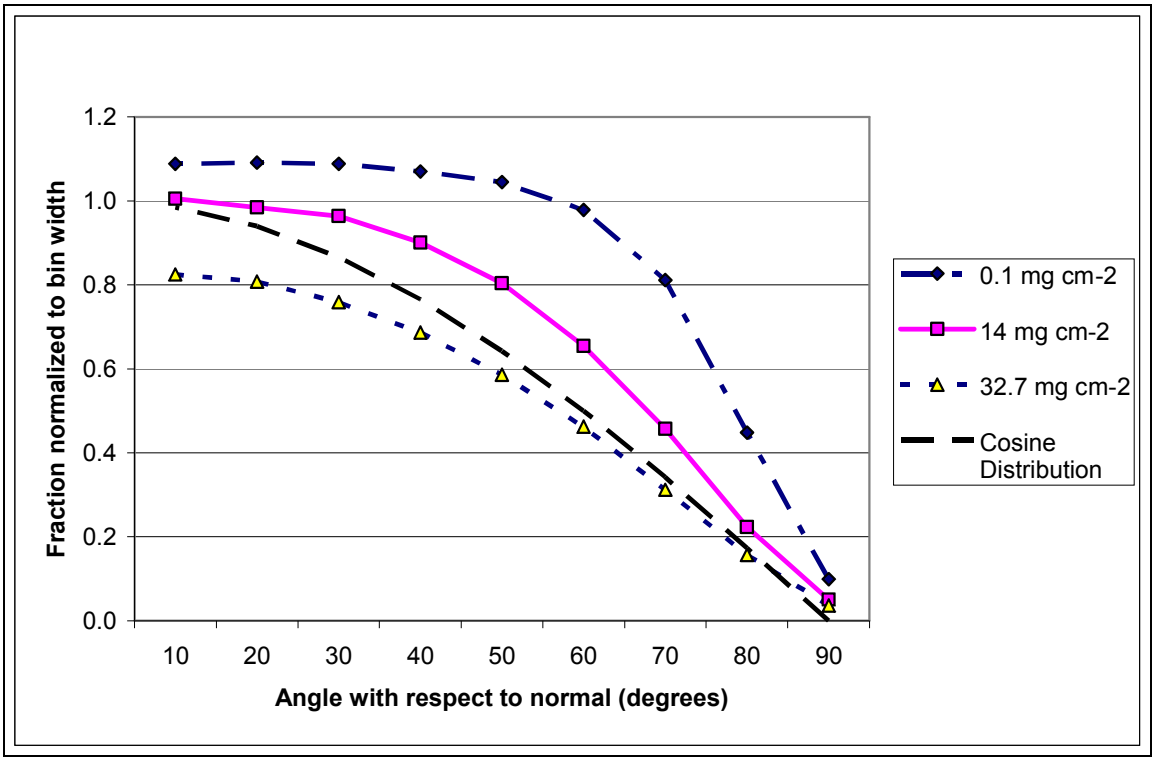

Figure 5-15. Direction of strontium-90 beta-particle tracks with respect to detector normal for 10 degree bin intervals as a function of areal density. Particles are initially started toward the plane of the detector window. Simulation results are provided for 0.1, 14, and 32.7 mg cm^{-2} sources. The expected cosine distribution for a weightless source is provided by equation 2-8.

The difference in the energy distribution and angular distribution of beta particles varies with areal thickness and also the maximum energy of the beta spectrum. As a result, parameters estimating attenuation by Mylar, air, and the detector window , scattering by the counting system geometry, and self-absorption within the strontium carbonate source are a function of the areal thickness of the source and likely to be correlated.

5.4.3 Estimated contributions from backscatter

The fractions of beta-particle histories initially directed two π away from the detector and scattered into the detector volume provide an estimate of the magnitude of the contribution from backscatter to the detector efficiency. Backscatter results may be presented as the fraction of beta-particle histories interacting within the detector volume, termed here the absolute backscatter fractions, or normalized to the geometrical efficiency as will be discussed below in section 5.5.2. Absolute backscatter fractions are presented in Tables 5-3, 5-6, 5-9, and 5-12 for carbon-14, strontium-90, strontium-89, and yttrium-90, respectively. Absolute backscatter fractions for sources with areal thickness of 0.1 and 35 mg cm^{-2} are compared with estimates by equation 2-6 from Tabata et al. (1971) based on average beta spectrum energies and the average atomic number for the filter and nylon support (Table 5-22).

Table 5-22. Summary of backscattered fraction from Monte Carlo simulation compared to backscatter coefficients for monoenergetic electrons measured in vacuum (Tabata et al., 1971) estimated for the average beta-particle energy and average Z for the filter (9) and nylon support (6.6)

Radionuclide	***Average Energy (MeV)***	***Backscatter Tabata et al. (Equation 2-6)***		***Absolute back-scattered fraction 0.1 mg cm^{-2}***	***Absolute back-scattered fraction 35 mg cm^{-2}***
		Filter	***Nylon***		
Carbon-14	0.050	0.08	0.05	0.030	0.0040
Strontium-90	0.199	0.07	0.04	0.090	0.052
Strontium-89	0.596	0.05	0.03	0.100	0.096
Yttrium-90	0.985	0.04	0.02	0.110	0.104

Important differences between the studies of backscatter summarized by Tabata et al. (1971) and the Monte Carlo simulation presented here are the comparison of estimates from monoenergetic electron data collected in a vacuum with spectral data collected

under typical counting conditions including attenuation, self-absorption, and scattering from other materials into the detector volume.

The backscatter fractions estimated following Tabata et al. are inversely related to the energy of the electron, where the average energy of the corresponding beta-particle spectrum is used here. As expected given the counting geometry, the absolute backscatter fractions for carbon-14 are less than the values predicted by equation 2-6 due to attenuation by Mylar, air, and the detector window. The absolute backscatter fractions from Monte Carlo simulations increases with the average beta-particle energies, and estimates by equation 2-6 decrease with increasing energy.

5.5 Estimation of detector counting efficiency by component parameters.

Parametric efficiency estimates by equation 2-1, in units of count rate per disintegration rate, assume that the parameters are independent. These parameters are correlated for the application and geometry of this study. The energy distributions of beta-particle histories deposited in the detector are a function of the areal thickness of the source as discussed in section 5.4.1. As the source areal thickness changes, the energy distribution and attenuation by intervening materials differ. The distributions in the direction of the beta-particle tracks are also a function of the areal thickness of the source as discussed in section 5.4.2. Both attributes of the beta-particle history are affected by backscatter and scatter into the detector that are a function of the maximum energy as well as the areal thickness of the source.

Parameter estimates for the components of equation 2-1 must also be in units such that the products of the factors result in units of count rate per disintegration rate. An estimate of the parameters of the efficiency equation incorporating the correlations is provided from Monte Carlo simulation results and empirical measurements by

$$R_m / A_R = G \bullet f_b' \bullet f_w' \bullet f_s' \bullet f_{sc}' \bullet \varepsilon_\beta \bullet f_m \bullet f_\tau \qquad \text{Equation 5-1}$$

where:

G = geometry factor of counting system (Table 3-7) (unitless)

f_b' = backscatter correction factor, from the pulse height fraction with the source direction biased two π downward and normalized by the geometrical efficiency, G;

f_w' = attenuation correction factor, from the pulse height fraction with the source direction biased two π upward and normalized by the pulse height fraction with the source direction biased two π upward and the cells for Mylar(4), air space(3) and window(2) void of interaction;

f_{sc}' = scatter into the detector cell, from the pulse height fraction with the source direction biased two π upward, no interactions for scattering cells including the metal ring (13), slide (17), and source spacer (18), as well as no attenuation in the cells for Mylar(4), air space(3), and window(2), and normalized by the pulse height fraction with the cells for Mylar(4), air space(3) and window(2) void of interaction;

f_s' = source self absorption factor, obtained from empirical fit to measurement data; and

ε_β, f_m, f_τ = 1.

5.5.1 Geometrical efficiency

The geometrical efficiency for the counting geometry was estimated by linear interpolation from tables published in Bland (1984) and described in section 3.4.3. The calculated geometrical efficiencies are found in Table 3.7 as a function of areal thickness. The geometrical efficiency of the simulations was evaluated by setting all interactions to zero and noting the fraction of particles entering the detector cell. When all cells are without interaction, the fraction of particles interacting within the detector

cell, corrected for particle weight, is 0.425, in agreement with the estimated geometrical efficiency of 0.425 for an areal thickness of 0.1 mg cm^{-2} (Table 5-23). This value is plotted in Figure 5-6. The values found in Table 3.7 were found for simulations at greater areal thicknesses.

Table 5-23. Fraction of electrons deposited in the detector volume for each modeled radionuclide, normalized by particle weight. Model with detector to slide distance of 0.2 cm, areal thickness 0.1 mg cm^{-2}.

Radionuclide	Average Energy (MeV)	F8 Tally	Tally Uncertainty	MCNP Particle Weight	Normalized Fraction	Uncertainty
Carbon-14	0.0503	0.419	0.012	0.987	0.425	0.012
Strontium-90	0.1986	0.423	0.012	0.997	0.425	0.012
Strontium-89	0.5958	0.424	0.012	0.999	0.425	0.012
Yttrium-90	0.9536	0.425	0.012	1.000	0.425	0.012

5.5.2 Scattering and backscatter

The contribution from scattering by components of the counting system and source geometry are not directly measurable due to the geometry of the counting system. The simulation results for surface current tallies provide insight into the cells traversed through flagging cells encountered, but the surface current tally does not directly correspond to the pulse height tally for the same simulation. Flagging particle histories by cell in pulse height tallies is not implemented in MCNP. In addition, surface current tallies flagged by cell do not distinguish electron tracks that may involve scattering from more than one cell. Surface current tallies identify the location of scattering by cell material. An example of these data is provided Table 5-24 for strontium-90, strontium-89, and yttrium-90 with areal thickness of 14 mg cm^{-2}. Carbon-14 is not included due to the low efficiency for sources at this areal thickness. Scattering into the detector volume occurs from two paths, backscatter from the filter, nylon support, and the source spacer, and scatter from the metal ring holding the detector window in place. Scattering from the

stainless steel support represented less than 1 percent of the contribution to the surface current tallies. Due to the geometry, histories scattering from the nylon filter support into the detector will also be recorded traversing the filter, resulting in correlation between the flagged surface current tallies. The filter is the predominate material for scattered beta-particles with histories reaching the detector window, with 4.9 percent of histories for strontium-90, 11.8 percent of histories for strontium-89, and 14.1 percent of histories for yttrium-90, respectively. The more energetic beta particles from strontium-89 and yttrium-90 also have significant fractions backscattering from the nylon filter support, with 8.5 percent and 11.3 percent of histories reaching the detector window for strontium-89 and yttrium-90, respectively. The ring/metal plate forming the base of the detector contributes from 0.8 percent to 1 percent of histories scattered into the detector.

Table 5-24. Percent of surface current (F1) tally flagged by cell traversed during the particle history for strontium carbonate sources with areal thickness of 14 mg cm^{-2}.

Flagged cell (cell number)	Strontium-90	Strontium-89	Yttrium-90
Filter (8)	**4.94%**	**11.75%**	**14.11%**
Plastic support, sides (9)	0.00%	0.00%	0.03%
Nylon support (10)	0.82%	**8.52%**	**11.28%**
Air space under support(11	0.00%	0.01%	0.33%
Metal plate and ring (13)	0.79%	**1.01%**	**1.08%**
Air space above slide (16)	0.11%	0.13%	0.13%
Slide (17)	0.10%	0.13%	0.14%
Source spacer (18)	**1.54%**	**2.16%**	**2.66%**

Similar patterns in the distribution of scattering and backscattering contributions are observed for simulations with areal thicknesses of 0.1 mg cm^{-2} and 32.7 mg cm^{-2}. Scattering increases for strontium-90 in thin sources due to the reduction in self-absorption and attenuation, and decreases for all radionuclides for thick sources because of increased self-absorption within strontium carbonate and attenuation by mylar, air, and the detector window. Model results for carbon-14 at 0.1 mg cm^{-2} indicate

16 percent of the surface current tally would have traversed the filter, with all other contributions less than 1 percent.

The scatter into the detector volume is estimated from the ratio of two simulations; both with beta particles biased two π upward to reduce the contribution from backscatter. The first has no interactions in scattering cells including the metal ring (13), slide (17), and source spacer (18), as well as no attenuation in the cells for Mylar(4), air space(3), and window(2). The second simulation is without interaction in Mylar(4), air space(3), and window(2). The ratio of the two pulse height tallies estimates the increase in from scattering by the metal ring (13), slide (17), and source spacer (18) and are provided in Table 5-27.

Backscatter estimates are obtained by normalizing the fraction of beta-particle histories initially biased two π downward that interact within the detector volume to the geometrical efficiency (Tables 5-3, 5-6, 5-9, and 5-12 for carbon-14, strontium-90, strontium-89, and yttrium-90, respectively). Scatter estimates are obtained from the ratio of Monte Carlo simulation pulse height tallies for model results with beta particles biased two π upward with no interactions in scattering cells for the metal ring (13), slide (17), and source spacer (18), with interactions in mylar(4), air space(3), and window(2) cells also held void, to model results biased two π upward with no interaction in Mylar(4), air space(3), and window(2) cells. The scattering cells were identified by flagging surface current tallies by source cell in Table 5-24 and backscatter results are presented in Table 5-25.

Table 5-25. Backscatter fraction normalized to geometrical efficiency from Tables 5-3, 5-6, 5-9, and 5-12.

Radionuclide	Areal thickness mg cm^{-2}	Backscatter (f_b')
C-14	0.1	1.071
	14	1.019
	32.7	1.009
Sr-90	0.1	1.21
	14	1.17
	32.7	1.12
Sr-89	0.1	1.254
	14	1.240
	32.7	1.222
Y-90	0.1	1.261
	14	1.252
	32.7	1.240

These results are comparable to backscatter factors available from Nader et al., (1954) for sources counted with an internal proportional counter. They reported backscatter factors range from approximately 1.1 for sulfur-35 (0.167 MeV) to approximately 1.25 for phosphorus-32 (1.70 MeV) for backing with atomic number 6. Nader et al. reported backscatter measurements as the ratio of the count rate with backing to the count rate with nearly weightless backing, normalizing the results to a 2 π geometry. Similar estimates are obtained in this study by normalizing the Monte Carlo simulation results to the geometrical efficiency.

5.5.3 Attenuation

The attenuation coefficients necessary for estimating the fraction reaching the detector volume for carbon-14, strontium-90, strontium-89, and yttrium-90 are not measurable by the absorber measurements due to the close proximity of the source and detector window. The attenuation by Mylar, air space, and detector window, and scatter into the

detector were estimated from the ratio of results for Monte Carlo simulations by biasing the initial source direction 2 π toward the detector to reduce the affect of backscatter and by manipulating the importance of cell interactions. Attenuation was estimated from the ratio of MCNP pulse height tallies from simulations with the initial direction of beta particles biased two π upward to the same simulation with no interaction occurring in Mylar (cell 4), the air space (3), and detector window (2), and are provided in Table 5-26.

Table 5-26. Attenuation in Mylar, air space, and detector window from MCNP model simulations.

Radionuclide	Areal thickness mg cm^{-2}	Attenuation fraction	Attenuation coefficient cm^{-2} mg
C-14	0.1	0.359	0.474
	14	0.484	0.336
	32.7	0.690	0.172
Sr-90	0.1	0.812	0.096
	14	0.898	0.050
	32.7	0.914	0.042
Sr-89	0.1	0.968	0.015
	14	0.969	0.015
	32.7	0.975	0.012
Y-90	0.1	0.998	0.001
	14	0.984	0.007
	32.7	0.987	0.006

The attenuation coefficients for sources with areal thickness of 32.7 mg cm^{-2} are similar to the values measured in absorbers by Baker and Katz (1953), with attenuation coefficients of 0.260 cm^2 mg^{-1} for carbon-14, 0.030 cm^2 mg^{-1} for strontium-90, 0.010 cm^2 mg^{-1} for strontium-89, and 0.005 cm^2 mg^{-1} for yttrium-90. The attenuation coefficients for sources with areal thickness of 32.7 mg cm^{-2} in Table 5-26 are close to the values reported by Baltakmens (1970), in Table 2-1, for aluminum and copper absorbers for strontium-90 (0.035 to 0.0354 cm^2 mg^{-1}, respectively), strontium-89 (0.0072 to 0.011 cm^2 mg^{-1}, respectively), and yttrium-90 (0.0049 to 0.006 cm^2 mg^{-1}, respectively).

5.6 Estimating efficiencies from component parameters

Parameter estimates for the components of the parametric efficiency by equation 5-1 are derived from measurements and Monte Carlo simulation results, and summarized for strontium carbonate areal thicknesses of 0.1, 14, and 32.7 mg cm^{-2} in Table 5-27. The MCNP pulse height fractions are from Table 5-14. The geometrical efficiencies are from Table 3-7.

The parametric efficiency estimate for sources with areal thickness of 0.1 mg cm^{-2} and the estimates from the Monte Carlo simulations agree within one to three percent for strontium-90, strontium-89, and yttrium-90. The result for carbon-14 at an areal thickness of 0.1 mg cm^{-2} underestimates the simulation result by 6 percent, with a difference in fractional efficiency of 0.012.

Table 5-27. Parametric efficiency estimates compared with MCNP fractions by radionuclide for sources with areal thicknesses of 0.1, 14, and 32.7 mg cm^{-2}.

Radionuclide	Areal thickness (mg cm^{-2})	MCNP Efficiency	Parametric Efficiency (R_m/A_R) =	Geometry (G) ×	Backscatter (f_b') ×	Attenuation (f_w') ×	Scatter (f_{sc}') ×	μ and Self-Absorption (f_s)	Parametric Efficiency/MCNP
Carbon-14		1S = 5%						μ=0.320	
	0.1	0.174	0.162	0.425	1.071	0.359	1.010	0.984	0.93
	14	0.040	0.047	0.429	1.019	0.484	1.002	0.221	1.17
	32.7	0.018	0.023	0.433	1.009	0.552	1.007	0.096	1.29
Strontium-90		1S = 2.4%						μ=0.050	
	0.1	0.438	0.424	0.425	1.21	0.812	1.017	0.998	0.97
	14	0.314	0.329	0.429	1.17	0.898	1.018	0.719	1.05
	32.7	0.230	0.220	0.433	1.12	0.914	1.003	0.492	0.96
Strontium-89		1S = 2.4%						μ=0.012	
	0.1	0.531	0.530	0.425	1.254	0.968	1.028	0.999	1.00
	14	0.476	0.489	0.429	1.240	0.969	1.031	0.921	1.03
	32.7	0.432	0.429	0.433	1.222	0.975	1.006	0.827	0.99
Yttrium-90		1S = 2.4%						μ=0.0066	
	0.1	0.546	0.551	0.425	1.261	0.998	1.031	1.000	1.01
	14	0.516	0.522	0.429	1.252	0.984	1.034	0.955	1.01
	32.7	0.486	0.480	0.433	1.240	0.987	1.006	0.899	0.99

Chapter 6. Conclusions

Counting efficiencies were determined by empirical measurement and Monte Carlo simulation for carbon-14, strontium-89, strontium-90, and yttrium-90 standards counted by low-background gas flow proportional counter for strontium carbonate precipitates in the range from 3 to 33 mg cm^{-2}. The maximum beta particle energies range from 0.156 MeV for carbon-14 to 2.28 MeV for yttrium-90. Counting efficiencies determined by empirical measurement and Monte Carlo simulations agree within the total expanded uncertainties of the measurements and the estimated uncertainties of the simulations.

The parameters required to estimate the counting efficiency are summarized as the best fit for sources with areal thickness of 14 mg cm^{-2} and the values corresponding to the range in strontium carbonate areal thickness from 0.1 mg cm^{-2} to 32.7 mg cm^{-2}. The geometrical efficiency (G) for this counting geometry is 0.429 with a range from 0.425 to 0.434 depending on source thickness, for a source holder to window distance of 0.2 cm.

Parameter estimates for backscatter (f_b), attenuation (f_w), and scattering (f_{sc}) into the detector are a function of areal thickness and estimated from Monte Carlo simulations. The fraction of beta-particles backscattered, f_b, defined as the fraction initially traveling away from the plane of the detector window and scattered into the detector volume, is normalized by the geometrical efficiency. It varies slightly with the maximum beta-particle energy and areal thickness of the precipitate as described in section 5.6. Backscatter ranges from 1.2 to 1.25 for strontium-89 and yttrium-90, and is a function of areal thickness for strontium-90 and carbon-14. Attenuation coefficients, f_w, estimated from simulation results, are also a function of the maximum energy and areal thickness of the precipitate as described in section 5.5.3. Scattering (f_{sc}) into the detector volume

contributes a small fraction ranging from 1 percent or less for carbon-14 to 3 percent for yttrium-90. These three parameters are correlated, with areal mass a common factor. Parameter estimates are summarized in section 5.6.

Self-absorption coefficients were fit to the measured efficiencies as a function of areal thickness in the range of 3 to 33 mg cm^{-2}. Fitted values were: 0.306 cm^2 mg^{-1} for carbon-14; 0.044 cm^2 mg^{-1} for strontium-90; 0.012 cm^2 mg^{-1} for strontium-89; and 0.0066 cm^2 g^{-1} for yttrium-90.

The intrinsic efficiency (ε_b) for the detector is 0.99 for yttrium-90 and 1.00 for lower energy beta emitters, with an estimated range from 0.98 to 1.00 for yttrium-90. The lower energy cutoff for beta-particle pulses is 0.3 keV deposited within the detector volume.

The Monte Carlo model provided efficiency estimates based on pulse height tallies in good agreement with measured values. The bias and uncertainties as 95 percent confidence limits for the model estimates, evaluated as the difference between Monte Carlo estimates and measured efficiencies, were: carbon-14, -0.0005 ± 0.005; strontium-90, -0.003 ± 0.018; strontium-89, -0.005 ± 0.021; and yttrium-90, 0.002 ± 0.030. The uncertainty of the Monte Carlo simulation as 95 percent confidence limits is estimated to be 10 percent for carbon-14 and 5 percent for strontium-90, strontium-89, and yttrium-90.

Fractional counting efficiencies and 95% confidence limits for single efficiency estimates for carbon-14 ranged from 0.107± 0.014 at 3.5 mg cm^{-2} to 0.025 ± 0.002 at 24.9 mg cm^{-2}. The greatest contribution to the measurement uncertainty is from the radionuclide concentration, contributing from 75 percent of the total uncertainty for counting

efficiencies for mass area less than 7 mg cm^{-2} to 86 percent for a mass area of 24.9 mg cm^{-2}.

Fractional counting efficiencies for strontium-89 ranged from 0.495 ± 0.022 at 5.7 mg cm^{-2} to 0.438 ± 0.029 at 31.4 mg cm^{-2}. The greatest contribution to the measurement uncertainty is from the carrier concentration, contributing from 56 percent of the total uncertainty for counting efficiencies for mass area less than 7 mg cm^{-2} to 72 percent for a mass area of 31.4 mg cm^{-2}.

Fractional counting efficiencies for strontium-90 ranged from 0.403 ± 0.018 at 2.9 mg cm^{-2} to 0.237 ± 0.006 at 33.3 mg cm^{-2}. The source of variability in counting efficiency measurements for strontium-90 varied with the source areal thickness. Measurements of small mass differences for sources at 3 mg cm^{-2} contributed 61 percent to the measurement uncertainty, and the uncertainty of the radionuclide concentration accounted for 19 percent. As the precipitate mass increased to 14 mg cm^{-2} and 33 mg cm^{-2}, the mass measurement uncertainties decreased and the principle sources of uncertainty were from the concentration of the radionuclide, 64 percent at 14 mg cm^{-2} to 61 percent for 33 mg cm^{-2}.

Fractional counting efficiencies for yttrium-90 ranged from 0.542 ± 0.024 at 2.9 mg cm^{-2} to 0.505 ± 0.012 at 33.3 mg cm^{-2}. The uncertainties for the yttrium-90 counting efficiencies are greater than for strontium-90 for the same mass area due to the double count method. Measurements of small mass differences for sources at 3 mg cm^{-2} contributed 61 percent to the measurement uncertainty, and the uncertainty of the radionuclide concentration accounted for 19 percent. As the precipitate mass increased to 14 mg cm^{-2} and 33 mg cm^{-2}, the uncertainties for mass measurements decreased and

the principle sources of uncertainty were the concentration of the radionuclide, 60 percent at 14 mg cm^{-2} to 66 percent for 33 mg cm^{-2}, and the concentration of the carrier, 14 percent at 14 mg cm^{-2} to 16 percent for 33 mg.

Specific conclusions and recommendations for the measurement process and Monte Carlo simulations are as follows.

6.1 Radiochemistry

Consistent efficiency measurements from a large number of sources, greater than 20, are producible only with carefully controlled processes that are consistently implemented. Particular attention to filtering conditions and drying precipitates are important for determining accurate areal thickness for precipitates and reproducible precipitate geometries.

6.1.1 Uncertainty

The largest contributor to counting efficiency uncertainty estimates at typical mass areas is the concentration of the radionuclide. The largest component of this measurement uncertainty is the uncertainty associated with the estimate of the initial activity. The contribution from the uncertainty of the radionuclide concentration is controlled by making standards gravimetrically with well characterized volumetric glassware. As expected, measurement of small differences in mass result in significant contributions to counting efficiency measurements, particularly for $SrCO_3$ precipitates below 7 mg cm^{-2}.

6.1.2 Carrier standardization

Gravimetric standardization is adequate for determining carrier concentrations, which is an important but small component of the total uncertainty budget for counting efficiency measurements. Independent measurement by ICP provides a means to assess potential bias by gravimetric standardization but does not offer a more precise measurement of carrier concentration.

It is important to standardize the drying of precipitates, conduct the carrier standardization with the same drying process, and minimize the uncertainties with gravimetric measurements. Uncertainties with gravimetric measurements can be assessed from linearity data typically collected in routine balance evaluation and maintenance.

6.1.3 Sample mass and density

Sample density may be affected by moisture and variations in filtering technique. Consistent filtering and washing procedures result in carrier recoveries of greater than 90 percent and reproducible densities. Avoiding measurements of small mass differences reduces the uncertainties introduced by gravimetric measurements at the low end of the linear range for typical analytical balances.

6.2 Monte Carlo simulation

A Monte Carlo model was constructed with MCNP and the results compared to the efficiency measurements. The results estimated from the model do not differ significantly when measured by Chi-Square goodness of fit (probability < 0.05) from the results measured for the four radionuclides, with maximum beta energies ranging from 0.156 MeV to 2.28 MeV. The energy deposition estimates from the model are consistent with the known performance characteristics of gas flow proportional counters, approximating the characteristic counting plateau observed for gas flow proportional counters.

The evaluation of measured efficiencies against model results, particularly those of the low beta-energy carbon-14, identified sources of discrepancies between the modeled and actual counting system. Specific parameters identified through this iterative procedure include the density of strontium carbonate; the composition of the detector window; and the distance from the source to the detector window. Specific conclusions from constructing the MCNP model and comparing results with measured values include the following.

6.2.1 Beta-particle spectra

The normalization routine used by MCNP for histogram distributions produces a bias in the normalized beta spectra. This bias is inherent in the routine “normh” and results in a lack of fit between the expected probabilities and the normalized probabilities from which MCNP samples beta particle energies. This normalization bias can be corrected by adding the probability removed below the low energy cutoff of 1 keV to the probability for the second energy bin (first non-zero energy bin) in the source definition.

In addition, the beta spectra provided in ICRU 56, Appendix D, are tabulated by energy intervals based on the lowest energy of the interval, while MCNP assumes that the energy intervals begin at 1 keV and the probabilities are provided for the greatest energy in the interval. As a result, it is necessary to translate the beta spectra probabilities from the ICRU distribution to the expected MCNP distribution.

6.2.2 Instrument parameters

The energy cutoff determined by the amplifier discriminator is needed to account for beta-particle interactions that may be excluded. Two methods are applicable to estimating the signal excluded by the amplifier: direct measurement of the pulse height from the amplifier output that is excluded and conversion to energy deposited; and direct measurement of the energy deposited by photoelectric interactions in the detector and estimation of the pulse height excluded. The energy cut-off for the counting system was evaluated from measurements with iron-55 5.9 keV x-rays and estimated to exclude events below 0.3 keV.

6.2.3 Material density

The geometry of the counting system, composition of materials, and the density of the materials are necessary for constructing a reasonable Monte Carlo model. Carbon-14 proved to be particularly sensitive to small changes in the model specifications affecting the geometry, particularly the spacing between the source surface and the plane of the detector window. The measured density of strontium carbonate precipitates and the

porous polyethersulfone based filter differed significantly from the physical density for these compounds and were found to affect the model results. The density for the detector window required measurement because of its unknown composition as a gold anodized hydrocarbon based film. Other materials including the nylon base and the Mylar film were found to have measured densities in agreement with published physical densities.

6.2.4 MCNP parameters

In addition to the beta spectra in the source definition, other MCNP parameters may affect model results including the selection of the energy binning algorithm and the number of energy sub-steps sampled in crossing small dimensions of the model. The selection of the energy binning algorithm affects how the electron stopping power is sampled and was implemented by the nearest group boundary algorithm. Another issue specific to this model is adequately sampling electrons crossing small dimensions of the model. This required evaluation and modification of the number of substeps sampled for specific materials. However, once the model specifications closely approximate the geometry and materials, it is found that reasonable changes in the parameter values result in small changes in the estimated detector efficiencies.

6.3 Summary

This dissertation investigated the counting efficiency calibration of a gas flow proportional counter with beta-particle emitters, providing estimates of the uncertainty and sources of variability in the calibration process. Additional information was developed regarding the composition of the detector window, the energy excluded by the amplifier discriminator, and the physical density of materials. A better understanding of the histogram normalization routine implemented within MCNP resulted from the construction and evaluation of a Monte Carlo model with MCNP. The difference in the specification of the probability distribution for beta-particle energy spectra in ICRU 56 Appendix D and MCNP requirements were described and a correction for the bias introduced during the normalization process for beta spectra was provided. The Monte Carlo simulation results agree within the uncertainty of analytical efficiency estimates.

Appendix A.

Efficiency measurements

Table A-1. Carbon-14 efficiency measurements, efficiency from self-absorption equation, and interpolated efficiencies from Monte Carlo simulation results.

Measured Counting efficiencies						E_0	0.174				
						μ'	0.304			MCNP	
Date	Number	Area Thickness (mg cm^{-2})	Counting Efficiency	Uncertainty (95% CL)	Area Thickness (mg cm^{-2})	Efficiency	Difference (Measured - Efficiency)	Area Thickness (mg cm^{-2})	Interpolated Efficiency	Difference (Measured - MCNP)
07/05/04	6	3.5	0.107	0.014	3.5	0.108	0.000	3.5	0.109	-0.001
07/05/04	7	3.5	0.106	0.014	3.5	0.108	-0.001	3.5	0.109	-0.002
08/13/04	2	3.5	0.105	0.012	3.5	0.107	-0.002	3.5	0.108	-0.003
07/23/04	6	3.6	0.106	0.012	3.6	0.105	0.001	3.6	0.106	0.000
07/23/04	7	3.6	0.102	0.012	3.6	0.105	-0.003	3.6	0.106	-0.004
08/06/04	1	4.7	0.088	0.010	4.7	0.093	-0.005	4.7	0.092	-0.005
07/05/04	4	6.9	0.072	0.008	6.9	0.073	-0.001	6.9	0.075	-0.004
07/05/04	5	7.0	0.070	0.008	7.0	0.072	-0.002	7.0	0.075	-0.005
07/23/04	4	7.1	0.071	0.008	7.1	0.071	0.000	7.1	0.074	-0.003
07/23/04	5	7.3	0.072	0.008	7.3	0.070	0.002	7.3	0.073	-0.001
07/23/04	3	10.6	0.052	0.010	10.6	0.052	0.000	10.6	0.052	0.000
07/05/04	3	10.7	0.049	0.006	10.7	0.051	-0.002	10.7	0.052	-0.002
07/23/04	2	14.2	0.041	0.004	14.2	0.040	0.001	14.2	0.039	0.002
07/05/04	2	14.4	0.040	0.004	14.4	0.039	0.001	14.4	0.039	0.001
08/06/04	8	14.8	0.036	0.004	14.8	0.038	-0.002	14.8	0.038	-0.002
08/06/04	4	15.2	0.036	0.004	15.2	0.037	-0.001	15.2	0.037	-0.001
08/06/04	3	15.4	0.039	0.004	15.4	0.037	0.002	15.4	0.037	0.002
08/06/04	7	15.5	0.036	0.004	15.5	0.037	0.000	15.5	0.037	0.000
07/05/04	1	15.5	0.040	0.004	15.5	0.037	0.003	15.5	0.036	0.003
07/23/04	8	15.5	0.039	0.004	15.5	0.037	0.002	15.5	0.036	0.003
07/23/04	1	15.6	0.039	0.004	15.6	0.036	0.003	15.6	0.036	0.003
08/06/04	6	15.6	0.037	0.004	15.6	0.036	0.000	15.6	0.036	0.000
08/06/04	5	17.0	0.037	0.004	17.0	0.033	0.004	17.0	0.033	0.004
08/13/04	3	23.3	0.027	0.003	23.3	0.025	0.002	23.3	0.024	0.003
08/13/04	4	24.9	0.025	0.003	24.9	0.023	0.002	24.9	0.023	0.002
		Number	25			Average	0.0001		Average	-0.0005
						Std Dev	0.0022		Std Dev	0.0026
									Std Error	0.0005

Table A-2. Carbon-14 efficiency measurement data for 07/05/04 with measured efficiency and total propagated uncertainty (1S).

Preparation Date			Radionuclide	Carbon-14						
7/5/2004			Concentration (C_A)		46282	min^{-1} mL^{-1}	5/26/2004			
			Na_2CO_3 Carrier (C_C)		41.43	mg mL^{-1}				
			Background Count Rate (R_b)			1.93	min^{-1}			
Number	Na_2CO_3 Carrier V_C	Expected Mass $V_C \cdot C_C$	Net Weight eq (3-2) W_{net}	Thickness eq (3-4) T_m	Yield eq (3-5) Y	Volume Radionuclide V_R	Activity eq (3-6) A_T	Total Count Rate R_g	Efficiency eq (3-7) E_R	Total Uncertainty
	mL	mg	mg	mg cm^{-2}		mL	min^{-1}	min^{-1}		(1S)
1-8	1.000	41.4	33.2	15.5	0.801	0.200	7.42E+03	298.11	0.040	0.002
2-8	0.800	33.1	30.7	14.4	0.926	0.200	8.57E+03	343.70	0.040	0.002
3-8	0.600	24.9	22.9	10.7	0.921	0.200	8.53E+03	423.12	0.049	0.003
4-8	0.400	16.6	14.8	6.9	0.893	0.200	8.27E+03	595.93	0.072	0.004
5-8	0.400	16.6	14.9	7.0	0.899	0.200	8.32E+03	583.47	0.070	0.004
6-8	0.200	8.3	7.4	3.5	0.893	0.200	8.27E+03	888.43	0.107	0.007
7-8	0.200	8.3	7.4	3.5	0.893	0.200	8.27E+03	882.08	0.106	0.007
8-8	1.000	41.4	32.0	15.0	0.772	0.200	7.15E+03	2.98		

Table A-3. Carbon-14 efficiency measurement data for 07/23/04 with measured efficiency and total propagated uncertainty (1S).

Preparation Date			Radionuclide	Carbon-14						
7/23/2004			Concentration (C_A)		46282	min^{-1} mL^{-1}	5/26/2004			
			Na_2CO_3 Carrier (C_C)		41.43	mg mL^{-1}				
			Background Count Rate (R_b)			1.93	min^{-1}			
Number	Na_2CO_3 Carrier V_C	Expected Mass $V_C \cdot C_C$	Net Weight eq (3-3) W_{net}	Thickness eq (3-4) T_m	Yield eq (3-5) Y	Volume Radionuclide V_R	Activity eq (3-6) A_T	Total Count Rate R_g	Efficiency eq (3-7) E_R	Total Uncertainty
	mL	mg	mg	mg cm^{-2}		mL	min^{-1}	min^{-1}		(1S)
1-8	1.000	41.4	33.3	15.6	0.804	0.200	7.44E+03	291.74	0.039	0.002
2-8	0.800	33.1	30.3	14.2	0.914	0.200	8.46E+03	347.95	0.041	0.002
3-8	0.600	24.9	22.7	10.6	0.913	0.400	8.45E+03	877.17	0.052	0.005
4-8	0.400	16.6	15.2	7.1	0.917	0.200	8.49E+03	603.03	0.071	0.004
5-8	0.400	16.6	15.6	7.3	0.941	0.200	8.71E+03	628.75	0.072	0.004
6-8	0.200	8.3	7.8	3.6	0.941	0.200	8.71E+03	925.87	0.106	0.006
7-8	0.200	8.3	7.8	3.6	0.941	0.200	8.71E+03	889.07	0.102	0.006
8-8	1.000	41.4	33.2	15.5	0.801	0.200	7.42E+03	291.18	0.039	0.002

Table A-4. Carbon-14 efficiency measurement data for 08/06/04 with measured efficiency and total propagated uncertainty (1S).

Preparation Date			Radionuclide	Carbon-14						
8/6/2004			Concentration (	46282	min^{-1} mL^{-1}	5/26/2004				
			Na_2CO_3 Carrier	41.43	mg mL^{-1}					
			Background Count Rate (R_b)			1.93	min^{-1}			
Number	Na2CO3 Carrier V_C	Expected Mass $V_C \cdot C_C$	Net Weight eq (3-3) W_{net}	Thickness eq (3-4) T_m	Yield eq (3-5) Y	Volume Radionuclide V_R	Activity eq (3-6) A_T	Total Count Rate R_g	Efficiency eq (3-7) E_R	Total Uncertainty
	mL	mg	mg	mg cm^{-2}		mL	min^{-1}	min^{-1}		(1S)
1-8	0.250	10.4	10.0	4.68	0.965	0.200	8.94E+03	786.95	0.088	0.005
2-8	0.250	10.4	10.1	4.72	0.975	0.200	9.03E+03			
3-8	1.000	41.4	33.0	15.43	0.797	0.200	7.37E+03	286.34	0.039	0.002
4-8	1.000	41.4	32.4	15.15	0.782	0.200	7.24E+03	262.33	0.036	0.002
5-8	1.250	51.8	36.4	17.03	0.703	0.200	6.51E+03	242.95	0.037	0.002
6-8	1.250	51.8	33.4	15.62	0.645	0.200	5.97E+03	221.23	0.037	0.002
7-8	1.500	62.1	33.1	15.48	0.533	0.200	4.93E+03	180.57	0.036	0.002
8-8	1.500	62.1	31.7	14.83	0.510	0.200	4.72E+03	172.58	0.036	0.002

Table A-5. Carbon-14 efficiency measurement data for 08/13/04 with measured efficiency and total propagated uncertainty (1S).

Preparation Date			Radionuclide	Carbon-14						
8/13/2004			Concentration (C_A)		46282	min^{-1} mL^{-1}	5/26/2004			
			Na_2CO_3 Carrier (C_C)		41.43	mg mL^{-1}				
			Background Count Rate (F		1.93	min^{-1}				
Number	Na2CO3 Carrier V_C	Expected Mass $V_C \cdot C_C$	Net Weight eq (3-3) W_{net}	Thickness eq (3-4) T_m	Yield eq (3-5) Y	Volume Radionuclide V_R	Activity eq (3-6) A_T	Total Count Rate R_g	Efficiency eq (3-7) E_R	Total Uncertainty (1S)
	mL	mg	mg	mg cm^{-2}		mL	min^{-1}	min^{-1}		
1-8	0.200	8.3	7.6	3.6	0.917	0.200	8.49E+03			
2-8	0.200	8.3	7.5	3.5	0.905	0.200	8.38E+03	883.80	0.105	0.006
3-8	1.400	58.0	49.8	23.3	0.859	0.400	1.59E+04	430.40	0.027	0.001
4-8	1.400	58.0	53.3	24.9	0.919	0.400	1.70E+04	419.61	0.025	0.001
5-8	0.000	0.0	0.0	0.0	NA	0.000	NA	598.60	NA	
6-8	0.000	0.0	0.0	0.0	NA	0.000	NA	542.03	NA	

Table A-6. Strontium-89 efficiency measurements, efficiencies from self-absorption equation, and fit to Monte Carlo simulation expected efficiencies.

Sr-89 Results						E_0	0.52			MCNP	
						μ	0.012				
Date	Number	Area Thickness (mg cm^{-2})	Counting Efficiency	Uncertainty (95% CL)	Area Thickness (mg cm^{-2})	Efficiency	Difference (Measured - Efficiency)	Area Thickness (mg cm^{-2})	Interpolated Efficiency	Difference (Measured MCNP)
4/15/1999	4-8	5.7	0.495	0.022	5.7	0.503	-0.007	5.7	0.504	-0.009
4/15/1999	3-8	5.7	0.479	0.022	5.7	0.503	-0.024	5.7	0.504	-0.025
4/15/1999	1-8	6.0	0.480	0.022	6.0	0.502	-0.021	6.0	0.503	-0.022
4/15/1999	2-8	6.1	0.471	0.022	6.1	0.501	-0.030	6.1	0.503	-0.031
2/28/1999	2-8	6.7	0.481	0.035	6.7	0.500	-0.019	6.7	0.500	-0.020
3/28/1999	1-8	7.6	0.507	0.037	7.6	0.497	0.010	7.6	0.497	0.010
2/28/1999	3-8	7.9	0.494	0.035	7.9	0.496	-0.002	7.9	0.496	-0.002
2/28/1999	1-8	8.0	0.486	0.035	8.0	0.496	-0.010	8.0	0.496	-0.010
3/28/1999	4-8	8.3	0.479	0.017	8.3	0.495	-0.016	8.3	0.495	-0.016
3/28/1999	2-8	8.6	0.511	0.037	8.6	0.494	0.017	8.6	0.493	0.018
2/28/1999	5-8	9.4	0.491	0.033	9.4	0.492	-0.001	9.4	0.490	0.001
2/28/1999	6-8	9.8	0.488	0.033	9.8	0.491	-0.003	9.8	0.489	-0.001
4/15/1999	6-8	11.1	0.461	0.013	11.1	0.487	-0.026	11.1	0.485	-0.024
4/15/1999	7-8	11.9	0.469	0.013	11.9	0.485	-0.016	11.9	0.482	-0.013
4/15/1999	8-8	12.0	0.478	0.013	12.0	0.484	-0.007	12.0	0.482	-0.004
4/15/1999	5-8	12.4	0.470	0.013	12.4	0.483	-0.013	12.4	0.481	-0.011
2/14/1999	5-8	13.0	0.467	0.031	13.0	0.482	-0.015	13.0	0.479	-0.012
2/14/1999	6-8	13.4	0.468	0.031	13.4	0.480	-0.012	13.4	0.478	-0.009
2/14/1999	4-8	13.8	0.473	0.031	13.8	0.479	-0.007	13.8	0.476	-0.004
2/14/1999	1-8	15.1	0.475	0.031	15.1	0.476	-0.001	15.1	0.473	0.003
2/28/1999	7-8	15.2	0.471	0.033	15.2	0.475	-0.005	15.2	0.472	-0.001
2/14/1999	2-8	15.5	0.473	0.031	15.5	0.474	-0.001	15.5	0.471	0.002
2/14/1999	3-8	15.9	0.464	0.031	15.9	0.473	-0.009	15.9	0.470	-0.006
3/28/1999	6-8	17.9	0.457	0.013	17.9	0.468	-0.011	17.9	0.465	-0.008
3/28/1999	5-8	18.5	0.453	0.012	18.5	0.466	-0.013	18.5	0.463	-0.010
3/28/1999	8-8	19.1	0.452	0.012	19.1	0.465	-0.013	19.1	0.462	-0.010
3/28/1999	7-8	19.4	0.453	0.012	19.4	0.464	-0.011	19.4	0.461	-0.008
3/19/1999	4-8	21.1	0.452	0.031	21.1	0.459	-0.008	21.1	0.457	-0.005
3/19/1999	2-8	21.3	0.460	0.031	21.3	0.459	0.001	21.3	0.456	0.004
3/19/1999	1-8	21.3	0.454	0.031	21.3	0.459	-0.005	21.3	0.456	-0.002
3/19/1999	3-8	21.4	0.466	0.031	21.4	0.459	0.007	21.4	0.456	0.010
3/19/1999	6-8	31.1	0.439	0.029	31.1	0.434	0.005	31.1	0.435	0.004
3/19/1999	8-8	31.2	0.450	0.029	31.2	0.434	0.017	31.2	0.434	0.016
3/19/1999	5-8	31.4	0.438	0.029	31.4	0.433	0.005	31.4	0.434	0.004
		Number	34			Average	-0.0071		Average	-0.0049
						Std Dev	0.0111		Std Dev	0.0105
									Std Error	0.0018

Table A-7. Strontium-89 efficiency measurement data for 02/14/99 with measured efficiency and total propagated uncertainty (1S).

Preparation Date		Radionuclide	Sr-89								
2/14/1999		Concentration (C_A)	825.46	min^{-1} mL^{-1}	1/25/1999	12:00 PM					
		$SrCO_3$ Carrier (C_C)	34.36	mg mL^{-1}							
		Background Count Rate (R_b)	2.22	min^{-1}							
Number	Volume Radionuclide V_R	Standard Weight	Carrier Volume V_C	Carrier Weight	Filter Weight W_f	Filter+Ppt Weight W_{f+ppt}	Net Weight eq (3-3) W_{net}	Yield eq (3-5) Y	Activity eq (3-6) A_T	Total Count Rate R_g	Efficiency eq (3-7) E_R	Total Uncertainty (1S)
	mL	g	mL	g	g	g	mg		min^{-1}	min^{-1}		
1-8	1.0000	0.9993	1.0000	1.0337	0.0212	0.0534	32.2	0.937	625.19	280.63	0.475	0.016
2-8	1.0000	1.0003	1.0000	1.0351	0.0210	0.0542	33.2	0.966	625.46	288.03	0.473	0.016
3-8	1.0000	0.9998	1.0000	1.0379	0.0210	0.0550	34.0	0.990	624.78	289.17	0.464	0.016
4-8	1.0000	1.0012	0.9000	0.9273	0.0213	0.0508	29.5	0.954	625.30	284.15	0.473	0.016
5-8	1.0000	1.0014	0.9000	0.9319	0.0210	0.0487	27.7	0.896	625.07	263.60	0.467	0.016
6-8	1.0000	1.0010	0.9000	0.9324	0.0212	0.0498	28.6	0.925	624.46	272.78	0.468	0.016
7-8	1.0000	0.0000	0.9000	0.9318	0.0209	0.0505	29.6	0.957	0	1.67		
8-8	1.0000	0.0000	1.0000	1.0380	0.0213	0.0545	33.2	0.966	0	2.77		

Table A-8. Strontium-89 efficiency measurement data for 02/28/99 with measured efficiency and total propagated uncertainty (1S).

Preparation Date		Radionuclide	Sr-89									
2/28/1999		Concentration (C_A)	825.46	min^{-1} mL^{-1}	1/25/1999	12:00 PM						
		$SrCO_3$ Carrier (C_C)	34.36	mg mL^{-1}								
		Background Count Rate (R_b)	2.22	min^{-1}								
Number	Volume Radionuclid V_R	Standard Weight	Carrier Volume V_C	Carrier Weight	Filter Weight W_f	Filter+Ppt Weight W_{f+ppt}	Net Weight eq (3-3) W_{net}	Yield eq (3-5) Y	Activity eq (3-6) A_T	Total Coun Rate R_g	Efficiency eq (3-7) E_R	Total Uncertainty (1S)
	mL	g	mL	g	g	g	mg		min^{-1}	min^{-1}		
1-8	1.000	1.0018	0.500	0.5189	0.0215	0.0385	17	99.0%	517.38	250.93	0.486	0.018
2-8	1.000	1.0029	0.500	0.5183	0.0208	0.0351	14.3	83.2%	517.65	209.4	0.481	0.018
3-8	1.000	1.0015	0.500	0.5183	0.0210	0.0379	16.9	98.4%	516.64	253.37	0.494	0.018
4-8	1.000	1.0038	0.650	0.6750	0.0209	0.0000					Lost	NA
5-8	1.000	1.0025	0.650	0.6731	0.0211	0.0413	20.2	90.4%	516.86	231.62	0.491	0.017
6-8	1.000	1.0019	0.650	0.6729	0.0209	0.0419	21	94.0%	516.25	239.05	0.488	0.017
7-8	1.000	1.0013	1.000	1.0369	0.0211	0.0536	32.5	94.6%	515.65	231.85	0.471	0.017
8-8	0.000	0.0000	1.000	1.0352	0.0212	0.0544	33.2	96.6%	0.00	2.38	Blank	

Table A-9. Strontium-89 efficiency measurement data for 03/19/99 with measured efficiency and total propagated uncertainty (1S).

Preparation Date			Radionuclide		Sr-89							
3/19/1999			Concentration (C_A)		825.46	min^{-1} mL^{-1}	1/25/1999	12:00 PM				
			$SrCO_3$ Carrier (C_C)		34.36	mg mL^{-1}						
			Background Count Rate (R_b)			2.22	min^{-1}					
Number	Volume Radionuclide V_R	Standard Weight	Carrier Volume V_C	Carrier Weight	Filter Weight W_f	Filter+Ppt Weight W_{f+ppt}	Net Weight eq (3-3) W_{net}	Yield eq (3-5) Y	Activity eq (3-6) A_T	Total Count Rate R_g	Efficiency eq (3-7) E_R	Total Uncertainty (1S)
	mL	g	mL	g	g	g	mg		min^{-1}	min^{-1}		
1-8	1.000	1.0003	1.400	1.4511	0.0227	0.0683	45.6	94.8%	516.61	174.87	0.353	0.016
2-8	1.000	1.0017	1.400	1.4527	0.0224	0.0679	45.5	94.6%	517.04	177.12	0.358	0.016
3-8	1.000	1.0009	1.400	1.4508	0.0223	0.0681	45.8	95.2%	516.33	180.02	0.362	0.016
4-8	1.000	0.9990	1.400	1.4498	0.0220	0.0672	45.2	94.0%	520.73	172.07	0.347	0.016
5-8	1.000	1.0004	2.000	2.0738	0.0218	0.0890	67.2	97.8%	515.77	173.7	0.340	0.015
6-8	1.000	1.0013	2.000	2.0769	0.0218	0.0882	66.4	96.6%	515.94	172.23	0.341	0.015
7-8	1.000	1.0022	2.000	2.0765	0.0220	0.0220	0	0.0%	516.11			
8-8	1.000	0.9960	2.000	2.0747	0.0220	0.0888	66.8	97.2%	512.63	176.15	0.349	0.015

Table A-10. Strontium-89 efficiency measurement data for 03/28/99 with measured efficiency and total propagated uncertainty (1S).

Preparation Date					Radionuclide Sr-89							
3/28/1999					Concentration (C_A)[a]		825.46	min^{-1} mL^{-1}	Date	1/25/1999	12:00 PM	
					Concentration (C_A)[b]		9926.34	min^{-1} mL^{-1}	Date	1/25/1999	12:00 PM	
					$SrCO_3$ Carrier (C_C)		34.36	mg mL^{-1}				
								Background Count Rate		2.22	min^{-1}	
Number	Volume Radionuclid V_R	Standard Weight	Carrier Volume V_C	Carrier Weight	Filter Weight W_f	Filter+Ppt Weight W_{f+ppt}	Net Weight eq (3-3) W_{net}	Yield eq (3-5) Y	Activity eq (3-6) A_T	Total Count Rate R_g	Efficiency eq (3-7) E_R	Total Uncertainty (1S)
	mL	g	mL	g	g	g	mg		min^{-1}	min^{-1}		
1-8[a]	0.675	0.6777	0.675	0.7000	0.0211	0.0373	16.2	0.6985	240.40	87.33	0.507	0.019
2-8[a]	0.675	0.6770	0.675	0.7031	0.0212	0.0395	18.3	0.7890	240.01	99.05	0.511	0.019
3-8[a]	0.675	0.6795	0.675	0.6941	0.0210	0.0000			240.76			
4-8[b]	0.675	0.5007	0.675	0.6957	0.0208	0.0385	17.7	0.7632	2134.44	782.2	0.479	0.009
5-8[b]	0.500	0.5058	1.350	1.3919	0.0214	0.0609	39.5	0.8516	2154.93	833.99	0.453	0.006
6-8[b]	0.500	0.5050	1.350	1.3955	0.0210	0.0592	38.2	0.8235	2150.29	812.19	0.457	0.006
7-8[b]	0.500	0.5053	1.350	1.3973	0.0206	0.0620	41.4	0.8925	2150.34	871.75	0.453	0.006
8-8[b]	0.500	0.5046	1.350	1.3982	0.0214	0.0622	40.8	0.8796	2146.13	855.49	0.452	0.006
a		activity added 825.46 min^{-1} mL^{-1}										
b		activity added 9925.1 min^{-1} mL^{-1}										

Table A-11. Strontium-89 efficiency measurement data for 04/15/99 with measured efficiency and total propagated uncertainty (1S).

Preparation Date												
4/15/1999				Radionuclide	Sr-89							
				Concentration (C_A)	9926.34	min^{-1} mL^{-1}		1/25/1999	12:00 PM			
				$SrCO_3$ Carrier (C_C)	34.36	mg mL^{-1}						
						Background Count Rate (R_b)			2.22	min^{-1}		
Number	Volume Radionuclide V_R	Standard Weight	Carrier Volume V_C	Carrier Weight	Filter Weight W_f	Filter+Ppt Weight W_{f+ppt}	Net Weight eq (3-3) W_{net}	Yield eq (3-5) Y	Activity eq (3-6) A_T	Total Count Rate R_g	Efficiency eq (3-7) E_R	Total Uncertainty (1S)
	mL	g	mL	g	g	g	mg		min^{-1}	min^{-1}		
1-8	0.415	0.4137	0.415	0.4307	0.0212	0.0341	12.9	90.47%	1255.02	547.75	0.480	0.011
2-8	0.415	0.4147	0.415	0.4297	0.0213	0.0344	13.1	91.87%	1257.33	546.53	0.471	0.011
3-8	0.415	0.4147	0.415	0.4303	0.0213	0.0335	12.2	85.56%	1273.97	524.2	0.479	0.011
4-8	0.415	0.4126	0.415	0.4307	0.0214	0.0336	12.2	85.56%	1249.52	531.65	0.495	0.011
5-8	0.830	0.8272	0.830	0.8557	0.0209	0.0474	26.5	92.92%	2503.67	1096.17	0.470	0.007
6-8	0.830	0.8274	0.830	0.8546	0.0211	0.0448	23.7	83.10%	2502.85	960.13	0.461	0.007
7-8	0.830	0.8262	0.830	0.8557	0.021	0.0464	25.4	89.06%	2497.79	1045.77	0.469	0.007
8-8	0.830	0.8265	0.830	0.8585	0.021	0.0467	25.7	90.12%	2497.27	1077.28	0.478	0.007

Table A-12. Strontium-90 and yttrium-90 counting efficiencies as a function of areal thickness with total propagated uncertainties (95% CL).

Date	Number	Mass Thickness (mg cm^{-2})	Strontium-90 Efficiency	Uncertainty (95% CL)	Yttrium-90 Efficiency	Uncertainty (95% CL)
02/21/00	5-8	2.9	0.403	0.018	0.542	0.024
11/11/01	5-8	3.0	0.410	0.018	0.555	0.025
11/11/01	6-8	3.0	0.407	0.018	0.533	0.024
02/21/00	2-8	3.2	0.392	0.017	0.545	0.023
11/11/01	4-8	3.5	0.402	0.016	0.556	0.020
11/11/01	1-8	3.8	0.394	0.015	0.532	0.012
11/11/01	2-8	3.9	0.393	0.015	0.536	0.020
11/11/01	3-8	4.0	0.384	0.014	0.534	0.020
11/04/01	8-8	4.1	0.389	0.014	0.548	0.020
11/04/01	5-8	4.2	0.397	0.014	0.523	0.019
11/04/01	6-8	4.2	0.390	0.014	0.531	0.019
01/08/00	5-8	4.5	0.412	0.013	0.558	0.018
01/08/00	8-8	4.6	0.388	0.012	0.536	0.017
11/04/01	1-8	4.7	0.391	0.013	0.510	0.017
01/08/00	6-8	4.9	0.391	0.012	0.541	0.017
11/04/01	2-8	4.9	0.388	0.013	0.512	0.017
11/04/01	3-8	4.9	0.387	0.013	0.515	0.017
11/04/01	4-8	4.9	0.386	0.013	0.532	0.018
08/04/02	1-8	6.9	0.363	0.011	0.538	0.015
08/04/02	3-8	7.2	0.364	0.011	0.528	0.015
01/08/00	2-8	7.5	0.368	0.009	0.520	0.013
08/04/02	2-8	7.6	0.353	0.011	0.505	0.015
08/04/02	4-8	7.6	0.353	0.011	0.532	0.015
01/08/00	4-8	7.6	0.365	0.009	0.521	0.013
01/08/00	3-8	7.7	0.360	0.009	0.535	0.014
08/04/02	7-8	9.2	0.349	0.011	0.531	0.014
08/04/02	5-8	9.4	0.348	0.010	0.525	0.014
08/04/02	6-8	9.5	0.344	0.010	0.524	0.014
07/29/00	4-8	12.3	0.319	0.008	0.513	0.013
07/29/00	1-8	12.4	0.328	0.008	0.517	0.013
09/03/01	7-8	14.2	0.284	0.007	0.559	0.014
09/03/01	8-8	14.2	0.318	0.008	0.519	0.013
09/03/01	2-8	17.2	0.303	0.008	0.531	0.013
09/03/01	3-8	17.7	0.300	0.007	0.494	0.012
09/03/01	1-8	18.0	0.305	0.008	0.514	0.013
09/03/01	6-8	21.9	0.305	0.007	0.475	0.012
09/03/01	5-8	22.1	0.275	0.007	0.505	0.012
09/07/01	3-8	24.8	0.276	0.007	0.490	0.012
09/07/01	2-8	24.9	0.271	0.007	0.451	0.011
09/07/01	1-8	25.5	0.265	0.006	0.491	0.012
09/07/01	5-8	26.4	0.264	0.006	0.498	0.012
09/07/01	4-8	29.4	0.249	0.006	0.499	0.012
09/07/01	6-8	29.7	0.250	0.006	0.494	0.012
02/21/00	8-8	29.8	0.237	0.006	0.464	0.011
02/21/00	7-8	30.1	0.233	0.006	0.479	0.012
02/21/00	6-8	30.4	0.233	0.006	0.473	0.011
09/07/01	7-8	32.6	0.240	0.006	0.485	0.012
09/07/01	8-8	33.3	0.237	0.006	0.505	0.012
Number of measurements			48		48	

Table A-13. Efficiencies estimated by self-absorption equation and differences from strontium-90 and yttrium-90 efficiency measurements.

Thickness (mg cm $^{-}$)	E_{0} = 0.430 Efficiency	μ= 0.044 Difference	E_{0} = 0.540 Efficiency	μ= 0.008 Difference
2.9	0.403	0.001	0.534	-0.008
3.0	0.403	-0.007	0.534	-0.021
3.0	0.402	-0.004	0.534	0.001
3.2	0.401	0.009	0.534	-0.012
3.5	0.399	-0.003	0.533	-0.023
3.8	0.396	0.002	0.532	0.000
3.9	0.395	0.002	0.532	-0.004
4.0	0.394	0.010	0.532	-0.002
4.1	0.394	0.005	0.532	-0.016
4.2	0.393	-0.004	0.532	0.008
4.2	0.393	0.002	0.532	0.001
4.5	0.390	-0.022	0.531	-0.027
4.6	0.389	0.001	0.531	-0.006
4.7	0.389	-0.002	0.531	0.021
4.9	0.387	-0.004	0.530	-0.011
4.9	0.387	-0.001	0.530	0.018
4.9	0.387	0.000	0.530	0.015
4.9	0.387	0.001	0.530	-0.002
6.9	0.371	0.008	0.526	-0.011
7.2	0.369	0.005	0.526	-0.002
7.5	0.366	-0.002	0.525	0.005
7.6	0.366	0.012	0.525	0.020
7.6	0.366	0.013	0.525	-0.007
7.6	0.366	0.001	0.525	0.004
7.7	0.365	0.005	0.525	-0.011
9.2	0.354	0.005	0.522	-0.009
9.4	0.352	0.004	0.521	-0.004
9.5	0.351	0.007	0.521	-0.003
12.3	0.332	0.013	0.516	0.003
12.4	0.331	0.003	0.516	-0.001
14.2	0.320	0.036	0.512	-0.047
14.2	0.320	0.002	0.512	-0.007
17.2	0.302	-0.002	0.507	-0.024
17.7	0.299	-0.001	0.506	0.012
18.0	0.297	-0.008	0.505	-0.009
21.9	0.276	-0.029	0.498	0.023
22.1	0.275	0.000	0.498	-0.007
24.8	0.262	-0.014	0.493	0.003
24.9	0.261	-0.010	0.493	0.041
25.5	0.258	-0.007	0.491	0.000
26.4	0.254	-0.010	0.490	-0.008
29.4	0.241	-0.008	0.485	-0.015
29.7	0.240	-0.010	0.484	-0.010
29.8	0.239	0.002	0.484	0.020
30.1	0.238	0.006	0.483	0.004
30.4	0.237	0.004	0.483	0.010
32.6	0.229	-0.011	0.479	-0.006
33.3	0.225	-0.012	0.478	-0.027
	Average	0.000		-0.003
	Std Dev	0.010		0.015
	Number	48		48

Table A-14. Evaluation of fit to MCNP efficiency estimates for strontium-90 and yttrium-90.

Areal thickness	Strontium-90 Efficiency		Yttium-90 Efficiency	
(mg cm^{-2})	Interpolated	Difference	Interpolated	Difference
2.9	0.402	-0.001	0.541	-0.001
3.0	0.401	-0.009	0.541	-0.014
3.0	0.401	-0.006	0.541	0.008
3.2	0.399	0.007	0.540	-0.005
3.5	0.397	-0.006	0.540	-0.016
3.8	0.393	-0.001	0.539	0.007
3.9	0.392	-0.001	0.539	0.002
4.0	0.391	0.007	0.538	0.004
4.1	0.390	0.002	0.538	-0.010
4.2	0.389	-0.008	0.538	0.014
4.2	0.389	-0.001	0.538	0.007
4.5	0.386	**-0.026**	0.537	-0.020
4.6	0.385	-0.003	0.537	0.001
4.7	0.384	-0.007	0.537	0.027
4.9	0.383	-0.009	0.536	-0.005
4.9	0.383	-0.005	0.536	0.024
4.9	0.383	-0.005	0.536	0.021
4.9	0.382	-0.003	0.536	0.004
6.9	0.366	0.003	0.531	-0.006
7.2	0.364	-0.001	0.530	0.002
7.5	0.361	-0.007	0.529	0.010
7.6	0.360	0.007	0.529	0.025
7.6	0.360	0.007	0.529	-0.002
7.6	0.360	-0.005	0.529	0.008
7.7	0.359	-0.001	0.529	-0.006
9.2	0.347	-0.002	0.525	-0.006
9.4	0.345	-0.003	0.525	-0.001
9.5	0.344	0.000	0.524	0.000
12.3	0.326	0.007	0.519	0.006
12.4	0.325	-0.003	0.519	0.002
14.2	0.313	**0.029**	0.515	**-0.044**
14.2	0.313	-0.004	0.515	-0.003
17.2	0.297	-0.006	0.510	-0.021
17.7	0.294	-0.006	0.509	0.015
18.0	0.292	-0.013	0.509	-0.005
21.9	0.276	**-0.029**	0.502	0.026
22.1	0.275	0.000	0.501	-0.003
24.8	0.263	-0.013	0.497	0.007
24.9	0.262	-0.008	0.497	**0.045**
25.5	0.260	-0.006	0.496	0.005
26.4	0.255	-0.009	0.495	-0.004
29.4	0.242	-0.007	0.490	-0.009
29.7	0.241	-0.009	0.490	-0.004
29.8	0.241	0.004	0.490	0.026
30.1	0.240	0.007	0.489	0.010
30.4	0.238	0.005	0.489	0.016
32.6	0.231	-0.009	0.486	0.001
33.3	0.2279	-0.009	0.4849	-0.020
	Average	-0.003		0.002
	Std Dev	0.009		0.015
	Number	48		48

Table A-15. Strontium-90 and yttrium-90 efficiency measurement data for 01/08/00 with measured efficiency and total propagated uncertainty (1S).

Preparation

Date: 01/08/00 01:00 PM | Radionuclide: Sr-90 | Activity: 947.3 min^{-1} mL^{-1} | Date: 06/26/97 | Carrier: 34.36 mg mL^{-1}

Yttrium ppt

Number	$SrCO_3$ Carrier ml	Y(OH)x Carrier ml	Filter Weight grams	Filter+ppt Weight grams	Net Weight mg Eq 3-3	Yield Eq 3-5	Volume Radionuclide mL
1	0.520	1	0.0207	0.0000	NA	NA	1.000
2	0.520	1	0.0209	0.0370	16.1	0.901	1.000
3	0.520	1	0.0203	0.0368	16.5	0.923	1.000
4	0.520	1	0.0205	0.0367	16.2	0.907	1.000
5	0.346	1	0.0215	0.0312	9.7	0.816	1.000
6	0.346	1	0.0205	0.0309	10.4	0.875	1.000
7	0.346	1	0.0200	0.0286	8.6	0.723	1.000
8	0.346	1	0.0210	0.0309	9.9	0.833	1.000

First Count

Background Count Rate: 2.31 min^{-1} | Count Time: 100 minutes

Number	Activity min^{-1} Eq 3-11	Count Date	Count Time	Total Count Rate min^{-1}	Net Count Rate min^{-1} Eq 3-2	Y-90 Ingrowth Eq 3-9	cpm from Y-90 Eq 3-12
1	0.0	01/08/00	02:58 PM	0.00	0.00	0.000	0.00
2	803.0	01/08/00	02:58 PM	306.50	304.19	0.021	8.79
3	823.0	01/08/00	05:59 PM	321.66	319.35	0.053	23.14
4	808.0	01/08/00	06:59 PM	323.69	321.38	0.063	26.43
5	727.1	01/08/00	07:59 PM	331.23	328.92	0.073	29.52
6	779.6	01/08/00	08:59 PM	342.37	340.06	0.083	34.95
7	644.6	01/08/00	10:00 PM	305.52	303.21	0.093	34.11
8	742.1	01/08/00	11:00 PM	330.75	328.44	0.103	40.85

Second Count

Number	Activity min^{-1} Eq 3-13	Count Date	Count Time	Total Count Rate min^{-1}	Net Count Rate min^{-1} Eq 3-2	Y-90 Ingrowth Eq 3-9
1	0.0	05/28/00	10:38 AM	0.00	NA	1.000
2	795.6	05/28/00	11:38 AM	714.91	712.6	1.000
3	815.4	05/28/00	12:38 PM	739.04	736.73	1.000
4	800.5	05/28/00	01:38 PM	718.58	716.27	1.000
5	720.4	05/28/00	02:38 PM	707.09	704.78	1.000
6	772.4	05/28/00	03:39 PM	729.40	727.09	1.000
7	638.7	05/28/00	04:39 PM	638.78	636.47	1.000
8	735.2	05/28/00	05:39 PM	687.93	685.62	1.000

Efficiency

Source Identification Date	Number	Thickness mg cm^{-2} Eq 3-4	Y-90 Efficiency Eq 3-14	Uncertainty (1S)	Sr-90 Efficiency Eq 3-15	Uncertainty (1S)	Comments
1/8/2000	1	NA	NA	NA	NA		Lost
1/8/2000	2	7.5	0.520	0.013	0.368	0.009	
1/8/2000	3	7.7	0.535	0.014	0.360	0.009	
1/8/2000	4	7.6	0.521	0.013	0.365	0.009	
1/8/2000	5	4.5	0.558	0.018	0.412	0.013	
1/8/2000	6	4.9	0.541	0.017	0.391	0.012	
1/8/2000	7	4.0	0.570	0.020	0.417	0.014	Low Yield
1/8/2000	8	4.6	0.536	0.017	0.388	0.012	

Table A-16. Strontium-90 and yttrium-90 efficiency measurement data for 02/21/00 with measured efficiency and total propagated uncertainty (1S).

Preparation

	Date	02/21/00		Radionuclide	Sr-90		Carrier
	Yttrium ppt	01:00 PM		Activity	3527.4 min^{-1} mL^{-1}		34.36 mg mL^{-1}
				Date	06/26/97		
Number	$SrCO_3$ Carrier ml	$Y(OH)_x$ Carrier ml	Filter Weight grams	Filter+ppt Weight grams	Net Weight mg	Yield	Volume Radionuclide mL
					Eq 3-3	Eq 3-5	
1	0.262	1.000	0.0221	0.0267	4.6	0.511	0.500
2	0.262	1.000	0.0210	0.0279	6.9	0.766	0.500
3	0.262	1.000	0.0207	0.0256	4.9	0.544	0.500
4	0.262	1.000	0.0209	0.0272	6.3	0.700	0.500
5	2.000	1.000	0.0205	0.0855	65.0	0.946	0.500
6	2.000	1.000	0.0207	0.0850	64.3	0.936	0.500
7	2.000	1.000	0.0207	0.0845	63.8	0.928	0.500
8	2.000	1.000	0.0208	0.0822	61.4	0.893	0.500

First Count

		Background	Count Rate	2.31	min-1		
			Count Time	100	minutes		
		Count	Count	Total	Net	Y-90	cpm
Number	Activity min^{-1}	Date	Time	Count Rate min^{-1}	Count Rate min^{-1}	Ingrowth	from Y-90
	Eq 3-11				Eq 3-2	Eq 3-9	see Eq 3-10
1	845.4	02/21/00	09:35 PM	436.86	434.55	0.089	47.64
2	1268.0	02/21/00	10:35 PM	567.33	565.02	0.099	68.23
3	900.5	02/21/00	11:35 PM	402.09	399.78	0.108	49.91
4	1157.8	02/22/00	12:35 AM	542.57	540.26	0.118	74.01
5	1564.8	02/21/00	05:34 PM	403.15	400.84	0.048	35.77
6	1548.0	02/21/00	06:34 PM	406.30	403.99	0.059	43.48
7	1535.9	02/21/00	07:35 PM	415.33	413.02	0.069	49.00
8	1478.2	02/21/00	08:35 PM	417.57	415.26	0.079	55.90

Second Count

		Count	Count	Total	Net	Y-90
Number	Activity min^{-1}	Date	Time	Count Rate min^{-1}	Count Rate min^{-1}	Ingrowth
	Eq 3-13				Eq 3-2	Eq 3-9
1	844.5	03/08/00	07:16 PM	917.18	914.87	0.985
2	1266.7	03/08/00	08:17 PM	1179.96	1177.65	0.986
3	899.5	03/08/00	09:17 PM	805.70	803.39	0.986
4	1156.5	03/08/00	10:17 PM	1086.23	1083.92	0.986
5	1563.2	03/08/00	11:17 PM	1096.80	1094.49	0.986
6	1546.3	03/09/00	12:18 AM	1093.55	1091.24	0.986
7	1534.3	03/09/00	01:18 AM	1067.98	1065.67	0.986
8	1476.6	03/09/00	02:18 AM	1060.04	1057.73	0.986

Efficiency

Source Identification		Thickness	Y-90		Sr-90	Uncertainty	
Date	Number	mg cm^{-2}	Efficiency		Efficiency	(1S)	Comments
		Eq 3-4	Eq 3-8		Eq 3-10		
2/21/2000	1	2.2	0.634	0.036	0.458	0.026	Yield 50%
2/21/2000	2	3.2	0.545	0.023	0.392	0.017	
2/21/2000	3	2.3	0.511	0.028	0.389	0.021	Yield 50%
2/21/2000	4	2.9	0.542	0.024	0.403	0.018	Ingrowth > 10%
2/21/2000	5	30.4	0.473	0.011	0.233	0.006	
2/21/2000	6	30.1	0.479	0.012	0.233	0.006	
2/21/2000	7	29.8	0.464	0.011	0.237	0.006	
2/21/2000	8	28.7	0.479	0.012	0.243	0.006	

Table A-17. Strontium-90 and yttrium-90 efficiency measurement data for 04/02/00 with measured efficiency and total propagated uncertainty (1S).

Preparation

	Date	04/02/00		Radionuclide	Sr-90		Carrier
	Yttrium ppt	01:00 PM		Activity	3527.4	min^{-1} mL^{-1}	34.84 mg mL^{-1}
				Date	06/26/97		
Number	$SrCO_3$ Carrier ml	$Y(OH)_x$ Carrier ml	Filter Weight grams	Filter+ppt Weight grams	Net Weight mg Eq 3-3	Yield Eq 3-5	Volume Radionuclide mL
1	1.600	1.000	0.0213	0.0718	50.5	0.906	0.500
2	1.600	1.000	0.0210	0.0735	52.5	0.942	0.500
3	1.600	1.000	0.0214	0.0729	51.5	0.924	0.500
4	1.600	1.000	0.0218	0.0714	49.6	0.890	0.500
5	2.000	1.000	0.0215	0.0876	66.1	0.949	0.500
6	2.000	1.000	0.0220	0.0866	64.6	0.927	0.500
7	2.000	1.000	0.0212	0.0866	65.4	0.939	0.500
8	2.000	1.000	0.0215	0.0860	64.5	0.926	0.500

First Count

		Background	Count Rate	2.31	min^{-1}		
			Count Time	100	minutes		
Number	Activity min^{-1} Eq 3-11	Count Date	Count Time	Total Count Rate min^{-1}	Net Count Rate min^{-1} Eq 3-2	Y-90 Ingrowth Eq 3-9	min^{-1} from Y-90 see Eq 3-10
1	1494.7	04/02/00	11:23 PM	433.03	430.72	0.106	84.35
2	1553.9	04/03/00	12:24 AM	452.77	450.46	0.116	94.92
3	1524.3	04/03/00	01:24 AM	451.14	448.83	0.126	102.43
4	1468.1	04/03/00	02:24 AM	446.70	444.39	0.135	103.66
5	1565.1	04/03/00	04:33 AM	440.28	437.97	0.155	129.14
6	1529.6	04/03/00	04:25 AM	436.20	433.89	0.154	121.50
7	1548.5	04/03/00	05:25 AM	NA	NA	0.163	NA
8	1527.2	04/03/00	05:25 AM	464.24	461.93	0.163	130.63

Second Count

Number	Activity min^{-1} Eq 3-13	Count Date	Count Time	Total Count Rate min^{-1}	Net Count Rate min^{-1} Eq 3-2	Y-90 Ingrowth Eq 3-9
1	1492.9	04/21/00	04:16 PM	1134.50	1132.19	0.993
2	1552.0	04/21/00	05:16 PM	1168.35	1166.04	0.993
3	1522.4	04/21/00	06:17 PM	1156.97	1154.66	0.993
4	1466.2	04/21/00	07:17 PM	1103.92	1101.61	0.993
5	1563.2	04/21/00	08:17 PM	1138.01	1135.7	0.993
6	1527.7	04/21/00	09:17 PM	1098.86	1096.55	0.993
7	1546.6	04/21/00	10:17 PM	NA	NA	0.994
8	1525.3	04/21/00	11:17 PM	1129.48	1127.17	0.994

Efficiency

Source Identification Date	Number	Thickness mg cm^{-2} Eq 3-4	Y-90 Efficiency Eq 3-8		Sr-90 Efficiency Eq 3-10		Comments
4/2/2000	1	23.6	0.530	0.013	0.232	0.006	Ingrowth > 10%
4/2/2000	2	24.6	0.526	0.013	0.229	0.006	Ingrowth > 10%
4/2/2000	3	24.1	0.534	0.013	0.227	0.006	Ingrowth > 10%
4/2/2000	4	23.2	0.522	0.013	0.232	0.006	Ingrowth > 10%
4/2/2000	5	30.9	0.532	0.013	0.197	0.005	Ingrowth > 10%
4/2/2000	6	30.2	0.517	0.013	0.204	0.005	Ingrowth > 10%
4/2/2000	7	30.6	NA		NA		Lost
4/2/2000	8	30.2	0.525	0.013	0.217	0.006	Ingrowth > 10%

Table A-18. Strontium-90 and yttrium-90 efficiency measurement data for 07/29/00 with measured efficiency and total propagated uncertainty (1S).

Preparation										
	Date	07/29/00		Radionuclide	Sr-90			Carrier		
	Yttrium ppt	03:00 PM		Activity	3527.4	min^{-1}	mL^{-1}	34.84	mg	mL^{-1}
				Date	06/26/97					
Number	$SrCO_3$ Carrier ml	$Y(OH)_x$ Carrier ml	Filter Weight grams	Filter+ppt Weight grams	Net Weight mg Eq 3-3	Yield Eq 3-5	Volume Radionuclide mL			
1	0.870	1.000	0.0206	0.0471	26.5	0.874	0.500			
2	0.870	1.000	0.0213	0.0289	7.6	0.251	0.500			
3	0.870	1.000	0.0214	0.0485	27.1	0.894	0.500			
4	0.870	1.000	0.0214	0.0477	26.3	0.868	0.500			
5	0.160	1.000	0.0207	0.0253	4.6	0.825	0.500			
6	0.160	1.000	0.0204	0.0244	4.0	0.718	0.500			
7	0.160	1.000	0.0207	0.0246	3.9	0.700	0.500			
8	0.160	1.000	0.0204	0.0244	4.0	0.718	0.500			
First Count										
		Background	Count Rate	2.31	min^{-1}					
			Count Time	100	minutes					
Number	Activity min^{-1} Eq 3-11	Count Date	Count Time	Total Count Rate cpm	Net Count Rate cpm Eq 3-2	Y-90 Ingrowth Eq 3-9	cpm from Y-90 see Eq 3-10			
1	1431.3	07/29/00	06:36 PM	500.18	497.87	0.038	28.38			
2	410.5	07/29/00	07:37 PM	173.56	171.25	0.049	10.87			
3	1463.7	07/29/00	08:37 PM							
4	1420.5	07/29/00	09:37 PM	505.73	503.42	0.069	50.46			
5	1351.0	07/29/00	10:37 PM	594.58	592.27	0.079	56.90			
6	1174.7	07/29/00	11:41 PM	572.90	570.59	0.090	37.65			
7	1145.4	07/30/00	12:38 AM	757.57	755.26	0.099	54.68			
8	1174.7	07/30/00	01:38 AM	674.68	672.37	0.109	49.47			
Second Count										
Number	Activity min^{-1} Eq 3-13	Count Date	Count Time	Total Count Rate min^{-1}	Net Count Rate min^{-1} Eq 3-2	Y-90 Ingrowth Eq 3-9				
1	1425.0	10/04/00	03:00 PM	1208.09	1205.78	1.000				
2	408.7	10/04/00	05:41 PM	384.28	381.97	1.000				
3	1457.4	10/04/00		0.00	NA	1.000				
4	1414.3	10/04/00	06:41 PM	1181.37	1179.06	1.000				
5	1345.0	10/04/00	07:41 PM	1253.30	1250.99	1.000				
6	1169.6	10/04/00	08:42 PM	953.05	950.74	1.000				
7	1140.3	10/04/00	09:42 PM	1252.58	1250.27	1.000				
8	1169.6	10/04/00	10:42 PM	1077.94	1075.63	1.000				
Efficiency										
	Source Identification		Thickness	Y-90	Uncertainty	Sr-90	Uncertainty			
	Date	Number	mg cm^{-2} Eq 3-4	Efficiency Eq 3-8	(1S)	Efficiency Eq 3-10	(1S)	Comments		
	7/29/2000	1	12.4	0.517	0.013	0.328	0.008			
	7/29/2000	2	3.6	0.542	0.022	0.391	0.015	Yield 25%		
	7/29/2000	3	12.7	NA		NA		Lost		
	7/29/2000	4	12.3	0.513	0.013	0.319	0.008			
	7/29/2000	5	2.2	0.532	0.031	0.396	0.023	first count 14 mi		
	7/29/2000	6	1.9	0.357	0.023	0.454	0.029	IEEE error		
	7/29/2000	7	1.8	0.482	0.032	0.612	0.040	IEEE error		
	7/29/2000	8	1.9	0.387	0.025	0.530	0.034	IEEE error		

Table A-19. Strontium-90 and yttrium-90 efficiency measurement data for 11/22/00 with measured efficiency and total propagated uncertainty (1S).

Preparation								
	Date	11/22/00		Radionuclide	Sr-90	min^{-1} mL^{-1}	Carrier	mg mL^{-1}
	Yttrium ppt	02:30 PM		Activity Date	3527.4 06/26/97		34.84	
Number	SrCO3 Carrier ml	Y(OH)x Carrier ml	Filter Weight grams	Filter+ppt Weight grams	Net Weight mg	Yield	Volume Radionuclide mL	
					Eq 3-3	Eq 3-5		
1	1.600	1.000	0.0207	0.0669	46.2	0.829	0.500	
2	1.600	1.000	0.0212	0.0731	51.9	0.931	0.500	
3	1.600	1.000	0.0212	0.0734	52.2	0.936	0.500	
4	1.600	1.000	0.0212	0.0738	52.6	0.944	0.500	
5	2.000	1.000	0.0205	0.0831	62.6	0.898	0.500	
6	2.000	1.000	0.0224	0.0506	28.2	0.405	0.500	
7	2.000	1.000	0.0211	0.0879	66.8	0.959	0.500	
8	2.000	1.000	0.0210	0.0892	68.2	0.979	0.500	

First Count								
		Background	Count Rate	2.31	min^{-1}			
			Count Time	100	minutes			
		Count	Count	Total	Net	Y-90	cpm	
Number	Activity min^{-1}	Date	Time	Count Rate min^{-1}	Count Rate min^{-1}	Ingrowth	from Y-90	
	Eq 3-11			(5)	Eq 3-2	Eq 3-9	see Eq 3-10	
1	1346.5	11/22/00	06:56 PM	401.10	398.79	0.047	31.43	
2	1512.6	11/22/00	07:57 PM	456.88	454.57	0.057	43.38	
3	1521.5	11/22/00		0.00	NA	NA		
4	1533.0	11/22/00	08:57 PM	450.38	448.07	0.067	50.74	
5	1459.6	11/22/00	09:57 PM	412.02	409.71	0.078	58.18	
6	657.5	11/22/00	10:57 PM	469.98	467.67	0.087	58.65	
7	1557.5	11/22/00	11:57 PM	443.41	441.10	0.097	72.50	
8	1590.1	11/23/00	12:58 AM	462.06	459.75	0.107	82.29	

Second Count							
		Count	Count	Total	Net	Y-90	
Number	Activity min^{-1}	Date	Time	Count Rate min^{-1}	Count Rate min^{-1}	Ingrowth	
	Eq 3-13			(5)	Eq 3-2	Eq 3-9	
1	1344.7	12/13/00	05:13 PM	1037.45	1035.14	0.996	
2	1510.6	12/13/00	06:14 PM	1167.35	1165.04	0.996	
3	1519.4	12/13/00			NA	NA	
4	1530.9	12/13/00	11:53 PM	1148.92	1146.61	0.996	
5	1457.6	12/13/00	08:14 PM	1101.55	1099.24	0.996	
6	656.6	12/13/00	09:15 PM	1079.41	1077.1	0.996	
7	1555.4	12/13/00	10:15 PM	1112.30	1109.99	0.996	
8	1588.0	12/13/00	11:15 PM	1144.64	1142.33	0.996	

Efficiency								
	Source Identification Date	Number	Thickness mg cm^{-2}	Y-90 Efficiency	Uncertainty (1S)	Sr-90 Efficiency	Uncertainty (1S)	Comments
			Eq 3-4	Eq 3-8		Eq 3-10		
	11/22/2000	1	21.6	0.498	0.012	0.273	0.007	
	11/22/2000	2	24.3	0.500	0.012	0.272	0.007	
	11/22/2000	3	24.4	NA	0.012	NA	0.007	Lost
	11/22/2000	4	24.6	0.491	0.012	0.259	0.006	
	11/22/2000	5	29.3	0.514	0.012	0.241	0.006	
	11/22/2000	6	13.2	1.020	0.012	0.622	0.007	Yield 40%
	11/22/2000	7	31.2	0.478	0.012	0.237	0.006	
	11/22/2000	8	31.9	0.483	0.012	0.237	0.006	

Table A-20. Strontium-90 and yttrium-90 efficiency measurement data for 09/03/01 with measured efficiency and total propagated uncertainty (1S).

Preparation

	Date	9/3/2001		Radionuclide	Sr-90		Carrier	
	Yttrium ppt	3:25 PM		Activity	3527.4	min^{-1} mL^{-1}	35.23	mg mL^{-1}
				Date	06/26/97			
	SrCO3	Y(OH)x	Filter	Filter+ppt	Net	Yield	Volume	
Number	Carrier ml	Carrier ml	Weight grams	Weight grams	Weight mg		Radionuclide mL	
					Eq 3-3	Eq 3-5		
1	1.250	1.000	0.0200	0.0585	38.5	0.874	0.500	
2	1.250	1.000	0.0207	0.0575	36.8	0.836	0.500	
3	1.250	1.000	0.0202	0.0580	37.8	0.858	0.500	
4	1.500	1.000	0.0208	0.0660	45.2	0.855	0.500	
5	1.500	1.000	0.0201	0.0674	47.3	0.895	0.500	
6	1.500	1.000	0.0202	0.0671	46.9	0.888	0.500	
7	1.000	1.000	0.0201	0.0504	30.3	0.860	0.500	
8	1.000	1.000	0.0202	0.0505	30.3	0.860	0.500	

First Count

		Background	Count Rate	2.31	min^{-1}			
			Count Time	100	minutes			
		Count	Count	Total	Net	Y-90	cpm	
Number	Activity min^{-1}	Date	Time	Count Rate min^{-1}	Count Rate min^{-1}	Ingrowth	from Y-90	
	Eq 3-11				Eq 3-2	Eq 3-9	Eq 3-12	
1	1394.0	09/03/01	06:17 PM	449.88	447.57	0.031	21.98	
2	1332.4	09/03/01	07:18 PM	435.46	433.15	0.041	29.22	
3	1368.6	09/03/01	08:18 PM	447.70	445.39	0.052	34.93	
4	1363.9	09/03/01		0.00	NA	NA	NA	
5	1427.1	09/03/01	09:19 PM	439.72	437.41	0.062	44.60	
6	1415.1	09/03/01	10:19 PM	482.52	480.21	0.072	48.45	
7	1371.3	09/03/01	11:19 PM	454.87	452.56	0.082	62.94	
8	1371.2	09/04/01	12:19 AM	503.15	500.84	0.092	65.45	

Second Count

		Count	Count	Total	Net	Y-90	
Number	Activity min^{-1}	Date	Time	Count Rate min^{-1}	Count Rate min^{-1}	Ingrowth	
	Eq 3-13				Eq 3-2	Eq 3-9	
1	1392.5	09/19/01	05:07 PM	1132.40	1130.09	0.985	
2	1331.0	09/19/01	06:08 PM	1102.24	1099.93	0.985	
3	1367.2	09/19/01	07:09 PM	1077.96	1075.65	0.985	
4	1362.4	09/19/01		0.00	NA	0.982	
5	1425.6	09/19/01	08:09 PM	1104.07	1101.76	0.985	
6	1413.6	09/19/01	09:09 PM	1096.03	1093.72	0.985	
7	1369.9	09/19/01	10:09 PM	1146.87	1144.56	0.985	
8	1369.9	09/19/01	11:10 PM	1138.25	1135.94	0.986	

Efficiency

	Source Identification		Thickness	Y-90	Uncertainty	Sr-90	Uncertainty	
	Date	Number	mg cm^{-2}	Efficiency	(1S)	Efficiency	(1S)	Comments
			Eq 3-4	Eq 3-14		Eq 3-15		
	9/3/2001	1	18.0	0.514	0.013	0.305	0.008	
	9/3/2001	2	17.2	0.531	0.013	0.303	0.008	
	9/3/2001	3	17.7	0.494	0.012	0.300	0.007	
	9/3/2001	4	21.1	NA		NA		Lost
	9/3/2001	5	22.1	0.505	0.012	0.275	0.007	
	9/3/2001	6	21.9	0.475	0.012	0.305	0.007	
	9/3/2001	7	14.2	0.559	0.014	0.284	0.007	
	9/3/2001	8	14.2	0.519	0.013	0.318	0.008	

Table A-21. Strontium-90 and yttrium-90 efficiency measurement data for 09/07/01 with measured efficiency and total propagated uncertainty (1S).

Preparation								
	Date	09/07/01		Radionuclide	Sr-90		Carrier	
	Yttrium ppt	03:30 PM		Activity	3527.4	min^{-1} mL^{-1}	35.23	mg mL^{-1}
				Date	06/26/97			
	SrCO3	Y(OH)x	Filter	Filter+ppt	Net	Yield	Volume	
Number	Carrier	Carrier	Weight	Weight	Weight		Radionuclide	
	ml	ml	grams	grams	mg		mL	
					Eq 3-3	Eq 3-5		
1	1.750	1.000	0.0203	0.0749	54.6	0.886	0.500	
2	1.750	1.000	0.0200	0.0733	53.3	0.865	0.500	
3	1.750	1.000	0.0198	0.0728	53.0	0.860	0.500	
4	2.000	1.000	0.0202	0.0831	62.9	0.893	0.500	
5	2.000	1.000	0.0200	0.0765	56.5	0.802	0.500	
6	2.000	1.000	0.0202	0.0837	63.5	0.901	0.500	
7	2.250	1.000	0.0198	0.0894	69.6	0.878	0.500	
8	2.250	1.000	0.0204	0.0917	71.3	0.899	0.500	

First Count		Background	Count Rate	2.31	cpm			
			Count Time	100	minutes			
		Count	Count	Total	Net	Y-90	cpm	
	Activity	Date	Time	Count Rate	Count Rate	Ingrowth	from	
Number	min^{-1}			min^{-1}	min^{-1}		Y-90	
	Eq 3-11				Eq 3-2	Eq 3-9	see Eq 3-10	
1	1411.7	09/07/01	06:39 PM	399.93	397.62	0.034	23.31	
2	1378.1	09/07/01	07:40 PM	402.80	400.49	0.044	27.50	
3	1370.3	09/07/01	08:40 PM	417.10	414.79	0.055	36.63	
4	1423.0	09/07/01	09:41 PM	402.72	400.41	0.065	46.03	
5	1278.2	09/07/01	10:41 PM	387.46	385.15	0.075	47.69	
6	1436.6	09/07/01	11:41 PM	421.55	419.24	0.085	60.25	
7	1399.6	09/08/01	12:41 AM	402.23	399.92	0.095	64.38	
8	1433.8	09/08/01	01:41 AM	418.03	415.72	0.105	75.73	

Second Count		Count	Count	Total	Net	Y-90	
	Activity	Date	Time	Count Rate	Count Rate	Ingrowth	
Number	min^{-1}			min^{-1}	min^{-1}		
	Eq 3-13				Eq 3-2	Eq 3-9	
1	1410.0	09/25/01	04:45 PM	1062.70	1060.39	0.991	
2	1376.4	09/25/01	05:46 PM	990.98	988.67	0.991	
3	1368.7	09/25/01	06:46 PM	1044.90	1042.59	0.991	
4	1421.3	09/25/01	07:46 PM	1060.10	1057.79	0.991	
5	1276.7	09/25/01	08:46 PM	970.27	967.96	0.991	
6	1434.9	09/25/01	09:47 PM	1064.07	1061.76	0.991	
7	1398.0	09/25/01	10:47 PM	1010.53	1008.22	0.991	
8	1432.1	09/25/01	11:47 PM	1059.63	1057.32	0.991	

Efficiency								
	Source Identification		Thickness	Y-90	Uncertainty	Sr-90	Uncertainty	
	Date	Number	mg cm^{-2}	Efficiency	(1S)	Efficiency	(1S)	Comments
			Eq 3-4	Eq 3-8		Eq 3-10		
	9/7/2001	1	25.5	0.491	0.012	0.265	0.006	
	9/7/2001	2	24.9	0.451	0.011	0.271	0.007	
	9/7/2001	3	24.8	0.490	0.012	0.276	0.007	
	9/7/2001	4	29.4	0.499	0.012	0.249	0.006	
	9/7/2001	5	26.4	0.498	0.012	0.264	0.006	
	9/7/2001	6	29.7	0.494	0.012	0.250	0.006	
	9/7/2001	7	32.6	0.485	0.012	0.240	0.006	
	9/7/2001	8	33.3	0.505	0.012	0.237	0.006	

Table A-22. Strontium-90 and yttrium-90 efficiency measurement data for 11/04/01 with measured efficiency and total propagated uncertainty (1S).

Preparation								
	Date	11/04/01		Radionuclide	Sr-90		Carrier	
	Yttrium ppt	07:30 PM		Activity	3527.4	min^{-1} mL^{-1}	35.23	mg mL^{-1}
				Date	06/26/97			
	SrCO3	Y(OH)x	Filter	Filter+ppt	Net	Yield	Volume	
Number	Carrier	Carrier	Weight	Weight	Weight		Radionuclide	
	ml	ml	grams	grams	mg		mL	
					Eq 3-3	Eq 3-5		
1	0.3500	1.0000	0.0199	0.0299	10.0	0.811	0.500	
2	0.3500	1.0000	0.0200	0.0304	10.4	0.843	0.500	
3	0.3500	1.0000	0.0198	0.0302	10.4	0.843	0.500	
4	0.3500	1.0000	0.0200	0.0305	10.5	0.852	0.500	
5	0.3000	1.0000	0.0199	0.0289	9.0	0.852	0.500	
6	0.3000	1.0000	0.0201	0.0291	9.0	0.852	0.500	
7	0.3000	1.0000	0.0198	0.0286	8.8	0.833	0.500	
8	0.3000	1.0000	0.0199	0.0286	8.7	0.823	0.500	

First Count								
		Background	Count Rate	2.31	cpm			
			Count Time	100	minutes			
		Count	Count	Total	Net	Y-90	cpm	
Number	Activity min^{-1}	Date	Time	Count Rate min^{-1}	Count Rate min^{-1}	Ingrowth	from Y-90	
	Eq 3-11				Eq 3-2	Eq 3-9	see Eq 3-10	
1	1287.8	11/04/01	10:12 PM	524.90	522.59	0.029	18.93	
2	1339.3	11/04/01	11:12 PM	548.50	546.19	0.039	27.01	
3	1339.3	11/05/01	12:12 AM	555.34	553.03	0.050	34.33	
4	1352.2	11/05/01	01:12 AM	566.77	564.46	0.060	43.13	
5	1352.2	11/05/01	02:13 AM	588.38	586.07	0.070	49.65	
6	1352.2	11/05/01	03:13 AM	587.51	585.20	0.080	57.54	
7	1322.1	11/05/01		0.00	NA	0.048	NA	
8	1307.1	11/05/01	04:13 AM	575.20	572.89	0.090	64.54	

Second Count							
		Count	Count	Total	Net	Y-90	
Number	Activity min^{-1}	Date	Time	Count Rate min^{-1}	Count Rate min^{-1}	Ingrowth	
	Eq 3-13				Eq 3-2	Eq 3-9	
1	1284.2	12/17/01	02:57 AM	1161.00	1158.69	1.000	
2	1335.6	12/17/01	03:57 AM	1206.04	1203.73	1.000	
3	1335.6	12/17/01	04:58 AM	1209.48	1207.17	1.000	
4	1348.4	12/17/01	05:58 AM	1240.70	1238.39	1.000	
5	1348.4	12/17/01	06:58 AM	1244.65	1242.34	1.000	
6	1350.7	11/21/01	09:07 PM	1238.20	1235.89	0.988	
7	1320.7	11/21/01	10:47 PM	0.00	NA	0.988	
8	1305.7	11/21/01	10:08 PM	1217.57	1215.26	0.988	

Efficicency								
	Source Identification		Thickness	Y-90	Uncertainty	Sr-90	Uncertainty	
	Date	Number	mg cm^{-2}	Efficiency	(1S)	Efficiency	(1S)	Comments
			Eq 3-4	Eq 3-8		Eq 3-10		
	11/4/2001	1	4.7	0.510	0.017	0.391	0.013	
	11/4/2001	2	4.9	0.512	0.017	0.388	0.013	
	11/4/2001	3	4.9	0.515	0.017	0.387	0.013	
	11/4/2001	4	4.9	0.532	0.018	0.386	0.013	
	11/4/2001	5	4.2	0.523	0.019	0.397	0.014	
	11/4/2001	6	4.2	0.531	0.019	0.390	0.014	
	11/4/2001	7	4.1	NA		NA		Discarded
	11/4/2001	8	4.1	0.548	0.020	0.389	0.014	

Table A-23. Strontium-90 and yttrium-90 efficiency measurement data for 11/11/01 with measured efficiency and total propagated uncertainty (1S).

Preparation

	Date Yttrium ppt	11/11/01 03:30 PM		Radionuclide Activity Date	Sr-90 3527.4 06/26/97	min^{-1} mL^{-1}	Carrier 35.23	mg mL^{-1}
Number	SrCO3 Carrier ml	Y(OH)x Carrier ml	Filter Weight grams	Filter+ppt Weight grams	Net Weight mg Eq 3-3	Yield Eq 3-5	Volume Radionuclide mL	
1	0.250	1.000	0.0197	0.0278	8.1	0.920	0.500	
2	0.250	1.000	0.0201	0.0285	8.4	0.954	0.500	
3	0.250	1.000	0.0197	0.0283	8.6	0.976	0.500	
4	0.250	1.000	0.0199	0.0273	7.4	0.840	0.500	
5	0.200	1.000	0.0200	0.0264	6.4	0.908	0.500	
6	0.200	1.000	0.0200	0.0265	6.5	0.923	0.500	
7	0.200	1.000	0.0201	0.0199	NA	NA	0.500	
8	0.200	1.000	0.0199	0.0199	0	0.000	0.500	

First Count

		Background Count	Count Rate Count Time	2.31 100	cpm minutes		
Number	Activity min^{-1} Eq 3-11	Date	Count Time	Total Count Rate min^{-1} (5)	Net Count Rate min^{-1} Eq 3-2	Y-90 Ingrowth Eq 3-9	cpm from Y-90 Eq 3-12
1	1459.7	11/11/01	06:41 PM	604.50	602.19	0.034	26.34
2	1513.8	11/11/01	07:43 PM	633.64	631.33	0.045	36.34
3	1549.8	11/11/01	08:44 PM	643.62	641.31	0.055	45.60
4	1333.6	11/11/01	09:44 PM	587.20	584.89	0.065	48.41
5	1441.7	11/11/01	10:44 PM	653.58	651.27	0.075	60.37
6	1464.2	11/11/01	11:44 PM	664.18	661.87	0.085	66.64
7	NA	11/11/01	11:44 PM	0.00	NA	NA	NA
8	0.0	11/11/01	11:44 PM	0.00	NA	0.085	0.00

Second Count

Number	Activity min^{-1} Eq 3-13	Count Date	Count Time	Total Count Rate min^{-1}	Net Count Rate min^{-1} Eq 3-2	Y-90 Ingrowth Eq 3-9
1	1457.9	11/30/01	02:47 PM	1348.33	1346.02	0.993
2	1511.9	11/30/01	04:44 PM	1402.16	1399.85	0.993
3	1547.9	11/30/01	05:44 PM	1418.79	1416.48	0.993
4	1331.9	11/30/01	06:45 PM	1273.95	1271.64	0.993
5	1439.9	11/30/01	07:45 PM	1388.15	1385.84	0.993
6	1462.4	11/30/01	08:45 PM	1372.46	1370.15	0.993
7	NA	11/30/01	10:47 PM	NA	NA	NA
8	0.0	11/30/01	11:47 PM	0.00	NA	0.993

Efficiency

	Source Identification Date	Number	Thickness mg cm^{-2} Eq 3-4	Y-90 Efficiency Eq 3-14		Sr-90 Efficiency Eq 3-15	Uncertainty (1S)	Comments
	11/11/2001	1	3.8	0.532	0.012	0.394	0.015	
	11/11/2001	2	3.9	0.536	0.020	0.393	0.015	
	11/11/2001	3	4.0	0.534	0.020	0.384	0.014	
	11/11/2001	4	3.5	0.556	0.020	0.402	0.016	
	11/11/2001	5	3.0	0.555	0.025	0.410	0.018	
	11/11/2001	6	3.0	0.533	0.024	0.407	0.018	
	11/11/2001	7	NA					Lost
	11/11/2001	8	0.0					Blank

Table A-24. Strontium-90 and yttrium-90 efficiency measurement data for 08/04/02 with measured efficiency and total propagated uncertainty (1S).

Preparation								
	Date	08/04/02		Radionuclide	Sr-90		Carrier	
	Yttrium ppt	03:26 PM		Activity	3527.4	min^{-1} mL^{-1}	35.23	mg mL^{-1}
				Date	06/26/97			
	SrCO3	Y(OH)x	Filter	Filter+ppt	Net	Yield	Volume	
Number	Carrier	Carrier	Weight	Weight	Weight		Radionuclide	
	ml	ml	grams	grams	mg		mL	
					Eq 3-3	Eq 3-5		
1	0.540	1.000	0.0199	0.0346	14.7	0.773	0.500	
2	0.540	1.000	0.0201	0.0363	16.2	0.852	0.500	
3	0.540	1.000	0.0200	0.0353	15.3	0.804	0.500	
4	0.540	1.000	0.0199	0.0361	16.2	0.852	0.500	
5	0.674	1.000	0.0199	0.0401	20.2	0.851	0.500	
6	0.674	1.000	0.0201	0.0405	20.4	0.859	0.500	
7	0.674	1.000	0.0201	0.0397	19.6	0.825	0.500	
8	0.674	1.000	0.0199	0.0400	20.1	0.846	0.500	

First Count								
		Background	Count Rate	2.31	cpm			
			Count Time	100	minutes			
				Total	Net	Y-90	cpm	
Number	Activity min^{-1}	Count Date	Count Time	Count Rate min^{-1}	Count Rate min^{-1}	Ingrowth	from Y-90	
	Eq 3-11				Eq 3-2	Eq 3-9	see Eq 3-10	
1	1205.1	08/04/02	07:25 PM	467.24	464.93	0.042	27.37	
2	1328.1	08/04/02	08:25 PM	506.80	504.49	0.053	35.29	
3	1254.3	08/04/02	09:25 PM	500.98	498.67	0.063	41.65	
4	1328.1	08/04/02	10:26 PM	522.58	520.27	0.073	51.56	
5	1326.8	08/04/02	11:26 PM	521.65	519.34	0.083	57.88	
6	1339.9	08/05/02	12:26 AM	528.51	526.20	0.093	65.25	
7	1287.4	08/05/02	01:26 AM	521.80	519.49	0.103	70.26	
8	1320.2	08/05/02	02:26 AM	529.60	527.29	0.112	76.44	

Second Count							
		Count	Count	Total	Net	Y-90	
Number	Activity min^{-1}	Date	Time	Count Rate min^{-1}	Count Rate min^{-1}	Ingrowth	
	Eq 3-13				Eq 3-2	Eq 3-9	
1	1203.9	08/19/02	05:06 PM	1074.27	1071.96	0.980	
2	1326.8	08/19/02	06:06 PM	1127.99	1125.68	0.980	
3	1253.1	08/19/02	07:06 PM	1108.20	1105.89	0.981	
4	1326.8	08/19/02	08:07 PM	1163.03	1160.72	0.981	
5	1325.5	08/19/02	09:07 PM	1146.90	1144.59	0.981	
6	1338.6	08/19/02	10:07 PM	1151.52	1149.21	0.981	
7	1286.1	08/19/02	11:07 PM	1122.08	1119.77	0.981	
8	1318.8	08/20/02	12:07 AM	1122.72	1120.41	0.986	

Efficiency								
	Source Identification		Thickness	Y-90	**Uncertainty**	Sr-90	**Uncertainty**	
	Date	Number	mg cm^{-2}	Efficiency	**(1S)**	Efficiency	**(1S)**	Comments
			Eq 3-4	Eq 3-8		Eq 3-10		
	8/4/2002	1	6.9	0.538	**0.015**	0.363	**0.011**	
	8/4/2002	2	7.6	0.505	**0.015**	0.353	**0.011**	
	8/4/2002	3	7.2	0.528	**0.015**	0.364	**0.011**	
	8/4/2002	4	7.6	0.532	**0.015**	0.353	**0.011**	
	8/4/2002	5	9.4	0.525	**0.014**	0.348	**0.010**	
	8/4/2002	6	9.5	0.524	**0.014**	0.344	**0.010**	
	8/4/2002	7	9.2	0.531	**0.014**	0.349	**0.011**	
	8/4/2002	8	9.4	0.515	**0.014**	0.342	**0.011**	Ingrowth > 10%

References

Agu, B. N. C., T. A. Burdett, and E. Matsukawa, 1958. The transmission of electrons through metallic foils. Proceedings Physics Society 72:727-732.

Albert, G. E. and L. Nelson, 1953. Contributions to the statistical theory of counter data. Annals Mathematical Statistics, 24:920.

APHA, 1992. Standard Methods for the Examination of Water and Wastewater, 18th edition. American Public Health Association, 1015 Fifteenth St. NW, Washington DC

ASTM, 1987. E319-68, Standard method of Testing Single-Arm Balances; U.S. Department of Commerce, National Institute of Standards and Technology, Handbook 44, Specifications, Tolerances, and Other Technical Requirements for Weighing and Measuring Devices.

Aten, Jr. A.H.W. 1950. Corrections for beta particle self absorption. Nucleonics 6(1): 68-74

Baker, R. G. and L. Katz, 1953. Absolute beta counting of thick planar samples. Nucleonics 7(2):14-19

Baily, N. A., and J. K. Steigerwalt, 1975. The relative influence of geometry and statistical fluctuations of energy loss on the distribution of energy deposition by charged particles in proportional counters. Health Physics 28:503-509.

Balfour, J. G., 1954. The effect of back-scattering of electrons on measurements in β-spectroscopy and absolute counting. Journal of Scientific Instruments 31:395-398.

Baltakmens, T., 1970. A Simple method for determining the maximum energy of beta emitters by absorption measurements. Nuclear Instruments and Methods, 82:264-268.

Baltakmens, T., 1977. Accuracy of absorption methods in the identification of beta emitters, Nuclear Instruments and Methods, 142:535-538.

Bayhurst, B. P. and R. J. Prestwood, 1959. A method for estimating beta-counting efficiencies. Nucleonics 17(3): 82-85.

Beismeister, J. F., (ed.), 1993. MCNP - General Monte Carlo N-Particle Transport Code, Version 4A , LA-1265-M.

Berger, M. J., 1963. Monte Carlo calculation of the penetration and diffusion of fast charged particles, in B. Alder, S. Fernback and M Rotenburg (eds.) Methods in Computational Physics: Advances in Research and Applications, pp.135-215. Academic Press, New York.

Berger, M. J., 1988. Electron Stopping Powers for Transport Calculations. In Jenkins, T. M., W. R. Nelson, and A. Rindi (editors), Monte Carlo Transport of Electrons and Photons, pp. 57-80. Springer Publishing Company, New York.

Berger, M. J., 1998. Applicability of the condensed-random-walk Monte Carlo method at low energies in high-Z materials. Radiation Physics and Chemistry 53:191-203.

Berger, M. J. and R. Wang, 1988. Multiple-Scattering angular deflections and energy-loss straggling. In Jenkins, T. M., W. R. Nelson, and A. Rindi (editors), Monte Carlo Transport of Electrons and Photons, pp. 21-56. Springer Publishing Company, New York.

Bland, C. J. 1984, Tables of geometrical factors for various source-detector configurations. Nuclear Instruments and Methods in Physics Research 223: 602-606.

Bowman, W. B., II, D. L. Swindle, and D. L. Henderson, 1976. Radiochemical determination of Sr-89 and Sr-90: A comparison of methods based on error analysis. Health Physics 31:495-500.

Burtt, B. P., 1949. Absolute beta counting. Nucleonics 5: 28-43.

Coryell, C. D, and N. Sugarman (editors), 1951. Radiochemical Studies: The Fission Products, Book 1: Parts I, II, III, IV - Papers 1 to 52. McGraw-Hill Book Co., New York.

Dapor, M. 1992. Monte Carlo simulation of backscattered electrons and energy from thick targets and surface films. Physical Review B, 46:618-625

Darlington, E. H., 1975. Backscattering of 10-100 keV electrons from thick targets. Journal Physics D: Applied Physics, 8:85-91.

DeGroot, M.H., 1986. Probability and Statistics. Addison-Wesley Publishing Company, Reading, Massachusetts.

Duval, C. 1963, Inorganic Thermogravimetric Analysis. Elsevier, Amsterdam.

Eckerman, K. F., R. J. Westfall, J. C. Ryman, and M. Cristy, 1994. Availability of nuclear decay data in electronic form, including beta spectra not previously published. Health Physics 67(4):338-345.

Elliott, N., D. W. Engelkemeir, and W. Rubinson, 1951. Angular dependence of X-ray intensity from radioactive sources: effect on determination of geometry factor. In C. D. Coryell and N. Sugarman (eds.) Radiochemical Studies: The Fission Products, Book 1 Parts I, II, III, IV - Papers 1 to 52, McGraw-Hill Book Co., New York.

Elliot, N., and E. Shapiro, 1951. An analysis of beta-ray scattering phenomena in sources and absorbers. In C. D. Coryell and N. Sugarman (eds.) Radiochemical Studies: The Fission Products, Book 1 Parts I, II, III, IV - Papers 1 to 52, McGraw-Hill Book Co., New York.

Ellison, S.L.R., M. Rosslein, and A. Williams, 2000. EURACHEM/CITAC Guide CG 4: Quantifying Uncertainty in Analytical Measurement, 2nd edition.

EML, 1997. The Procedures Manual of the Environmental Measurements Laboratory, HASL-300. 28th edition, February, 1997. Nancy A. Chieco, Editor. U. S. Department of Homeland Security, 201 Varick St. 5th Floor, New York, NY 10014.

Emsley, J., 1989. The Elements. Clarendon Press, Oxford.

Engelkemeir, D. W., J. A. Seiler, E. P. Steinberg, and L. Winsber, 1951. Investigation of the effects on counting of self-scattering due to source weight. In C. D. Coryell and N. Erlich, M., Pruitt, J.S. and C.G. Soares, 1985. Standard beta particle and monoenergetic electron sources for the calibration of beta-radiation Instrumentation. Report NUREG/CR 4266/NBSIR 85-3169, National Bureau of Standards, Gaithersburg, MD...

Evans, R. D., 1955. The Atomic Nucleus. Robert E. Krieger Publishing Company, Malabar, Florida.

Frank, H., 1959. Multiple scattering and back-diffusion of fast electrons after passage through thick layers. Zeitshrift fuer Naturforschung, 14a: 247-261.

Franzen, W. and L.W. Cochran, 1962. Pulse ionization chambers and proportional counters, In A. H. Snell (ed.), Nuclear Instruments and their uses, Volume I: Ionization detectors, scintillators, Cerenkov counters, amplifiers: assay, dosimetry, health physics. John Wiley and Sons, New York.

Gleason, G. I., J.D. Taylor, and D.L. Tabern, 1951. Absolute beta counting at defined geometries. Nucleonics 8(5):12-21.

Goudsmit, S. and J.L. Saunderson, 1940. Multiple scattering of electrons. Physical Review 57:24-29.

Goudsmit, S. and J. L Saunderson, 1940. Multiple scattering of electrons. II. Physical Review 58:36-42.

Greene, R.E., R.S. Pressly, and F.N. Case, 1972. A review of alpha source preparation methods and applications. ORNL-4819, Oak Ridge National Laboratory, Oak Ridge, Tennessee.

Grozev, P.A., E.I. Vapirev, and L.I. Botsova, 1992. Energy distribution of beta particles transmitted through an absorber. International Journal Radiation Applied Isotopes. Part A, Applied Radiation Isotopes, 43: 383-387

Halbleib, J. A. 1988. Structure and operation of the ITS Code System. In Jenkins, T. M., W. R. Nelson, and A. Rindi (editors), Monte Carlo Transport of Electrons and Photons, pp. 249-261. Springer Publishing Company, New York.

Halbleib, J. A. 1988. Applications of the ITS codes. In Jenkins, T. M., W. R. Nelson, and A. Rindi (editors), 1988. Monte Carlo Transport of Electrons and Photons, pp. 263-284. Springer Publishing Company, New York.

Halbleib, J. A. and W. H. Vandevender, 1976. Cyltran: A cylindrical-geometry multimaterial electron/photon Monte Carlo transport code. Nuclear Science and Engineering 61:288.

Hankins, D.E. 1985. Effect of air-scattered beta particles on instrument and dosimeter response, Health Physics 49: 435-441.

Hogan, O.H., P.E. Zigman, and J.L. Mackin, 1964. Beta Spectra II. Spectra of individual negatron emitters. U.S. Naval Radiological Defense Laboratory, USNPDL-TR-802, 16 December, 1964.

Hogg, R. V. and A. T. Craig, 1978. Introduction to Mathematical Statistics, MacMillan Publishing Co., Inc. New York.

Horowitz, Y. S., C. R. Hirning, P. Yuen, and P. Wong, 1994. Monte Carlo calculations of monoenergetic electron depth dose distributions in LiF chips: skin dose correction factors for beta rays. Health Physics 67(4):330-337.

Hunger, H. J. and L. Küchler, 1979. Measurements of the electron backscattering Coefficient for Quantitative EPMA in the Energy Range of 4 to 40 keV. Physica Status Solidi 56:K45-K48.

ICRP, 1983. ICRP Publication 38, Radionuclide transformations. International Commission on Radiation Protection. Pergamon Press, Oxford.

ICRU, 1979. ICRU Report 31. Average energy required to produce an ion pair. International Commission on Radiation Units and Measurements, Bethesda, Maryland.

ICRU, 1997. ICRU Report 56. Dosimetry of external beta rays for radiation protection. International Commission on Radiation Units and Measurements, Bethesda, Maryland.

Jaffey, A. H., 1953. Solid angle subtended by a circular aperture at point and spread sources: formulas and some tables. Review of Scientific Instruments 25(4):349

Jenkins, T. M., W. R. Nelson, and A. Rindi (editors), 1988. Monte Carlo transport of electrons and photons, Plenum Press, New York.

Johansson, L., G. Sibbens, T. Altzitzoglou, and B. Denecke, 2002. Self-absorption correction in standardization of ^{204} Tl. Applied Radiation and Isotopes 56: 199-203.

Jun, I. 2003. Benchmark study for energy deposition by energetic electrons in thick elemental slabs: Monte Carlo results and experiments. IEEE Transactions on Nuclear Science 50(5):1732-1739.

Kalmon, B., 1953. Experimental method for determination of counting geometry. Nucleonics 11(7):56-59.

Kanter, H., 1957. Back-scattering of electrons in the energy range between 10 and 100 keV. Annalen der Physik 20:144-166.

Knoll, G. F., 2000. Radiation detection and measurement, John Wiley and Sons, New York.

Krieger, H. L. and E. L. Whittaker, 1980. Prescribed procedures for measurement of radioactivity in drinking water. EPA-600/Y-80-032

LANL, 2005. MCNP – A general Monte Carlo N-Particle transport code, Version 5. Volume I: Overview and Theory. LA-UR-03-1987. April 24, 2003, revised October 3, 2005.

LANL, 2006. MCNP/MCNPX: Monte Carlo N-Particle transport code system including MCNP5 1.40 and MCNPX 2.5.0 and data libraries. Distributed by ORNL RSICC, CCC-730 MCNP/MCNPX

Lockwood, G.J., L.E. Ruggles, G.H. Miller, J.A. Halbleib, 1981. "Calorimetric measurement of electron energy deposition in extended media -- theory vs. experiment," SAND 79-0414, Sandia National Laboratories.

Lorence, Jr., L.J., and D. E. Buetler, 1997. Radiation transport phenomena and modeling Part A: codes, Part B: applications and examples. SAND 97-2135, Sandia National Laboratories.

Martin, J. W., J. Yuan, S. A. Hoedl, B.W. Filippone, D. Fong, T. M. Ito, E. Lin, B. Tipton and A. R. Young, 2003. Measurment of electron backscattering in the energy range of neutron β-decay. Physical Review C. 68(055503):1-8.

Martin, J. W., J. Yuan, M. J. Betancourt, B.W. Filippone, S. A. Hoedl, T. M. Ito, B. Plaster, and A. R. Young, 2006. New measurment and quantitative analysis of electron backscattering in the energy range of neutron β-decay. Physical Review C. 73(15501):1-6.

MacPherson, M. S., C. K. Ross, and D. W. O. Rogers, 1995. A technique for accurate measurement of electron stopping powers. Medical Physics 22:950.

MacPherson, M. S., C. K. Ross, and D. W. O. Rogers. 1996. Measured electron stopping powers for elemental absorbers. Medical Physics 23:797.

Mann, W. B. and H. H. Seliger, 1958. Preparation, maintenance, and application of standards of radioactivity", Nat. Bureau Standards (U.S.) Circular 594

MARLAP, 2004. Multi-Agency Radiological Laboratory Analytical Protocols Manual (Final) Volume I (EPA 402-B-04-001A), Volume II (EPA 402-B-04-001B), Volume III (EPA 402-B-04-001C).

Masket, A. V., 1957. Solid angle contour integrals, series, and tables, Review of Scientific Instruments 28(3):191.

McCroan, K. D., 2005. GumCalc v 1.0. Freeware developed for the MARLAP project. http://mccroan.com/Gumcalc.htm.

Merrit, J.S, Taylor, J.G.V., and Campion, P.V. (1959). Self-absorption in sources prepared for 4pi beta counting. Canadian Journal Chemistry 37: 1109.

Molière, G., 1947. Theorie der streurng schneller geladener teilchen I: einzelstreuung am abgeschirmten Coulomb-Feld, Z. Naturforsch 2a: 133.

Morin, R. L.(editor), 1988. Monte Carlo simulation in the radiological sciences, CRC Press, Inc., Boca Raton, Florida.

Murthy, M.S. S., 1971. Shape and average energy of beta-particle spectra. International Journal of Applied Radiation and Isotopes 22:111-123.

Nader, J. S., G. R. Hagee, and L.R. Setter, 1954. Evaluating the performance of the internal counter. Nucleonics 12: 29-31.

Nahum, A. E. 1988. Overview of photon and electron Monte Carlo. In Jenkins, T. M., W. R. Nelson, and A. Rindi (editors), Monte Carlo transport of electrons and photons. pp. 3-20. Springer Publishing Company, New York.

Nath, R., 1988. Monte Carlo simulations in radiation therapy, In Morin, R. L.(editor), Monte Carlo Simulation in the Radiological Sciences, CRC Press, Inc., Boca Raton, Florida.

Nervik, W.E. and P.C. Stevenson, 1952. Self scattering and self absorption of betas by moderately thick samples. Nucleonics 10(3):18-22.

Neter, J., W. Wasserman, and M. H. Kutner. 1990. Applied linear statistical models: regression, analysis of variance, and experimental designs. Irwin, Homewood, Illinois.

Neubert, G., and S. Rogachewski, 1980. Backscattering coefficient measurements of 15 to 60 keV electrons for solids at various angles of incidence. Physica Status Solidi 59:35-41.

N.C.R.P., 1978, A handbook of radioactivity measurements procedures, NCRP Report No. 58, National Council on Radiation Protection and Measurements, Washington, D.C.

Novey, T. B., and N. Elliott, 1951. An analysis of the effects on absorption curves of scattering of beta-radiation by absorbers. In C. D. Coryell and N. Sugarman (eds.) Radiochemical Studies: The Fission Products, Book 1 Parts I, II, III, IV - Papers 1 to 52, McGraw-Hill Book Co., New York.

Novey, T. B., 1950. RaDEF Standard sources for beta-disintegration rate determinations. Review of Scientific Instruments 21(4):280.

Pregenzer, A. L, 1985. Monte Carlo calculations of low energy backscatter coefficients. Nuclear Instruments and Methods in Physics Research. 136:562-565

Price, W. J., 1964. Nuclear radiation detection, 2nd edition,
McGraw-Hill Book Company, New York.

Rester, D. H., and J. H. Derrickson, 1970. Electron backscatter measurements for perpendicular and non-perpendicular incidence at 1.0 MeV bombarding energy. Nuclear Instruments and Methods 86: 261-267.

Schaart, D. R., J. T. M. Jansen, J. Zoetelief, and P. F. A. de Leege, 2002. A comparison of MCNP4C electron transport with ITS 3.0 and experiment at incident energies between 100 keV and 20 MeV: influence of voxel size, substeps, and energy indexing algorithm," Phys.Med. Biol., 47:1459-1484.

Scott, W. T., 1963. The theory of small-angle multiple scattering of fast charged particles. Reviews of Modern Physics, 35(2):231-313.

Seliger, H. H., 1950. Saturation backscattering of positive electrons, Physical Review 78:491.

Seliger, H. H., 1952. The backscattering of positrons and electrons, Physical Review 88(2):408.

Seliger, H. H. and A. Schwebel, 1954. Standardization of beta-emitting nuclides. Nucleonics 12(7):54-63.

Seltzer, S. M. 1988. Cross Sections for Bremsstrahlung production and electron-impact ionization. In Jenkins, T. M., W. R. Nelson, and A. Rindi (editors), Monte Carlo Transport of Electrons and Photons, Plenum Press, New York.

Shimizu, R. and S. Ichimura, 1983. Direct Monte Carlo simulations of scattering processes of kV electrons in aluminum; comparison of theoretical N(E) spectra with experiment. Surface Science 133:250-266.

Snell, A. H. (ed.), 1962. Nuclear Instruments and their uses, Volume I: Ionization detectors, scintillators, Cerenkov counters, amplifiers: assay, dosimetry, health physics. John Wiley and Sons, New York.

Steinberg, E. P., 1962. Counting methods for the assay of radioactive samples, In A. H. Snell (editor), Nuclear instruments and their uses, Volume I: Ionization detectors, scintillators, cerenkov counters, amplifiers: assay, dosimetry, health physics. John Wiley and Sons, New York.

Suzor, F. and G. Charpak, 1952. Energy dependence of electron backscattering. Jounal de Physique et le Radium 13:1-10.

Tabata, T., 1967. Backscattering of electrons from 3.2 to 14 MeV. Physical Review 162(2):336-347

Tabata, T., R. Ito, and S. Okabe, 1971. An empirical equation for the backscattering coefficient of electrons. Nuclear Instruments and Methods 94(1971): 509-513.

Taylor B. N., and C. E. Kuyatt, 1994. Guidelines for evaluating and expressing the uncertainty of NIST measurement results, NIST Technical Note 1297, 1994 edition, National Institute of Standards and Technology.

Tennelec, undated. Instruction manual: LB 1000 low background counting system.

Trump, J. G. and R. J. Van de Graaff, 1949. The secondary emission of electrons by high energy electrons. Physical Review 75:44-45.

Turner, J. E., 1986. Atoms, radiation, and radiation protection. Pergamon Press, New York.

USNRC, 2007. Quality Assurance for radiological monitoring programs (Inception through normal operations to License Termination) -- effluent streams and the environment, Revision 2, ML071790506, July, 2007.

Van der Eijk, W., W. Oldenhof, and W. Zehner, 1973. Preparation of thin sources," Nuclear Instruments Methods 112: 343.

Weast, R. C., M. J. Astle, and W. H. Beyer, 1985. CRC Handbook of Chemistry and Physics. CRC Press, Inc., Boca Raton, Florida.

X-5 Monte Carlo Team, 2005. MCNP - A general Monte Carlo N-particle transport code, version 5. Volume I: Overview and Theory LA-UR-03-2987. April 24, 2003, revised October 3, 2005.

Yankwich, P.E., T.H. Norris and J Huston, 1947. Correcting for the absorption of weak beta-particles in thick samples. Analytical Chemistry 19(7):439-441.

Zumwalt, L. R., 1950. Absolute beta counting using end-window Geiger Mueller counters and experimental data on beta-particle scattering effects, Report MONC-397, U.S. Atomic Energy Comm. Document AECU-567.